University of Nottingham
UK | CHINA | MALAYSIA

Bacterial biofilm interactions with human immune cells

Thesis submitted to the University of Nottingham for the degree of Doctor of Philosophy

Kelly Lee

July 2022

Table of Contents

List of Figures

List of Tables

Abstract

The human immune system is vast, and ranges from physical barriers to cellular mediators which coordinate to protect the host from the environment and pathogens. Bacterial cells have been shown to interact with various immune receptors which contribute to pathogen recognition, clearance and memory. Importantly, C-type lectin receptors (CLRs) interact with polysaccharides and are involved in the innate stages of immune recognition and decision-making during infection. Specifically, the CLRs MR, Dectin-2 and DC-SIGN all interact with high-mannose structures, which are abundant in multiple pathogens.

Pseudomonas aeruginosa is a ubiquitous, Gram-negative bacterium that causes opportunistic infection in immunocompromised hosts, and is particularly associated with both diabetes and cystic fibrosis patients. Additionally, *Staphylococcus aureus* is a commensal organism and a common resident of the skin microbiome. *P. aeruginosa* and *S. aureus* pose a burden to the global healthcare system as ESKAPE organisms, and possess the ability to switch between a planktonic, free-swimming growth mode to biofilm, characterised by development of bacterial communities within an extracellular matrix (ECM).

Our lab has previously demonstrated that both *P. aeruginosa* biofilms and purified biofilm carbohydrates from PAO1 biofilm-overproducing mutants, are able to interact with CLRs DC-SIGN, MR and Dectin-2, which all play a role in early immune decision making and modulation. During this study, we were able to optimise assays to confirm binding of these lectins to ECM polysaccharides from *P. aeruginosa*, namely Pel and Psl, as well as introduce a new species, *S. aureus* (SH1000), into our *in vitro* biofilm model which

displayed potential GalNAc ligands. Due to binding artifacts identified in the culture medium, *P. aeruginosa* biofilm growth was optimised in DMEM-BSA. Binding of all three CLRs was maintained for whole biofilms in this new medium, but to purified product, only DC-SIGN binding was observed. Optimisation of this work is ongoing.

To investigate cellular interactions during infection, a 3D co-culture model using a skin-like collagen matrix was designed and optimised to investigate interaction of human immune cells (monocyte-derived dendritic cells, moDCs) with *P. aeruginosa* (PAO1) biofilms in the context of cytotoxicity, cytokine production and surface marker expression. In this model, moDCs maintained high viability up to 24 h when cultured with live bacteria, although cytokine profiles were altered in the presence of bacteria. Specifically, chemoattractant protein MCP-1 was specifically downregulated in the presence of bacteria compared to other inflammatory cytokines (TNF-α, IL-1β) which were upregulated in the same conditions. Neither cytotoxicity nor cytokine profile was altered in the absence of DC-SIGN, indicating a certain level of redundancy in this context, contrary to earlier binding data. Additionally, surface markers (HLA-DR, CD11b, DC-SIGN, MR) were downregulated in the presence of PAO1 compared to uninfected cells when analysed by flow cytometry. After further investigation, this reduction was shown to be independent of secreted bacterial proteases, LPS stimulation or the general interaction of collagen with the immune cells.

The findings displayed during this study have provided novel contributions to our understanding of the immune response to bacterial biofilms, in context of polysaccharide interaction with CLRs and whole biofilms with immune cells in a wound-like setting, and have given us some exciting insight into how bacteria modulate immune responses during chronic infection. Although not without limitations, the work conducted here

provides some interesting routes for future investigation, potentially highlighting new avenues for therapeutic research and disease control.

Acknowledgements

I'd first like to give my most deep and sincere thank you to my primary supervisor, Luisa Martinez-Pomares, for everything she's done for me throughout this PhD. At a time when I felt lost and was unsure of my place in academia, you reminded me that I could still thrive and took the time to build me up to the confident scientist I have become. I couldn't have asked for a wiser, more caring or inspiring supervisor, and I feel blessed to have been your student. My second supervisor, Miguel Cámara, your ideas and expert advice have been instrumental during my project, and your enthusiasm and encouragement never fail to brighten my week. Thank you for giving me the opportunity to be your student. I would also like to thank my doctoral training program, the MRC IMPACT DTP, for both their financial support and for giving me so many training and development opportunities throughout my PhD which have allowed me to fulfil my dream.

I also feel incredibly lucky to have carried out my PhD in such a brilliant lab, over the years you've all helped and guided me, handled my chaos, laughed and cried with me and been great friends as well as colleagues. Darryl, you've been there since day one and from you've kept me right all the way. You own this lab, and I'm glad to have been part of it, 감사합냐다. Sonali, thank you for teaching me the ways of the immune cells and for always being there with a word of advice and encouragement. Simone, you're an inspiration and the king of antibodies, I've learned so much from you. Khawalah and Nusrat, I couldn't have asked for better padawans, you're going to do the most amazing things. Previous members Oli and Yasir, Dan Scott and David Onion, the NBIC crew, everyone from D44 and D61, Rebecca Cooper, Iona Willingham and I'm sure a hundred others that have provided so much help and advice during my project, I want to say thank you to all of you.

My rock, my best friend, mi familia and the person that makes me always want to be better. Sami, I would never have gotten through this without your guidance, your sword and you forever reminding me that of course it's hard, it's supposed to be. We will run a lab together one day, it's been manifested. Thank you.

All throughout my PhD, my dad has given me so many important truths and the most real advice. You're the most brutally honest and unrelenting man, but also the most supportive and caring. I love you for all of it more than anything. Mum, you've always been my biggest cheerleader and you've always got my back, I love and thank you for always being there. Dawn, for your endless encouragement and believing in me unconditionally, thank you.

Iona, when I don't believe in myself, you do, and when we're in the lab together I can never stop smiling. You take me out of my comfort zone and have given me so many incredible memories, I can't wait to make more with you. Tyla, you've gotten me through the craziness of thesis writing. You're always on hand for a cuppa, a rant or a cuddle I can't express how important you are to me. Shaun, Josh, Alex and Fran, the tight jeans double Ds, I've never laughed so much than when I'm with you all. You've taken me into your lives and I never want you to let me go. Thank you for being the best friends I could have asked for in Nottingham, you've all made this city a blast. Adam, my oldest and most dear friend, you've supported me from the start and are always there for a pint when I need it. Thank you for always being there.

When I moved to Nottingham from Glasgow, there was excitement but also fear. Kate and Peter have been there for me all this time from the homeland, making sure I never forget that no matter the distance, they've always got my back. Thank you both of you.

List of Publications

Written articles

ORCID ID: 0000-0002-9499-1081

Carbohydrates from Pseudomonas aeruginosa biofilms interact with immune C-type lectins and interfere with their receptor function. Sonali Singh, Yasir Almuhanna, Mohammad Y. Alshahrani, Douglas W. Lowman, Peter J. Rice, Chris Gell, Zuchao Ma, Bridget Graves, Darryl Jackson, **Kelly Lee**, Rucha Juarez, Janice Koranteng, Sirina Muntaka, Daniel A. Mitchell, Ana C. da Silva, Farah Hussain, Gokhan Yilmaz, Francesca Mastrotto, Yasuhiko Irie, Paul Williams, David L. Williams, Miguel Cámara and Luisa Martinez-Pomares. npj Biofilms Microbiomes. 7, 87 (2021). https://doi.org/10.1038/s41522-021-00257-w

Poster presentations

Polysaccharides of Staphylococcus aureus and Pseudomonas aeruginosa biofilms elicit immune responses via C-type lectin receptors. **Kelly Lee,** Sonali Singh, Yasir Almuhanna, Darryl Jackson, Miguel Cámara, Luisa Martinez-Pomares. Microbiology Society conference 2021

Polysaccharides of Staphylococcus aureus and Pseudomonas aeruginosa biofilms elicit divergent immune responses via C-type lectin receptors. **Kelly Lee**, Yasir Almuhanna, Sonali Singh, Shaun Robertson, Miguel Cámara & Luisa Martinez-Pomares. University of Nottingham PGR Symposium 2020.

*Variation in Staphylococcus aureus and Pseudomonas aeruginosa biofilm composition leads to varied immune responses via C-type lectin receptors***. Kelly Lee**, Yasir Almuhanna, Sonali Singh,

Rucha Kelkar, Shaun Robertson, Miguel Cámara & Luisa Martinez-Pomares. British Society of Immunology Congress 2019.

Oral presentations

Modelling host-pathogen interactions in the context of chronic wounds. **Kelly Lee**, Darryl Jackson, Miguel Cámara & Luisa Martinez-Pomares. 32nd European Congress of Clinical Microbiology and Infectious Diseases. Lisbon 2022. Applied for and awarded **Research Academy Travel Prize** (£500) and **IMM Divisional Travel Grant** (£500).

Polysaccharides of Staphylococcus aureus and Pseudomonas aeruginosa biofilms elicit an immune response via C-type lectin receptor engagement. **Kelly Lee**, Darryl Jackson, Miguel Cámara & Luisa Martinez-Pomares. University of Nottingham PGR Symposium 2021 (Online).

Pseudomonas aeruginosa biofilms display carbohydrate ligands for C-type lectin receptors that interfere with their receptor function. Sonali Singh, Yasir Almuhanna, Mohammad Y. Alshahrani, Douglas Lowman, Peter J. Rice, Chris Gell, Zuchao Ma, Bridget Graves, Darryl Jackson, **Kelly Lee**, Rucha Kelkar, Janice Koranteng, Dan Mitchell, Ana Silva, Farah Hussain, Gokhan Yilmaz, Francesca Mastrotto, Yasuhiko Irie, Paul Williams, David Williams, Miguel Cámara, Luisa Martinez-Pomares, The FASEB Microbial Glycobiology Conference 2020 (Online). Awarded prize for **Best Short Talk.**

List of Abbreviations

APC – Antigen presenting cell

BSA – Bovine serum albumin

CDC – Centre for Disease Control and Prevention

CFU – Colony forming unit

CLR – C-type lectin receptor

Con A – Concanavalin A

CRP – C-reactive protein

CTLD – C-type lectin-like domain

DAMP – Damage-associated molecular pattern

DBA – *Dolichos biflorus* agglutinin

DC – Dendritic cell

DC-SIGN - Dendritic cell-specific intercellular adhesion molecule-3

DMEM – Dulbecco's Modified Eagles Medium

dsRNA – double-stranded RNA

ECM – Extracellular matrix

EGF – Epidermal growth factor

ELISA – Enzyme-linked immunosorbent assay

FPLC – Fast protein liquid chromatography

FPRs – N-formyl peptide receptors

GalNAc – *N*-acetylgalactosamine

GlcNAc – *N*-acetylglucosamine

HAI – Hospital-acquired infection (healthcare-associated infection)

HKCa – Heat-killed *Candida albicans*

HO-1 – Haem oxygenase-1

ICAM – Intercellular adhesion molecule

Ig – Immunoglobulin

IL – Interleukin

LPS – Lipopolysaccharide

MAC – Membrane Attack Complex

MCP-1 – Monocyte chemoattractant protein 1

MAPK – Mitogen-activated protein kinase

MASP – MBL-associated serine proteases

MBL – Mannose binding lectin

MHC – Major histocompatibility complex

moDC – Monocyte-derived dendritic cell

MR – Mannose receptor

NET – Neutrophil extracellular trap

NF-κB – Nuclear factor kappa B

NK – Natural killer

NHSN – National Healthcare Safety Network

NLR – Nod-like receptor

PAMP – Pathogen-associated molecular pattern

PBMC – Peripheral blood mononuclear cell

PFA – Paraformaldehyde

PIA – Polysaccharide intercellular adhesion

PNA – Peanut agglutinin

Psl – Polysaccharide synthetic locus

PRR – Pattern Recognition Receptor

RCA I – *Ricinus communis* agglutinin

RLR – Rig-I-like receptor

SBA – Soybean agglutinin

SDS-PAGE – Sodium dodecyl sulfate–polyacrylamide gel electrophoresis

S1P – Sphingosine-1-phosphate

siRNA – short interfering RNA

TCR – T cell receptor

TLR – Toll-like receptor

TNF-α – Tumour necrosis factor alpha

TSB – Tryptic soy broth

UEA I – *Ulex europaeus* agglutinin I

VEGF – Vascular endothelial growth factor

WGA – Wheat germ agglutinin

WTA – Wall teichoic acid

Chapter 1. Introduction

1.1 Immune response during wound healing and infection

The immune system has evolved over time to defend the body from infection by the plethora of pathogens and traumas it is exposed to throughout its lifetime. Fundamentally, functioning of the immune system stems from its ability to differentiate between what is 'self' and what is 'non-self', and from this, determine what aspects of these entities are of benefit or detriment to the overall health of the host. The immune system is shaped from birth to tolerate non-self-antigens, such as ingested food and the extensive bacterial microbiome, which in itself has been implicated in countless benefits including utilisation of indigestible foodstuffs, protection from neurodegeneration and cancer (1-3). However, many microorganisms, are recognised as pathogenic, requiring clearance from the body due to their ability to cause disease. Further, the balance between pro- and anti-inflammatory signals are instrumental in controlled progression from trauma and colonisation to healing and resolution of infection. Many different cell types are involved in this defence, each with their own unique characteristics that contribute to the immune attack on pathogens. Alongside this, non-cellular agents aid the response, culminating in the re-establishment of homeostasis and health.

1.1.1 Barriers, immune complexes and innate immunity during acute wound healing and infection

The skin and mucocilliary systems are physical barriers that represent the first line of defence against infection, preventing pathogens from accessing internal tissues. The skin is made up of subcutaneous tissue (hypodermis), the dermis and the outermost epidermis that all play a role in physically preventing pathogen entry and environmental

damage (4). The epidermis provides a waterproof external layer, while the dermis contains sebum-secreting hair follicles, sweat glands and connective tissue that provide a hostile environment for pathogens due to excessive salt and oils as well as a lack of nutrients (5, 6). It is because of this harsh environment that members of the skin microbiome, the natural microbial community that inhabits various body sites, have adapted to populate this environment (7). The skin microbiome acts as a protective population by producing molecules that inhibit pathogen colonisation, out-competing any pathogenic cells that do attach and playing a role in immune education (7). Further, innate effector proteins and small molecules are produced constitutively by many cells within barrier sites before any trauma has occurred, shielding the tissues from invasive onslaught. In the lung, epithelial cells produce antimicrobial peptides such as defensins and cathelicidins, which are directly involved in pathogen killing and immune cell recruitment (8).

A wound is defined as a cut or other impact to tissues, in this case skin, which compromises barrier integrity. Over the decades, the timeline of wound healing has been well described. In summary, the initial stages are characterised by inflammation, which subsides on entering the next, anti-inflammatory and proliferative stage, concluding in extracellular matrix (ECM) remodelling and scar formation (**Figure 1.1**). During the earliest stages of inflammation, coagulation occurs within the wound site, initiated by the degranulation of platelets and mast cells and the formation of a fibrin-rich clot. Within, plasmin from plasminogen acts as a fibrolytic enzyme, which when knocked out severely impairs wound healing (9). Platelets, that lack a cell nucleus and are discoid in shape when inactive and dendritic when active, express various pattern recognition receptors (PRRs) able to directly interact with the wound environment and release pro-

inflammatory mediators when appropriate. Alongside this, it has also been theorised that platelets are able to stimulate mast cell degranulation (10). Indeed, this phenomenon has been observed *in vitro* in a human cardiac model (11).

Following initial degranulation, epithelial restitution occurs, where epithelial cells undergo sheet migration to cover the wound surface to provide a preliminary structure from which healing can occur. Cells migrate via cell-cell and cell-matrix adhesions from f-actin-rich protrusions of Rac1-β1 integrin, pulling cells forwards while attaching to exposed matrix fragments (12). Further, matrix metalloproteinases are involved in cleavage of exposed matrix as well as the basal lamina which allows for the migration of fibroblasts to the wound bed (13).

Disruption of vasculature and blood flow, blockage by the fibrin clot and increased influx of highly metabolically active immune cells during injury induces a local hypoxia during the pro-inflammatory stage of healing, which plays a role in acute as well as chronic wounds. Hypoxia initiates proliferation of fibroblasts and causes them to secrete transforming growth factor-β1 (TGF-β1), which is a key marker in healing (14). However, normoxia must be restored for effective healing, as proper collagen deposition and remodelling and maintenance of fibroblast proliferation requires substantial oxygen in the environment. Here, hypoxia-inducible factor-1 (HIF-1) is a transcription factor which activates genes involved in increasing oxygen delivery to wound, constituting a heterodimer of α- and β-subunits, where the β-subunit is constitutively expressed and α is regulated by oxygen level (15).

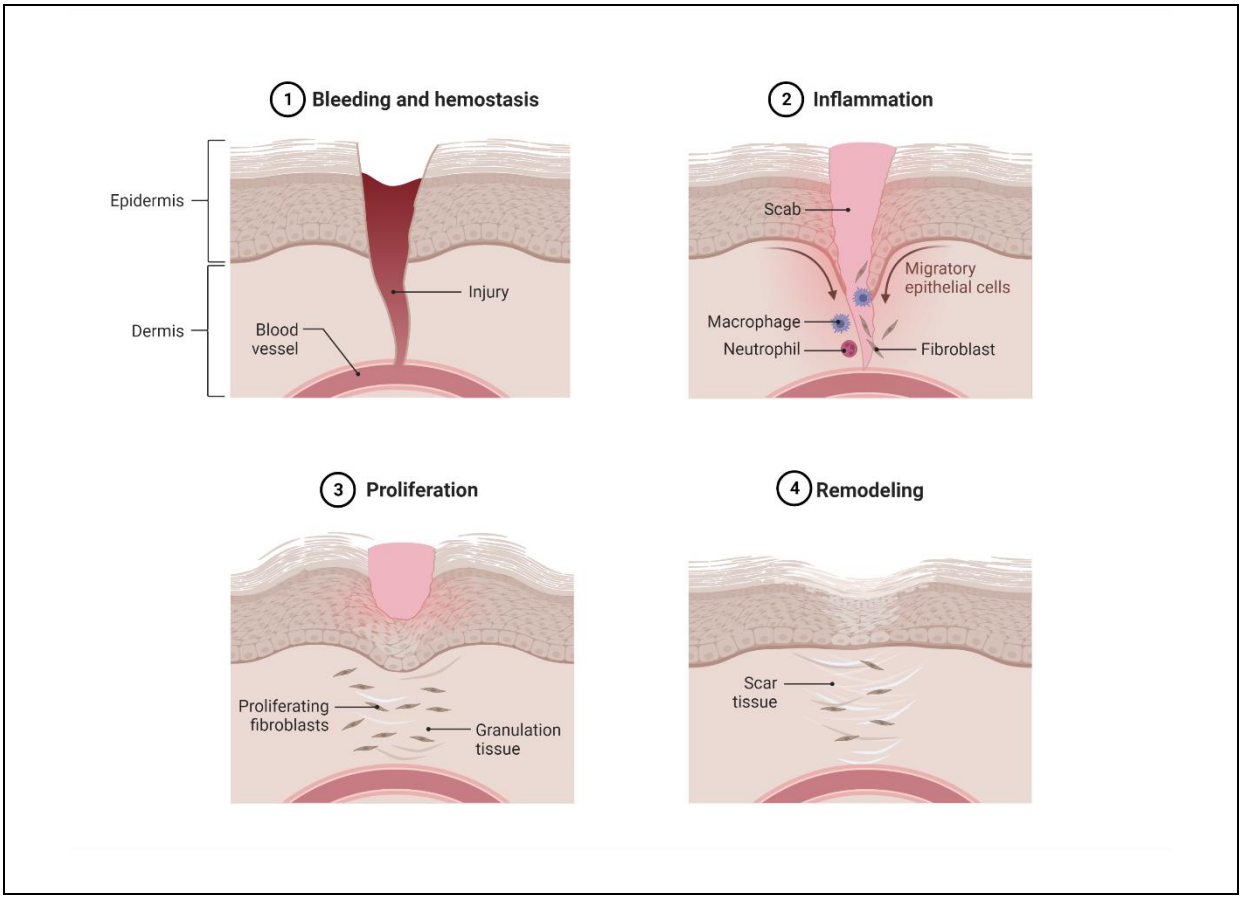

***Figure 1. 1: Stages of acute wound healing**. Immediately after injury, hemostasis occurs and a fibrin clot develops to form a provisional matrix within the wound bed. Platelets release growth factors such as PDGF, TGF-β and VEGF that initiate repair. Second is the inflammation phase within the first day of initial trauma, and it initiated by neutrophil attachment to blood vessel endothelia for migration to the wound site while epithelial cells undergo restitution, reinforcing the matrix. Following inflammation, the proliferation phase, favours promotion of anti-inflammation, where dermis-resident macrophages and activated monocytes migrate to the wound site alongside epithelial Langerhans cells to phagocytose neutrophils, remove denatured ECM and secrete fibroblast- and epidermal-stimulating growth factors to promote production of granulation tissue, replacing the normal dermis with a dense collagen and capillary networks. Finally, remodelling occurs where unorganised granulation tissue is replaced by scar tissue, where ECM organisation is much closer to that of normal skin. Image generated using templates in Biorender.com and in book chapter (16).*

1.1.1.1 Non-cellular responses during wound healing

Damaged cells release danger signals (damage-associated molecular patterns, DAMPs) that alert residing immune cells, triggering production of pro-inflammatory cytokines and chemokines. Chemokines diffuse into the bloodstream and promote chemotaxis of peripheral leukocytes, which migrate upstream against the concentration gradient. They

are distinguished into groups based on their conserved cysteine residues. For example, the GROα chemokine (CXCL1) with a C-X-C motif is expressed by epithelial cells as well as immune cells, and has potent neutrophil chemoattractant activity (17). Also, monocyte chemoattractant protein 1 (MCP-1 or CCL2) has a C-C motif and is produced during injury or infection, and functions by recruiting monocytes, dendritic cells and T lymphocytes to the site of inflammation (18). At the site of trauma, local immune cells produce pro-inflammatory cytokines that enter the bloodstream and signal other cells. Most notably, interleukin (IL)-1β, IL-6 and tumour necrosis factor-α (TNF-α) are associated with the promotion of pro-inflammation (19). IL-1β has a range of functions, including the promotion of immune cell proliferation and differentiation and is associated with pyroptosis. Here, IL-1β is released as a result of gasdermin D processing, responsible for pore forming, during inflammasome activation (20). IL-6, produced by macrophages, is involved in fever and upregulation of neutrophil haematopoiesis (21); it is able to cross the blood brain barrier and directly affect temperature regulation in the hypothalamus by producing the prostaglandin E_2. TNF-α is also produced predominantly by macrophages and promotes cell proliferation and activation and apoptosis (22).

1.1.1.2 Complement system

The complement system acts as an accessory (a complement) to immune cells and humoral components to clear damaged cells and pathogens. Many complement components circulate freely in the blood as inactive forms and are produced by various cells, predominantly hepatocytes in the liver, but also epithelial cells, macrophages and monocytes (23). Activation of the complement system occurs via three different pathways, the classical, lectin and alternative pathways (**Figure 1.2**), all of which involve a cascade of proteolytic cleavages that culminate in homologous active products, variants

of the protease C3-convertase (24). In the classical pathway, the C1-complex is formed in response to IgG or IgM bound to antigen (immune complexes), although the protein C1q is able to bind directly to some surface antigens due to its flexible globular head region, providing a range of specificity (25). Perhaps most importantly, C1q can directly bind phosphatidylserine and dsDNA, promoting opsonisation and enhancing the immunosuppressive qualities of apoptotic cells (26-28). Additionally, C1q binds bacterial lipid A, LPS and porins, contributing to positive feedback of opsonisation and complement activation (29). The C1-complex is formed of C1q, 2x C1r, 2x C1s (C1qr2s2). Binding to antibody Fc portion leads to the activation and cleavage of C1r, a serine protease that cleaves C1s while C1r2s2 cleaves C4 and C2 from plasma, and the newly formed C2b and C4b combine to form a C3-convertase (C4b2b complex). C3-convertase cleaves C3 to C3a/b, the latter contributing to the formation ofaC5 convertase (C4b2b3b) alongside lone C3b directly decorating the pathogen surface. C5 convertase cleaves C5 to C5a, an anaphylatoxin that promotes inflammation and cellular activation, alongside C3a, and C5b, assembling with C6-9 to form the membrane attack complex (MAC). MAC is lytic and functions by binding and forming a pore within the membrane of its target cell, ending in cell death (30).

Unlike the classical pathway, the alternative pathway is constitutively activated at a low level by spontaneous hydrolysis of C3 due to its instability in the aqueous environment (31). However, the C3b-like cleavage product produced by this spontaneous cleavage is quickly inactivated by factor H or factor I, alongside residual C3b from C3-convertase complex in other pathways, preventing cumulative pro-inflammation (31). The alternative pathway does not require antibodies for activation, rather an internal thioester of C3 covalently binds with amino/hydroxyl groups on self- or pathogen cell

surfaces, preventing factor I/H inactivation and allowing it to bind factor B and factor D, ultimately forming C3bBb, an alternative C3-convertase (32). C3-convertase is stabilised by factor P, and this complex initiates a positive feedback loop, where new C3b binds the same cell surface as its precursor, recruiting B, D and P and restarting the process (32). Unlike self-cells, pathogens are generally unable to regulate complement surface levels, thus distinguishing self from non-self, based on surface complement decoration levels, leading to opsonisation and phagocytosis (33). Covalent binding of C3 convertase to another C3b forms C3bBbC3bP, the alternative C5 convertase, performing the same role as in the classical pathway.

Finally, the lectin pathway follows a similar route to the classical pathway, replacing C1q with mannose binding lectin (MBL) and ficolins. Here, MBL binds mannose structures on the surface of pathogens, activating MBL-associated serine proteases (MASP)-1 and MASP-2 to split C4 and C2 as in the classical pathway (34). Classical C3-convertase is formed of C4b and C2b, and the cascade continues in the same way proceeding its formation. Ficolins are similar to MBL and directly bind the pathogen surface (35). Ficolins also interact with MASP to produce the classical C3-convertase (34).

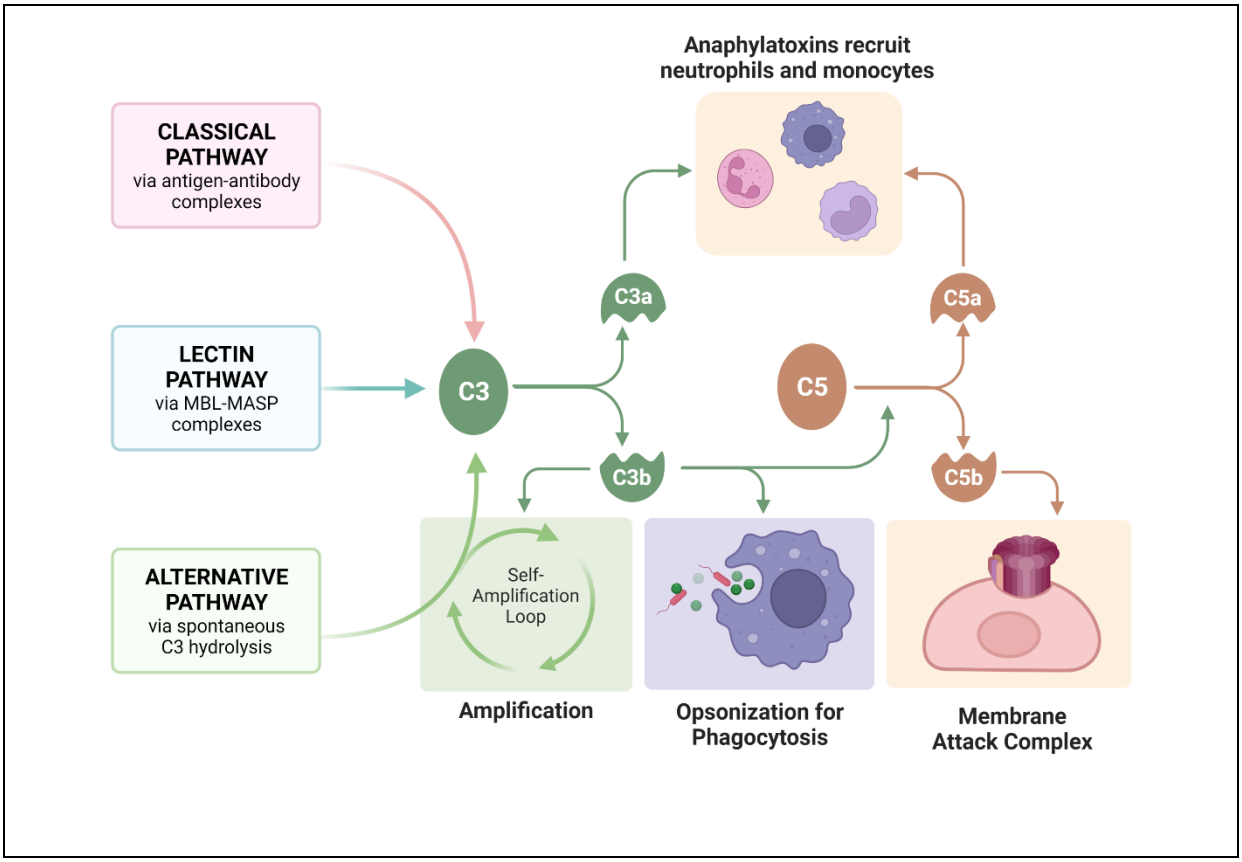

Figure 1. 2: Schematic depicting complement activation pathways. *Complement may be activated via the classical, alternative or lectin pathways. The classical pathway relies primarily on formation of the C1-complex (C1qr2s2) via recognition of antigen-antibody complexes, leading to the production of C3-convertase. The lectin pathway is activated when MBL complexes with MASP and binds microbial carbohydrates to form the C3-convertase. From here, C3 cleaves to form C3a (for chemotaxis and cell activation after complexing with C5a) and C3b (for opsonisation for phagocytosis and to complex with C4b2b to form C5-convertase). C5 cleaves to C5a (see above) and C5b, part of the membrane attack complex. In the alternative pathway, C3 is spontaneously activated by C3 hydrolysis, forming C3b, which contributes to the self-amplification loop of the other pathways. Figure generated using template on Biorender.com alongside (24).*

Alongside complement, pentraxins, including the C-reactive protein (CRP), are a group of pentameric proteins that increase during inflammation. CRP binds to the lipoproteins and polysaccharides at the surface of pathogenic or apoptotic cells and interact with C1q of the complement system, promoting formation of the MAC (36). All of these early inflammatory products or acute phase mediators increase in production in the presence of inflammation.

1.1.1.3 Resolution of inflammation

The transition from pro- to anti-inflammation is vital to the effective and timely healing of a wound, and dysregulation can lead to formation of a chronic wound, which will be discussed at length later in this section. The regulation of this shift to anti-inflammation is complex and not fully understood, but there are a number of key factors that that influence the wound environment at this time, as well as behaviours by immune cells, primarily macrophages.

Resolution of inflammation is required for the re-establishment of homeostasis. In part, this is achieved by the activation and signalling of N-formyl peptide receptors (FPRs) that are expressed by phagocytes and epithelial cells. This signalling cascade activates the NADPD oxidase NOX1, facilitating epithelial cell migration and mucosal wound repair (37). Further, pro-resolution macrophages are induced by apoptotic neutrophils, promoting their effector function in reverse migration and phagocytic clearance of inflammatory neutrophils from the wound bed and induction of anti-inflammation (38).

Epithelial migration and wound contraction facilitates the deposition of raw materials for collagen-rich granulation tissue and new vasculature, while epidermal growth factor (EGF) and TGF- β1 promote barrier repair (14). Major tissue and ECM remodelling occurs at the latest stage of the wound healing process. Fibroblasts, keratinocytes and endothelial cells restore dermis, epidermis and vasculature respectively, while macrophages secrete matrix metalloproteinases to breakdown ECM (39). Following this, most macrophages themselves apoptose, allowing skin to return to normal state as well as stimulating epithelial hair follicle stem cells for hair regeneration (39, 40). Subsets of macrophages that are resistant to apoptosis have been shown to be critical for promotion of fibrosis in pulmonary models (41). Apoptosis also occurs with myofibroblasts and

vascular cells after remodelling has taken place (42). T cells, namely Th2, infiltrate at this late stage and aid resolution and remodelling (43). The severity of scarring is dependent on the level of dysregulation on the proliferation of regenerative cells, be it excessive or insufficient.

1.1.2 The adaptive response

While the innate immune system is effective in the rapid recognition and clearance of pathogens and damaged tissue, the adaptive system provides a more refined response to specific antigens that initiates more slowly. However, although commonly described as divergent aspects of the overall response, both the innate and adaptive arms are interlinked and intricately coordinated to best protect the host. Both innate and adaptive cells play a role in immunosurveillance and wound healing, and in many ways rely on each other for immune action after activation. In addition, several cell subsets have been associated with bridging the gap between innate and immune responses during wound healing, including gamma delta T cells, Langerhans cells and plasmacytoid dendritic cells (44). In addition, natural killer (NK) cells are, strictly speaking, classed as innate immune cells, and are involved in targeting and killing virus-infected host cells by recognising danger signals expressed on surface of doomed cells (45). Adaptive immunity constitutes two general arms, humoral and cell-mediated responses, mediated by B and T lymphocytes. These cells are activated on interaction with free/native or processed antigens.

In the context of T cells, activation relies on engagement of the T cell receptor (TCR) with processed antigens (peptides) presented in the Major Histocompatibility Complex (MHC). Antigen presenting cells (APCs) such as dendritic cells (DCs) and macrophages are able to internalise, process and present specific antigens via the MHC class II, specific

for ACPs, to CD4 T cells initiating potent effector pathways and immunological memory (**Figure 1.3**) (46). Conversely, antigens may also be presented by MHC I which is present on most cell types and is an indicator of intracellular infection, and facilitates recognition by CD8 T cells, resulting in cellular killing. Unlike innate immune cells whose receptors are germline encoded and show little variability, receptors in lymphoid cells undergo recombination within organs of the lymphatic system from gene fragments, which lends to an incredible variability in their specificity (46).

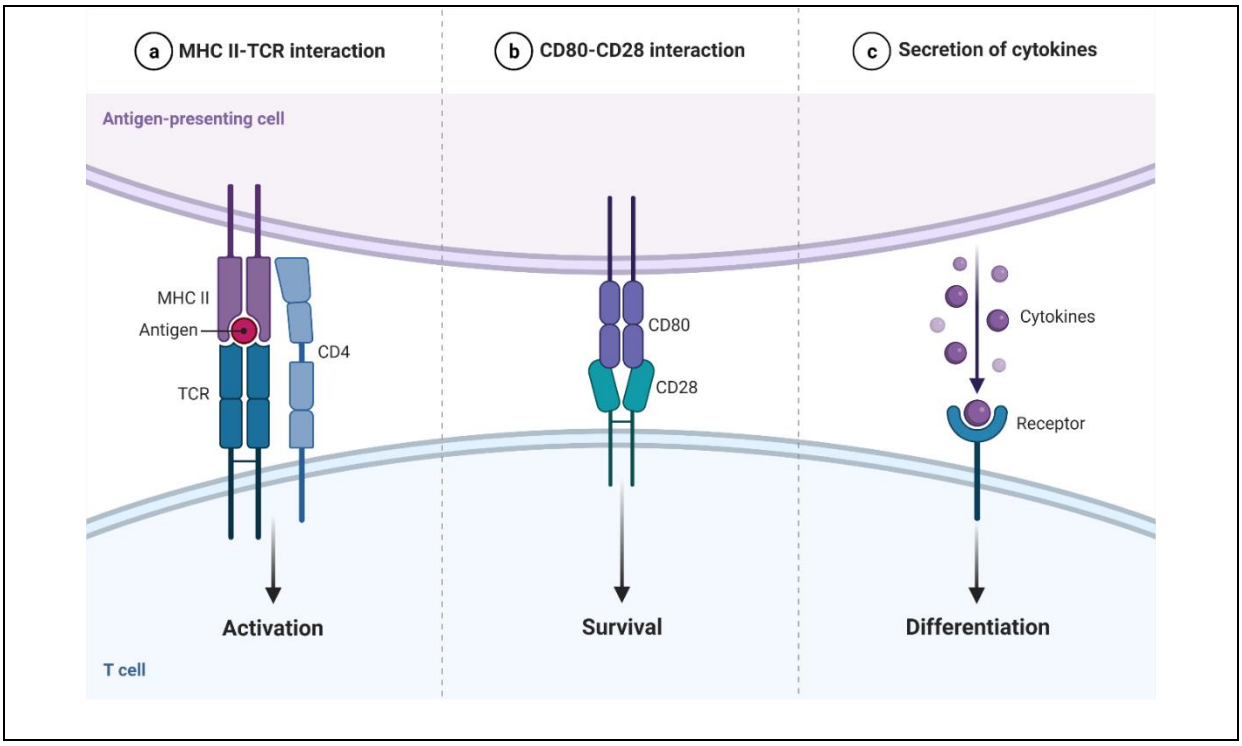

Figure 1. 3: Presentation of antigen by APC via MHC II. Image generated using Biorender.com template and (46).

On activation by CD4 T cells, B cells, initially induced to produce immunoglobulin (Ig)M after antigen recognition through the B cell receptor (BCR), produce more specific antibodies of different classes as part of the humoral response that play various roles, including opsonisation, inactivation of toxins, signalling for cell destruction and activating complement. In addition to IgM antibodies occupy 4different classes: IgG, IgE, IgA and IgD, that all have specific roles. Alongside antibody production, B cells have been

implicated in additional functions, such as antigen presentation and cytokine secretion, particularly immune suppression via IL-10 secretion (47).

1.2 Specific roles of immune cells within wounds and infection

As implicated in the overview above, wound repair and infection clearance relies on the coordinated effects of various cell types that control the balance between pro-inflammation, cell killing and immune dampening. Here, we will discuss the specific roles of important immune cells both resident in tissues and those recruited to the site of wounds and infection.

1.2.1 Macrophages

The role of macrophages in wounds was recognised as early as 1975, where guinea pigs with depleted macrophages had impaired healing (48). Although results were highly interpretational in this study, over the subsequent decades more robust data has been gathered by many other groups. Generally, there are two main macrophage subsets. Firstly, bone marrow-derived monocytes circulate in blood then migrate to tissue before differentiation to macrophages and secondly, tissue resident macrophages with different functions depending on their location (49). For example, Kupffer cells in the liver are highly phagocytic for breakdown and recycling of red blood cells, while alveolar macrophages in the lung release reactive cytotoxic oxidants to clear large quantities of airborne pathogens and allergens (50). In general, reduced macrophage numbers are associated with slower healing (42), but with specific effects depending on the stage. If macrophages are depleted during early stages of inflammation there is impaired closure and granulation tissue formation. In contrast, if depleted during the early proliferative stage, wounds showed haemorrhaging, curbed closure and tissue maturation. If depleted during late tissue maturation phase, no effect was observed (51).

Resting macrophages secrete low levels of mediators, and on exposure to DAMPS, microbe-derived products (MAMPs) or cytokines, they undergo classical activation to

become M1-polarised, producing classical inflammatory cytokines IL-1β, IL-6, IL-12, TNFα and reactive nitrogen/oxygen species as well as leukocyte chemoattractants. These cells also perform extensive phagocytosis (52). M1 macrophages are associated with early wounds, and like neutrophils, if not carefully controlled during healing, excessive secretion of damaging products target lipid, DNA and proteins and activate transcription factors which amplify inflammation further. On the resolution from pro-inflammation, classically activated macrophages transition to alternatively activated, M2-polarised macrophages which secrete IL-1R antagonist, IL-10, TGF-β1 and vascular endothelial growth factor (VEGF), a pro-angiogenic factor produced primarily by macrophages, but also keratinocytes and platelets (53). VEGF is a growth factor which stimulates fibroblast to produce osteopontin and promote scar tissue formation (54). Canonically, alternatively activated macrophages are induced by IL-4 and IL-13. However, M2 cells can be further divided into subsets with different activation pathways: M2a which are activated by IL-4 and IL-13 as mentioned, M2b by immune complexes, IL-1β and endotoxin/lipopolysaccharide (LPS), and M2c by IL-10, TGF-β and glucocorticoids (55). In wounds, M2-like macrophages and are stimulated cumulatively by anti-inflammatory cytokines, glucocorticoids, prostaglandins or lipid/glucose metabolism modulators released my M1s, and on activation promote the healing phenotype by producing lipoxins, prostaglandin E_2 metabolites, resolvins and protectins (56). Interestingly, characteristic markers of late-stage macrophages are CD206 (mannose receptor, MR) and arginase-1, however these are not fully canonical M2 cells, as they also produce TNF-α and IL-6 which are more heavily associated with M1 cells, supporting the suggesting that there are potential multiple hybrid macrophage phenotypes in one wound at any one time (56).

One major role of macrophages is the phagocytosis of apoptotic cells, such as neutrophils that have taken up pathogens, followed by the release M2-like anti-inflammatory mediators including IL-10 and TGF-β1 to dampen further inflammation. In addition, M2-polarised macrophages actively antagonise M1s by inhibiting pro-inflammatory mediators (56). Macrophage heme oxygenase-1 (HO-1) is an antagonist of inflammation due to its multiple roles in heme homeostasis, anti-apoptotic action and inhibition of pro-inflammatory cytokines. HO-1 can exhibit both anti-inflammatory and anti-apoptotic functionality and is also inducible within the cell under specific conditions. Indeed, HO-1 deficiency in mice and humans has been linked with increases in inflammation (57). Apoptotic cells biphasically upregulate HO-1 production in macrophages during co-culture, in both the short- and long-term. In addition, supernatants from apoptotic cells also stimulate naïve macrophages to upregulate HO-1 at both the transcriptional and translational level, as inhibiting p38 (mitogen-activated protein kinase, MAPK, signalling) and Janus kinase (Jak pathway) signalling prevented expression at early and late phase respectively (58). Experimental knockdown of HO-1 with siRNA diminishes Bcl-2, Bcl-XL and Adora A2A produced by macrophages in the presence of apoptotic cell-conditioned medium (58). The initial early stage of HO-1 upregulation is dependent on sphingosine-1-phosphate (S1P) which activates survival pathways and anti-apoptotic proteins Bcl-1 and Bcl-XL in macrophages (59). Conversely, at the late stage, VEGF A is responsible for upregulation of HO-1 via autocrine signalling, its release facilitated by S1P (58).

1.2.2 Dendritic cells

DCs are phagocytic, professional antigen presenting cells that harbour long cellular extensions that allow for broad coverage of their resident tissues and coordinate the adaptive response to a plethora of pathogens. DCs generally have a similar gene

expression profile to macrophages, and a correlation has even been observed between Langerhans cells, resident APCs of the epidermis, and wound healing, where increased numbers led to better outcomes (39). However, DCs are relatively rare in the blood, accounting for only 0.1-1% of total mononuclear cells, although DCs are abundant in resident tissues and may be produced by differentiation of circulating monocytes on recruitment to tissue (60). DCs differ from other phagocytes in their ability to actively migrate from their resident tissues to draining lymph nodes, allowing them to communicate quickly and effectively with other immune cells leading to T cell activation, a process unique to DCs (61). Antigen capture may occur via three pathways, phagocytosis, receptor-mediated endocytosis or pinocytosis (62). There are several classes of dendritic cells in humans and mice, with 2 major groups, the plasmacytoid (pDCs) and conventional (cDCs), all of which derive from haematopoetic stem cells in the bone marrow (63). DCs are further classified based on their location or surface marker expression. Each has a specific function with unique profile of antigen capture and presentation, each of which occurring in different locations. Generally, pDCs play a role in antiviral responses via IFN induction, while cDCs are more classical APCs, facilitating the Th1, 2, 17 and Treg polarisation (64). In addition, cDCs are also able to promote cytotoxic T cell activation via IL-12p70 and MHCI-peptide presentation (64).

DCs generally exist as one of two states, immature and mature. The former are mostly widespread, have high phagocytic capacity and express low surface levels of antigen presentation proteins, including MHCII and costimulatory molecules, and are weak inducers of T cell activation and proliferation (65), but are highly effective in antigen recognition and capture via PRRs (66). Following recognition of antigens and activation the DCs mature, adapting their transcriptional and metabolic profiles to enable migration

to secondary lymphoid organs from peripheral tissues, where they upregulate MHCII and costimulatory molecules for the presentation of antigen to CD4+ T cells and CD8+ T cells, inducing their activation and proliferation (67).

In vitro, human monocyte-derived (mo)DCs are most often utilised proceeding isolation of CD14+ monocytes from blood using positive selection, which are treated with GM-CSF and IL-4 for differentiation, generating a large number of cells that show high similarity to immature DCs (68, 69). This is necessary due to low numbers of both pDCs and cDCs in the periphery as mentioned previously, the isolation of which proving challenging (70). However, the relevance of moDCs is a controversial area, due to the debate as to whether these immature DC-like cells are too far removed from true differentiation or proliferation of monocyte precursors (71). It has also been shown that alterations in the purification protocol for CD14+ monocytes has downstream effects on the moDC progeny, namely in their proliferative capacity, but population do maintain their viability and surface expression of CD11c (60). Indeed, in a study comparing moDCs and primary DCs in immunotherapy found that during metastatic melanoma vaccination, moDCs showed considerably less effectiveness than primary cells, with much reduced survival, indicating that these cells may be insufficient in other *in vitro* studies (72).

For effective priming of T cells for anti-pathogen activity, DCs secrete different cytokine profiles to determine T cell flavour following detection of antigen, this is discussed in more depth in Section **1.3.4**. During infection, pathogens may modulate this cytokine response to facilitate their survival. For example, supernatants from both mucoid and non-mucoid *Pseudomonas aeruginosa* strains have been described to induce IL-10 production by moDCs, more so than other bacterial species, enhancing the Th2-type response, perhaps favouring long-term infection via competition with the Th1, pro-

inflammatory response (73). Indeed, it has been indicated during murine experimentation that Th2 response is due to pulmonary DC-mediated inhibition of the Th1 response, although more generally via negative IL-6 regulation of IL-12 (74).

1.2.3 Neutrophils

Originating in the bone marrow, neutrophils are powerfully phagocytic cells with a short lifespan, which make up the major fraction of blood leukocytes, and are the first responders during infection. Neutrophils are one of the main mediators of pathogen clearance and communicate with dendritic cells and macrophages (75). Neutrophils contain a multi-lobed nucleus and have a granulated cytoplasm, with primary and secondary granules. Primary granules contain hydrolytic enzymes such as elastase, azurocidin and myeloperoxidases, while secondary granules contain cathelicidin, lactoferrin and cathepsin G, all of which contribute to the killing of ingested cells (76). The initial, aggressive hydrolytic attack on pathogens by neutrophils, deemed the respiratory burst, involves extensive secretion of hydrogen peroxide and superoxide anions during increased oxygen consumption. These corrosive products are able to unselectively degrade phagosome contents (77). Alongside the respiratory burst, neutrophil extracellular traps (NETs) play a major role in pathogen clearance. NETs are large DNA-based structures that arise through chromatin de-condensation and cell lysis, congealing various proteins including products of the granules which trap extracellular pathogens and degrade them (78). However, there has been debate in recent years as to whether NET formation always ends in cell death, as neutrophils can maintain membrane integrity and motility *in vitro* after NET expulsion very early after activation, maintaining phagocytic function even after losing their nuclear, histone-rich DNA (79).

In the context of wound healing, neutrophils are instrumental in the initial phases of the pro-inflammatory response, preventing establishment of infection as described above. Generally, neutrophils are not present in healthy skin, but are recruited to sites of injury by damaged cells and alter their gene expressions for a pro-inflammatory state compared to resting circulating cells (80). Unfortunately, due to the extensive arsenal of secreted products, neutrophils also cause collateral tissue damage which greatly affects both the speed of healing but also the quality, for example in relation to scar tissue formation (81). However, this highly inflammatory state is paradoxically a cue for initiation of the anti-inflammatory stage of healing, as neutrophils often undergo apoptosis after fulfilling their role in the wound bed which are then phagocytosed by macrophages, triggering the resolution of pro-inflammation (82, 83).

1.2.4 T cells

T cells are lymphocytes that develop in the bone marrow and mature in the thymus, expressing T cell receptors (TCRs) that are uniquely encoded to engage specific antigens. T cells are activated within lymph nodes and spleen. Antigens are presented to them by DCs and other APCs, and proceed to migrate to their target site for effector function, while a subset linger as memory cells (84). For successful recognition, processed antigens are complexed with the MHC of the presenting cell, which engages directly with the TCR (**Figure 1.3**).

T cells are classically divided into two main groups, CD4+ (T helper) and CD8+ (T killer), and are associated predominantly with adaptive immunity, as part of the delayed immune response to infection. CD4+ cells interact with MHCII where the antigens presented tend to be exogenous, for example from an phagocytosed bacterium, while CD8+ interact with endogenous antigens from within the cell, such as virus-infected, on

MHC I (24). In addition, DCs that phagocytose infected self-cells are able to present antigens from the infected cell on MHC I to activate CD8+ cells, in a process termed cross-presentation (85). Within these groups, T cells may be further subdivided to naïve, effector and regulatory, the latter remaining in circulation for many months or years after their activation (86). In addition to classical T cells, populations of innate-like γδT cells that are involved in initiation and propagation of the immune response and NK cells (discussed in in Section **1.1.2**), whose function is analogous to that of T killer cells, but are much more rapidly effective and do not require the MHC (87).

Generally, activated CD4+ cells are referred to as one of 4 groups: Th1, Th2, Th17 and T regulatory cells. Th1 and Th2 cells have major discernible features that differentiate their function. Th1 cells are stimulated by IL-12, allowing them to produce IFNγ and IL-2, prompting a cell-mediated response by activating mononuclear phagocytes, CD8+ cells and NK cells for killing intracellular pathogens such as bacteria and viruses. Th2 cells are induced by IL-4 and produce IL-4, IL-5, IL-10 and IL-13, promoting antibody-mediated response by B cells. Th2s are also associated with the immune response to parasitic infection (46). Here, Th2-associated interleukins are associated with IgE production and eosinophilic response related to atopy, while IL-10 promotes anti-inflammation and subduing of the Th1 phenotype (88). Th17 cells are induced by IL6, IL-1β and TGF-β and produce IL-17 and IL-21, contributing considerably to the inflammatory response and neutrophil recruitment for elimination of extracellular pathogens (89). Indeed, recent studies have also indicated that Th17 responses may contribute to pathology in diseases like cystic fibrosis due to extensive tissue damage, while during our own study, decrease in lung function is directly correlated with IL-17 production (90, 91). After activation, a small subset of T cells become quiescent as memory T cells. These cells remain in the

body for years after the initial exposure to antigen, in some cases the rest of the lifetime, and allow for a rapid and potent immune response and clearance of pathogen if a second exposure occurs (92). These cells are much of the basis for vaccine development. CD8+ cells function primarily to clear intracellular pathogens by killing infected cells. They do this in direct contact with the infected cells, which enter apoptosis after exposure to perforins and granzymes exocytosed from the T cell similarly to NK cells (93).

1.3 Immune recognition via pattern recognition receptors

To recognise pathogens, innate immune cells utilise receptors able to distinguish unique microbiological structures, often in the context of tissue damage caused by their various virulence factors. Pathogen-associated molecular patterns (PAMPs) tend to be highly conserved amongst microorganisms and are recognised by PRRs (**Figure 1.4**), which initiates activation of the immune system leading to cells signalling, recruitment and pathogen clearance (94). PRRs constitute 4 main groups, including the Toll-like receptors (TLRs), Nod-like receptors (NLRs), RIG-I-like receptors (RLRs) and C-type lectin receptors (CLRs) that are expressed primarily on innate immune cells (94). Innate immune activation through PRR engagement is one of the earliest responses to infection, with several signalling cascades contributing and leading to the expression and secretion of cytokines and chemokines that aid in the inflammatory response and increases cell killing capability via recruited cells primed with specific effector function (95). Often, genes that are expressed in response to infection are regulated by the transcription factor nuclear factor kappa B (NF-κB), which is activated though many of the PRR signalling cascades, although others are also present and will be discussed subsequently.

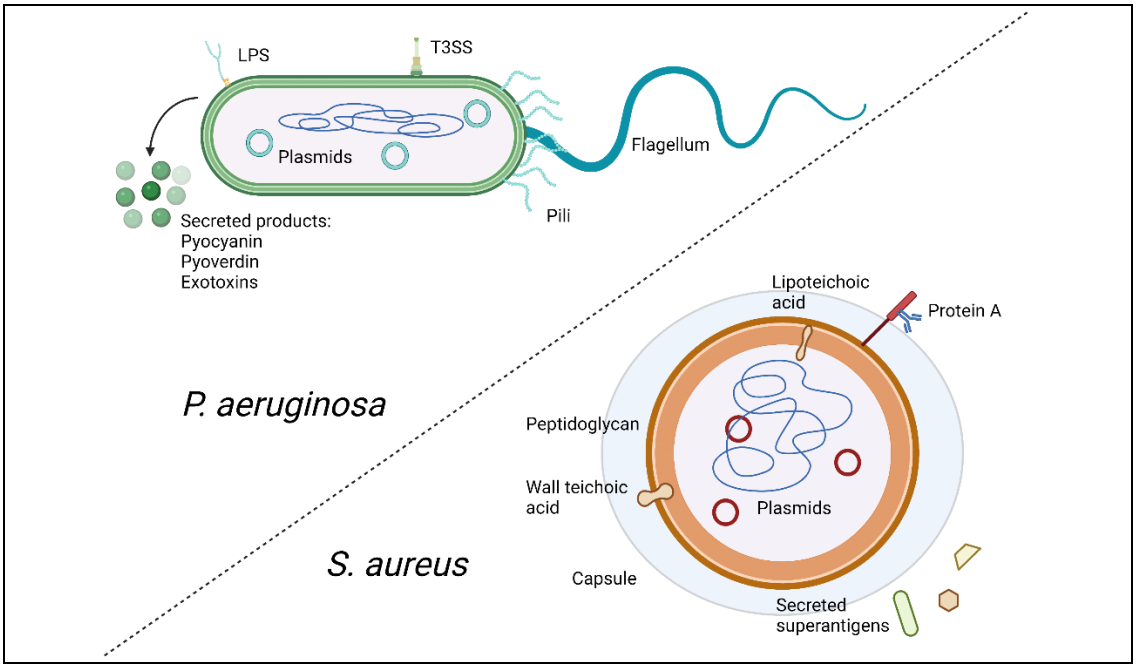

Figure 1. 4: PAMPs recognised by the immune system during bacterial infection*. During this study, P. aeruginosa and S. aureus were used utilised for experiments. During acute infection, each of these species produce various virulence factors that interfere with the host defences to promote inflammation via the pathways explored in this section. Planktonic P. aeruginosa cells have flagella and type IV pili that facilitate adhesion to the host surface. The flagellin that constitutes these structures is recognised by TLR-5 and TLR-11 (Table 1.1). Further this Gram-negative species produces the T3SS, which facilitates cytotoxin ExoS and ExoU injection to the host cell and is recognised by the inflammasome NLRC4. Additionally, LPS is recognised by TLR-4. Pyocyanin and pyoverdine are also highly inflammatory, as well as exotoxins and proteases that can destroy host complement and extracellular matrix. In contrast, S. aureus is a Gram-positive species with much more peptidoglycan in their cell wall, alongside wall teichoic acid and lipoteichoic acid that is recognised by TLR-1/2. Protein A is also produced that can bind. Figure inspired by (96, 97) and produced using BioRender.com.*

1.3.1 Toll-like receptors

TLRs comprise the best characterised group of PRRs. These receptors are embedded in the plasma membrane either on the cell surface or endosomes and consist of a leucine-rich extracellular repeat region, a transmembrane domain and Toll-interleukin-1 receptor domain that resides intracellularly (95). There are 13 described TLRs: TLR-1 to -13. TLR-3 and -7-13 are situated in the endosomes and recognise nucleic acids, including dsRNA, ssRNA and unmethylated Cytosine-phosphor-Guanine (CpG)-DNA (the unmethylated form unique to bacteria), with TLR-10 acting as a negative regulator (**Table 1.1**). Humans lack TLRs 11, 12 and 13. Other TLRs (TLR2/6, TLR2/1, TLR4 and TLR5) are plasma membrane anchored and recognise extracellular PAMPs, with many ligands being bacterial products (**Table 1.1**) (98, 99).

Table 1. 1: Human and mouse TLRs, their locations and specificities.

	Location	**Ligands**	**Human/mouse**
TLR-1/2	Cell membrane	Triacyl lipopeptides, lipoteichoic acid	Human, mouse
TLR-2/6	Cell membrane	Diacyl lipopeptides (100)	Human, mouse
TLR-3	Endosome	Viral double-stranded RNA (dsRNA), small-interfering RNA (siRNA)	Human, mouse
TLR-4	Cell membrane	LPS	Human, mouse
TLR-5	Cell Membrane	Flagellin	Human, mouse
TLR-7	Endosome	Viral single-stranded RNA (ssRNA), streptococcus B RNA (100)	Human, mouse
TLR-8	Endosome	Viral and bacterial RNA (100)	Human, mouse
TLR-9	Endosome	Viral and bacterial DNA (unmethylated CpG-DNA)	Human, mouse
TLR-2/10	Endosome	dsRNA (101)	Human
TLR-11	Endolysosome	Flagellin, *Toxoplasma gondii* profilin	Mouse
TLR-12	Endosome	*T. gondii* profilin (100)	Mouse
TLR-13	Endosome	Bacterial 23S RNA	Mouse

Regarding specific ligands, cells from many bacterial species are highly motile due to their flagella. Flagellin is recognised by TLR-5 and recognises the *P. aeruginosa* single polar flagellum in its planktonic form, which is highly immunogenic (102). In addition, Gram-

negative species such as *P. aeruginosa* produce LPS as a virulence factor, which is recognised by the TLR-4 and MD-2 complex. Finally, lipoproteins produced by *P. aeruginosa* are also recognised by a heterodimer of TLR-2 and TLR-1, which recognises triacyl lipopeptides (103). Alternatively, TLR-2 is also able to form heterodimers with TLR-6 that recognises diacyl lipopeptides that are characteristic of Gram-positive bacteria, such as *Staphylococcus aureus* (104). Indeed, it has been shown that mice depleted of TLR-2 are highly susceptible to *S. aureus* infection (105). Interestingly, although TLR-2 has been implicated in the recognition of *S. aureus* peptidoglycan, this appears to be specific to that species. Rather, in other species, TLR-2 predominantly recognises lipoteichoic acids or lipoproteins from Gram-positive or –negative species respectively (106). Regarding intracellular TLRs, these receptors are able to recognise nucleic acids of bacterial or viral origin, as well as self-DNA the context of autoimmunity (100). Although most heavily associated with viral infection, endosomal TLRs are also important during bacterial infection. For example, bacterial DNA that contains extensive unmethylated CpG-DNA and bacterial RNA of 23S ribosome are recognised by TLR-9 and -13 respectively (107-109). In addition, rather than TLR-5, flagellin that has entered the endolysosome engages with TLR-11 (110). Combined, the recognition of these ligands by their respective receptors triggers a consortium of signalling pathways that heavily influences the immune decisions going forward.

To produce an appropriate immune response, a signalling cascade occurs from the initial receptor interaction, leading to transcription of required pro-inflammatory genes. Almost all TLRs signal via the MyD88 adaptor molecule, activating the Myddosome complex followed by TAK1 via polyubiquitination. Activation of TAK1 leads to the activation of the IKK-NF-κB and –MAPK pathways, leading to phosphorylation and

degradation of NF-κB's inhibitory protein, IκBα, allowing NF-κB to enter the nucleus and initiate pro-inflammatory gene expression. Further, TAK1 activates p38, ERK1/2 and JNK of the MAPK family, mediating AP-1 transcription factor activation and mRNA stabilisation of inflammatory response genes (100, 111). In contrast, TLRs 3 and 4 (once translocated to the endosome) utilise the alternative TRIF/TRAM pathway. Here, TRIF interacts with TRAF 3 and 6, the latter leading to TAK1 and MAPK/NF-κB as in the MyD88 pathway. In contrast, TRAF3 recruits kinases TBK1 and the IKK complex (IKKi with NEMO), phosphorylating IRF3 and IRF7 transcription factors for nuclear translocation and production of type I interferons (95, 100).

1.3.2 Inflammasome

Inflammasomes are a group of innate immune sensors that regulate the caspase cascade and promote inflammation in response to microbes and other irritant molecules via IL-1β and IL-18. The inflammasome complex is made up of multiple PRRs, which act as caspase-1-activating scaffolds in response to stimuli (112). The role of caspase-1 is to cleave the inactive pro-IL-1 and pro-IL-18 cytokines to their bioactive counterparts, IL-1β and IL-18 and activation of gasmerdin D, resulting in release of IL-1β and IL-18 and pyroptosis (113, 114). Unlike apoptosis, cell death by pyroptosis is extremely pro-inflammatory due to the release of cell contents to the surrounding environment post-plasma membrane rupture, including cytokines and cleaved DNA (i.e. DAMPs) (115). Inflammasomes are most closely associated with auto-inflammatory diseases such as neurodegenerative disease (Parkinson's disease, multiple sclerosis) and metabolic disease (type 2 diabetes, atherosclerosis), exacerbating pathology in response to DAMPs in the patient (114).

On detection of DAMPs or PAMPs in the cytosol, inflammasomes assemble in various combinations depending on the stimuli, but ultimately, as mentioned above, act as a scaffolds for pro-caspase-1 recruitment which on oligomerisation self-cleaves to active caspase-1 (116). A cysteine-dependant protease, caspase-1 cleaves pro-IL-1β/-18 to form their active forms (117). Although the exact mechanism for inflammasome assembly is unclear, classification of inflammasomes depend on the protein in the initial stimuli-receptor scaffold, the most studied being nucleotide-binding oligomerisation domain, Leucine-rich Repeat and Pryrin domain containing (NLRP) NLRP3, NLRC4 and AIM2. The former, NLRP3, recognises the broadest range of ligands and is closely associated with TLR-4 activation by LPS, and is assembled in response to NF-κB upregulation, cellular potassium efflux, mitochondrial release of ROS, cardiolipin and DNA and cathepsin release to the cytosol from lysosomes (118, 119). In contrast, NLRC4 inflammasome is activated by a limited number of stimuli, that complex with NLRC4 via the NAIP proteins, implicating NLRC4 as solely a scaffold protein as opposed to a receptor in its own right (120, 121). In humans, the NAIP protein binds bacterial type III secretion system (T3SS) needle protein, found in Gram-negative bacteria such as *P. aeruginosa*, which leads to complexing with NLRC4 and caspase-1 activation (120). During infection, bacteria utilise T3SS to deliver a range of exotoxins to circumvent host immunity, serving various functions for limitation of host cytosol catalytic activity, even facilitating intracellular survival in epithelial cells in the case of exoS (122, 123). Finally, unlike the NLR-inflammasomes, AIM2 inflammasome directly binds its stimulus, pathogen-origin cytosolic dsDNA, and on binding activates the PYD domain of AIM2, recruiting apoptosis-associated speck-like protein containing C-terminal caspase recruitment domain (ASC) and facilitating caspase-1 activation (124).

1.3.3 C-type lectin receptors

Amongst PRRs, CLRs are an important subset that, when engaged, can induce gene expression in isolation or by modulating other receptor signalling pathways, such as TLRs. These receptors are able to recognise ligands via one or more recognition domains, including the characteristic folded structure of the C-type lectin-like domain (CTLD), and are either membrane-bound (in the case of those discussed below) or soluble as with MBL (125). Generally, most CLRs recognise structures that contain the sugars mannose, fucose and/or glucan, that are present on both self-moieties and various pathogens including bacteria, fungi and viruses. On recognition, ligands are internalised by the phagocytic cell and allow for degradation and antigen presentation to other immune cells for immune decision making (126). Recognition is often calcium-dependant, including the mannose receptor (MR, CD206) and dendritic-cell-associated C-type lectin (Dectin)-2 (CLEC6A) and dendritic cell-specific intercellular adhesion molecule-3 (DC-SIGN, CD209), while other such as the Dectin-1 (CLEC7A) do not require calcium. There are several major CLRs expressed by immune cells, each with distinct signalling pathways to induce effector molecules.

1.3.3.1 Mannose receptor

The mannose receptor family comprises group I CLRs, including several endocytic receptors that recognise a broad range of ligands (127). The most studied receptor of this family is MR, which was the first of its type to be identified. MR contains 3 extracellular domains and is the sole member of the family to contain a functional cysteine-rich (CR) domain. Alongside the CR domain, MR also constitutes a fibronectin type-II (FNII) domain and eight CTLDs. The CR domain recognises sulphated glycans, while the FNII and CTLDs recognise collagen and mannosylated/fucosylated/*N*-acetyl glucosamine ligands

respectively. Mannose/fucose recognition through CTLDs only occurs in the presence of calcium (128). Among CTLDs CTLDs 1-3 weakly bind carbohydrate while CTLDs 4-8 show much higher affinity, with multivalent binding allowing a cumulative higher avidity (129). When the MR is engaged, clathrin-mediated endocytosis occurs leading to ligand internalisation, requiring a tyrosine residue on MR's cytoplasmic tail (130). Within endosomes the receptor is released due to endosome acidification (131). Binding of MR to the FcRy-chain adaptor molecule is required for localisation at the macrophage cell surface, similarly to other CLRs macrophage-inducible C-type lectin (Mincle), Dectin-2 and macrophage C-type lectin (MCL, (132-134)). The downstream signalling pathways of MR are relatively unclear, but it has been suggested that microRNA transcribed alongside the MR MRC1 gene is able to actively downregulate target genes at the RNA level and inhibit tumour growth (135).

MR is expressed by macrophages, DCs and selected endothelial cells. Expression levels are highly variable, particularly amongst macrophages and DCs, and is affected by their differentiation states (127). The expression of MR in macrophages is upregulated by various cytokines including IL-4, IL-10 and IL-13, while IFNγ and LPS have been shown to inhibit production (136). It has also been shown that MR acts as a marker for activated macrophages, particularly indicating the immunosuppressive phenotype (137). However, some contradicting evidence has suggested during our own work, where MR shows upregulation in the pro-inflammatory, M1-type macrophage population, as well as downregulation of MR expression by LPS compared to IFNγ (unpublished). The uptake of antigens by MR is also associated with antigen presentation by dendritic cells to T cells, with increasing numbers of MR+ dendritic cells being identified within lymph nodes during innate stimulation *in vivo* (138). MR has also been indicated as a homeostatic

regulator of endogenous ligands (127, 131). The role of MR in infectious disease is fairly uncertain, although recognition of various pathogens has been described, including *C. albicans*, *Leishmania*, HIV, *Klebsiella* and *Streptococcus spp.* (127, 131). Although able to recognise many ligands on these pathogens, MR is not essential for the phagocytosis of pathogens, with *C. albicans* and *Leishmania* internalisation able to occur in both the wild-type and MR- cells (139, 140). However, recent studies have identified that both MR and TLR-2 are directly involved in phagosome maturation after internalisation of *Leishmania* (141), hence indicating that the biological response via MR requires cooperation with other receptors. In further agreement, an MR-TLR-4 cooperation is required for the proliferation and differentiation of T cells during *Paracoccidioides brasiliensis* infection of DCs (142).

1.3.3.2 *Dectin-1 and Dectin-2*

Dectin-1 is expressed on macrophages, neutrophils and DCs and is made up of a immunoreceptor tyrosine-based activation motif (ITAM)-like containing cytoplasmic tail, stalk region and a single extracellular CTLD (143). This receptor primarily binds β1,3-linked glucan, a substance present in the cell wall of many important fungal species (144). However, Dectin-1 is also known to bind to *Mycobacterium tuberculosis*, which does not express β-glucans, suggesting this receptor has a broader ligand repertoire than first suspected (145). Dectin-1 is involved in phagocytosis as well as in production of reactive oxygen species in neutrophils. The signalling pathways of this receptor are well characterised, with a cascade via spleen tyrosine kinase (Syk)-caspase recruitment domain family member 9 (CARD9) resulting in upregulation of an array of products, such as TNFα, IL-2, IL-10, ROS and IL-12 (146). During infection, presence of Dectin-1 is important for phagocytosis of pathogens, with depletion *in vivo* resulting in impaired

recovery from fungal infection as well as a reduction in IL-17 production (147, 148), and increased susceptibility to mucosal *C. albicans* infection (149). Further, Dectin-1 has been implicated in co-ordination with TLR-2, where coordination acts as an agonist for glucan internalisation, transcription factor activation, pro-inflammation and ROS production (150).

Similarly, Dectin-2 is a receptor that recognises mainly fungal and bacterial antigens, specifically α1-2 or α1-4 linked mannose structures, and is expressed on macrophages monocytes, neutrophils and some subsets of DCs (151-155). This receptor generally shows low surface levels but is upregulated during pro-inflammation. The mechanism, however, is unclear (156).

Dectin-2 has no intracellular signalling motif, but rather on engagement of ligand interacts with Fc receptor-γ common chain, phosphorylating Syk for activation of the CBM protein cluster (containing CARD9, B-Cell lymphoma 10 and mucosa-associated lymphoid tissue lymphoma translocation protein 1), culminating in activation of NF-κB that induces upregulation of two cytokines of apparent opposite function, TNF-α and IL-1 receptor antagonist (IL-1ra) (157). In addition, Syk activation facilitates production of ROS, instrumental in pathogen killing and inflammasome activation for production of mature IL-1β (158). Dectin-2 is most heavily associated with anti-fungal immunity, where deficiency is associated with decreased murine survival on infection with *C. albicans,* perhaps due to reduced IL17 production in deficient mice, instrumental in clearance of acute fungal infection (159).

1.3.3.3 DC-SIGN

DC-SIGN, is a type II, membrane-bound receptor expressed on both mature and immature DCs and macrophages, and is associated with antigen internalisation and presentation as

well as adhesion to T cells, neutrophils and the mucosal endothelium for cellular communication (160). The receptor is a homo-tetramer bound at the neck repeat region, with a transmembrane domain and cytoplasmic tail that contains internalisation and recycling motifs. The extracellular carbohydrate recognition domain (CRD) is able to recognise high mannose and fucose structures present on various pathogens in a calcium-dependent manner (161). Due to its tetrameric structure DC-SIGN is able to form multivalent interactions with its ligands, granting enhanced avidity (161). DC-SIGN broad glycan specificity creates an interesting conundrum for its biological significance in both pathogen- and self-recognition, as fucose and mannose ligands are common moieties in various mammalian glycans, including Lewis blood antigens, endothelial receptors and various metabolic proteins.

On interaction with its mannose or fucose ligands, DC-SIGN modulates the TLR-4 response through the NF-κB pathway. On binding, DC-SIGN activates the Ras GTPase within the cytoplasm, which in turn activates RAF1 by phosphorylating it at Tyr340, Tyr 341 and Ser 388. In this activated state, RAF1 phosphorylates NF-κB subunit p65, activating the transcription factor. In its activated state, NF-κB binds CREB-binding protein which acetylates various lysine residues of p65, increasing its transcriptional capability and hence, allowing it to enter the nucleus and more effectively enhance target gene expression. The presence of acetylated lysines on p65 also increases NF-κB stability, resulting in longer persistence in the nucleus, culminating in an increase of NF-κB-induced transcription of target genes, including the cytokine IL-10 (145). Increased production of IL-10 suggests the induction of an anti-inflammatory phenotype.

Initially, DC-SIGN was identified to bind to the HIV-1 glycoprotein gp120, residing in the viral envelope, hence theorised to facilitate viral entry to host cells (162). However, later

work identified receptor engagement as a transport mechanism for viral particles to CD4+ T-cells, promoting infection (162). Alongside HIV, DC-SIGN is able to bind to other organisms, including Gram-negative bacterium *Helicobacter pylori* and the helminth *Schistosoma mansoni*, both of which express glycoproteins that resemble the Lewis^X antigen (163). Of the species able to interact with DC-SIGN, one overarching factor is their propensity for chronic infection. This, alongside general upregulation of IL-10 on ligand engagement, suggests an involvement in immune modulation by the pathogens to favour immune suppression and anti-inflammation. As a specific example of this, the pathogen *Mycobacterium tuberculosis* has been shown to diminish IL-12 production while enhancing IL-10 in DCs, relying on DC-SIGN engagement, promoting a Th2-type type response and bacterial persistence (164).

Alongside direct response to pathogens via cytokine production, DC-SIGN facilitates antigen uptake and presentation on MHC class I or II by APCs, promoting antigen specific CD4 or CD8 T cell responses (165). Also, DC-SIGN is able to bind to intercellular adhesion molecules (ICAM)-2 on the endothelium and ICAM-3 on resting T-cells. During the former, interaction of the receptor with its ligand promotes tethering and rolling of the immature DC along the endothelium, ultimately allowing transendothelial migration from the vascular lumen into tissues where they are able to elicit the required immune response (166). Binding of DC-SIGN to ICAM-3 on resting T-cells is one of the principal interactions for triggering the adaptive immune response. This interaction is of high affinity and is essential for initiation, as blocking of DC-SIGN results in an inhibition of T cell proliferation (66). Finally, DC-SIGN is able to interact with fucose residues on Lewis blood group antigens at varying affinities (163). Indeed, in a recent study, changes in fucosylation patters in blood group antigens of oral cancer cells have been implicated in

enhanced DC-SIGN recognition and metastasis of cancer cells (167). It is clear from this range of ligands, that DC-SIGN is an incredibly versatile receptor that may be involved in many processes involving DCs and selected macrophages.

1.4 Hospital acquired infections, antibiotic resistance and the ESKAPE organisms

Throughout medical history, it has been recognised that clinicians could contract disease when handling patients, through wounds caused by medical equipment or performing autopsies, and that transmission was reduced when physicians washed between patients (168). However, there was little compliance with suggested measures amongst clinicians until the publication of Koch's postulates in the 1890s, where opinion quickly changed and measures were taken to protect both patients and medical professionals by improving infection control (169). Hospital acquired (healthcare-associated) infections (HAIs) are nosocomially acquired infections that are not present, or are incubating, on initial admission to hospital, manifesting around 48 h post-admission. Due to their heavy burden on the healthcare system, HAIs are closely monitored by the Centre for Disease Control Prevention (CDC) and National Healthcare Safety Network (NHSN), with the aim of preventing HAI and protecting patients. Within recent years, most individual hospitals have implemented surveillance and prevention systems to control HAIs in patients (170). Precautions are organised based on various indications that depend on the microorganism, namely standard precautions for all patients, contact precautions, droplet precautions and airborne precautions, for patients suspected to transmit via physical contact, sneeze/coughs and breathing respectively (170). The impact of HAIs exceeds the individual patient level, as these multidrug-resistant pathogens often circulate in communities.

Infections may occur from environmental opportunistic pathogens, as with *Pseudomonas aeruginosa*, or human commensals, as with *Staphylococcus aureus*, and include central line-associated bloodstream infections (CLABSIs), catheter-associated urinary tract

infections (UTIs), surgical site infections, hospital-acquired pneumonia, ventilator-associated pneumonia (VAP) and *Clostridium difficile* infection (171). In the USA, HAI is considered a leading cause of death and the most common complication in the hospital environment (172). Across other high-income countries, around 5-15% of hospitalised patients contract HAI, increasing to up to 30% in patients admitted to intensive care, where chronic illness alongside immune deficiency increases susceptibility to infection (173). HAI is of great importance to society in various ways, causing high levels of mortality and morbidity that culminate in longer hospital stays and resulting in a huge economic burden, with HAI in the USA predicted to cost between $28 and $45 billion every year as of 2018 (168). In the UK, the National Health Service (NHS) has adopted national evidence-based guidelines, termed epic3, as a preventative strategy against HAI from 1998, which is regularly reviewed and available through government sources (174).

In the annual report by the CDC in 2020, it was stated that the emergence of COVID-19 had a major impact on hospitals and their available levels of care in 2021, and that as a result, progress made in the control of HAI was significantly hindered. It was predicted that the standardized infection ratio (SIR) of various HAIs was increased, importantly 35% for VAE, 20% for CLABSIs and 15% for methicillin-resistant *S. aureus* (MRSA, (175)). Although reassuringly, these increases appear to be a direct result of the pandemic, as in recent years, much improvement has been made in the prevention of these infections (175, 176).

Countless bacterial species can cause infection in humans, with many developing mechanisms of resistance over time, circumventing the immune system as well as antibiotics. The ESKAPE species (*Enterococcus faecium, Staphylococcus aureus, Klebsiella pneumoniae, Acinetobacter baumannii, Pseudomonas aeruginosa*, and *Enterobacter spp*.)

are a group of pathogens of paramount concern to global health, particularly in nosocomial infection, where antibiotic resistant strains readily develop (177). Indeed, since the implementation of the first antibiotics in the 1940s, penicillin resistance became a considerable clinical issue by the end of the decade, with the first report of MRSA as early as 1962 in the UK (178). Further, since the introduction of antibiotics to treat serious infections in humans, their use has expanded beyond the medical setting and into various other practices, including agriculture and the home, where increasing globalisation and selective pressure have allowed for these resistant strains to become widespread (179-181). In recent years, there has been a decline in discovery of new antibiotics, forcing new incentives for the development of antibiotic alternatives, including bacteriophage therapy, nanoparticle delivery systems and live bio-therapeutics (182).

1.4.1 *Pseudomonas aeruginosa*

P. aeruginosa is a ubiquitous bacterial species able to survive in numerous environments, including soil and abiotic surfaces. *P. aeruginosa* can also opportunistically colonise human tissues including the lung epithelium and skin. In particular, *P. aeruginosa* is associated with cystic fibrosis and chronic wounds and burns which will be discussed in later sections. *Pseudomonas spp*. are Gram-negative, motile rods with a large genome, encoding many metabolic pathways that facilitate its adaptability in a broad range of niches (183). Generally, healthy individuals harbour low risk of *P. aeruginosa* infection, as host barriers are effective in its recognition and clearance. Conversely, at high-risk are those immunocompromised in the population, often in the context of healthcare facilities including hospitals and nursing homes. Importantly, in the intensive care unit (ITU), up to 43% of patients may be colonised with *P. aeruginosa*, most of which acquiring the

infection from that location as a HAI (184). *P. aeruginosa* is classically associated with chronic infection, facilitated by its plethora of virulence factors and immune suppression capabilities (185).

LPS is present in all Gram-negative organisms as a major cell membrane constituent, and is important in both virulence and the host immune response (186). LPS is composed of 3 major regions, lipid A, core oligosaccharide and the O-antigen, and is a major structural component of the outer cell membrane that regulates membrane permeability to both hydrophobic and hydrophilic compounds (186, 187). Lipid A released from cell lysis is responsible for the majority of *P. aeruginosa* infection symptoms; mostly by initiating septic shock due to excessive over-stimulation of the innate immune system (188). The extent of inflammation due to LPS is related to the level of acetylation of lipid A, as tri- or tetra-acetylated lipid A causes much lower inflammation than penta- or hexa-acetylated forms due to a diminished ability to activate TLR-4 (189). The O-antigen is a polysaccharide of varying length which is synthesised separately to the Lipid A and core oligosaccharide fragments and attached later. It is due to this that there is high LPS heterogeneity on the outer membrane surface of 'capped' (O-antigen-containing) and uncapped LPS, generally referred to as smooth and rough in the literature (186). O-antigen structure is highly variable between and within species, with *P. aeruginosa* able to produce two: common polysaccharide antigen (CPA) and O-specific antigen (OSA, (190)). The former has a conserved structure of repeating [→3)d-Rha(α1→3)d-Rha(α1→2)d-Rha(α1→], and is required for engagement of certain immune receptors by *P. aeruginosa*, including DC-SIGN (191). As discussed in Sections **1.4.1** and **1.4.2**, LPS is important for bacteria recognition by multiple platforms, including TLR-4 and the NLRP3 inflammasome, associated with pro-inflammation. LPS also shows variation depending

on the type of infection which contributes to its immune recognition. For example, during cystic fibrosis, *P. aeruginosa* adapts to increase acylation of LPS lipid A over time, causing excessive pro-inflammation via enhanced recognition by TLR-4 and NF-κB-mediated responses (192).

Alongside LPS, *P. aeruginosa* produces various proteases with various roles in virulence and are particularly troublesome during wound healing. Importantly, pseudolysin and protease IV are able to module wound healing both *in vitro* and *in vivo*, by inhibiting fibroblasts, keratinocytes and endothelial cell migration and impeding collagen deposition, as well as promoting elevated IL-6 in the surrounding tissue (193). The elastase LasB degrades many host proteins, including immunoglobulins, complement factors, cytokines and NETs, and has been associated with flagellin degradation, inhibiting immune recognition (194-196). Another protease, *P. aeruginosa* small protease (PASP) is a secreted serine protease that is instrumental in corneal degradation in bacteria keratitis (197). Finally, exotoxins ExoS, ExoT, ExoU and ExoY are directly injected into host cells via the T3SS, all of which contributing to the promotion of apoptosis-like death of host cells (198).

This opportunistic pathogen poses many risks relating to antibiotic resistance. *P. aeruginosa* is able to mutate rapidly during infection and gain resistance during treatment, leaving many antibiotic classes unusable, including β-lactams, aminoglycosides and fluoroquinolones (199). Multidrug resistant strains are also prevalent worldwide and are associated with longer hospital stays and economic burden (200). β-lactam resistance develops via AmpC cephalosporinase mutation. In addition, enzymes that directly modify aminoglycosides reduce their binding affinity for the 30S ribosomal subunit, blocking their activity (201). Resistance to a broad range of antibiotic

classes is facilitated by upregulation of efflux pumps of the resistance-modulation-division family that occur through a selection of mutations in regulatory genes due to antibiotic pressure. These large efflux systems cross both plasma membranes and the periplasmic space, allowing for direct expulsion of toxic compounds (202). General treatment regimens for *P. aeruginosa* infection include at least two antibiotic classes in tandem, reducing the likelihood of resistance by necessitating dual mutations. New drugs implemented against *P. aeruginosa* include combinations of carbapenems, β-lactamase inhibitors and cephalosporins (200).

1.4.2 *Staphylococcus aureus*

S. aureus is a Gram-positive bacterium that commensally occupies the nasal squamous epithelium of up to 30% of the population, from which it is able to spread to the skin and other regions (203). Commensal carriers within the population are an important reservoir within the hospital environment. Patients at highest risk are the very young and the elderly, with lowest rates of infection in young adults. Other at-risk patients include the immunocompromised, intensive care patients and those undergoing haemodialysis (204). Most frequently, *S. aureus* is associated with skin infections that stem from commensal colonisation, but may also be community acquired, ranging in severity from superficial epidermal infections like impetigo to deeper, life-threatening infections such as like necrotising fasciitis (205). Another frequent class of condition caused by *S. aureus* are respiratory tract infections. These are usually nosocomial and tend to be chronic, and are associated with important clinical conditions such as cystic fibrosis (205).

S. aureus is a versatile, opportunistic pathogen that, like *P. aeruginosa*, encodes many virulence factors within its genome, allowing for its broad range of disease phenotypes. Many virulence factors are encoded on mobile genetic elements, which can be transferred

between strains by horizontal transfer. Key virulence factors include numerous toxins and superantigens. (206). For example, systemic toxic shock syndrome (TSS) occurs when a patient is infected with a strain expressing toxic shock syndrome toxin 1, a superantigen that causes various acute symptoms including fever, rash, hypotension and involves one or more organ systems (207). Enterotoxins SE-A to -E, are also superantigens and are associated with TSS. Superantigens function via the unspecific activation of T cells in the absence of antigen processing, leading to excessive production of pro-inflammatory cytokines (206). Another class of toxins have specific cellular targets, including the hemolysins. Of these, alpha-toxin is responsible for the lysis of host erythrocytes. Alpha-toxin binds ADAM1, forming a betabarrel pore within the plasma membrane allowing for loss of cellular contents and ultimately, osmotic lysis (206). *S. aureus* also produces a range of proteins that inhibit neutrophil proteases, including neutrophil elastase, proteinase 3 and cathepsin G, compromising immune responses to infection (208).

Gram-positive bacteria including *S. aureus* differ from Gram-negatives in their considerable peptidoglycan layer that makes up the majority of the cell wall, playing a vital role in cellular integrity and host-pathogen interaction (209). Peptidoglycan is made up of alternating *N*-acetylmuramic acid and *N*-acetylglucosamine residues connected by short stem peptides of L-alanine, D-*iso*glutamine, L-lysine and D-alanine, and is recognised by various PRRs, resulting in pro-inflammatory cytokine secretion and leukocyte recruitment (209, 210). Situated amongst the cell wall, wall teichoic acids (WTAs) bind peptidoglycan and are recognised by various innate immune receptors, including langerin and macrophage galactose-type lectin (MGL), which when engaged modulate immune cell cytokine secretion (211).

As mentioned earlier in this section, MRSA was reported as early as 1962, with cases increasing rapidly during the 1980s (212). Resistance to methicillin is due to expression of the penicillin-binding protein PBP2a encoded by mecA gene, which has low affinity for β-lactams. The mecA gene was acquired as part of the staphylococcal cassette chromosome mec (SCCmec), a large mobile genetic element that is transferred horizontally among *Staphylococcus* strains (213, 214). Since emergence, multiple strains of MRSA have been reported in numerous countries, and rather than being confined to the hospital setting, these new MRSA isolates are community acquired and are often able to infect healthy hosts (213). Currently, the standard treatment for MRSA is vancomycin. However, strains with reduced susceptibility to vancomycin have recently been identified; bearing mutations in genes that promote cell wall thickening, reducing access of the drug to peptidoglycan precursors (215).

1.5 Biofilms as bacterial virulence factors

An important virulence factor that promotes bacteria survival and persistence, is the ability to switch from planktonic to the biofilm mode of growth, exhibiting divergent surface structures to their planktonic counterparts (**Figure 1.5**). Generally, biofilms are bacterial and/or fungal communities of one or more species exhibiting group behaviour, showing reduced sensitivity to antibiotic and immune clearance (216). Surfaces able to harbour biofilm communities range from biological tissues to abiotic substances such as industrial piping and medical devices. Biofilms are also able to grow in the absence of a surface, relying solely on cell-cell interactions.

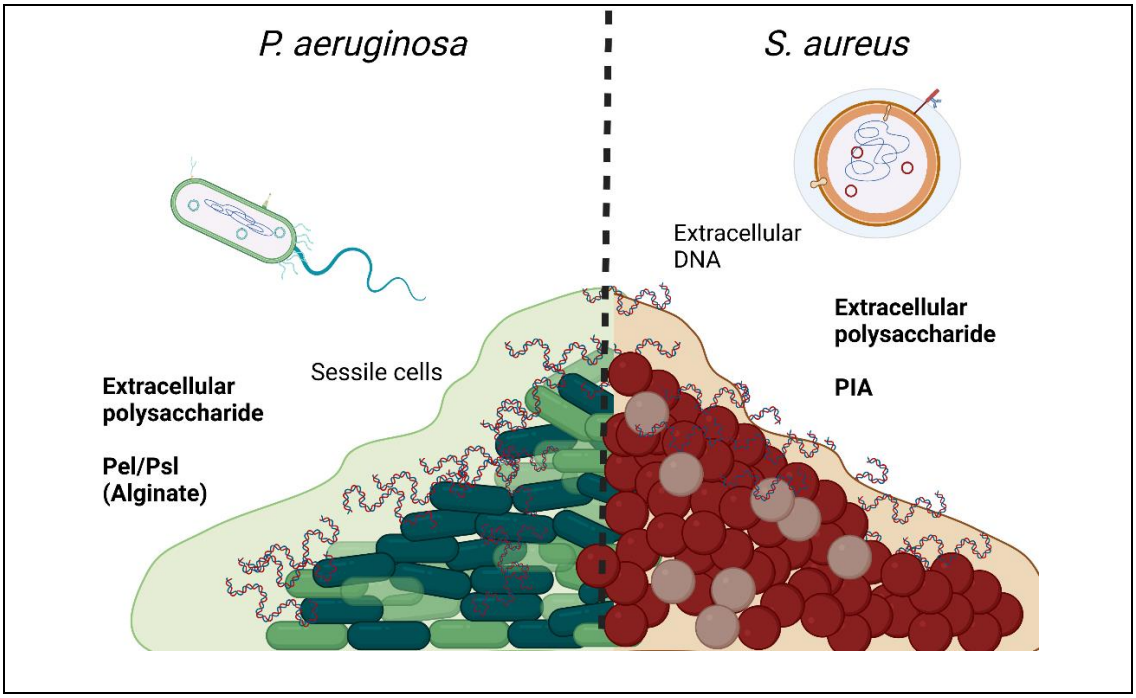

Figure 1. 5: Evolution of bacterial PAMPs during transition from planktonic to the biofilm mode of growth. *In biofilms, bacteria adopt new surface structures that contribute to their immune recognition and virulence which will be explored during this section. From (Figure in section 1.3), P. aeruginosa sheds its flagellum and pili as well as its T3SS to form immobile forms. Both P. aeruginosa and S. aureus biofilms maintain a portion of the population as sessile cells, losing metabolic activity that confers increased resistance to environmental stresses, including antibiotic treatment and nutrient starvation. Further, extracellular DNA is produced which provides structural stability, and is associated with immune receptors such as RAGE and TLR-9. Another major structural component and route for immune recognition is extracellular polysaccharides. In P. aeruginosa, Pel, Psl and alginate are associated with biofilms, and are predicted to bind innate immune receptors. Importantly for this study, Psl contains a high proportion of mannose, and can interact with immunomodulatory receptors DC-SIGN, MR and Dectin-2. In contrast, S. aureus produces PIA in high-carbohydrate biofilms, as is relevant to this project, containing a high proportion of GlcNAc, and is associated with inflammation, although specific interactions are unclear. Figure inspired by (96, 217) and produced using BioRender.com.*

1.5.1 The biofilm cycle

Biofilms form from individual planktonic cells in five distinct phases *in vitro* (**Figure 1.4**), although there are disparities when considering biofilms *in vivo*, these will be discussed later. Initially, individual cells approach and reversibly attach to a surface, followed by permanent adhesion and initiation of replication. Fixed bacteria multiply during stage three and expand to immature biofilm micro-colonies that begin to show some phenotypes that are characteristic of biofilms. Namely, the general biofilm structure contains both latent and metabolically active bacterial cells, various proteins and carbohydrates and extracellular DNA (eDNA) that make up the 3D structure. Later in the maturation phase, biofilm becomes established, with complex networks that trap nutrients and allow for water distribution and waste removal. Finally, dispersal of bacteria via sheer stress in the environment or due to nutrient changes and active shedding, releases cells that have reverted to the planktonic state and allows for colonisation of new surfaces during propagation, completing the cycle (218).

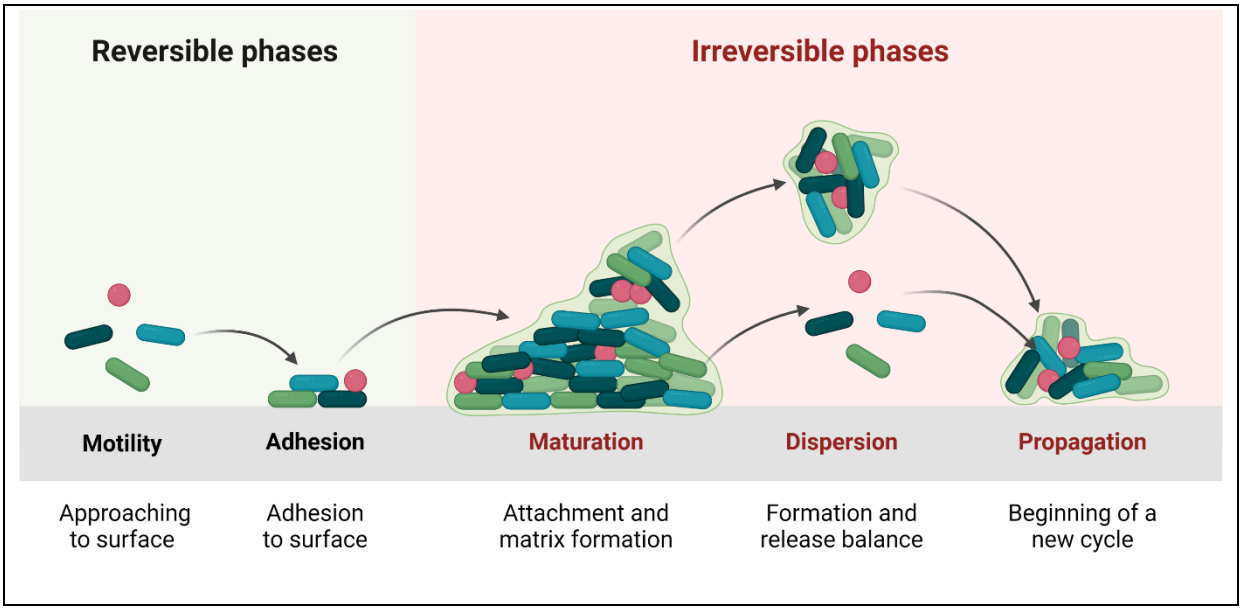

Figure 1. 6: The classical biofilm cycle as observed in vitro. *Planktonic bacteria approach a surface and irreversibly attach. Few individual cells permanently adhere and begin replication to form small aggregates. The irreversible phase begins with biofilm maturation, where small aggregates increase in size and develop their matrix, containing eDNA,*

proteins and carbohydrates. In mature biofilms, small aggregates or individual, planktonic bacteria are dispersed for propagation at new sites to re-initiate the cycle. Figure was generated using Biorender.com and using (216, 218).

1.5.2 Extracellular DNA

Within biofilms, cells are embedded within large 3-dimentional structures composed of extracellular polymeric substances (EPS), with pore spaces for nutrients that create a protective environment for the inhabitant cells while adhering them to a surface (219). The EPS is an amalgamation of many components, with much of the biomass attributable to polysaccharides and extracellular DNA (eDNA), but also includes lipids, proteins, carbohydrates and other biomaterials that together determine the overall characteristics of the biofilm, including its water content, porosity and charge. This incredible plasticity allows adaptation to countless environmental stresses (220). The production of eDNA is abundant across many bacterial species, including the ESKAPE organisms, solidifying its importance in these structures (221). Indeed, eDNA has various functions within the biofilm. Firstly, it constitutes a major structural component, and exposure to DNase abrogates biofilm development, particularly in *S. aureus* and *S. epidermidis* strains (222). With *P. aeruginosa,* eDNA appears most important in early biofilm development, as DNase treatment of mature biofilm (post-84 h) does not significantly affect biofilm structure in an *in vitro* flow-cell model (223). In contrast, acidification due to presence of eDNA has been shown to confer resistance to aminoglycosides in *P. aeruginosa*, with even planktonic cells showing increased resistance in the presence of eDNA in its growth medium (224). Generally, eDNA facilitates immune recognition via TLR-9, leading to inflammation, but TLR-9-independent activation of neutrophils in response to eDNA has been described (225).

1.5.3 Lipids

Lipids are utilised primarily by fungal biofilms to facilitate their own pathogenicity and protection within the biofilm, as well as determining morphological parameters which allow for attachment to different surfaces (226). This is also relevant in other species, including *E. coli*. In the biofilms, sphingolipids and ergosterol form lipid rafts that maintain membrane integrity during hyphal development as well as modulating protein distribution (227). This proves an interesting route for preventative measures, as inhibition of sphingolipid or ergosterol synthesis pathways completely abrogate biofilm formation in *C. albicans* (228). *C. albicans* is frequently observed clinically in poly-microbial communities, with secreted prostaglandin lipid secretions directly promoting growth of *S. aureus* within proximity, providing a scaffold for stability (229, 230).

1.5.4 Quorum sensing

For many species, establishing biofilms requires cellular communication within the population to globally regulate various pathways, in a process known as quorum sensing (QS). With increasing population density, small molecule autoinducers in the environment accumulate and are detected by cells in the vicinity. At a certain threshold, transcriptional regulators are activated that enable various pathways, including those involved in biofilm formation (231). Generally, in Gram-negative bacteria, autoinducers are of the acyl-homoserine lactone class of molecules. These molecules are soluble and bind specific receptors within the inner cell membrane or cytoplasm (232). Gram-positive species differ in that auoinducers are small oligopeptides that are synthesised on the ribosome and modified within the cell. These molecules are actively transported from the cell and in contact with another cell, bind membrane sensor kinases that activate

response regulators that trigger or repress target QS genes. Interactions are often cross-species, highlighting the high complexity in biofilm social behaviours (233).

1.5.5 Antimicrobial resistance

Biofilms are tolerant to many antimicrobials and modulate the host inflammatory response facilitating microbial survival under high environmental stress. Mechanisms of tolerance to anti-microbials within the biofilm environment differ from those in planktonic bacteria. Planktonic bacteria susceptible to antibiotics lose some sensitivity when in the biofilm environment, even when antibiotic can freely diffuse within the matrix, and sensitivity is restored once dispersed, suggesting a more adaptive means of resistance (234, 235). There are four main hypotheses for this, including: 1) incomplete diffusion of antibiotic into the biofilm, 2) varying metabolic gradient within the biofilm leaving subsets of cells metabolically inactive and therefore non-susceptible, 3) an adaptive stress response in some cell subsets and 4) development of "persister cells" in the presence of antibiotic (234). Due to the adaptive aspect of this resistance, biofilm disaggregation to generate antibiotic-susceptible planktonic cells is an option for clinical application. In a recent murine model, rapid disaggregation of a wound biofilm caused sepsis in the host in the absence of antibiotics, but when dispersed during antibiotic treatment, the host was protected and wound size reduced over seven days (236).

1.5.5 The immune response to biofilms

The immune response to infection is complex, with the biofilm mode of growth eliciting immune responses that differ from those against planktonic cells. Recognition of biofilm encourages production of various inflammatory cytokines to control infection that have limited success and contribute to extensive collateral tissue damage within the host (237). Biofilms produced across species are extremely divergent, with each harbouring

different components that affect the overall structure and hence, specific immune interactions. These specific interactions will be discussed in the following sections.

1.5.6 *P. aeruginosa* biofilms

P. aeruginosa biofilms harbour various protein and carbohydrate components that provide structural characteristics as well as dictate host-pathogen interactions within their niche. Biofilm development depends on the small molecule messenger cyclic-di-GMP (cdiGMP), which is regulated by antagonising proteins encoded by *wspR* and *wspF*, with disruption of the latter causing biofilm overproduction (238). There are 3 major polysaccharides associated with the *P. aeruginosa* biofilm matrix, namely alginate, Pel and polysaccharide synthetic locus (Psl).

1.5.6.1 Alginate

Alginate is most associated with mucoid strains, made up of D-mannuronic acid and L-guluronic acid (239). These strains often over-produce alginate, and are commonly isolated from cystic fibrosis patients, showing high levels of antibiotic resistance. Non-mucoid strains convert to mucoidy after initial colonisation of the lung, perhaps due to exposure to immunological stress (240). In non-mucoid strains, Pel and Psl are the dominant biofilm polysaccharides. Interestingly, it has been suggested that coexistence of both mucoid and non-mucoid *P. aeruginosa* in the cystic fibrosis lung provides selective benefits, with both variants contributing to immune evasion and infection persistence (241).

1.5.6.2 Psl

Psl is composed of repeating units of D-mannose, L-rhamnose and D-glucose, and is either cell associated or soluble, which are high and low molecular weights respectively (242). Production is mediated by the Psl locus, which consists of 15 genes, 13 of which essential

for Psl production (7). In particular, *PslA* and *PslB* are important for structurally sound biofilm formation, with disruptions showing compromised biofilm structures that were poorly adhesive in the strain PAO1 (243, 244).

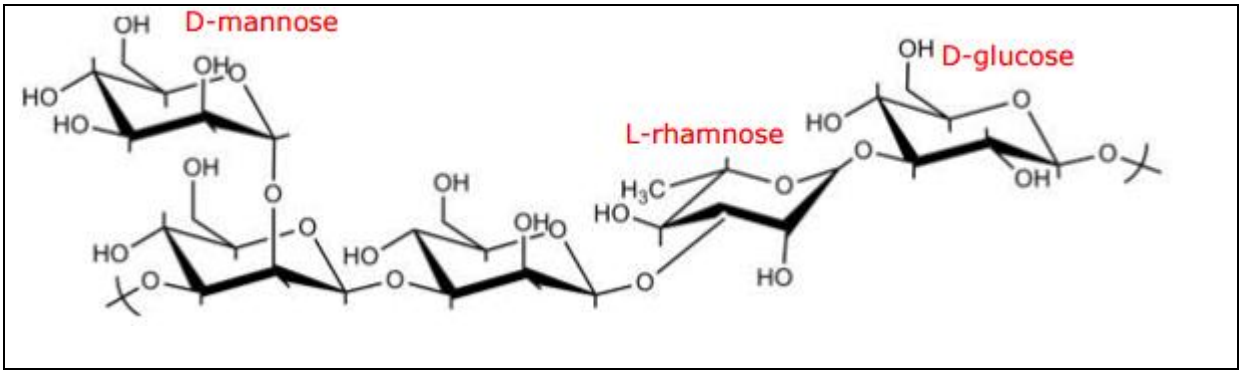

Figure 1. 7: Chemical composition of P. aeruginosa Psl, adapted from (245).

Psl anchors to the cell surface and promotes cell to cell interactions within biofilms via its helical distribution around the cell surface (246). It provides strength to the EPS matrix as well as flexibility and viscosity (247). However, Psl is not strictly essential for biofilm formation; as the individual disruption of Psl or Pel can be compensated by upregulation of the alternative polysaccharide during extended culture (244). In addition, during a study earlier this year, neither deletion nor overproduction of Psl affected bacterial numbers in a murine *in vivo* model, but that single knock-out of Psl showed fewer, larger and more closely associated bacterial aggregates as visualised by immunohistochemistry (248).

It is broadly understood that Psl facilitates immune evasion by inhibiting complement activation and by hindering the killing activity of macrophages and neutrophils (249, 250). Specifically, *P. aeruginosa* produces a serine protease inhibitor, ecotin, which directly binds Psl and inactivates neutrophil elastase. Our own study supports these ideas, where purified, high-mannose carbohydrate purified from a Psl-overproducing strain of PAO1 did not elicit any change in immune cell cytokine response compared to

controls (191). In contrast, biofilms with Psl or alginate within the matrix have also been shown to be most efficient at activating neutrophils (251, 252), calling into question the true effect of Psl on these immune cells, but supporting the idea that persistent *Pseudomonas* infection promotes dysregulation of inflammation, hampering resolution. Clinically, up to 99% of isolates are predicted to produce Psl, leaving it a promising target for drug discovery. Indeed, antibodies against Psl are currently under development that bind biofilms and inhibit biofilm formation at the early stages (253).

1.5.6.3 *Pel*

Pel is a polymer made up of partially acetylated *N*-acetylgalactosamine (GalNAc) and *N*-acetylglucosamine (GlcNAc) with 1→4 glycosidic linkages. Due to its acetylation, it has an overall positive charge, theorised to contribute to structural stability by cross-linking eDNA in the matrix. This interaction is able to compensate for loss of Psl in some cases (254). Synthesis is the Pel operon (*pelA-G*) is regulated by cdiGMP, with adhesion of planktonic cells to a surface triggering a spike in cdiGMP production, resulting in enhanced pelA transcription as little as 30 min after attachment (255). Importance of Pel in biofilm formation is strain dependent. In Psl-dominant strains such as laboratory PAO1, Pel is not essential for biofilm formation, although on knockout of Psl genes, Pel is upregulated to compensate for its absence (244). In contrast, in the highly virulent lab strain PA14, Pel is the primary matrix polysaccharide and is essential for biofilm formation (244). Immunologically, small colony variants of *P. aeruginosa* that overproduce Pel and Psl are highly persistent in the cystic fibrosis lung and chronic wounds, stimulating excessive pro-inflammation (252). As with Psl, single knock-out of Pel during an *in vivo* murine model produced larger, closely associated aggregates compared to the double-producers. However, deletion of both Pel and Psl resulted in

fewer, smaller aggregates as well as fewer overall bacterial numbers. Interestingly, deletion of Pel in this model, but not Psl, resulted in a lower ratio of immune cells in relation to bacteria, suggesting that Pel is less able to activate immune cells than Psl. Finally, it was concluded that in strains lacking both Pel and Psl, tolerance to gentamycin was significantly reduced, supporting the idea that increased biofilm biomass is protective to the bacteria during antibiotic treatment (248).

1.5.6.4 *Protein*

Proteins play a pivotal role in biofilm formation, via initial coordinating initial attachment alongside interaction with polysaccharides within the matrix to enhance stability (256). In the planktonic state, *P. aeruginosa's* singular Type IV pili coordinates initial surface attachment alongside eDNA (257). Unique to biofilms over planktonic *P. aeruginosa*, CdrA adhesin is a lectin, described to bind Psl as well as Pel via its carbohydrate binding domain to promote overall stability and aggregation by controlling specific localisation of Psl within the biofilm, as well as protection from immune proteases (258, 259). However, Psl is not essential for biofilm aggregation by CdrA, as protein-protein interactions are still capable of maintaining structure under shear stress (260). Another lectin, LecB, provides a similar structural role to CdrA, but binds cells to the host surface as well as each other, although recent evidence has shown an ability to also bind Psl (261).

1.5.6.5 *Quorum sensing*

Biofilm production is regulated by many overlapping mechanisms through QS, with *P. aeruginosa* utilising 3 main QS systems: las, rhl and the *Pseudomonas* quinolone signal (pqs). Las and rhl utilise *N*-acetylhomoserine lactones as small signalling molecules. The las system is associated with toxin production, as well as coordinating biofilm formation, with mutations in the lasI gene resulting in flat biofilms with poor structural integrity

(262). Rhl is also associated with biofilm formation, particularly production of Pel (263). The pqs system utilises alternative autoinducers, the 2-alkyl-4-quinolones, produced by the *pqsABCDE* operon. These molecules regulate many secreted virulence factors and are also important in biofilm formation (264). During biofilm development, pqs upregulates cell autolysis and hence the production of eDNA to make up the matrix. Culture of the laboratory strain PAO1 in the presence and absence of pqs highlighted its requirement for biofilm production, with biofilms having significantly more surface coverage when pqs is present (265). Additionally, 2 *Pseudomonas* QS molecules (3-oxo-C12-HSL and pqs) are able to directly affect the host immune response, reducing IL-12 production in murine DCs during LPS stimulation that showed reduced capacity to induce T cell proliferation and activation (266).

1.5.7 *S. aureus* biofilms

S. aureus strains are commensal in many individuals and able to attach to abiotic medical equipment, allowing them to form biofilms able to persist and cause infection in immunocompromised hosts (205). During *S. aureus* infection associated to biofilm formation there is a rapid inflammatory response, to produce IL-2 and TNF-α, likely causing the tissue damage that promotes *S. aureus* attachment and establishment (237). In addition, *S. aureus* biofilms have been observed to circumvent its TLR-2- and TLR-9-dependant recognition and clearance in an *in vivo* mouse catheter infection model, leading to a decrease in M1-charateristic secretions (TNF-α, IL-1β, CCL2, CXCL2, iNOS) and an increase M2-like phenotype (increased arginase-1) of exposed macrophages, with bacteria being actively phagocytosed but escaping killing. Paradoxically, this suggests that these *S. aureus* biofilms promote the opposite of the pro-inflammatory environment characteristic of chronic wounds, including those colonised with *P. aeruginosa* (267).

1.5.7.1 Quorum sensing

Overall biofilm formation in *S. aureus* is also coordinated through QS. The accessory gene regulator (agr) locus is a two-operon system under the control of two promoters P2 and P3, which drive transcription of operons RNAII and RNAIII respectively. Of these, the operon RNAII produces the autoinducer for the system. After export, the autoinducer may bind to and activate the response regulator protein AgrC, inducing transcription of RNAII and RNAIII (268). The RNAIII transcript is a small RNA that regulates various virulence factors at the post-transcriptional level by binding mRNAs, forming RNA duplexes that are recognised and degraded by endoribonuclease III (269). QS affects biofilm formation at several stages, with the agr having various, and sometimes conflicting, roles across *Staphylococcus* species. In *S. epidermidis*, initial adhesion is facilitated in mutants with disrupted agr, while in *S. aureus*, this effect is not observed (270). Agr mutants also result in biofilms of greater thickness compared to wild-type strains without any associated cell death, suggesting a role in biofilm detachment and spreading of infection, likely through a depletion in phenol-soluble modulins encoded by RNAIII (231). Agr mutations can either promote or inhibit biofilm formation and vary susceptibilities to antibiotics, but generally, it is accepted that high activity of agr is associated with toxin and exoenzymes during acute disease, while low activity is associated with chronic infection, such as in biofilm formation (271, 272). Indeed, biofilm production has been observed in some strains of *S. aureus* deficient in the ica polysaccharide suggesting an alternative ica-independent mechanism in certain cases (273).

1.5.7.2 Polysaccharide intracellular adhesin

Polysaccharide intercellular adhesin (PIA), made up of repeating units of linear *N*-acetylglucosamine, is the major polysaccharide in *S. aureus* biofilms encoded by the *ica*

locus (**Figure 6**). PIA is heavily involved in cell-cell adherence (274). As with Pel and Psl of *P. aeruginosa*, PIA acts as a structural substance that surrounds individual bacteria within the biofilm matrix, alongside negatively charged eDNA and WTAs to promote formation and maintenance of the 3D structure (275). Interestingly, there is conflicting data on the importance of PIA and the *ica* operon during *Staphylococcus* infection. It has been observed that in murine infection models, *ica*-positive *S. aureus* shows better *in vivo* survival than the knock-out, and in a co-infection model with *C. albicans*, only *ica*-positive *S. epidermidis* was lethal amongst conditions (276, 277). In contrast, absence of PIA did not affect infection outcomes for *S. aureus* or *S. epidermidis* in a guinea pig or mouse *in vivo* model, although strains used during these studies were shown to be agr-dysfunctional, which may have contributed to overall biofilm production in general (278, 279).

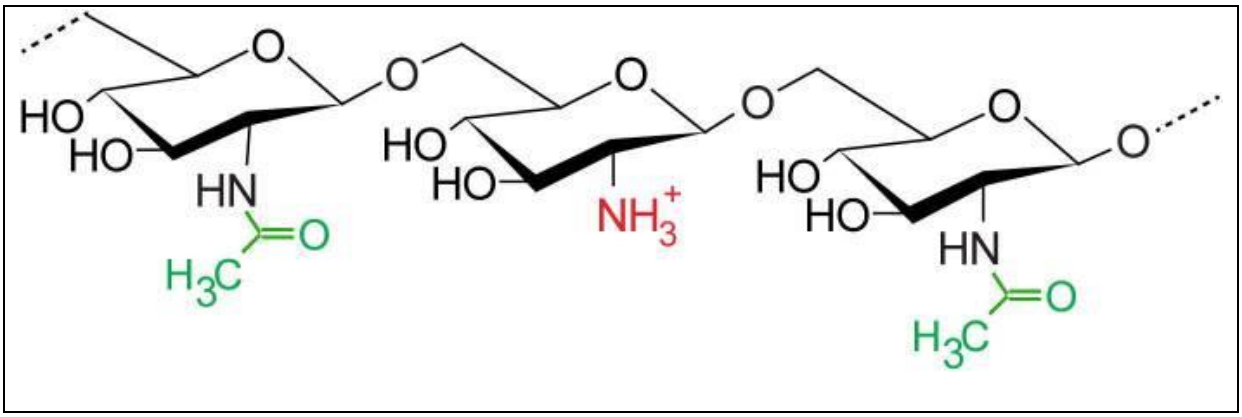

Figure 1. 8: Chemical structure of S. aureus PIA, adapted from (280).

The role of PIA in immune interaction has been investigated in multiple studies. In *S. aureus*, absence of PIA led to increased IL-12 production by murine DCs, alongside increased complement-mediated bacterial killing, supporting the idea discussed above that *S. aureus* biofilms that contain PIA promote reduced inflammation (267, 281, 282). However, in other studies, PIA-positive bacteria have been shown to promote inflammation both *in vivo* and *ex vivo*, with increased complement activation and

neutrophil recruitment (283, 284). Further, purified PIA itself has been shown to promote inflammation, inducing IL-6, IL-8 and MCP-1 via TLR-2 stimulation (285). It must be taken into consideration however, that the purification process may not have removed 100% of other biofilm contaminants, including secreted pro-inflammatory molecules that remain adhered to PIA.

1.5.7.3 Protein

Various *S. aureus* proteins aid in biofilm formation, including Protein A, *S. aureus* surface protein G (SasG) and fibronectin binding proteins A and B. Here, biofilm architecture is extremely plastic, with different effectors being produced in response to varying stimuli. Hence, biofilms are generated with varying combinations of EPS components that best suit the infection environment, aiding overall survival (286). Protein A is a small *S. aureus* surface protein that binds the Fc-portion of antibodies, whose binding inhibits antibody mediated opsonisation and phagocytosis (287, 288). Cross-linking to the B cell receptor triggers excessive non-specific proliferation of splenic B cells, leading to mass apoptosis and impaired systemic response (289). SasG is a binding protein, facilitating adherence to epithelial cells (290), while fibronectin binding proteins aid in biofilm stability by adhering to host extracellular matrix (291).

1.6 Bacterial co-infection during disease

In the clinic, it is rare for bacteria to grow in single-species colonies, but rather are found as complex poly-microbial communities whose attributes differ considerably from those of monoculture. Species live and interact with each other within biofilm, and communicate to best utilise the environment and protect themselves from external stresses (292). In some diseases, specific combinations of bacteria are associated with infection, such as in the chronic lung condition cystic fibrosis as well as in extensive burns and chronic wounds.

As discussed throughout this section, bacteria are generally accepted to adopt two growth types, planktonic and biofilm. The mechanisms of the biofilm lifestyle have been investigated extensively *in vitro,* denoting stages of attachment by individual planktonic cells, biofilm maturation and dissociation. However, *in vivo*, bacteria tend to form aggregates (293). Although bacteria in chronic wounds show many similarities with *in vitro* biofilms, suspended aggregates tend to be smaller, with species unevenly distributed throughout the infection site, with formation and regulation, similar to aggregates described in the environment (294). In **Table 1.2**, summaries are given for important in vitro and ex-vivo skin models that have been described in the literature to simulate the true wound environment more closely. Specific parameters used have been described which were taken into close consideration during the later stages of this project.

Table 1. 2: summary of existing in vitro and ex-vivo models used for bacterial biofilm infection in host-like conditions, predominantly in a wound-like setting.

Model	Context	Parameters	References
Human skin equivalents	Investigation of fibroblast and keratinocyte roles during re-epithelialisation of the dermal-epidermal junction during wound healing.	Use of hydrated 4 mgmL^{-1} collagen (rat-tail) gels mixed with normal human fibroblast suspension in Dulbecco's modified Eagle Medium were seeded with human keratinocytes from normal breast tissue to construct an epidermis and maintained at the air-liquid interface. The construct was fed with three parts DMEM and one part Ham's F12 medium supplemented with 5% HyClone calf serum (Greiner, Nurtingen, Germany) with 1mM hydro-cortisone, 1mM isoproterenol, 0.1mM insulin (Sig-ma-Aldricht, Zwijndrecht, The Netherlands), 1% human serum 1x10^{5} M L-carnitine, 1x10^{2} M L-serine, 1mM DL-α-tocopherol-acetate and a lipid supplement containing 25mM palmitic acid, 15mM linoleic acid, 7mM arachidonic acid and 2.4x10^{5} M bovine serum albumin. Wounds were introduced via superficial incision or full thickness trauma by cold-burn.	(295)
Bacterial infection of collagen matrix	Investigation of bacterial infections on non-solid surfaces in a 3D, wound- and soft tissue-like infection model to investigate hallmarks of biofilm growth, including embedded matrix aggregates, antibiotic resistance, and bacterial organization similar to those in *in vivo* infected wounds.	Clinically relevant species *P. aeruginosa* (PAO0001) and *S. aureus* (ATCC:6538) were grown planktonically in TSB medium then seeded to a 3D rat-tail collagen type I matrix (BD Biosciences, San Jose,CA, USA) in synthetic wound fluid (50% foetal calf serum and 50% physiological NaCl in 0.2% peptone) to produce biofilms. In later experiments, biofilms were also treated with antibiotics ciprofloxacin and rifampicin. Morphological analysis was performed by light and confocal microscopy and compared to in vivo chronic wounds.	(296)
Ex vivo porcine skin explant model of bacterial biofilm infection	Biofilm phenotype is highly dependent on the growth environment, and can contribute to virulence and resistance, promoting chronic wound longevity. Using a porcine skin explant closely recapitulates an *in vivo* wound, allowing for testing effects of antimicrobial agents.	Porcine skin biopsies were extracted and sterilized using a range of methods before culture in liquid, solid or semi-solid TSB medium (agar for semi-solid) with planktonic bacteria (*P. aeruginosa* PAO1 and *S. aureus* ATCC 35556). Biofilms were analysed under various treatment conditions by histology, microscopy and viable colony counting.	(297)
Artificial dermis model	Bacterially infected chronic wounds are difficult to effectively treat with conventional methods, largely due to quorum sensing which regulates biofilm formation, although there are few drugs utilising this system.	Artificial dermis was produced in two layers as found *in vivo*, with an upper spongey layer of chemically cross-linked hyaluronic acid atop a spongey sheet of hyaluronic acid with collagen (cross-linked using ethyleneglycol diglycidyl ether, EX810 (Nagaseksei, Hyogo, Japan) as described by (Mineo et al. 2012). This method was modified to saturate the dermis with Bolton Broth with 50% plasma (Sigma-Aldrich) with 5% laked horse blood. Artificial dermis was infected with *S. aureus* (mu50) and/or *P. aeruginosa*	(298)

		(QSIS2, PAO1, MH340, MH710). Activated cellulose gauzes impregnated with vancomycin and/or quorum sensing inhibitor were placed over the dermis surface immediately or 24 h after infection to test inhibitory and eradicatory properties respectively.	
Basal perfusion model	Topical antimicrobials used in wound dressings were screened using a range of taxonomically defined facultative and wound pathogens in a 3D wound model to assess antimicrobial tolerance in mixed-species biofilms.	For this model, significant bacterial pathogens *Streptococcus pyogenes* and *P. aeruginosa* were isolated from infected clinical wounds while MRSA NCTC 11939 and *Bacteriodes fragilis* NCTC 9343 were obtained via Public Health England and co-culture optimised in simulated wound fluid (49% (v/v) Mueller-Hinton broth, 49% FCS and 2% laked horse blood (Oxoid, Basingstoke, UK)). Medium was fed through a central inlet and filtered continuously to bacteria grown on a solid surface, removing waste and excess medium continually. Temperature and atmospheric CO_2 was maintained by housing system in an aerobic incubator.	(299)
Macrophage-facilitated innate wound healing	Tumour-associated macrophages express proteins like those associated with a healing phenotype in wounds, and that expression is facilitated by IL-6 in a collagen-rich environment leading to tumour metastasis.	Primary macrophages and monocytes were isolated from murine tumour tissue or human donors (peripheral CD14+ monocytes differentiated to *in vitro*-derived macrophages using M-CSF) and seeded to type-I collagen (BIO RAD) matrix for transendothelial migration assays, viability testing and protein analysis.	(300)
Ex vivo human skin infection model	Although chronic wounds are researched extensively in the field, there are limitations in using in vitro studies due to their stark differences to human infections. Here, a simple human skin explant model was designed to compare wound healing characteristics during infection vs sterile conditions.	Excess skin was obtained from elective panniculectomy and adipose tissue removed before washing and explants wounded with a biopsy punch tool before culture in DMEM (Thermo Fisher Scientific, Waltham, MA) supplemented with 10% FBS (Atlanta Biologicals, Flowery Branch, GA). Clinical *S. aureus* isolate UAMS-1 was inoculated to wound surface. The epithelium was maintained at the air-liquid interface and DMEM medium replaced every 24 h to select for adherent bacteria and biofilm formation. Skin wounds were collected after 72 h for histological analysis, imaging, bacterial quantification, qPCR abd protein quantification.	(301)
In vivo-like biofilms using a porcine lung model	*P. aeruginosa* infection of the cystic fibrosis lung is associated with increased mortality, substantially due to antibiotic resistance. An *ex vivo* pig lung model was optimised to mimic these chronic infections more closely.	Porcine lungs were donated from a local butcher and the ventral surface heat sterilized. Bronchiole sections were extracted and alveolar tissue removed before washing and culture in a mixture of artificial sputum medium developed from the average concentrations of ions, free amino acids, glucose, and lactate in CF sputum samples as described in (Palmer *et al.* 2007) with or without supplementation of macromolecules from CF sputum described in (Turner et al. 2015). This was further supplemented with agar and ampicillin. *P. aeruginosa* were introduced by needle prick before incubation. Bacteria were quantified and their virulence factors analysed.	(302)

1.6.1 Biofilms in cystic fibrosis

Cystic fibrosis is a severe genetic condition, requiring intense treatments and long hospital stays due to its effects on multiple organ systems. Cystic fibrosis patients harbour one or more mutations in the cystic fibrosis conductance regulator (CFTR) gene, leading to a dysfunctional protein and deregulation of osmotic balance within the lung, the most common mutation being the F508 deletion (303, 304). CTFR regulates the passage of chloride ions and water across epithelia involved in mucus secretion, resulting in highly viscous mucus. Difficulty in mucus clearance creates a prime environmental niche for bacterial and fungal infection, and is therefore highly associated with HAI (305). Over time, persistent inflammation from chronic infection alongside permanent lung damage lead to pulmonary hypotension and hypoxia, ultimately resulting in patients requiring constant positive-pressure ventilation or lung transplantation (292).

The two bacterial species most highly associated with lung infection in cystic fibrosis are *S. aureus* and *P. aeruginosa*, causing chronic infections that are exceptionally resistant to antibiotics and immune clearance. Generally, the cystic fibrosis lung is colonised by *S. aureus* during childhood, the flora developing during adolescence and adulthood, leaving *P. aeruginosa* the dominant species, although co-existence throughout life has been observed (306). The major pathology observed during cystic fibrosis lung infection is attributed to *P. aeruginosa* while *S. aureus* appears less virulent, although this may be attributable to fewer studies, particularly in children (183). Generally, bacterial aggregates are not observed on the lung epithelium, but within mucus surrounded by neutrophils (307).

Various *P. aeruginosa* exoproducts contribute to pathology, including LPS and pyocyanin that promote inflammation (308). During infection, the innate immune response is exacerbated, including neutrophil accumulation with excessive respiratory burst, and evidence of neutrophil dysfunction. *P. aeruginosa* also produces DdDHL, a neutrophil chemoattractant, followed by rhamnolipids that initiate neutrophil lysis (309). These characteristics are similar to those associated with chronic wounds (310, 311). The cystic fibrosis lung generally contains increased levels of activated complement. Although perhaps counterintuitively, *P. aeruginosa* elastase and alkaline protease have been shown to inactivate it (310). Indeed, the Th2 type immune response is common in cystic fibrosis patients with chronic *P. aeruginosa* infection, inducing high levels of IL-4 (312). In addition, IL-17 often found in the sputum of cystic fibrosis patients, characteristic of the Th17 response, and indeed, during this disease, naïve T cells show a predisposition to take on the Th17 phenotype (313, 314). Both of these T cell responses have also been shown to co-exist during cystic fibrosis, as significant increases in both Th2 (IL-5/IL-13) and Th17 (IL-17A) cytokine profiles have been observed in clinically symptomatic patients, which is augmented during *P. aeruginosa* (315).

1.6.2 Severe burns

Severe compromise of the skin barrier through burns leaves an exposed surface enabling bacterial colonisation and biofilm formation. Many commercial topical drugs and wound dressings do not inhibit biofilm formation, highlighting the requirement for the development of alternative treatments and dressings to promote healing (316). *P. aeruginosa* is commonly associated with these infections, with its ubiquity in the environment and as a skin commensal increasing likelihood of exposure before healing (183). *P. aeruginosa* hinders the healing process in tissues, due to biofilm production in

the cutaneous epithelium and deep tissue spreading, with the elastase LasB preventing remodelling of extracellular matrix and promoting collagen degradation. Supporting this, a murine burn study using various QS mutants, showed that strains lacking the las and rhl systems cause significantly less mortality than the PAO1 wild-type, as well as decreased dissemination to distant sites (317). In another study, burn wound exudates from patients were used to stimulate growth of a range of bacterial species. Here, PAO1 was the only strain able to grow within the exudate, even promoting enhanced production of multiple virulence factors, including pyocyanin and pyoverdin (318).

S. aureus is often associated with *P. aeruginosa* in burns. The interactions between these species are poorly understood, but *P. aeruginosa* produces various factors that inhibit *S. aureus* growth *in vitro*, although *in vivo* the relationship is more nuanced (319). In particular, if *S. aureus* is already established due to prior colonisation as a commensal, addition of *P. aeruginosa* does not result in complete out-competition, forming a mixed-species biofilm (320). In fact, in certain cases, *S. aureus* benefits from *P. aeruginosa*; due to some exoproducts produced by certain *P. aeruginosa* strains, *S. aureus* is granted significant protection from tobramycin and ciprofloxacin. Conversely, other exoproducts tested actually increased killing by vancomycin, such as LasA endopeptidase (319). Together, these studies suggest a complex relationship between *S. aureus* and *P. aeruginosa* in the context of burns, the combination likely to alter not only susceptibility to antibiotic stresses, but also recognition by the immune system and its response to biofilms.

1.6.3 Diabetes and chronic wounds

Diabetes mellitus is a metabolic condition, characterised by dysregulated hyperglycaemia, resulting in numerous health complications if left untreated. As of 2020,

around 10% (537 million) of the adult population is estimated to harbour this condition, with up to 90% attributable to Type 2 diabetes (321). Diabetes manifests through two major routes. Type 1 diabetes is an autoimmune disease, where depletion of pancreatic beta cells results in insufficient insulin production, preventing glucose uptake in cells (322). In contrast, Type 2 diabetes is caused by an intolerance to insulin that develops over time, the most common factors being obesity and insufficient exercise (323). While both manifestations can be treated by regular insulin injections, Type 2 diabetes may be prevented and controlled by a healthy diet and lifestyle (323). Acute complications can be life threatening, including diabetic ketoacidosis and hyperosmolar hyperglycaemia, with 6.7 million reported deaths in 2021 (321, 324). In the long-term, diabetes is associated with kidney and cardiovascular disease, nerve damage and foot ulcers (325). In the latter, dysregulation in wound healing leads to wound chronicity, due to the various biochemical, vascular and neuropathic effects of hyperglycaemia (326). In addition, peripheral neuropathy often results in initial wounds going unnoticed and hence, untreated, leading to chronicity. These things combined prevent proper leukocyte migration to the wound bed, leaving them vulnerable to infection.

Chronic diabetic wounds are made up of granulation tissue with collagen, new capillaries, ECM and immune cells, and it is frequently observed that consistent stimulation of ROS/RNS, inflammatory cytokines, immune complexes and complement in acute wounds often results in infection, with increased risk of reinfections after treatment due to healing delay (327). *Staphylococcus* and *Pseudomonas* aggregates are observed in soft tissues, exhibiting high antibiotic tolerance, implying that the highly hydrated environment with extensive collagen and elastin is favourable for aggregate formation (328). In a longitudinal study of persisting venous leg ulcers, 93.5% of wounds were

colonised by *S. aureus* while 52.2% were colonised with *P. aeruginosa* (329), with *S. aureus* present at the wound surface, while *P. aeruginosa* remained deep in the wound bed. In biopsied leg ulcer samples, these deep-set *P. aeruginosa* aggregates are surrounded by polymorphonuclear neutrophils, and are more prevalent in diabetic vs non-diabetic wounds (330, 331). Ulcers co-infected with both species also tend to be larger than those infected with *S. aureus* alone (329). These differences in characteristics highlight the fact that multiple species within a wound might provide unique roles in pathology. Importantly, isolates from human wound infections show poor biofilm formation *in vitro*, while biofilm-deficient lab mutants can form aggregates in murine *in vivo* models, suggesting that these aggregates are the default growth mode during infection, perhaps due to the highly polymer- and nutrient-rich environment (332).

1.8 Hypothesis and aims

The overarching aim of this project was to investigate the interaction between bacterial biofilms with innate immune cells in the context of chronic wounds, with a focus on the role of biofilm carbohydrates. During this thesis, we explore these interactions in three different contexts:

1. Previously, work was conducted in the lab to characterise *P. aeruginosa* biofilms through the lens of carbohydrate interactions using lectins of varying specificity. Here, we aimed to optimise new species and growth conditions, with the hypothesis that **the combinations of CLRs ligands will differ in *S. aureus* compared to *P. aeruginosa,* as well as in different growth conditions.**

The specific aims for this section were:

- Optimise growth of both planktonic and biofilm cultures of *S. aureus* SH1000 in relevant media types.

- Characterise and compare SH1000 biofilm characteristics in relation to PAO1.

- Re-design and optimise biofilm production in new media types for greater control of media composition that will enable in depth biochemical analysis.

2. *P. aeruginosa* biofilm carbohydrate was purified previously in the lab, identifying ligands for various lectins. Here, we endeavoured to purify carbohydrate from whole *S. aureus* biofilms and *P. aeruginosa* biofilms grown in minimal medium, and hypothesised that **using this product, we may be able to more clearly identify the ligands for the lectins, and infer how these carbohydrates specifically influence immune recognition and responses.**

The aims in this section were:

- Optimise growth of *S. aureus* SH1000 biofilms in TSB for carbohydrate extraction and purification.

- Compare SH1000 biofilm carbohydrate characteristics to those from PAO1Δ*wspF*Δ*pel.*

- Re-design and optimise biofilm production in a new media for carbohydrate extraction, purification and characterisation.

3. We aimed to establish the biological relevance of CLR binding to biofilms. In this section, we investigated immune cell interactions with whole biofilms, using 2D and 3D wound models, and hypothesised that **interaction of immune cells with biofilms will promote inflammation.**

The aims of section 3 were:

- Normalise live biofilm cell numbers using known OD_{600nm} values of planktonic cultures.

- Optimise 2D infection assays using live bacterial cultures and 96-well plate format.

- Design a novel 3D model to mimic the chronic wound environment.

Chapter 2. Analysis of carbohydrate composition of *P. aeruginosa* and *S. aureus* biofilms using lectins

2.1 Introduction

Innate immune cells recognise pathogens via specific receptors able to distinguish structures unique to microorganisms, deemed pathogen associated molecular patterns (PAMPs). PAMPs tend to be highly conserved across multiple species, allowing for global recognition by pattern recognition receptors (PRRs), contributing to immune activation and pathogen clearance via expression and secretion of cytokines and chemokines that aid in the inflammatory response and increase cell killing capability (94, 95). Often, genes expressed in response to infection are regulated by the transcription factor NF-κB, which is activated though many of the PRR signalling cascades (333).

Notably, bacterial flagellin, lipopolysaccharide (LPS) and peptidoglycan are recognised by Toll-like receptors (TLRs), which induce the transcription of pro-inflammatory genes via activation of MyD88 and ultimately NF-κB, or the type I interferon response via TRIF in the case of LPS (95). Further, carbohydrate-specific C-type receptors (CLRs) are associated with the recognition of biofilm EPS, which could result in changes in the production of cytokines and immune activation, but as yet little is understood about specific mechanisms (125, 334).

CLRs engage with ligands via one or more recognition domains, including the characteristic folded structure of the C-type lectin-like domain (CTLD), which are either membrane-bound or soluble depending on the receptor, and recognise polysaccharides (125). Some common CLR ligands are composed of mannose, fucose and glucose, and are present on various bacterial, fungal and viral pathogens (125). There are several major

CLRs expressed by immune cells, each with distinct signalling pathways to induce effector mechanisms. Often, receptor-ligand binding is calcium-dependant, as is the case for the mannose receptor (MR, CD206), Dectin-2 (CLEC6A) and Dendritic Cell-Specific Intercellular adhesion molecule-3-Grabbing Non-integrin (DC-SIGN, CD206) that are the focus of this chapter, and the rest of the chapters going forward (191, 335). As well as self-structures, ligands for DC-SIGN exists on a broad range of pathogens (161).

DC-SIGN is a membrane-bound receptor expressed on dendritic cells (DCs) and selected dermal and IL-4 treated macrophages, and is associated with antigen internalisation and presentation, and DC adhesion to T cells, neutrophils and the mucosal endothelium (160). The receptor naturally exists as a tetramer, with an extracellular carbohydrate recognition domain (CRD) that engages with high-mannose and –fucose structures. Due to its tetrameric structure, it is able to form multivalent interactions with its ligands, allowing for enhanced avidity (336).

The mannose receptor family comprises the group I CLRs and includes several endocytic receptors that recognise a broad range of ligands (127). Perhaps the best described is the MR, expressed by DCs and macrophages and containing two sugar binding sites, the 8 CTLD domains bind to mannose, fucose and N-acetyl-glucosamine and the cysteine-rich domain recognises sulphated glycans. MR binds collagen through the fibronectin type II domain (337). Mannose and fucose recognition through CTLDs is calcium-dependant (128). Among CTLDs, domains 1-3 weakly bind carbohydrate while 4-8 show much higher affinity due to multivalent binding leading to increased avidity (129). The exact signalling pathways of MR are unclear, but it has been suggested that in humans, alongside the mRNA for the MR protein, microRNA miR-511-5P (miR-511-3P in mouse) is also transcribed from MR intron 5 plays some role in its function. Generally, miR-511-

3P has been described to play various roles in inflammation and tumour growth. Although it is not affected by antagonists or blocking antibodies for the MR protein, knockout of MR also facilitates the knockout of the microRNA, meaning that during this knockout, cellular affects occur as a combination of both losses (135, 338). Interestingly, as MR is present on exosomes, it is suggested that miR-511-5P would also be contained in these exosomes to modulate systemic inflammation.

Similarly, Dectin-2 is a neutrophil, monocyte, macrophage receptor that recognises mainly fungal and bacterial antigens, specifically α1-2 or α1-4 linked mannose structures (151). Dectin-2 has no intracellular signalling motif, but rather interacts with Fc receptor-γ common chain that allows for intracellular signalling though Syk, culminating in activation of NF-κB that induces upregulation of TNF-α and IL-1ra (157).

P. aeruginosa can hinder the healing process in wounds due to biofilm production in the cutaneous epithelium and deep tissue spreading. Further, elastase LasB prevents remodelling of extracellular matrix and promotes collagen degradation, as well as degrading various antimicrobial agents, including mucins and surfactants (339-341). Important virulence factors like elastase are controlled by the Las QS system (342). In one study, burn wound exudates from patients were used to stimulate cultures of *P. aeruginosa*, *S. aureus* and *Acinetobacter baumanni*. Here, PAO1 was the only strain able to grow within the exudate, with an increased production of certain virulence factors including pyocyanin and pyoverdine as well as upregulation of QS molecule pqsA (318). *S. aureus* is often associated with *P. aeruginosa* in burns and chronic wounds, with ulcers co-infected with both species tending to be larger than those infected with *S. aureus* alone (329). The specific interactions between these two species is poorly understood, but findings suggest that *P. aeruginosa* produces various factors that inhibit *S. aureus* growth

(319). However, once *S. aureus* is already established, addition of *Pseudomonas* does not lead to complete out-competition and the species are able to co-exist, although whether this was in a homogenous mix or as aggregates was not determined in this study (320). Co-culture of these species also affects antibiotic sensitivity, with exoproducts from some *P. aeruginosa* strains providing significant protection to *S. aureus* from tobramycin and ciprofloxacin (319). Conversely, other exoproducts increased killing of *S. aureus* by vancomycin, such as the LasA endopeptidase (319). Together, these studies suggest a complex relationship between *S. aureus* and *P. aeruginosa* in the context of burns and wounds, the combination likely to alter not only susceptibility to antibiotic stresses, but also recognition by the immune system and its response to biofilms.

In the early stages of my project, we focused on the introduction of *S. aureus* to our *in vitro* infection models alongside the comparison of *S. aureus* and *P. aeruginosa* biofilms in terms of biofilm production, immune receptor binding and 3D architecture, with an ultimate goal of optimising a polymicrobial *in vitro* model that includes *Candida albicans*. Due to knowledge gained on this route however, the aims evolved to investigate changes in the environmental conditions for *P. aeruginosa* alone, unravelling the effects this has on biofilms.

2.2 Hypothesis

Historically, our laboratory has produced biofilms *in vitro* to characterise their compositions via the comparative binding activities of various clinically relevant lectins, focusing primarily on *P. aeruginosa* laboratory strain PAO1, selected EPS mutants and clinical isolates (191). Therefore, the initial focus for this project was the investigation of biofilms produced by another clinically important ESKAPE organism *S. aureus*, whose general characteristics, importantly the carbohydrate composition, varies from that of *P. aeruginosa.* Hence, we hypothesised that once biofilm formation was optimised using our model, that **the combinations of CLRs binding will differ in *S. aureus* compared to *P. aeruginosa*, giving indication as to their divergent downstream immune responses.**

2.3 Aims

Previously, production of *P. aeruginosa* biofilms with different carbohydrate compositions was optimised in a 96-well format for analysis using ELISA-type assays. However, it is dogma in microbiology that different species often harbour vastly different characteristics in both growth and pathogenicity based on environmental conditions. Hence, incorporation of *S. aureus* into this model may pose challenges, in part related to various unique *P. aeruginosa* and *S. aureus* virulence factors that may interfere with co-culture. The overall aim of this chapter is to optimise *S. aureus* biofilm production using our 2D 96 well model to study the combined interactions with innate immune receptors. From here, we endeavoured to adapt the model for more in-depth biochemical characterisations of biofilm carbohydrates to investigate their roles in immune interaction. Towards these aims, we partook various routes of investigation.

- Optimise growth of both planktonic and biofilm cultures of *S. aureus* SH1000 in relevant media types.

- Characterise and compare SH1000 biofilm characteristics in relation to PAO1, including:

    - Growth-phase time signatures using OD_{600nm}.

    - Biofilm biomass using crystal violet analysis.

    - Biofilm carbohydrate composition via engagement of lectin receptors of varying specificity, including Fc- and biotin-conjugated human and plant lectins using ELISA-based assays and confocal microscopy.

- Re-design and optimise biofilm production in new media types for greater control of media composition that will enable in depth biochemical analysis.

2.4 Materials and Methods

2.4.1 Bacterial strains and culture conditions

Biofilms were produced by first streaking glycerol stocks onto LB agar which were incubated overnight at 37 °C. Strains used throughout this project are described in **Table 2.1**. Single colonies were inoculated to 5 mL X-Vivo15 (Lonza, BEBP02-061Q) and incubated overnight at 37 °C, 200 rpm. Overnight cultures were corrected to OD_{600nm} of 0.01 (*P. aeruginosa*, PAO1-L) or 0.1 (*S. aureus,* SH1000) in 20 mL pre-warmed X-Vivo15 and incubated for 3 h at 37 °C, 200 rpm in 250 mL conical flasks. The OD_{600nm} of the 3 h cultures was corrected to 0.04 in X-Vivo15 and 100 µL seeded to relevant wells of a 96-well TC-treated (Corning Costar, 3596) or Maxisorb (Thermo Scientific Nunc, 439454) plate and incubated at 37 °C, 5% CO_2 for 16 or 24 h. In some instances, remaining culture at 0.04 OD_{600nm} was incubated overnight at 37 °C to produce new overnight cultures to be used as planktonic cells controls.

Table 2. 1: Bacterial strains used in experiments described in this thesis. (PAO1-ΔLasR synthesised in-house and kindly donated by Dr. Samuel Fenn, University of Nottingham, UK; ** wspF were mutants kindly donated by Dr. Yashuhiko Irie, University of Tartu, Estonia).*

Strain	Relevant characteristics	Carbohydrate production	Original isolation	Refs.
P. aeruginosa PAO1-L (Lausanne)	Wild-type, physiological cyclic-di-GMP, normal biofilm growth, serogroup O2/O5, type b flagellum, moderate virulence	Pel+psl+	High similarity to Holloway's original PAO isolate	(91, 343)
PAO1-L*ΔwspF*	High levels of cdiGMP, biofilm overproducer	Pel+++psl+++	PAO1 origin	(238)**
PAO1-L*ΔwspFΔpel*	High levels of cdiGMP, biofilm overproducer	Pel-psl+++	PAO1 origin	(344)**
PAO1-L*ΔwspFΔpsl*	High levels of cdiGMP, biofilm overproducer	Pel+++psl-	PAO1 origin	(344)**
PAO1-L*ΔwspFΔpelΔpsl*	High levels of cdiGMP, biofilm deficient	Pel-psl-	PAO1 origin	(258)**
PAO1-L*ΔlasR*	Normal biofilm production, deficient in major proteases	Pel+psl+	PAO1 origin	-*
S. aureus SH1000	Normal biofilm production	PAI	Clinical sepsis isolate, lab strain	(345)

2.4.2 PCR for confirmation of bacterial strains

To confirm mutations in relevant genes in bacterial strains used (**Section 2.4.1, Table 2.1**), PCR was used using primers for *wspF*, *pelA* and *pslC/D* (**Table 2.2**) Bacterial overnight cultures were produced in X-Vivo15 (37 °C, 200 rpm) and 1 µL inoculated into PCR reaction mixture containing 1X GoTaq G2 green master mix (including loading buffer, Promega, M7822) with 0.1 µM of each forward and reverse primers (**Table 2.2**) in nuclease-free water (Sigma-Aldrich, P119E). The final volume of each reaction mixture was 25 µL. Initial denaturation was performed for 5 min, 96 °C followed by 30 amplification cycles (denaturation 30 s, 95 °C; annealing 30 s, 55 °C; extension 30 s, 72 °C) and a final 5 min extension (72 °C) and hold at 4 °C. A fraction of the reaction (15 µL) was loaded into 1% agarose gel (11 388 991 001, Roche) in Tris-acetate-EDTA buffer (Scientific Laboratory Supplies (SLS), 93283) with 0.01% Sybergreen safe stain

(Invitrogen, S33102) and electrophoresed at 100 volts for 1 h. For each gel, a 1 kb marker was used for reference (Invitrogen, 10787018).

Table 2. 2: Primers used for PCR to confirm gene expression in strains used*. Primers were kindly donated by Dr. Yashuhiko Irie, University of Tartu, Estonia.*

Gene	Forward primer (5'-3')	Reverse primer (5'-3')
wspF	AAGATTCAGAACGTCGGCTG	GATGTGATTGTTGGTCCCCG
pslC/D	GGTCTACCATTCCCACGATTAC	TCAGCTCGTTGGCGATTT
pelA	CCCTATCCGTTCCTCACCTC	TACTGGGCCTCGAAGTTCTC

2.4.3 Crystal violet assay to quantify biofilm biomass

To confirm consistency of growth with regards to biomass, biofilms were produced as in 2.4.1 and crystal violet assay performed. In brief, wells containing cultures were washed 3x with 200 µL HPLC-grade water and incubated for 1 h at room temperature in 125 µL 1% (w/v in water) crystal violet solution in the dark. Wells were washed 3x as before and the stain solubilised in 70% ethanol and 125 µL transferred to sterile wells, diluted 1:2 in ethanol for a total volume of 250 µL. Absorbance was measured at 595 nm using a Multiscan FC (Thermo Scientific).

2.4.4 Growth curves for bacterial strains

To determine the growth characteristics of *S. aureus* and *P. aeruginosa* strains, growth curves were performed in X-Vivo15 and RPMI-1640 media (Sigma, R0883). Overnight cultures of bacteria were produced as described in Section **2.4.1** and corrected to OD_{600nm} 0.01 and 100 µL of inoculated to a 96-well Maxisorp plate. Culture plates were incubated for 18 h at 37 °C with OD_{600nm} recorded at 30 min intervals using a Spark® Multimode Microplate Reader (Tecan).

2.4.5 Lectin binding assay to whole biofilms (Enzyme-linked immunosorbent assay)

Binding assays were used to test interaction of various lectins to biofilms. Biofilms were produced in 96-well Maxisorp plates as described in Section **2.4.1**. Alongside bacterial cultures, wells were coated with controls consisting of relevant glycopolymers (Lectinity, α-D-galactose-PAA, 0023-PA; α-L-Fucose-PAA, 0027-PA; Lewis^X-PAA, 0044-PA), heat-killed *Candida albicans* (HKCa, produced in-house) or Zymosan from *S. cerevisiae* (Merck, 12352200) at 2 μgmL^{-1} in 50 µL PBS and incubated for 24 h, 37 °C. After incubation, wells containing biofilms were fixed for 10 min, 4 °C with 2% paraformaldehyde (supplier) in PBS without Ca^{2+} or Mg^{2+} and were washed 3x with 200 µL TSB buffer (10 mM Tris-HCl pH7.5, 10 mM $CaCl_2$, 154 mM NaCl and 0.05% (v/v) Tween 20 (Sigma-Aldrich, P1379)). Biofilms and controls were incubated with 50 µL of protein; Fc-DC-SIGN (2-10 μgmL^{-1}, R&D Systems), MR CTLD4-7-Fc (2-10 μgmL^{-1}, produced in-house), or Dectin-2-Fc (2-10 μgmL^{-1}, mouse, Enzo, ALX-522-126-C050; human, Stratech, 12352202) for 2 h, RT. Wells were washed 3x with TSB then incubated with 50 µL anti-human Fc-conjugated to alkaline phosphatase (AP, Sigma-Aldrich, A9544) diluted 1:1000 in TSB for 1 h, RT. Wells were washed 2x with TSB and once with AP buffer (100 mM Tris HCl pH 9, 100 mM NaCl, 1 mM $MgCl_2$ in HPLC water), except for Dectin-2-Fc wells which were washed 3x with TSB. For all experiments, 50 µL of p-Nitrophenyl phosphate substrate solution (1 $mgmL^{-1}$ PNPP tablet and 0.2 M Tris buffer tablet (SLS, N2770-50SET), in HPLC water) was added to each well and incubated at in the dark at RT. Absorbance was read at 405 nm between 5 and 30 min at 5-min intervals.

For later experiments, biotinylated plant lectins (Lectin Kit I: Biotinylated, Vector Laboratories, BK-1000) were utilised as an alternative to Fc-conjugated lectins to assess

biofilm carbohydrate compositions. For these, the protocol format was the same, changing only specific reagents as follows:

- TSB buffer was supplemented with 2 mM $MnCl_2$.

- Plant lectins conjugated to biotin were prepared at a range of concentrations in TSB before 2 h incubation.

- Instead of IgG conjugated to AP, washed wells containing bound lectin were incubated with 50 µL Neutravidin-AP (2 μgmL^{-1}, Thermo Fisher Scientific, 31002) for incubation in the dark, 1 h.

2.4.6 Production of biotinylated tetrameric DC-SIGN for lectin binding assays

Tetrameric DC-SIGN was kindly donated by Professor Jesús Jiménez-Barbero (CIC bioGUNE, Bizkaia Science and Technology Park, Bilbao, Spain). Biotinylation was performed using Protocol 1 from the Roche Biotin Protein Labelling kit (11 418 165 001). Biotin-7-NHS was prepared in DMSO (2 $mgmL^{-1}$) and 30 µg tetrameric DC-SIGN (1 $mgmL^{-1}$ in PBS) in a 0.5 mL Eppendorf and incubated at RT for 2 h, stirring gently to not introduce bubbles. After incubation, solution was added to the gel filtration column then flushed in 2.5 mL PBS. Protein was eluted with 3 mL PBS and collected in 0.5 mL fractions. Protein concentration was determine by reading absorbance at 280 nm by nanodrop.

2.4.7 Confocal imaging of biofilms

During this project, we optimised biofilm growth in DMEM-BSA medium which was analysed as described in previous sections. In order to compare biofilm architecture in DMEM-BSA vs X-Vivo15, we utilised confocal microscopy. Biofilms were produced as in Section **2.4.1**. Exponential-phase cultures were seeded in 8-well confocal-compatible

chambers (300 µLwell^{-1}, OD_{600nm} = 0.04, ibidi, 80826) and incubated 16 h at 37 °C, 5% CO_2. Supernatants were aspirated and biofilms fixed for 10 min, 4 °C using 4% PFA in PBS. Following washing 3x in TSB buffer, cell membranes were stained on ice in 100 µLwell^{-1} FM 1-43 FX membrane dye (2 µgmL^{-1} in PBS, Thermo Fisher Scientific, F35355) for 30 min. This, and all proceeding incubation steps were performed in the dark, with 3x washes in TSB between steps. Fc-DC-SIGN (5 µgmL^{-1} in TSB) in 50 µL was added to wells and incubated 2 h, RT. After washing, 100 µL goat anti-human IgG conjugated to Alexa Fluor 647 (10 µgmL^{-1}, in PBS with 3% (v/v) donkey serum, Merck, D9663) was added to wells to visualise lectin binding distribution and incubated for 1 h, 4 °C. Finally, DNA was stained using 100 µL HOECHST (2 µgmL^{-1} in PBS) for 15 min, RT. Samples were stored in 0.1% (w/v) sodium azide in TSB in the dark at 4 °C for imaging. Confocal images were acquired using Zeiss LSM 700 microscope using a 40x /1.2 water objective. Fluorescence emission was collected 405-435 nm (HOECHST), 488-518 nm (FM 1-43 FX membrane dye) and 488-589 nm (Alexa Fluor 647) at a pixel time of 2.55 µs and 2% laser power. Z-stacks presented were in the dimension of x=200 x y=200 x z=60 µM and analysed using Zen Blue and Image J software.

2.4.8 Statistical analysis

All statistical analysis was performed in GraphPad Prism (version 80; San Diego, CA, USA). Significance was calculated by standard t-test or one- or two-way ANOVA. P-value less than 0.05 was considered statistically significant and level of significance is indicated in the figures: ns > 0.05, * <0.05, ** <0.01, *** <0.001 and **** <0.0001. Details of specific statistical tests are included in figure legends.

2.5 Results

2.5.1 Characterisation and growth characteristics of planktonic and biofilm SH1000 and PAO1-P strains in X-Vivo15 medium.

EPS makes up a considerable portion of the biofilm architecture, with *P. aeruginosa* exhibiting one or a combination of three polysaccharides, Pel, Psl and/or alginate depending on the strain (244). For this project, mutants of the strain PAO1 were utilised that overproduced Pel and/or Psl to assess biofilm binding characteristics. Variations in c-di-GMP levels in the cytoplasm directly regulate various pathways, including the *pel* and *psl* operons. In the mutants, c-di-GMP is upregulated due to a Δ*wspF* mutation which promotes biofilm overproduction (238). We utilised these mutants with a range of polysaccharide production profiles in order to determine their relative roles in immune receptor interaction, and later, in whole immune cell responses to biofilms. Before proceeding with assays, mutations in the *pel*, *psl* and *wspF* genes within strains were confirmed by PCR using primers for *wspF*, *pslC/D* and *pelA* (**Table 2.1, Figure 2.1**). In all biofilm overproducing mutants, the *wspF* gene was absent as expected, as well as the combinations of *pel* and *psl* mutations.

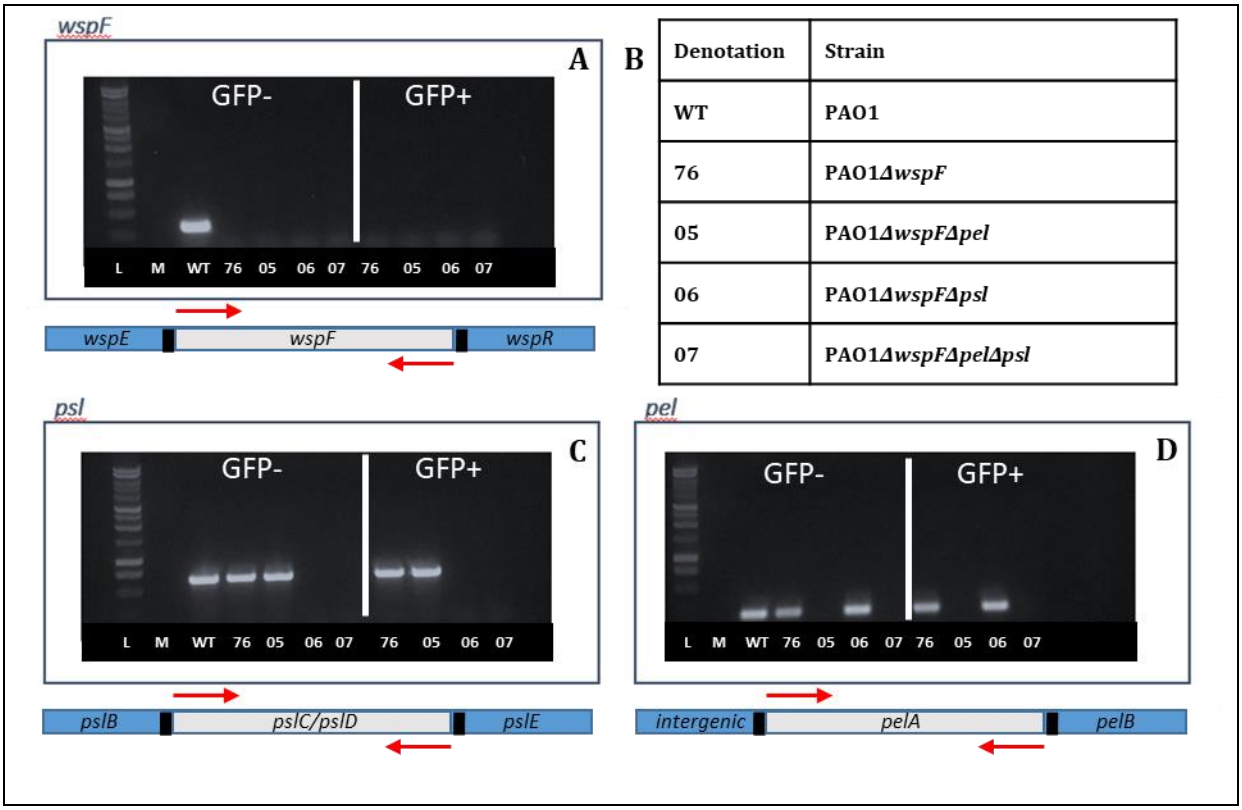

Figure 2. 1: PCRs to confirm correct genetic profiles in mutant strains*. Overnight cultures in X-Vivo15 were produced for relevant strains and 1 µL seeded to 24 µL of PCR master mix (1X GoTaq G2 green master mix 0.1 µM of each forward and reverse primers, nuclease-free water) and PCRs ran for 30 amplification cycles (denaturation 30 s, 95 °C; annealing 30 s, 55 °C; extension 30 s, 72 °C) before gel electrophoresis with 1 kb DNA ladder (L) and media alone (M). Representative images show that only wild-type PAO1 strain contained the wspF gene (**A**) Psl was only present in PAO1 wild-type, PAO1ΔwspF and PAO1ΔwspFΔpel and the GFP-tagged counterparts (**C**), while Pel was present in PAO1 wild-type, PAO1ΔwspF and PAO1ΔwspFΔpsl and the GFP counterparts (**D**) n=3.*

From work conducted previously in the laboratory, the conditions for biofilm growth using PAO1 with its *ΔwspF* mutants was already established, and biofilms generally produced as described in Section **2.4.1**, with various alterations depending on the specific assay. The original route for investigation during this project was to optimise *S. aureus* biofilm growth using these methods, with the ultimate aim to produce polymicrobial biofilms with these species. To determine the characteristics of *S. aureus* SH1000 (345) in relation to PAO1, growth curves were performed to compare the time required to reach mid-log phase from the initial inoculum. Based on the growth curve data, both PAO1 and

the biofilm-deficient PAO1*ΔwspFΔpelΔpsl* strains reached mid-log phase at approximately 3 h in X-Vivo 15 as expected (**Figure 2.2A**). However, SH1000, although reaching stationary phase at a greater cell density, reached mid-log phase slower, at around 5 h (**Figure 2.2A**). Due to this, it was decided that inoculation opacity for *S. aureus* should be increased compared to that of *P. aeruginosa* in order to reach adequate cell density in the same 3 h time-frame. Although not exactly in mid-log phase at this time, a satisfactory proportion of cells will have reached exponential phase by this point for successful biofilm formation.

For biofilm growth, a range of SH1000 OD_{600nm} values between 0.01 and 0.32 were seeded in 100 µL X-Vivo15 into Maxisorp plates and incubated for 24 h before performing Crystal Violet assay for biomass quantification. Biofilm formation was observed at all inoculums, interestingly a trend towards increased biofilm biomass when using lower cell density was observed, with highest variation between replicates occurring at the lower inoculums (**Figure 2.2B**). This inverse effect is potentially due to rapid depletion of resources and higher incidence of cell death due to the relatively small volume and long timeframe. An OD_{600nm} value of 0.04 was selected to remain consistent with PAO1 strains.

Once *S. aureus* biofilm generation was optimised, we aimed to compare growth characteristics between strains and media types. Unlike SH1000, PAO1 strains were unable to produce biofilm in RPMI-1640 (**Figure 2.2C**). This was unsurprising, as were also unable to produce growth curves from planktonic cultures using this medium (data not shown).

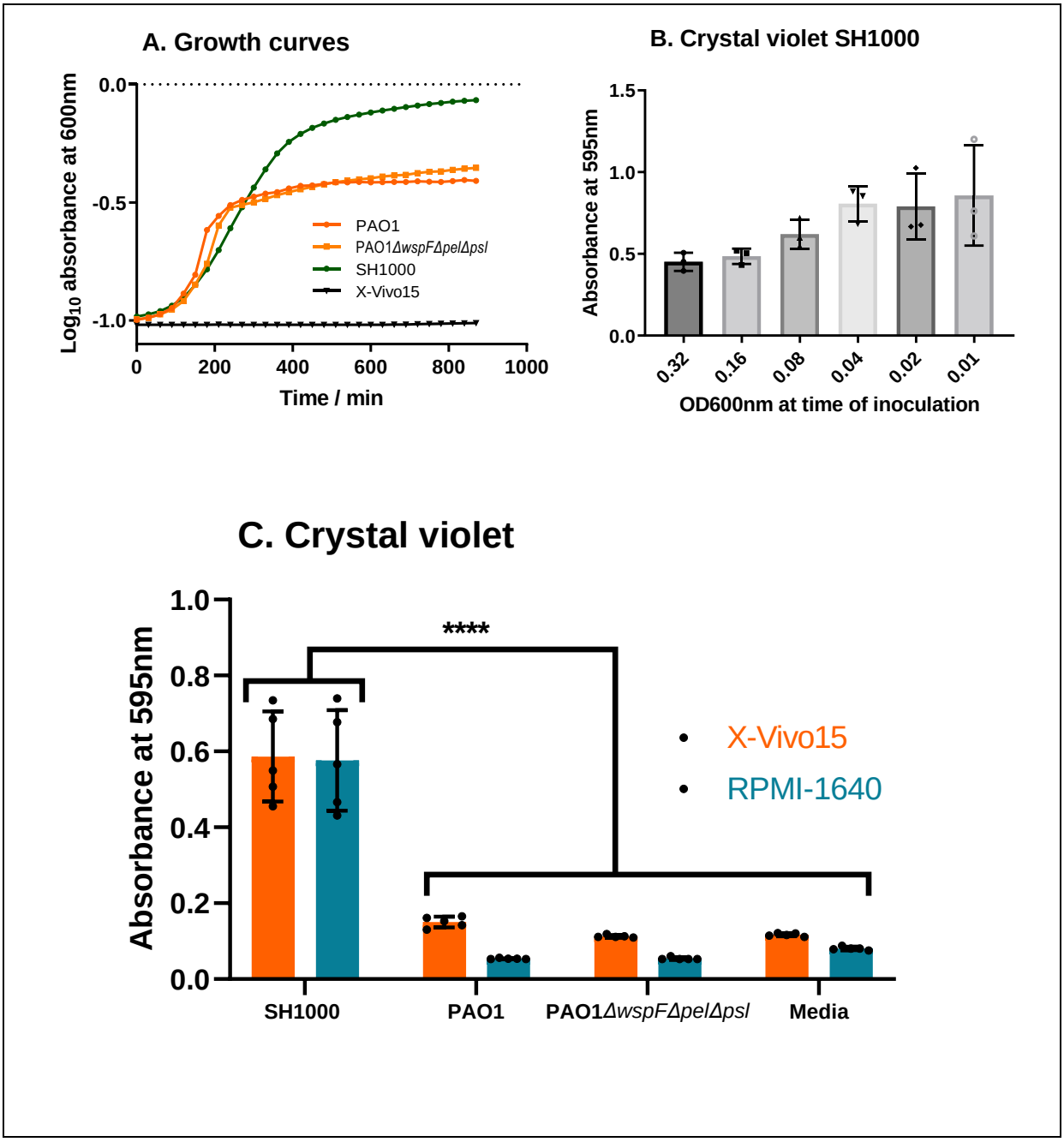

Figure 2. 2: Optimisation of S. aureus growth using established laboratory culture methods. *(**A**) Overnight cultures of PAO1 wild-type, PAO1ΔwspFΔwspFΔpelΔpsl (biofilm deficient) and SH1000 were corrected to an OD_{600nm} of 0.01, seeded to 96-well plates and incubated for 18 h at 37 °C, reading OD_{600nm} at 30 min intervals. SH1000 took 5 h to reach mid-log, while PAO1 strains took 3 h. Panel shows results from the single experiment performed, as this formed the basis for growth conditions going forwards. For following experiments, overnight cultures of SH1000 were corrected to an OD_{600nm} of 0.1 for 3 h culture to reach mid-log phase. SH1000 exponential-phase cultures were corrected to a range of OD_{600nm} values before 24 h incubation and crystal violet analysis to optimise final seeding opacity. Here, 0.04 was chosen as the optimum optical density for biofilm formation (**B**, n=3). Crystal violet analysis was performed to compare biofilms grown in X-Vivo15 and RPMI-1640 (**C**, n=5). SH1000 biomass was significantly higher than both PAO1 strains when analysed by two-way*

ANOVA ($(F_{3,32}) = 148.5$, $p = <0.0001$), but when corrected for multiple comparisons using Šídák's multiple comparisons test, there was no difference in SH1000 growth across media types (p=0.9984). PAO1 growth was not supported by RPMI-1640.

2.5.2 Comparison of binding activity of Fc-conjugated C-type lectin receptors CTLD4-7 (MR), DC-SIGN and Dectin-2 to whole mono-species biofilms grown in X-Vivo15 shows high, significant levels of DC-SIGN binding.

While learning the binding assay protocol during early experiments, it was observed that Fc-DC-SIGN was able to bind X-Vivo15 in an ELISA binding assay. It was important therefore, that when these experiments were repeated for my thesis, that this potential artefact be investigated. The CLRs DC-SIGN, MR CTLD4-7 and Dectin-2 were the key lectins investigated here, as these are the most physiologically relevant due to their expression on a range of immune cells, including DCs (191). In previous experiments, the Fc-chimeric proteins for MR CTLD4-7, Dectin-2 and DC-SIGN were prepared at a concentrations of 2 and 10 μgmL^{-1} and exposed to biofilms formed by PAO1 wild-type as well as the mutant strains lacking the *wspF* gene, responsible for regulating cytoplasmic c-di-GMP concentration, and hence in its overproduction enhancing biofilm overproduction (238). However, as Fc-DC-SIGN bound to X-Vivo15 at 10 μgmL^{-1}, but binding was completely abrogated at 2 μgmL^{-1}, to similar levels to the negative control (**Figure 2.3C**), it was decided therefore, to introduce a concentration, 5 μgmL^{-1}, to determine the critical point for losing background binding. As expected, high levels of binding were observed to $Lewis^X$ and fucose, but not saline or galactose (**Figure 2.3B**). A dose effect of lectin concentrations was clear, and highest levels of binding observed in PAO1*ΔwspF*, corresponding to highest biofilm biomass (**Figure 2.3A, C**). Interestingly, a low level of binding was observed to planktonic bacteria (PAO1*ΔwspFΔpelFΔpsl*), and at high levels to PAO1 wild-type, which both have low to no biomass when measured by crystal violet (**Figure 2.3A, C**). This observation suggests that Fc-DC-SIGN binding does

not correlate directly with crude biomass, but rather smaller fluctuations in proportion of specific ligands that could be present in planktonic cells. Of these, DC-SIGN is an extremely versatile receptor that recognises mannose and fucose- containing structures both host- and pathogen-derived (66, 160).

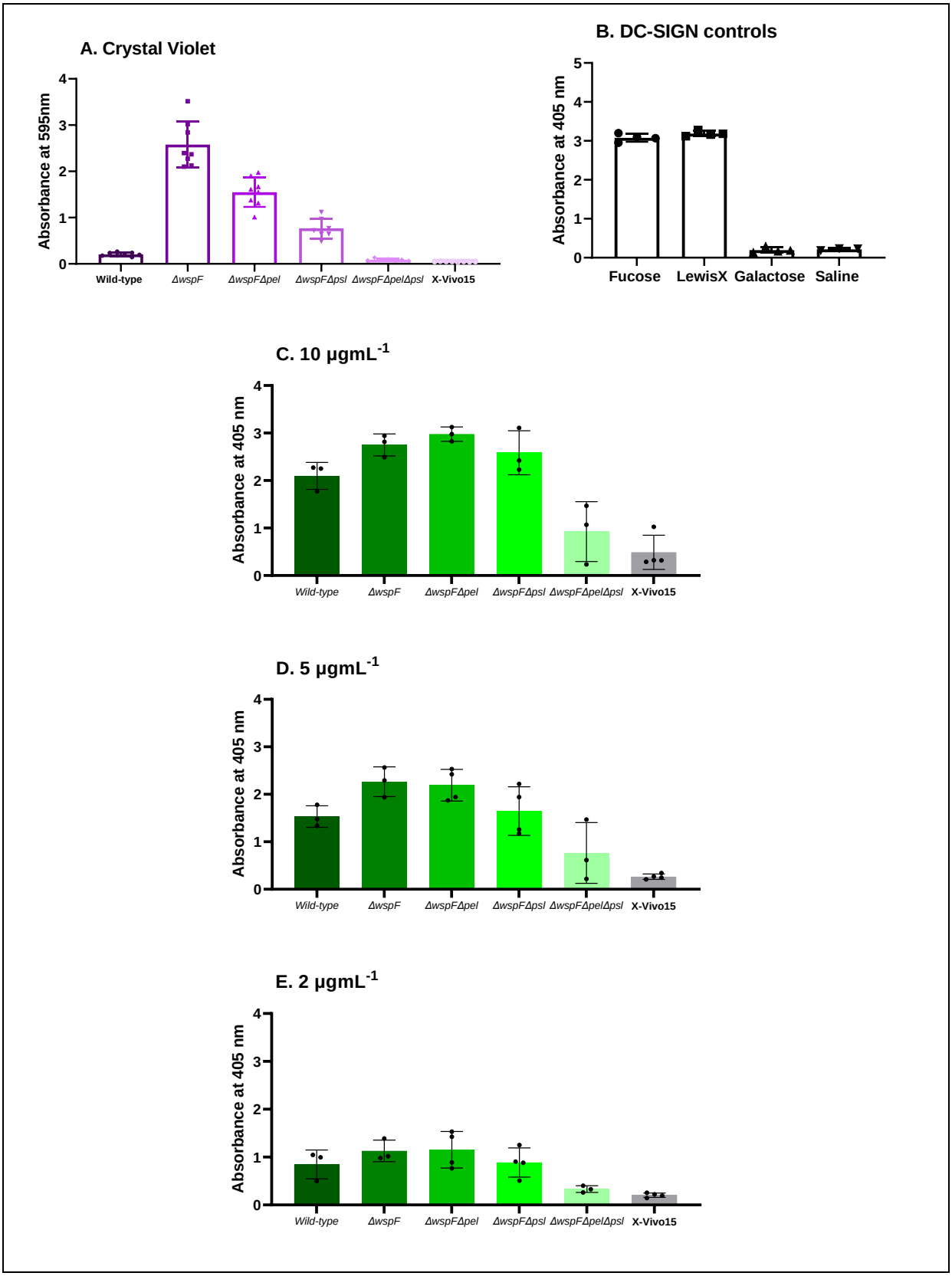

Figure 2. 3: Binding of Fc-DC-SIGN to (C) PAO1 strains and (B) controls. *Biofilms were produced as described in* ***Section 2.4.1*** *alongside relevant sugar controls before fixation and washing. Lectins were prepared at 10, 5 or 2 μgmL^{-1} in TSB buffer and exposed to biofilms and controls for 2 h, before washing and incubation with IgG2 secondary antibody*

*conjugated to alkaline phosphatase. Colour development reagent was added, and absorbance measured at 405 nm. Crystal violet analysis was performed in parallel. Crystal violet analysis showed biofilm biomass consistency across experiments (**A**, n=8). Fc-DC-SIGN bound to positive control sugars fucose and Lewis^X as expected, and not negative controls galactose and saline (**B**). Binding to X-Vivo15 was observed at 10 µgmL^{-1} by Fc-DC-SIGN (**C**), but at no other concentrations, and bound all strains in a dose-dependent manner (**C-E**). Results were analysed using Graphpad Prism 9, and one-way ANOVA showed significant differences in biofilm production between strains at 10 (($F_{5,13}$) = 24.37, p = <0.0001), 5 (($F_{5,15}$) = 15.19, p = <0.0001) and 2 µgmL^{-1} ($F_{5,15}$) = 8.582, p = 0.0005). Secondary antibody alone showed very low levels of binding (n≥3).*

The mannose-specific CTLD4-7-Fc lectin was able to bind fucose but not galactose or Lewis^{X} as described in the literature (136). Further, at both 2 and 10 μgmL^{-1}, CTLD-4-7-Fc bound PAO1*ΔwspF*, reaching significance at 10 μgmL^{-1}, while showing low to undetectable levels for PAO1 wild-type and planktonic PAO1*ΔwspFΔpslΔpel*, in stark contrast to Fc-DC-SIGN (**Figure 2.4A**). Reassuringly, at both concentrations tested, CTLD4-7-Fc did not bind X-Vivo15, showing similar values to the negative controls (**Figure 2.4B**).

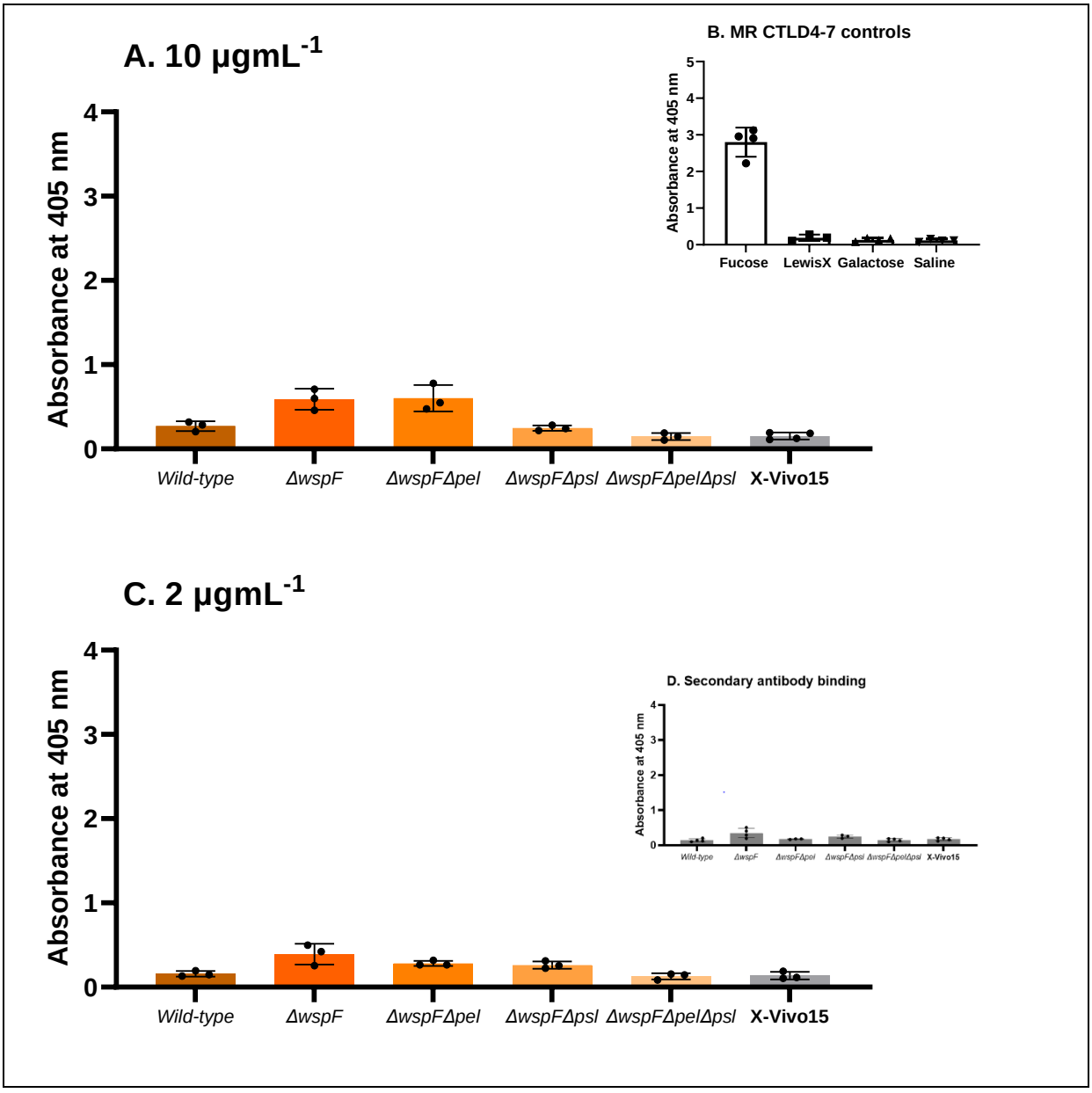

Figure 2. 4: Binding of MR CTLD4-7-Fc to (A, C) PAO1 stains and (B) controls. *Biofilms were produced as described in* ***Section 2.4.1*** *alongside relevant sugar controls before fixation and washing. Lectins were prepared at 10, 5 or 2 µgmL^{-1} in TSB buffer and exposed to biofilms and controls for 2 h, before washing and incubation with IgG2 secondary antibody conjugated to alkaline phosphatase. Colour development reagent was added, and absorbance measured at 405 nm. Crystal violet analysis was performed in parallel (**Figure 2.3**). MR CTLD4-7-Fc bound to positive control sugar fucose as expected, and not negative controls galactose, Lewis^{X} and saline (**B**). Binding to X-Vivo15 was not observed at any concentration tested, but bound biofilms in a dose-dependent manner (**A, C**). Results were analysed using Graphpad Prism 9, and one-way ANOVA showed significant differences in biofilm production between strains at 10 ($(F_{5,13}) = 17.93$, $p = <0.0001$) and 2 µgmL^{-1} ($F_{5,12}$) = 8.566, p = 0.0012). Secondary antibody alone showed very low levels of binding (n≥3).*

Similarly, mouse (m)Dectin-2-Fc also engages high mannose structures. In these experiments, and in work conducted previously (191), HKCa was used in place of Zymosan as a positive control due to its cell wall containing high proportions of mannose-containing polysaccharides (346). However, although mDectin-2-Fc did effectively bind its HKCa control, it was at very low levels (**Figure 2.5B**), perhaps due to the age of samples. Therefore, we elected to switch to Zymosan to properly control concentration for subsequent, as this is widely accepted (152). Here, binding to X-Vivo15 was low for both lectin concentrations, even at 10 μgmL^{-1}, confirming that binding of MR CTLD4-7-Fc and Dectin-2-Fc is much more specific than in Fc-DC-SIGN, and in this case not an artefact of media interaction (**Figure 2.4A, 2.5A, C**). As with CTLD4-7-Fc, the highest binding was observed to PAO1*Δ*wspF*, which decreased in correlation with decreasing biomass of the strains (**Figure 2.5A, C**). However, this did not reach significance, likely due to reduced ligand availability in these biofilms compared to that of Fc-DC-SIGN. For most of these experiments, in order to maintain consistency with previous work in the lab (191), mDectin-2-Fc was used for binding assays (**Figure 2.5A**). In order to make this more clinically relevant, we tested human (h)Dectin-2-Fc under the same conditions as mouse, which produced similar results, even slightly higher in the psl over-producing strains (PAO1*Δ*wspF* and PAO1*Δ*wspFΔpel*) (**Figure 2.5C**). For the Pel over-producer PAO1*Δ*wspFΔpsl*, the signal produced by the secondary antibody control was troublingly high for mouse and human Dectin-2-Fc. This issue was encountered previously in the lab and the reason is unclear but could relate to the biofilm structure of PAO1*Δ*wspFΔpsl* having a slight positive charge due to Pel polysaccharide, more likely to hold on to the negatively-charged phosphate groups of the alkaline phosphatase conjugated to the antibody.

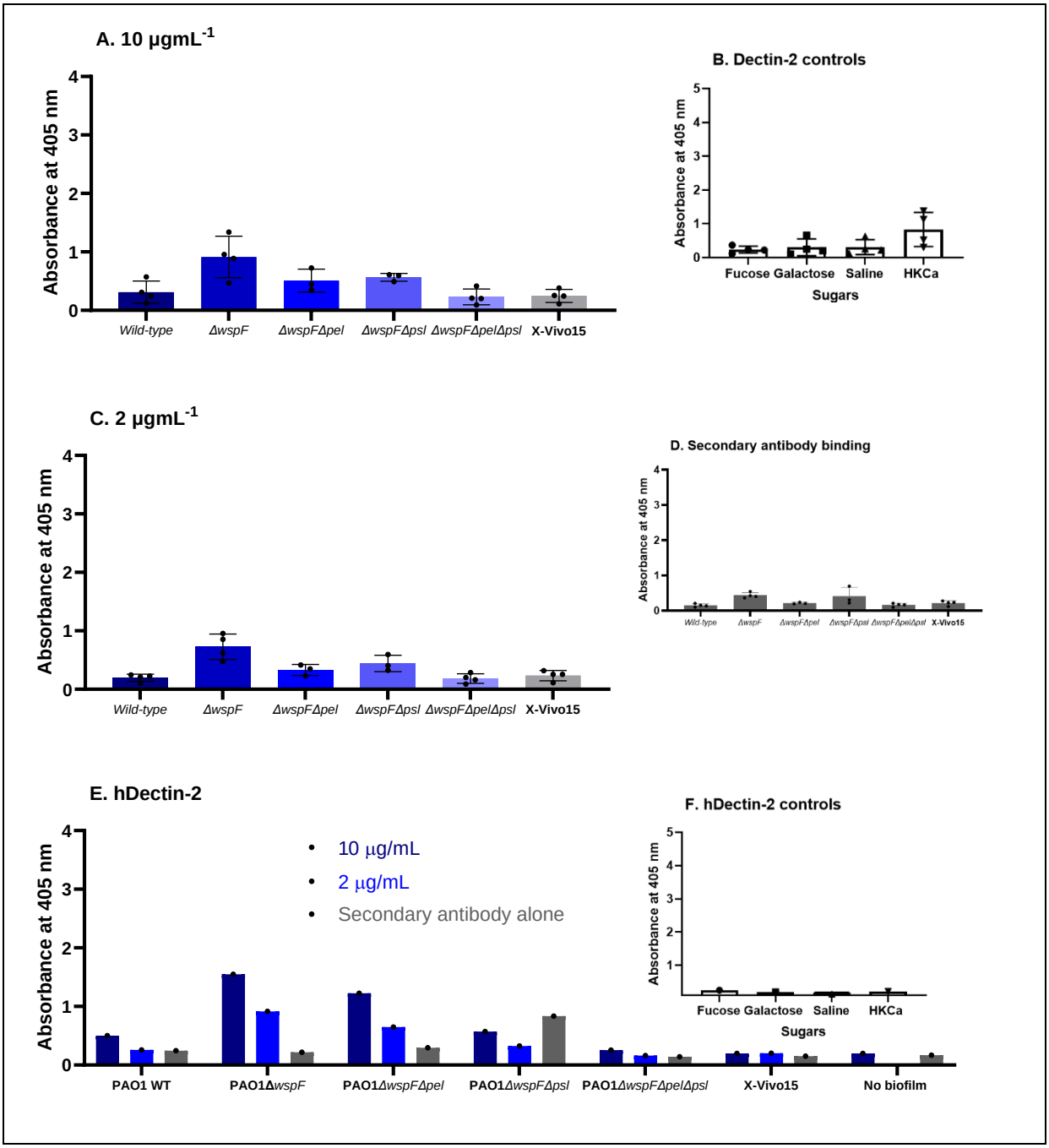

Figure 2. 5: Binding of murine Dectin-2-Fc to (A, C) PAO1 stains and (B, D) controls. *Biofilms were produced as described in* ***Section 2.4.1*** *alongside relevant sugar controls before fixation and washing. Lectins were prepared at 10 and 2 µgmL^{-1} in TSB buffer and exposed to biofilms and controls for 2 h, before washing and incubation with IgG2 secondary antibody conjugated to alkaline phosphatase. Colour development reagent was added and absorbance measured at 405 nm. Binding to X-Vivo15 was not observed. Murine Dectin-2-Fc bound to positive control HKCa as expected, and not negative controls galactose, fucose and saline (**B**). Binding to X-Vivo15 was not observed at any concentration tested, but bound biofilms in a dose-dependent manner (**A, C**). Results were analysed using Graphpad Prism 9, and one-way ANOVA showed significant differences in biofilm production between strains at 10 ($(F_{5,16}) = 6.454$, $p = 0.0018$) and 2 µgmL^{-1} ($F_{5,16}$)*

*= 10.66, p = 0.0001). Secondary antibody alone showed very low levels of binding (n≥3). Human Dectin-2-Fc bound at similar levels to murine, but was unable to bind positive control (**E-F**), n=1.*

However, these experiments were not suitable for testing lectin binding characteristics in *S. aureus*, as most strains of this species produce the virulence factor Protein A, specific for antibody Fc-portions and would hence interfere with the assay (287). Therefore, an alternative approach was to utilise proteins tagged with biotin- or poly-His. From collaborators, we acquired DC-SIGN in its tetrameric form (347), and proceeded to attempt biotinylation. By designing the procedure in accordance with kit guidelines, we were able to collect relevant fractions, with 0.7 mg protein content (70% of the initial amount). From here, we performed a binding assay to control sugars to determine whether biotinylation was successful. Unfortunately, although DC-SIGN-biotin binding was observed to its usual positive controls, it also bound all the negative, including empty wells (data not shown). This observation may be due to over-saturation of the tag to the protein, causing it to over-develop even in negative control wells. In future, when more tetrameric DC-SIGN is acquired from collaborators, we will attempt the biotinylation process again, using a lower ratio of tag:lectin to prevent this.

2.5.3 Comparison of binding activity of biotinylated plant lectins to whole biofilms grown in X-Vivo15 shows high levels of binding to components of X-Vivo15 medium.

Outwith the investigation into biotinylated DC-SIGN, we utilised commercial biotinylated plant lectins of various specificities to investigate their various binding characteristics to biofilms to provide some insight into polysaccharide composition. Of particular interest in the case of *S. aureus* biofilms is the lectin WGA, which binds *N*-acetylglucosamine (GlcNAc), the carbohydrate reported to be present in *S. aureus* biofilms (348). Further, *Dolichos biflorus* agglutinin (DBA), *Ricinus communis* agglutinin (RCA I) and *Glycine max* (soybean) agglutinin (SBA) specifically engage *N*-acetylgalactosamine (GalNAc) ligands, which is of similar structure to GlcNAc (**Figure 2.20**). Per the specificities described in **Table 2.3**, positive controls were selected that were expected to effectively bind the lectins.

Table 2. 3: Plant lectins used to determine biofilm binding characteristics alongside specificities and positive controls.

Lectin	**Ligand**	**Positive control**
Con A	Mannose, glucose	HKCa
DBA	GalNAc	HKCa
PNA	Galactose	Galactose
RCA I	Galactose, GalNAc	Galactose
SBA	GalNAc	HKCa
UEA I	Fucose	Fucose
WGA	GlcNAc	HKCa

Due to the concerns raised in the previous section concerning background binding to X-Vivo15 medium, it was important to control for this. When exposed to the culture medium alone, only DBA, PNA and UEA I showed no background binding, while Con A, WGA, RCA I and SBA all produced high signals (**Figure 2.6A**). Due to the medium being purchased externally, we are uncertain of the exact composition, although it has been confirmed that glucose is present while mannose is not. As it is a rich tissue culture medium, it is likely that many polysaccharides are present, many of which may interact with these lectins. One explanation for this could be that due to biofilm fixation and several washing steps, pure X-Vivo15 no longer remained at the surface of the biofilm, but rather individual components were incorporated into the matrix during its construction, such as glucose, while the PNA ligands were lost. Further, it is difficult to predict the specific ligand within the medium, since as mentioned above the complete composition is not disclosed by the manufacturer, but we may infer that in the case of the biofilms, SBA shows higher specificity to its described ligand GalNAc, unlike DBA, which may show some promiscuity as with DC-SIGN. In contrast to our observations, early studies have reported binding of SBA to both *S. aureus* and *S. epidermidis* clinical isolates, although binding was outcompeted using low concentrations of pure GalNAc (349, 350).

To determine if binding to X-Vivo15 diminished with reduced lectin concentration, Con A was incubated with X-Vivo15 as well as *S. aureus* and *P. aeruginosa* biofilms grown in this medium between 10 and 2 μgmL^{-1} of Con A-biotin. For all conditions tested, binding was not affected by reduction in lectin concentration (**Figure 2.6B**). Therefore, lectins that strongly bound culture medium, were discarded in subsequent experiments.

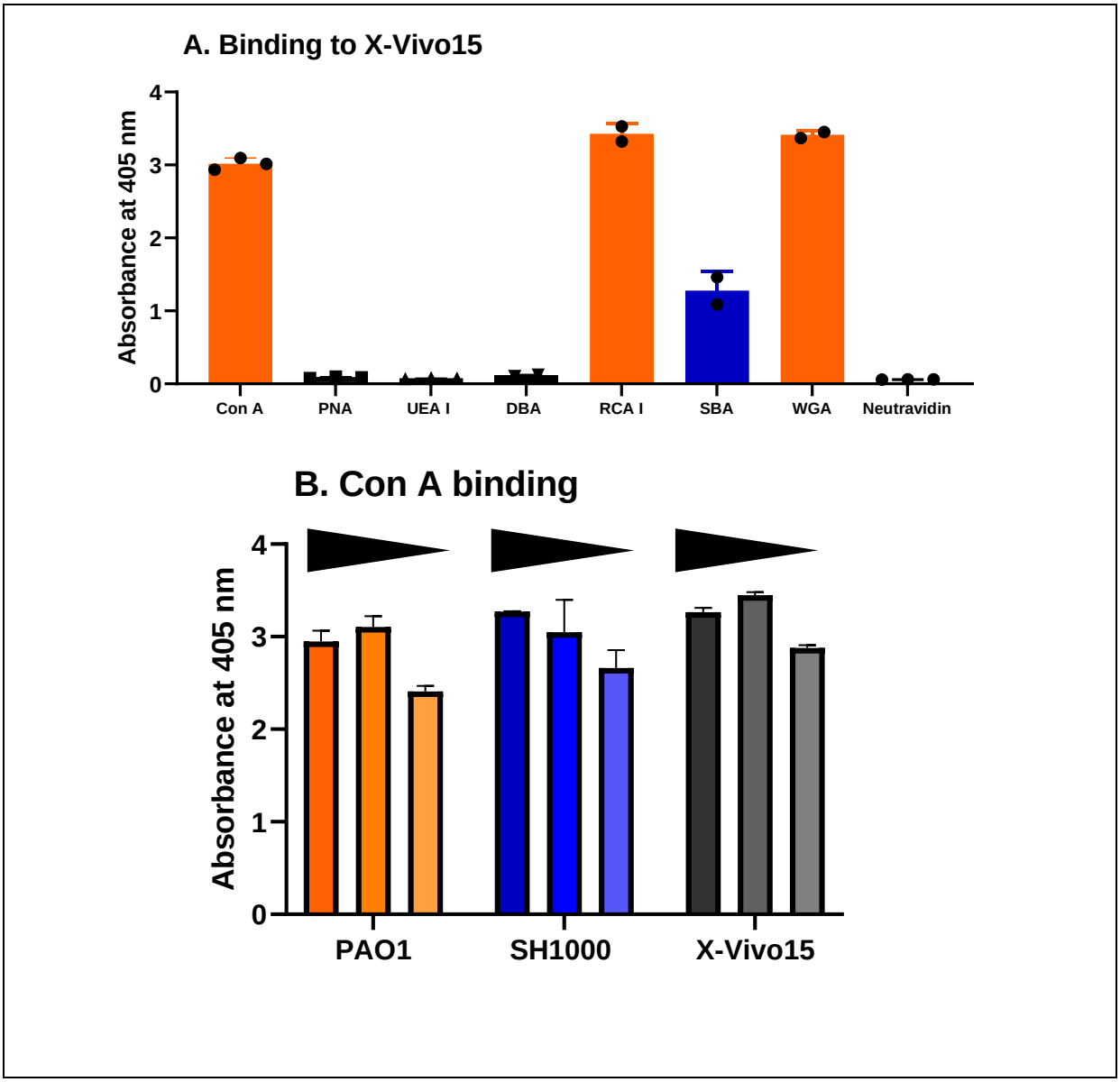

Figure 2. 6: Binding of biotinylated plant lectins to (A) X-Vivo15 and (B) Con A binding to whole biofilms and X-Vivo15*. Biofilms were prepared, fixed and washed in 96-well Maxisorp as described in* ***Figure 3-5****. Lectins were loaded to relevant wells (50 µL, 5 µgmL^{-1}) and incubated for 2 h, followed by 3x washes in TSB. Wells were loaded with Neurtravidin conjugated to alkaline phosphatase (50 µL, 2 µgmL^{-1}) and incubated in the dark for 1 h. Wells were washed 2x in TSB and 1x in AP buffer then colour development reagent was added and absorbance read at 405 nm. RCA I, WGA, and Con A also bound X-Vivo15 culture medium at very high levels compared to biofilms, SBA also bound X-Vivo15, but to a lesser extent (**A,** Con A, UEA I, PNA, DBA, Neutravidin, n=3; RCA I, SBA, WGA, n=2). Con A binding did not decrease in decreasing seeding concentrations (**B,** 5-1 µgmL^{-1}, n=2). Results were analysed using Graphpad Prism 9.*

Going forward, DBA, UEA I, PNA and Con A for reference were tested against their predicted positive controls. Here, Con A and DBA bound their expected HKCa control (**Figure 2.7A**), while UEA I bound fucose (**Figure 2.7B**). Therefore, the data may be considered for interpretation. Interestingly, DBA also bound fucose, impugning the quoted specificity of this lectin from the supplier. This was surprising, as in the literature, fucose has not been described to act as its ligand. We cannot be certain here however that this result was not an artefact, as the two biological replicates were extremely different, with one showing undetectable binding as expected (**Figure 2.7B**). Unfortunately, PNA was unable to bind any of the controls tested (**Figure 2.7C**). Similarly, SBA is also specific to GalNAc yet was unable to bind its control, although it showed some binding to X-Vivo15 alone (**Figure 2.6A, 2.7A**).

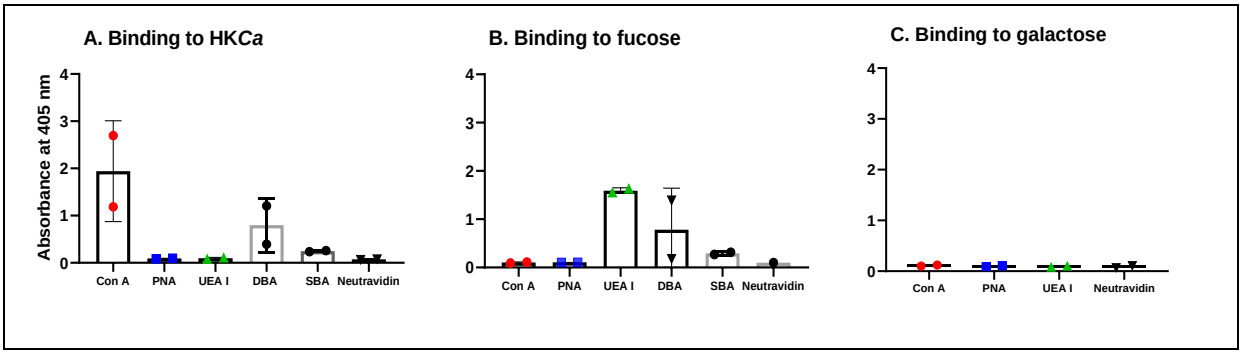

Figure 2. 7: Lectin binding to designated control sugars used for binding experiments. *(**A**) HKCa (2x10⁶ ppm in 50µL saline), (**B**) fucose or (**C**) galactose (each 2 µgmL⁻¹ in 50 µL saline) was loaded to 96-well Maxisorb plates and incubated overnight at 37 °C. After 3x washes in TSB, lectins were loaded to relevant wells (5 µgmL⁻¹ in 50 µL) and incubated for 2 h, followed by 3x washes in TSB. Wells were loaded with Neurtravidin conjugated to alkaline phosphatase (2 µgmL⁻¹ in 50 µL) and incubated in the dark for 1 h. Wells were washed 2x in TSB and 1x in AP buffer then colour development reagent was added and absorbance read at 405 nm. Con A, UEA I and DBA bound expected positive controls, but DBA also bound fucose unexpectedly. PNA did not bind its expected positive control. Neutravidin alone bound no controls tested (n=2). Results were analysed using Graphpad Prism 9.*

Following, PAO1 or SH1000 biofilms were exposed to lectins to gain some insight into carbohydrate composition. Here, PNA also failed to detect ligands in either biofilm (**Figure 2.8**). Regardless, the lack of binding is not unexpected as galactose has not been described as a biofilm-associated polysaccharide in either species (351), and is more associated with biofilms of other species, for example non-pathogenic, soil bacterium *Bacillus subtilis* (352). However, *S. aureus* is able to utilise galactose monomers as a carbon source (353). Further, although UEA I did bind its fucose control, it did not bind to either biofilm, confirming the lack of fucose within the EPS of either biofilm previously described (351, 354). Of greater significance was the interaction of DBA, which specifically bound SH1000 but not PAO1. Although the ligand is specific for GalNAc, the likely ligand here was GlcNAc within the *S. aureus* PIA which has been described previously to be part of the EPS (280). However, there have been previous observations that GalNAc is indeed present in some strains of *S. aureus,* for example the strain ST395, where the CLR macrophage galactose-type lectin (MGL, CD301) is able to engage GalNAc residues in teichoic acid, resulting in increased skin inflammation (211). It is important therefore, that further investigations to determine true polysaccharide composition in this biofilm model, as this may hold clinical significance. This idea is explored in the following section.

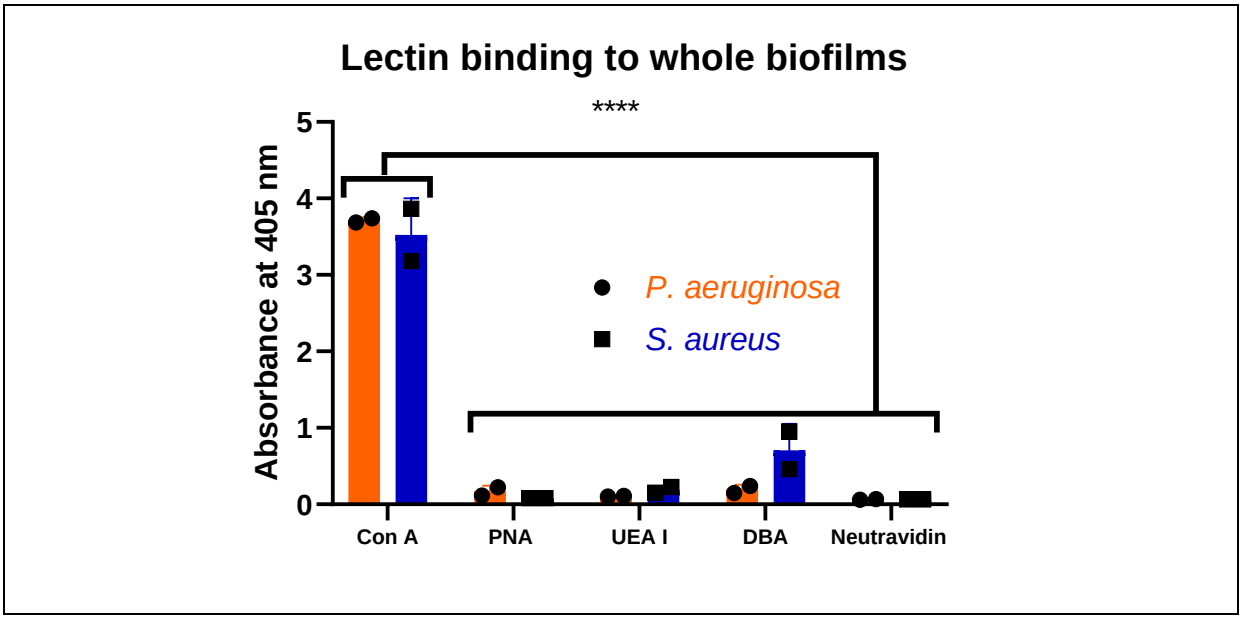

Figure 2. 8: Binding of biotinylated plant lectins to whole biofilms*. Biofilms were prepared, fixed and washed in 96-well Maxisorp as described in* ***Figure 2.3-5****. Lectins were loaded to relevant wells (50 µL, 5 µgmL^{-1}) and incubated for 2 h, followed by 3x washes in TSB. Wells were loaded with Neurtravidin conjugated to alkaline phosphatase (50 µL, 2 µgmL^{-1}) and incubated in the dark for 1 h. Wells were washed 2x in TSB and 1x in AP buffer then colour development reagent was added, and absorbance measured at 405 nm. DBA, Con A and UEA I bound controls as expected, but PNA and SBA did not (****Figure 2.7 A-C, Table 2.1****). PNA was included here however, as it was unable to bind X-Vivo15, unlike SBA . Con A binding to X-Vivo15 was also high, but was included for continuity. Neutravidin alone produced no signal. Using Graphpad Prism 9, two-way ANOVA showed significant differences in biofilm production between lectins (($F_{4,10}$) = 257.5, p = <0.0001), but not between strains (($F_{1,10}$) = 0.5462, p = 0.4769). Šídák's multiple comparisons test concluded that for both species, Con A was able to bind significantly more than all other lectins (p=<0.0001).*

2.5.4 Optimisation of whole biofilm growth in DMEM medium provides better congruity with healthy and diabetic conditions while maintaining significant binding by Fc-DC-SIGN to whole biofilms and binding by plant lectins.

Throughout the previous experiments shown in this chapter, we were able to produce biofilms and characterise them using various lectins to gain some insights into biofilm architecture. However, it could not be ignored that these characteristics are heavily dependent on the environment in which the bacteria grow (355). In both species used, we were able to produce robust and consistent biofilms in X-Vivo15 medium, a rich, tissue culture medium that can support both bacterial and human cells, an important requirement for later experiments. One considerable downside here was that we did not know the complete composition beyond key components including glucose, L-glutamine and phenol red, which vary depending on product. The remaining composition is not disclosed by the manufacturer. This is particularly problematic due to the binding of some receptors, importantly DC-SIGN, to the media alone, as we cannot accurately infer the specific component responsible, or control it. Therefore, it was decided to identify a new culture medium in which we could produce biofilms as well as maintain human immune cells, that provides no inherent ligands for the lectins being investigated.

As *Pseudomonas* and *Staphylococcus spp.* are not particularly fastidious, it was decided to begin with a tissue culture medium in consideration of the immune cells to be used later. Dulbecco's Modified Eagle medium (DMEM) is a well-established culture medium which has a broad array of uses, including growth of neural, immune and muscle cell lines. This medium is also well defined, with a plethora of different formulations available. After a comparison of the different compositions, we proceeded with DMEM-D5921, which

contains most key salts and amino acids, but lacks L-glutamine, calcium carbonate or HEPES (**Figure 2.9**). The advantage here was that while the medium remained minimal, we were able to supplement with relevant components, namely the HEPES buffer and L-glutamine, the latter supplemented, as it is known to degrade over time. Another important factor when determining media was the glucose content. Most media types contain 2 gL^{-1} glucose to ensure a rich carbon source for cells, but is more congruous with diabetic blood glucose levels, rather than normal physiological, between 70 to 140 $mgdL^{-1}$ (356).

	D5546	D5648	D5671	D5796	D5921	D4947	D6046	D6171
	[1×]	[powder]	[1×]	[1×]	[1×]	[1×]	[1×]	[1×]
COMPONENT	g/L	g/L	g/L	g/L	g/L	g/L	g/L	g/L
Inorganic Salts								
$CaCl_2$	0.2	0.2	0.2	0.2	0.265	0.265	0.2	0.265
$Fe(NO_3)_3 \cdot 9H_2O$	0.0001	0.0001	0.0001	0.0001	0.0001	0.0001	0.0001	0.0001
$MgSO_4$	0.09767	0.09767	0.09767	0.09767	0.09767	0.09767	0.09767	0.09767
KCl	0.4	0.4	0.4	0.4	0.4	0.4	0.4	0.4
$NaHCO_3$	3.7	—	3.7	3.7	3.7	3.7	3.7	3.7
NaCl	6.4	6.4	6.4	6.4	6.4	6.4	6.4	4.4
NaH_2PO_4	0.109	0.109	0.109	0.109	0.109	0.109	0.109	0.109
Amino Acids								
L-Alanyl-L-Glutamine	—	—	—	—	—	—	—	—
L-Arginine • HCl	0.084	0.084	0.084	0.084	0.084	0.084	0.084	0.084
L-Cystine • 2HCl	0.0626	0.0626	0.0626	0.0626	0.0626	0.0626	0.0626	0.0626
L-Glutamine	—	0.584	—	0.584	—	0.584	0.584	—
Glycine	0.03	0.03	0.03	0.03	0.03	0.03	0.03	0.03
L-Histidine • HCl • H_2O	0.042	0.042	0.042	0.042	0.042	0.042	0.042	0.042
L-Isoleucine	0.105	0.105	0.105	0.105	0.105	0.105	0.105	0.105
L-Leucine	0.105	0.105	0.105	0.105	0.105	0.105	0.105	0.105
L-Lysine • HCl	0.146	0.146	0.146	0.146	0.146	0.146	0.146	0.146
L-Methionine	0.03	0.03	0.03	0.03	0.03	0.03	0.03	0.03
L-Phenylalanine	0.066	0.066	0.066	0.066	0.066	0.066	0.066	0.066
L-Serine	0.042	0.042	0.042	0.042	0.042	0.042	0.042	0.042
L-Threonine	0.095	0.095	0.095	0.095	0.095	0.095	0.095	0.095
L-Tryptophan	0.016	0.016	0.016	0.016	0.016	0.016	0.016	0.016
L-Tyrosine • 2Na • $2H_2O$	0.10379	0.10379	0.10379	0.10379	0.12037	0.12037	0.10379	0.10379
L-Valine	0.094	0.094	0.094	0.094	0.094	0.094	0.094	0.094
Vitamins								
Choline Chloride	0.004	0.004	0.004	0.004	0.004	0.004	0.004	0.004
Folic Acid	0.004	0.004	0.004	0.004	0.004	0.004	0.004	0.004
myo-Inositol	0.0072	0.0072	0.0072	0.0072	0.0072	0.0072	0.0072	0.0072
Niacinamide	0.004	0.004	0.004	0.004	0.004	0.004	0.004	0.004
D-Pantothenic Acid • ½Ca	0.004	0.004	0.004	0.004	0.004	0.004	0.004	0.004
Pyridoxal • HCl	—	0.004	—	—	—	—	—	—
Pyridoxine • HCl	0.00404	—	0.00404	0.00404	0.00404	0.00404	0.00404	0.00404
Riboflavin	0.0004	0.0004	0.0004	0.0004	0.0004	0.0004	0.0004	0.0004
Thiamine • HCl	0.004	0.004	0.004	0.004	0.004	0.004	0.004	0.004
Other								
D-Glucose	1.0	4.5	4.5	4.5	1.0	1.0	1.0	4.5
HEPES	—	—	—	—	—	—	—	5.958
Phenol Red • Na	0.0159	0.0159	0.0159	0.0159	—	—	0.0159	0.0159
Pyruvic Acid • Na	0.11	—	—	—	—	—	0.11	—
ADD								
Glucose	—	—	—	—	—	—	—	—
L-Glutamine	0.584	—	0.584	—	0.584	—	—	0.584
$NaHCO_3$	—	3.7	—	—	—	—	—	—

Figure 2. 9: Composition of DMEM-D5921 (red) as described by manufacturer, Sigma-Aldrich.

We selected DMEM-D5921 as it contains a physiological glucose level and allows us to alter it down the line to compare normal to diabetic conditions. On seeding bacterial colonies however, this medium was not able to support planktonic growth. To remedy this, the media was further supplemented with 5% (w/v) bovine serum albumin (BSA). Interestingly, it has been previously described that although BSA inhibits homoserine lactone quorum signalling in *P. aeruginosa in vitro*, growth was still supported. Further, during this study, inhibition of this signalling by *P. aeruginosa* reduced killing of *S. aureus in vitro*, promoting its growth in co-culture (357). Here, *P. aeruginosa* was able to produce planktonic cultures in DMEM-5% BSA, but interestingly not *S. aureus* (**Figure 2.10**). Going forward, experiments continued with *P. aeruginosa* alone.

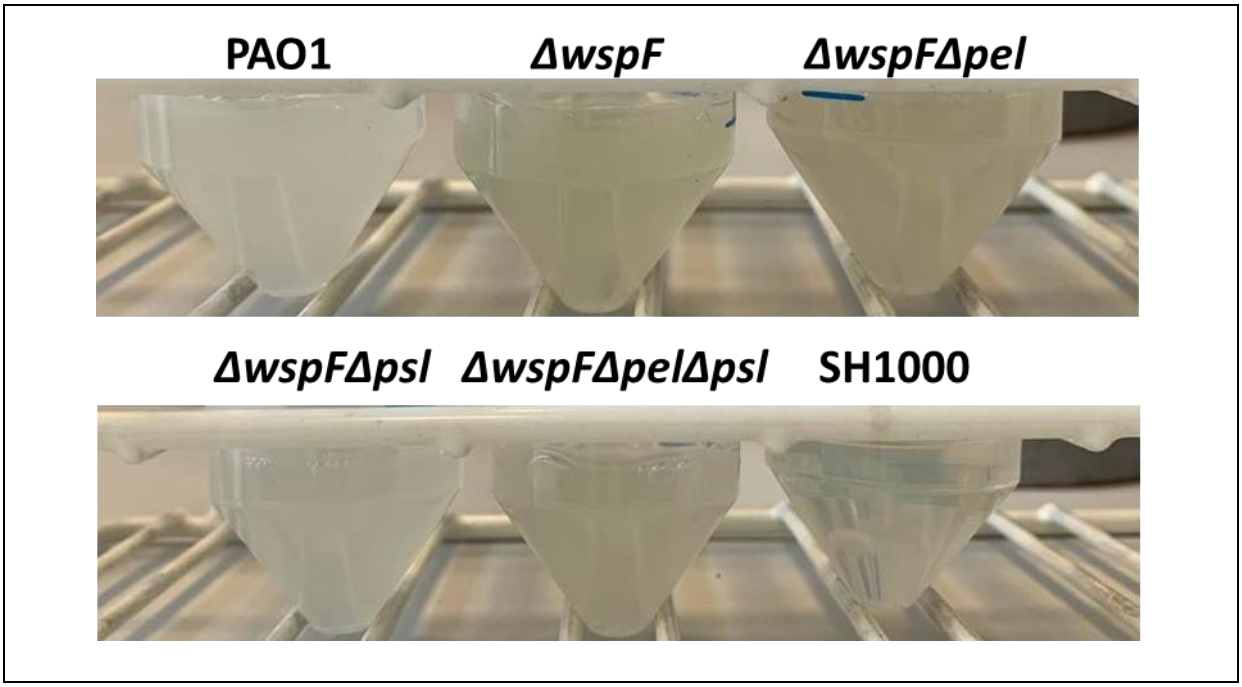

Figure 2. 10: Planktonic growth of P. aeruginosa PAO1 is supported in DMEM-BSA, but not S. aureus SH1000. *Overnight cultures were produced in DMEM-BSA and incubated overnight at 37 °C, 200 rpm. All cultures were opaque, indicating bacterial growth, except S. aureus SH1000 (bottom right).*

Crystal violet assays illustrated that as shown previously, PAO1 wild-type and the biofilm non-producer PAO1Δ*wspF*Δ*pel*Δ*psl* exhibit very little biofilm biomass when cultured in DMEM-5%BSA, while PAO1Δ*wspF* produced the most biofilm under these conditions, comparable to that in X-Vivo15 (**Figure 2.11**). PAO1Δ*wspF*Δ*pel* biofilms showed comparable biomass to PAO1Δ*wspF*, but greater than its equivalent grown in X-Vivo15. Interestingly, PAO1Δ*wspF*Δ*psl* failed to significantly produce detectable biofilm biomass, although when compared to this strain produced in X-Vivo15, there was no significant difference.

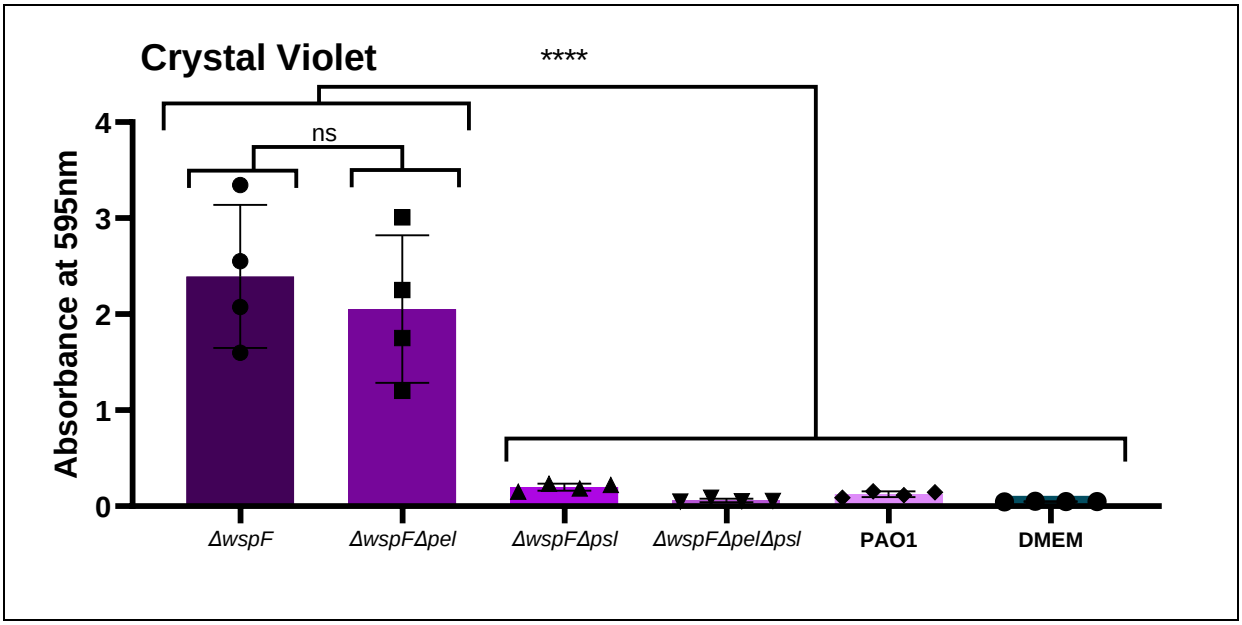

Figure 2. 11: P. aeruginosa biofilms produced in DMEM-BSA have divergent biomass characteristics to those grown in X-Vivo15. *Biofilms were produced as described in Section* ***2.4.1*** *and crystal violet analysis was performed alongside binding assays. Biofilms were comparable to X-Vivo15 for PAO1, ΔwspF and ΔwspFΔpelΔpsl. Biomass was higher than X-Vivo15 for ΔwspFΔpel, but lower for ΔwspFΔpsl. Stars denote significant biofilm production in comparison to media alone. (**D**, n=4). Using Graphpad Prism 9, one-way ANOVA showed significant differences in biofilm production between strains ($(F_{5,18}) = 25.23$, p = <0.0001). Tukey's multiple comparisons test concluded PAO1ΔwspF and PAO1ΔwspFΔpel had significantly more biomass than all other strains (p=<0.0001), but not to each other (p=0.8757).*

When binding assays were performed, there were consistently lower signals for all CLRs tested, particularly apparent in PAO1*ΔwspF* and PAO1*ΔwspFΔpel,* where biomass was almost identical to that of X-Vivo15 biofilms, supporting the assumption that specific composition has changed between these two biofilms (**Figure 2.12**). For MR CTLD4-7-Fc binding was low to undetectable for all strains except PAO1*ΔwspFΔpsl,* although here, secondary antibody negative control was equivalent to tested lectin concentrations, so discredits this observation (**Figure 2.12B**). In contrast, for both Dectin-2-Fc and Fc-DC-SIGN, binding remained similar for most strains, with the striking exception of PAO1*ΔwspFΔpsl,* which showed comparable binding to PAO1*ΔwspF*, despite the fact that biofilm was almost undetectable in relation to biomass, further showing that these biofilms present new mannose-containing ligands within the EPS (**Figures 2.12A, C**). In addition, Fc-DC-SIGN did not significantly bind to PAO1 wild-type grown in DMEM-BSA (**Figure 2.12A**). In these conditions, the lack of Psl in the PAO1*ΔwspFΔpsl* strain may have triggered over-compensation in some other biofilm component, mostly likely Pel, but perhaps some other polysaccharide not yet described. In order to identify this ligand, it would be beneficial to biochemically characterise purified carbohydrates from biofilms grown under these conditions, which will be the focus of the next chapter.

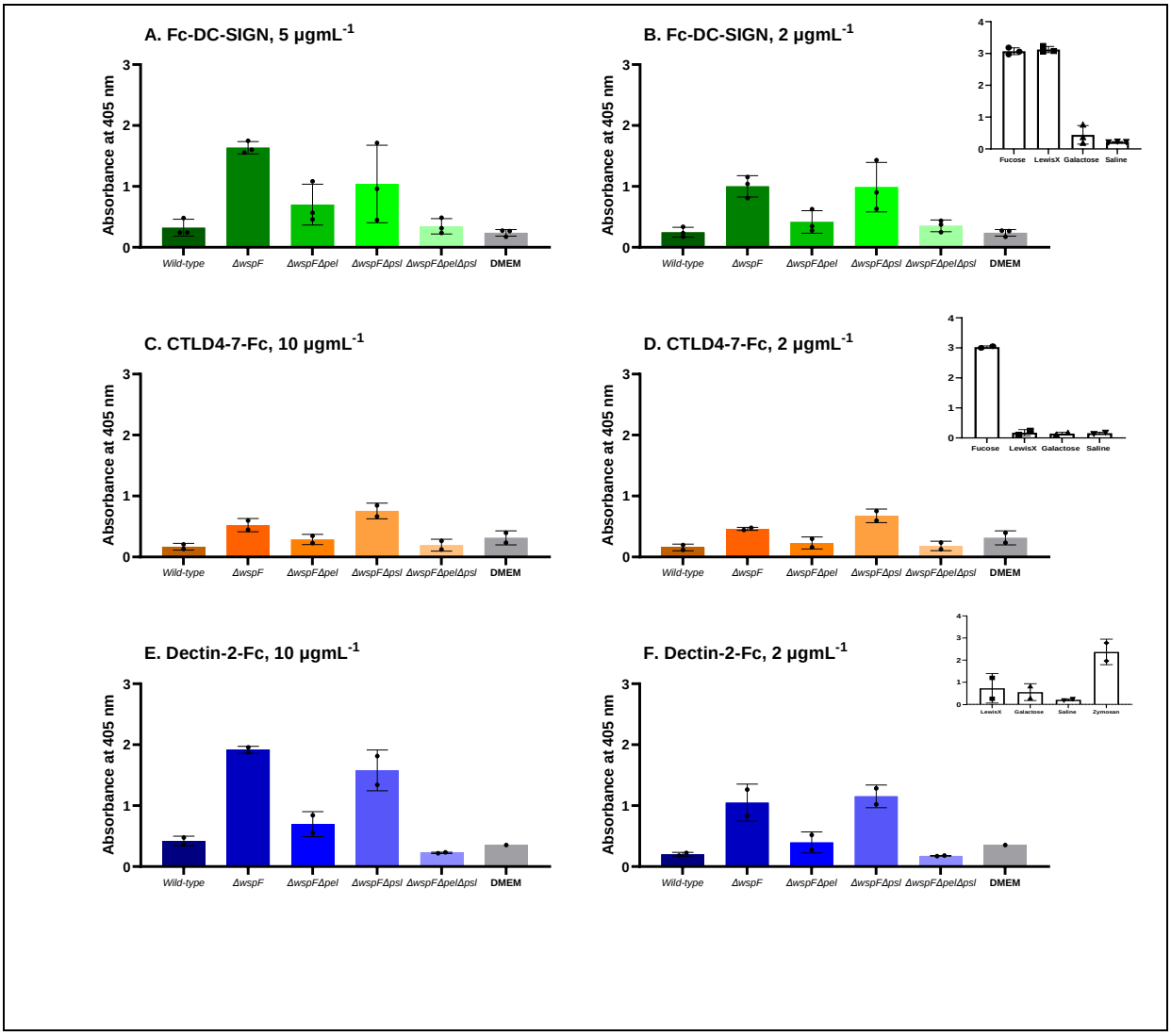

Figure 2. 12: Binding of (A-B) Fc-DC-SIGN, (C-D) MR CTLD4-7-Fc and (E-F) Dectin-2-Fc to PAO1 biofilms grown in DMEM-BSA alongside control polysaccharides. *Biofilms were produced as described in* ***Figures 2.3-5*** *alongside relevant sugar and media controls before fixation and washing. Lectins were prepared at 10, 5 or 2 µgmL^{-1} in TSB buffer and exposed to biofilms and controls (10 µgmL^{-1} only) for 2 h, before washing and incubation with IgG2 secondary antibody conjugated to alkaline phosphatase. Colour development reagent was added and absorbance measured at 405 nm. Secondary antibody alone showed very low levels of binding. (DC-SIGN, n=3; MR CTLD4-7 and hDectin-2 n=2). Results were analysed using Graphpad Prism 9 and one-way ANOVA. For Fc-DC-SIGN, significant differences in biofilm production between strains was observed at 5 (($F_{5,12}$) = 9.366, p = 0.0008) and 2 µgmL^{-1} ($F_{5,12}$) = 9.289, p = 0.0008). For CTLD4-7-Fc, significant differences in biofilm production between strains was observed at 10 (($F_{5,6}$) = 9.924, p = 0.0073) and 2 µgmL^{-1} ($F_{5,6}$) = 10.61, p = 0.0061). For Dectin-2-Fc, significant differences in biofilm production between strains was observed at 10 (($F_{5,5}$) = 28.93, p = 0.0011) and 2 µgmL^{-1} ($F_{5,5}$) = 11.59, p = 0.0089). Secondary antibody alone showed very low levels of binding in all experiments.*

2.5.5 Visualisation of DC-SIGN ligands in 2D biofilms generated in DMEM-BSA using confocal microscopy.

As discussed earlier, previous work in the lab focused on characterising CLR binding patterns using confocal microscopy, visualising ligand clusters within the 3D biofilm architecture (191). Here, biofilms were produced in static or flow conditions before visualising ligands for CLRs of interest, cell membranes and DNA, giving us an idea of their distributions. We were interested therefore, in repeating this process with biofilms produced in DMEM-5%BSA as in the previous section to identify any changes in the structure, especially considering the differences in overall binding levels for the three lectins tested (**Figure 2.12**). The growth protocol was adapted for confocal-compatible wells, and 16 h biofilms of the PAO1 wild-type produced in both X-Vivo15 and DMEM-BSA were incubated with Fc-DC-SIGN and staining for DNA and cell membranes.

During this experiment, DMEM-BSA biofilms produced mushroom-shaped protrusions similar to that of X-Vivo15 biofilms (**Figure 2.13**). Protrusions tended to be smoother overall however, with a less prominent dip in the structure in the X-Vivo15 biofilms (**Figure 2.13A** – arrow). Further, in DMEM-BSA biofilms, eDNA distribution appears much more extensive than in X-Vivo15 biofilms, completely saturating the upper surface of the mushroom-structure (**Figure 2.13B** - blue). Bacterial cells also showed differences in distribution, as in X-Vivo15, cell distribution appeared compact and organised around the mushroom structure (**Figure 2.13A** - green), while in DMEM-BSA, bacteria seemed to be more disorganised, showing fringed distribution some distance from the main structure (**Figure 2.13B** – green).

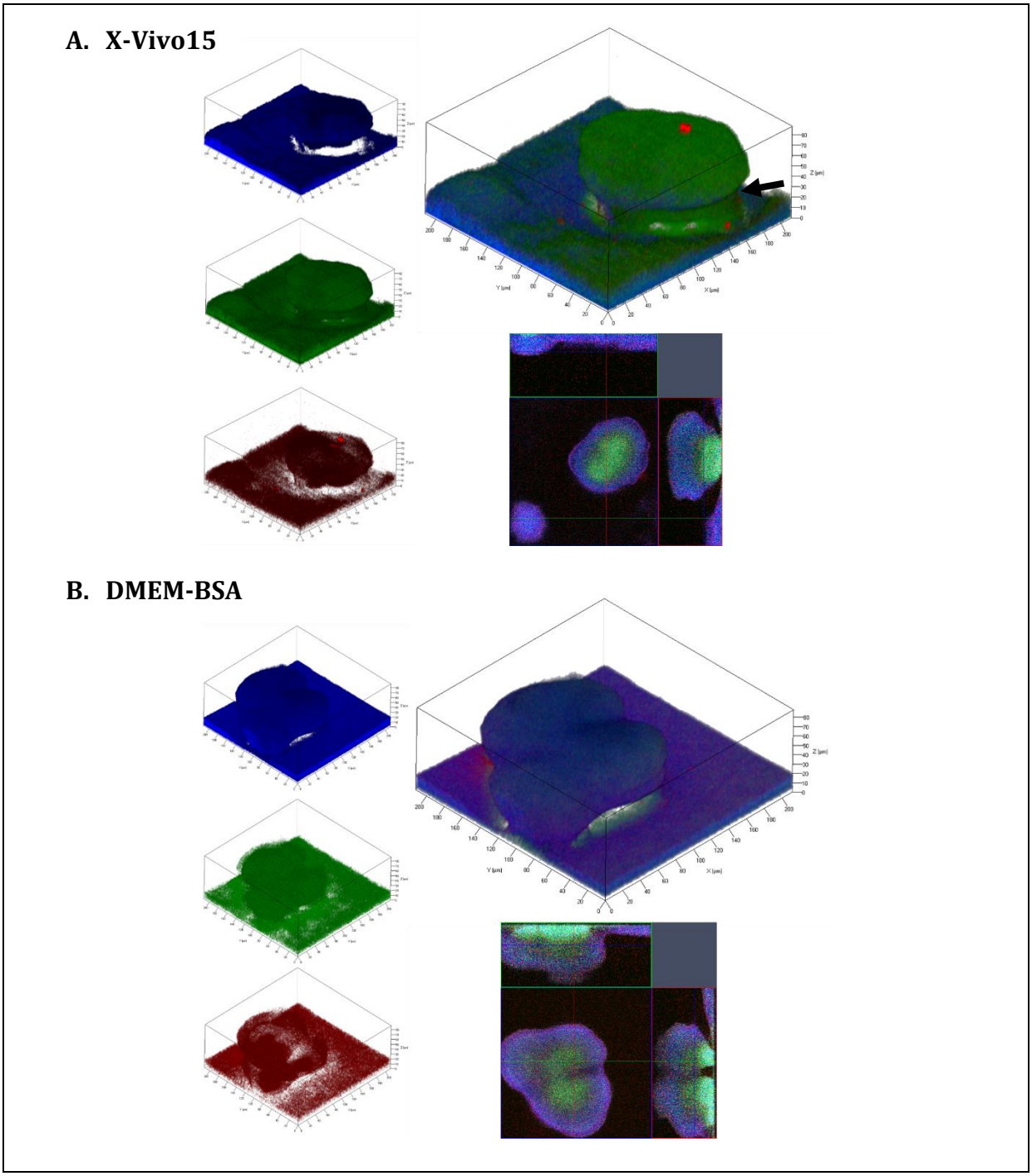

Figure 2. 13: Confocal imaging of biofilms produced in (A) X-Vivo15 and (B) DMEM-BSA shows similar biofilm architecture. *Biofilms were produced for 16 h as described in Section 2.4.1 in µ-Slide VI 0.4 slides before staining with HOECHST (blue), FM 1-43X FX membrane dye (green) and Alexa Fluor 647 (red) bound to Fc-DC-SIGN before imagining and Z-stack construction using a Zeiss LSM 700 microscope using a 40x /1.2 water objective. Images were analysed using Zen Blue and Image J software. Biofilms showed mushroom-like protrusions in both conditions, but in X-Vivo15, eDNA and DC-SIGN distribution was more extensive (**A**). In DMEM-BSA, bacterial cells were less compact around the structure and showed spreading around the periphery (**B**) and had less prominent shelf structures (**B** – arrow).*

Finally, DC-SIGN binding appeared similarly spatially distributed in both biofilms (**Figure 2.12** – red), although to a much greater extent in X-Vivo15 biofilms. When overlays are shown without eDNA (blue), DC-SIGN binding is clearer (**Figure 2.13**). Here, biofilms grown in X-Vivo15 show multiple large clusters of DC-SIGN throughout the structure, while in DMEM-BSA, DC-SIGN seems to cluster around the base of the mushroom structure.

2.6 Discussion and future work

During this chapter, we formed several conclusions. Firstly, that it is possible to work with multiple species within the context of our established biofilm model, although each species must be carefully optimised depending on their growth characteristics (**Figure 2.2**). Further, on production of biofilms, we were able to infer characteristics of the EPS architecture via the binding of Fc- and biotin-conjugated lectins of various specificity, primarily indicating the presence of high-mannose structures (**Figures 2.3, 2.5**). Finally, that when altering the environmental conditions, overall binding of Fc-DC-SIGN, MR CTLD4-7-Fc and Dectin-2-Fc also changes, indicating alterations in EPS composition, although distribution of Fc-DC-SIGN remains consistent with that in X-Vivo15 when visualised using confocal (**Figure 2.7-8**). Combining this information, the key message we may infer, is that biofilm production is both robust and highly plastic, producing carbohydrates that differentially interact with lectin receptors which may lead to differences in immune response within the host.

Throughout the overarching biofilm project in the lab, *ΔwspF* mutants of PAO1 have been utilised, characterised by increased cytosolic levels of c-di-GMP, combined with controlled combinations of Pel and Psl carbohydrate (238, 258, 343, 344). The result of these mutations is the overproduction of biofilm (with the exception of PAO1*ΔwspFΔpelΔpsl*) which allows us to focus on these specific carbohydrates during binding ELISAs and other immunological assays, to determine their role in immune modulation (238). However, there is some dispute in the integrity of these strains, as we are relying on the assumption that the only significant consequence of increased cdiGMP levels is the overproduction of biofilm products. Within the cell, proteins encoded by *wspF* and *wspR* act as antagonists for cdiGMP production, so on either knockout, cdiGMP

is able to go unchecked (238). In nature, cdiGMP regulation by these proteins is controlled upstream by diguanylate cyclase (DCG) and phosphodiesterase (PDE) proteins in a chemosensory-like signalling system, where cdiGMP levels are fine-tuned depending on the environmental niche, regulating virulence and early biofilm development (358). Namely, 39 genes were identified with a DCG or PDE binding-domain during a systematic, whole-genome sequence of *P. aeruginosa* PAO1 and PA14 that on validation directly influenced cdiGMP levels either locally or globally within the cell, resulting in hyper-biofilm pellicle formation and disruption to type-three secretion system and type IV pili production and reduction (359). Interestingly, mutations in these genes did not significantly affect survival during murine infection. Similarly, during a longitudinal study of *P. aeruginosa* colonisation in the cystic fibrosis lung, various isolates with *wspF* mutations were identified, resulting in increased cdiGMP, which may promote bacterial persistence but were not clearly associated with any specific increase in morbidity (360, 361). This is relevant however, as it proves that this mutation is not strictly artificial, but is manifesting *in vivo* during these types of chronic infection. It is important to note for this project, that there has been no indication in the literature that fluctuations in cdiGMP and biofilm production result in changes to the specific structure of Pel or Psl carbohydrate. Both in this and the following chapter, the key focus is on the interactions with specific carbohydrate ligands that appear within biofilm EPS, and hence the effect on other virulence factors should be inconsequential, with any exceptions explored individually in this section. For later assays, when immune cells were incorporated to the biofilm model, we negated this risk by adopting the wild-type *P. aeruginosa* strain PAO1, with the aim of progressing to mixed-species and clinical isolates in the future.

During binding assays to *P. aeruginosa* biofilms in X-Vivo 15, one consistent observation was the robust binding of DC-SIGN, to a much greater extent than the other CLRs tested, MR CTLD4-7 and Dectin-2 (**Figure 2.3**). This was also observed in previous work conducted in the lab, where DC-SIGN ligands were distributed broadly with punctate clusters both within biofilm matrix as well as bacterial aggregates, perhaps engaging with individual bacterial cells expressing CPA LPS required for binding (186, 191). Generally, binding of MR and Dectin-2 was lower than that of DC-SIGN in these biofilms, perhaps due to slight differences in their specificity, avidity and accessibility, in contrast to confocal analysis of biofilms grown in flow-conditions where Dectin-2 showed more robust binding than MR (191). Biofilms are complex by nature, so for these highly specific lectins, various other components such as eDNA, proteins and other fragments may provide some steric hindrance, preventing effective binding. In contrast, DC-SIGN is relatively broad in its binding specificity, and may show a certain level of promiscuity with its ligands within the biofilms (362). In addition, the experimental conditions may have played a role in comparative binding of the lectins. Biofilms do incorporate carbohydrates into their 3D matrix, but considerable amounts are also secreted into the surrounding aqueous fraction, which during this assay would be lost during numerous washing steps. This being the case, the lower levels of binding by MR CTLD4-7 and Dectin-2 may be due to a preference for the secreted carbohydrates which are not represented in the final readings.

In addition, biofilms produce several secreted products that may compete for ligands of MR and Dectin-2. Namely, the lectins CdrA and LecB are produced by *P. aeruginosa* and are instrumental in biofilm formation by interacting directly with mannose-structures in Psl to reinforce the 3D structure and overall integrity of the biofilm (259, 261, 363). In

future work, it will be interesting to purify and characterise these *Pseudomonas*-secreted lectins, perhaps in competition with the human CLRs that we have explored here to compare affinity with known ligands, whole biofilms and biofilm carbohydrates. In performing this work, we may be able to validate this suggestion. We know from work discussed later in this thesis that purified biofilm carbohydrate is able to displace known ligands for these three lectins, but at relatively high concentrations, particularly with Dectin-2, which highlights the idea that these binding pockets are highly dynamic, and hence switching of ligands between receptors may occur readily.

To incorporate *S. aureus* into these analyses, we attempted to biotinylated purified tetrameric DC-SIGN to assess binding without the risk of secreted Protein A influencing the results by binding and blocking the Fc-portion of our lectins. We were interested in this line of investigation for two main reasons, (i) to compare binding capabilities of Fc-chimeric c vs tetrameric DC-SIGN and (ii), to compare DC-SIGN interactions between *S. aureus* and *P. aeruginosa*. In nature, DC-SIGN exists as a homo-tetramer, which lends to its binding promiscuity and broad range of ligands, including both pathogen- and self-antigens (364, 365). Although these proteins show good levels of binding (**Figure 2.3-5**), it is difficult to accurately infer how the receptor will behave in the tetramer form, as we do not know the proportions at which binding avidity will increase, if at all. In the case of Fc-DC-SIGN, although marketed as a monomer, due to the protein neck region the recombinant proteins likely arrange as dimers or higher level polymers in solution. However, this native form of DC-SIGN is not readily available commercially, and expressing and purifying a correct form of the tetramer in-house was not possible for our laboratory. However, tetrameric DC-SIGN interactions with blood group antigens have been solved via NMR, interestingly showing that the receptor can directly bind αGalNAc

moieties, albeit weakly, lending to potential interactions with *S. aureus* biofilms (347). This laboratory kindly donated some of their unlabelled protein to us, which we endeavoured to conjugate with biotin using an established kit protocol. Unfortunately, binding was exceptionally high in all conditions tested, including negative controls, indicating that the protein was over-saturated and hence 'sticky,' showing no specificity. We have yet to obtain more of this protein from our collaborators, but work will commence at the earliest opportunity for this investigation.

In relation to point (ii) above, plant lectins were utilised to begin analysis of *S. aureus* biofilms. As discussed in Section **2.5**, controls were selected per their specificities as described in the literature. HKCa is comprised of the whole fungal organism, the cell wall of which is complex and contains polymers of GlcNAc, β-(1-3)-and β-(1-6)-glucans, which should facilitate binding of *Triticum vulgaris* (wheat germ) agglutinin (WGA) and Concanavalin A (Con A) (366). We also expected that GalNAc-specific lectins would bind HKCa due to its similar structure to GlcNAc (**Figure 2.15**). The positive controls for *Arachis hypogaea* (peanut) agglutinin (PNA), RCA I and *Ulex europaeus* agglutinin I (UEA I) were more straightforward, corresponding to the specific sugar specificities galactose or fucose.

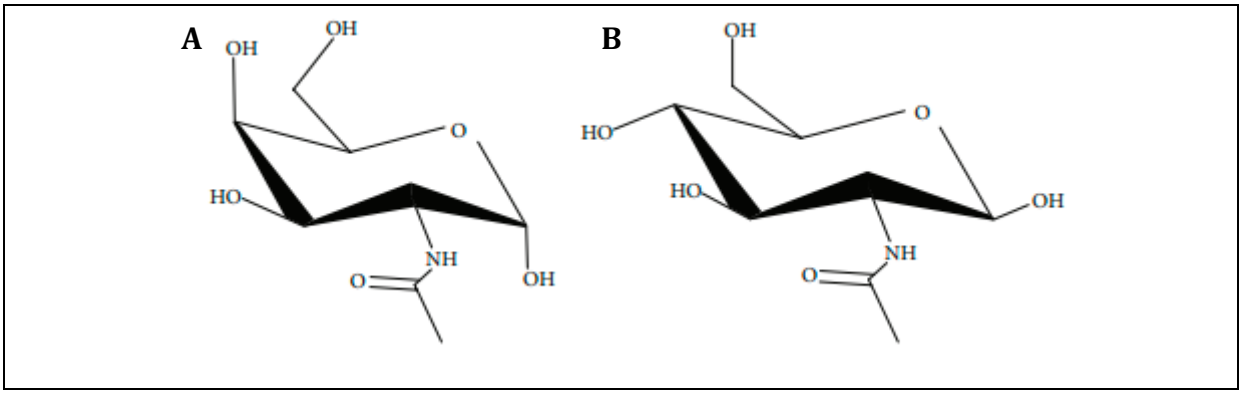

Figure 2. 14: Chemical structures of (A) GalNAc and (B) GlcNAc. Adapted from (367).

What became immediately apparent was that a majority of the lectins within the set purchased had ligands within the X-Vivo15 medium alone, even at low concentrations, which proved them unsuitable for experiments going forward due to difficulty distinguishing between biofilm-specific and media-derived interactions (**Figure 2.6A**). The Con A lectin is historically known to bind glucose as well as mannose, so is not necessarily surprising here (368), but ligands for the other lectins are less clear. Without independent composition analysis of X-Vivo15, perhaps by mass spectrometry, it is impossible to determine potential ligands in this medium, so further exploration was halted. However, now that biofilm growth is optimised in new media, it would be interesting to revisit these lectins to identify any new interactions. In spite of this, *S. aureus* biofilms themselves may still provide ligands. Although the major polysaccharide component of *S. aureus* biofilms is GlcNAc, it has been reported that up to 52.8% of the *S. epidermidis* EPS constitutes mannose (351). Therefore, although Con A shows overwhelming binding to glucose here, it is possible that if *S. aureus* EPS has a similar, previously unreported mannose-containing component, it would facilitate binding of Con A. Notably, it has been previously observed that Con A can bind *S. aureus*, although ligands were more likely found in the high-sugar glycocalyx, as well as the biofilm slime layer (369).

In future, if *S. aureus* is going to be more thoroughly established within the lab, we would benefit from incorporating other clinically relevant lectins alongside CLRs already established. A broad range have been described to bind *S. aureus* which would provide a good basis. Most Gram-positive bacteria, including *S. aureus*, produce wall teichoic acid (WTA), a structural component of the cell wall that binds peptidoglycan, and generally constitutes a poly-ribitolphosphate backbone decorated with GlcNAc, but does exist in

other forms (370). WTA is also important for the interplay between *S. aureus* and other species, and has been implicated in synergy with *C. albicans* during chronic infection (371, 372). WTA engages with the CLR Langerin (CD207) which is expressed by dermal Langerhans cells and has been observed to engage some *S. aureus* strains (373). Langerin is an endocytic, recycling receptor that is uniquely associated with Birbeck Granules which mediate degradation and antigen presentation to T cells (374, 375). Further, MGL is a macrophage and DC receptor that binds some forms of WTA, namely those containing poly-glycerolphosphate and GalNAc (211). MGL is a CLR expressed on DCs and activated macrophages able to recognise both self- and non-self-ligands, modulating cytokine output and T cell polarisation (376). During both of the above studies, engagement of these receptors led to alterations in cytokine output. These lectins have ligands in substances most heavily associated with *S. aureus* biofilms, but are still important for our work. Clinically, biofilms are rarely monoculture, but exist as poly-microbial communities that interact and influence each other's behaviour, with the most common two species being *S. aureus* and *P. aeruginosa* (316). Therefore, it is important to obtain a comprehensive binding profile for each lectin, for each monoculture, in order to compare to the profile of mixed cultures, giving us insight as to cumulative signalling changes downstream, ultimately providing clues as to the overall immune response.

Alternatively to carbohydrate-specific lectins, other innate receptors may be involved in recognition of alternative biofilm structures. Biofilms are highly heterogeneous, containing proteins and extracellular nucleic acid alongside their EPS (216, 219, 222). It is already well established that TLRs bind various common bacterial structures, including peptidoglycan, LPS and lipoteichoic acids (95), but other receptors have been described. For example, the Receptor for Advanced Glycation End-products (RAGE) binds the

intracellular DNA-binding protein high mobility group protein B1 (HMGB-1) during *S. aureus* skin infection, leading to NF-κB induction and inflammation (377). Additionally, PAR proteins are G-protein coupled receptors, activated on cleavage by proteases, a plethora of which are produced by *Pseudomonas* (LepA and Epa) as well as *Staphylococcus* (Aureolysin, SspB) *spp.* (378-381). Several PAR proteins are expressed on various immune cells including dendritic cells, and on activation induce NF-κB activation via the phospholipase C-protein kinase C signalling cascade, as well as increase production of CCL18, promoting recruitment of naïve T cells and T regs (382, 383). It is generally understood receptor engagement, signalling and action does not occur in isolation, but rather there are more nuanced, synergistic effects from multiple engagements, culminating in a complex overall response to infection by the host. We may assume therefore, that it is likely the case here and rather than individual receptors, it is the combined binding profile that will give us the most clues as to the direction of the overall immune response.

The switch from X-Vivo15 medium to DMEM-BSA for biofilm growth was optimised during this chapter, showing that this medium was able to support *P. aeruginosa* cultures, but not *S. aureus* (**Figure 2.10**), and that biofilms formed of *P. aeruginosa* show slightly different biomass and binding characteristics to those observed previously. Generally, the lower biomass in DMEM-BSA cultures may be as a result of the general minimal nature of the medium, unlike X-Vivo15 that is rich for tissue culture. The most interesting reduction in biomass is perhaps for PAO1*ΔwspFΔpsl*, where Pel is overproduced, as biofilm production is completely abrogated in this medium, yet binding by Fc-DC-SIGN and hDectin-Fc remains high (**Figures 2.11-12**). Generally, it is not surprising that these two lectins bind this strain, as a similar result was observed in X-Vivo15 where the high-

mannose Psl was not present (**Figures 2.9 and 2.11**). Here, if biofilm lacked robustness, as has previously been described in biofilms lacking Psl (244), combined with lack of nutrients in the media, the multiple washing steps may have dislodged the majority of bacteria. However, prior to this, remaining Pel carbohydrate may have adhered to the assay plate in a similar way to sugar controls, providing binding material for lectins. Further, as mentioned previously, Pel is made up of GlcNAc and GalNAc which has been shown to directly bind Dectin-2, albeit at a lower level than to mannose ligands, which may have contributed here (151). Dectin-2 has also been reported to bind LPS in various species via mannosylated O-antigen, including to *E. coli* 09a and *Hafnia alvei (384)*. DC-SIGN also readily binds core LPS of various other pathogens via GlcNAc residues, including *Salmonella*, *E. coli* K12 and *Yersinia pseudotuberculosis* (385), which may have contributed to binding in PAO1*ΔwspFΔpsl*. Additionally, DC-SIGN has been shown to uniquely bind *Neisseria gonorrhoeae* variant A, a sexually transmitted bacterial infection, via terminal GlcNAc residues of its surface lipooligosaccharide (LOS), while unable to bind varients B and C where the terminal LOS residues constitute galactose and GalNAc respectively (386).

During confocal analysis, we observed differences in the overall biofilm architecture between in DMEM-BSA compared to X-Vivo15, namely a decreased eDNA, less compact bacterial cell distribution around protrusions and less DC-SIGN binding. It was promising that biofilms grown in DMEM-BSA showed the same general shape as those in X-Vivo15, as these structures have been described previously in multiple media types (191, 387, 388). It is suggested that this mushroom-shape structure is formed with motile bacteria at the top (cap) with non-motile at the bottom (stalk), and in mature biofilms, the cap region forms a fluid-filled cavity containing planktonic bacteria that are released during

dissemination (389). As this work was preliminary, we unfortunately did not provide a secondary antibody-only control during this experiment. Work in the laboratory is currently underway to optimise confocal imaging, as was performed here, using dynamic biofilm flow systems and 3D imaging within a collagen matrix. Therefore, these experiments will be repeated with relevant controls. Importantly however, in previous assays where the same Fc-DC-SIGN was used during imaging, secondary antibodies showed undetectable signals when tested. Also, during binding assays performed in this chapter, we also displayed low to undetectable background in the secondary antibody controls. We are hopeful therefore that these results are real, and not a result of a secondary antibody binding artefact.

In conclusion, during this chapter, we have demonstrated interactions of specific immune receptors with *P. aeruginosa* and *S. aureus* biofilms in a static, 2D culture model, as well as adapt for new media types. This has highlighted clear variations between both species and between environments. We have also visualised these biofilms by confocal microscopy, confirming differences in biofilm architecture and DC-SIGN distribution within the 3D structure. In doing this, we have strengthened the idea that bacteria will readily adapt to their environments, altering the landscape and providing diverse ligands for immune cells that may steer the infection progression and wound healing in patients.

Chapter 3. Preparation and analysis of purified EPS from biofilms

3.1 Introduction

Polysaccharides are one of the most abundant macromolecules in nature, constituting sugar monomers linked by glyosidic bonds that play various roles across clades, including plants, animals, bacteria and fungi (390). Compared to their monomeric counterparts, polysaccharides and other natural macromolecules such as proteins and nucleic acids show a range of properties due to their complex secondary and tertiary structures, and contribute to energy storage, cell structure and communication (391).

To form persistent biofilms on abiotic or biological surfaces, bacteria utilise several structural components within their EPS, including polysaccharides. Monocultures of different bacterial species may be characterised by their polysaccharide production. For *P. aeruginosa*, alginate, Pel and polysaccharide synthetic locus (Psl) form part of the EPS produced by isolates, with the specific combination dictating some of the physical characteristics of the biofilm (244). Alginate is made up of D-mannuronic acid and L-guluronic acid and is associated with mucoid strains of *Pseudomonas*, commonly isolated in the lungs of cystic fibrosis patients, where biofilms are highly persistent and tolerant to antibiotic and immune clearance (392). In non-mucoid strains, Pel and Psl are the dominant biofilm polysaccharides. Pel holds an overall positive charge from partially acetylated residues of *N*-acetylgalactosamine (GalNAc) and *N*-acetylglucosamine (GlcNAc), produced by strains including the lab strain PA14 (244). However, the complete structure of Pel is still unsolved. Due to its positive charge, Pel likely plays a role in cross-linking with eDNA in the EPS matrix to promotes structural stability. Although

usually present alongside Psl in biofilms, it has been described to compensate for loss of Psl in some strains (243, 254). Psl is formed of repeating units of D-mannose, L-rhamnose and D-glucose, its production mediated by the *psl* locus, which consists of 15 genes (243, 244). Of these, *pslA* and *pslB* are the most studied, and appear essential for biofilm formation, perhaps due to their upstream position compared with the rest of the locus, with disruptions resulting in compromised structure and surface adhesion (243, 244). Psl strongly associates with the bacterial cell surface and promotes cell-cell interactions within the matrix (246). Switching from planktonic to biofilm growth with concomitant production of Pel and Psl is promoted by increased cytoplasmic concentration of the second-messenger cdiGMP, which is in turn regulated environmentally, importantly via proteins encoded by *wspR* and *wspF*, with disruption of the latter causing biofilm overproduction (238). Further, the Las, Pqs and Rhl quorum sensing systems are heavily associated with biofilm production, with Rhl particularly important in the production of Pel (262-265). Importantly, the presence Pel and Psl together is not strictly essential for biofilm formation; as disruption of one or the other can be compensated by mutations in genes that upregulate synthesis of the other polysaccharides during extended culture (244).

Polysaccharide intracellular adhesin (PIA) contains repeating units of linear *N*-acetylglucosamine and is the major polysaccharide associated with *S. aureus* biofilms. Similarly to Pel and Psl of *Pseudomonas*, PIA has a mechanical role, surrounding bacteria within the matrix alongside eDNA and proteins, promoting adherence and formation of 3D structures (275). The production, modification and export of PIA is primarily coordinated by genes of the *icaADBC* locus which is present in most clinical isolates, the loss of which abrogates the ability to form biofilm in most cases (274). However, biofilm

production has been observed in some *ica*-deficient strains of *S. aureus*, suggesting an alternative *ica*-independent mechanism (273). Various proteins also play a role in biofilm formation, including Protein A, SasC and SasG and fibronectin binding proteins A and B. Further, the accessory gene regulator (*agr*) locus is a two-operon quorum sensing system that operates a dual, post-transcriptional system that regulates various virulence factors and biofilm components (269). Namely, different mutations within *agr* can either promote or inhibit biofilm formation and vary susceptibilities to antibiotics (271). Due to these overlapping systems, it is difficult to determine the specific contributions of each individual component in PIA production, especially due to the highly plastic nature of *Staphylococcus* biofilms depending on their environment. Hence, each biofilm is fine-tuned in its structure and composition to best suit the infection environment, aiding in persistence and survival (286).

In nature, bacteria rarely exist in single-species colonies, but are found as complex poly-microbial communities whose attributes are dependent on specific interactions between species in the structure. By actively interacting with their own as well as neighbouring species within biofilm, they may best utilise the environment and protect themselves from external stresses (292). In some diseases, specific combinations of bacteria are associated with infection, such as in the chronic lung condition cystic fibrosis as well as in extensive burn wounds. *S. aureus* and *P. aeruginosa* are associated with both of these and coexist to cause chronic infections with extensive morbidity.

Immune cells recognise polysaccharides and differentiate between self and non-self, modulating the overall immune outcome through differential engagement of CLRs. A result of this is the production of various biomaterials in medicine are being developed,

including vaccine adjuvants for increased vaccine efficacy, implant coatings for reduced complement activation and rejection and viral entry inhibitors (390, 393, 394).

3.2 Hypothesis

Previously, we produced *P. aeruginosa* and *S. aureus* biofilms *in vitro* to characterise their compositions via the comparative binding profiles of various lectins including Fc- and biotin-conjugated. From this, we gained some insight into the composition, namely the presence of high-mannose ligands within *P. aeruginosa* biofilms, and GalNAc ligands unique to *S. aureus* biofilms within our model. However, due to the inherent complexity of whole biofilms, it is difficult to infer the specific component that is producing these ligands. Therefore, we endeavoured to purify carbohydrate from whole biofilms, and hypothesised that **using a biochemically characterised product, we may be able to identify the ligands more clearly for the lectins, and more accurately infer how these carbohydrates specifically influence immune recognition and responses.**

3.3 Aims

Previously, production of *P. aeruginosa* biofilms with different carbohydrate compositions was optimised in a 96-well format for analysis using ELISA-type assays. However, it is dogma in microbiology that different species often harbour vastly different characteristics in both growth and pathogenicity based on environmental conditions. The overall initial aim of this chapter was to optimise *S. aureus* biofilm production under conditions suitable for carbohydrate purification. Findings indicated the existence of carbohydrates in the media of choice tryptic soy broth (TSB) that interfered with our experimental model. This led to the optimisation of alternative culture conditions, in this case for PAO1Δ*wspF*Δ*pel*, to avoid potential artefacts and compare with our previous findings.

The specific objectives were:

- Optimise growth of S. aureus SH1000 biofilms in TSB for carbohydrate extraction and purification.

- Compare SH1000 biofilm carbohydrate characteristics to those from PAO1Δ*wspF*Δ*pel*, including:

    - Total carbohydrate and total protein quantification.

    - Engagement of receptors of varying specificity, including Fc- and biotin-conjugated human and plant lectins, as well as a newly designed competition ELISA.

    - Cytotoxicity analysis using human immune cells.

- Re-design and optimise biofilm production in a new media (DMEM-containing bovine serum albumin, BSA) for carbohydrate extraction, purification and characterisation.

3.4 Materials and Methods

3.4.1 Optimisation of *S. aureus* biofilm growth in TSB for carbohydrate extraction and purification

In order to study the specific recognition of biofilm carbohydrates by purified lectins and whole human immune cells, EPS was purified from biofilms grown in TSB. For the final protocol, SH1000 was streaked from glycerol stocks to LB agar and incubated overnight at 37 °C. A single colony was inoculated to 20 mL sterile TSB (Sigma-Aldrich, 22092)) supplemented with 3% (w/v) NaCl (TSB-NaCl, (217)) and incubated overnight at 37 °C, 200 rpm then entire culture inoculated to 1 L pre-warmed TSB-NaCl and incubated 5 days, 37 °C, 100 rpm. Culture was fixed in 0.219% (v/v) formaldehyde and incubated at RT, 100 rpm for 1 h, then carbohydrate solubilised in 285 mM NaOH for 3 h, RT, 100 rpm. The resulting solution was centrifuged at 16,000 x *g* (Beckman Coulter, Avanti centrifuge, JLA 10.500 rotor), 4 °C for 1 h and supernatant diluted 1:1 in HPLC water. Supernatants underwent vacuum filtration through a CytoOne® 0.2 µM filtration unit (Starlab, CC6032-9233) to remove remaining bacteria before storage overnight at 4 °C.

Supernatants were dialysed against HPLC water at RT using VIVAFLOW 200, 12-14 kDa molecular weight cut-off membrane (MWCO, Sartorius, VF20H0) to a volume <100 mL. To precipitate proteins and nucleic acid, 20% (w/v) tri-chloro-acetic acid (Sigma-Aldrich, 91230) was added and sample incubated on ice for 30 min before centrifugation at 16,000 x *g*, 4 °C for 1 h (Beckman Coulter, Avanti centrifuge, JLA 16.250 rotor). Supernatant was collected to a glass bottle and 1.5x volume ice-cold, 95% (v/v) ethanol added to precipitate carbohydrates from lipids. Solution was incubated 20 h, -20 °C and centrifuged at 16,000 x *g*, 4 °C for 1 h. Supernatant was discarded and pellet re-suspended in 7.5 mL HPLC water. Pre-chilled, 100% ethanol was added (142.5 mL for a final 95%

v/v) and extract stored 20 h, -20 °C. Extract was centrifuged at 16,000 x *g*, 4 °C for 1 h, supernatant discarded and pellet re-suspended in 5 mL HPLC water. Final extract was dialysed against 4 L HPLC water using 8-10 kDa MWCO Spectra/Poe Float-A-Lyzer G2 Dialysis Device (Sigma-Aldrich, Z726508) at 4 °C, 24 h and final product lyophilised and stored at -80 °C.

Purified carbohydrate from 3 preparations was pooled and fractionated on a HiPrep 26/60, Sephacryl S-200 HR gel filtration column (GE Healthcare, 17-1195-01) to acquire fractions containing products of ≥17 kDa. The void volume of <17kDa was also collected. The column was calibrated using protein standards (1511901, BioRad) to produce a standard curve where the retention time of known molecular weights could be calculated. Fractions were collected and pooled before lyophilisation and resuspension in 5 mL sterile endotoxin-free water. Samples were dialysed using 8-10 kDa MWCO Spectra/Poe Float-A-Lyzer G2 Dialysis Device dialysis and lyophilised again before reconstitution in endotoxin-free water for a final concentration of 5 $mgmL^{-1}$.

3.4.2 Biochemical analysis of carbohydrate preparation

3.4.2.1 *Coomassie and silver staining*

Sodium dodecyl sulphate polyacrylamide gel electrophoresis (SDS-PAGE) is a technique used to separate proteins within a sample according to size and electrophoretic mobility. SDS-PAGE gels were produced at 1.5mm thickness and 30% Acrylamide/Bis Solution (37.5:1), which were stored at 4 °C after polymerisation. Samples and ladders were denatured at 90 °C, 5 min in 1X loading buffer (Bio Rad, B70245) followed by 5 min incubation on ice. Samples were centrifuged at 13,000 rpm 1 min and 10 µL (30 µg) solution loaded to relevant wells of SDS-PAGE gel. In one well, 10 µL of protein ladder (Bio Rad, P77125) with 1X loading buffer was added for fragment size determination.

Gels were loaded into the electrophoresis unit and submerged in tris-glycine electrophoresis buffer (Bio Rad, 1610772) and ran at 30 mA for 60-90 min, until the dye front reached the bottom of the gel.

The Coomassie Blue staining procedure was used to visualise proteins separated during the SDS-PAGE gel. The gel was incubated overnight, RT, 100 rpm in 0.015% Coomassie Brilliant Blue R (Sigma, B6529) dye in de-stain solution (25% isopropanol, 10% acetic acid, 65% distilled water) to bind proteins. The dye was aspirated and replaced with fresh de-stain solution and incubated in a sealed container with gentle rocking. This was repeated periodically until the optimum visualisation was reached. After de-staining, the gel was photographed.

Silver staining, around 50-fold more sensitive than Coomassie and ideal for identifying low concentrations of protein was performed using the PlusOne Silver staining kit (Pierce, 24612). SDS-PAGE gels were fixed for 60 min in acetic acid supplemented with 30% ethanol (v/v) then incubated overnight in sensitisation solution (830 mM sodium acetate and in 30% ethanol, 5% sodium thiosulfate and 0.125% glutaraldehyde (v/v) in HPLC water). After sensitisation, gels were washed 15min, 4x in distilled water then incubated with 2.5% (w/v) silver nitrate in H_2O for 60 min. Gels were washed 2x in H_2O for 1 min then developed for 4-6 min in developing solution (235 mM sodium carbonate in water). Stopping solution (39 mM EDTA-Na2•2H_2O in HPLC water) was added and incubated for 60 min before photographs taken.

3.4.2.2 *Bicinchoninic acid assay*

The bicinchoninic acid assay (BCA) is a biochemical assay used to determine the total concentration of protein in a solution using (Pierce, 23225). Control protein albumin (Sigma-Aldrich, P5369) was diluted in HPLC water for a standard curve (0 and 2000

µgmL-1) and 10 µL added in duplicate to a 96-well flat-bottomed plate. Samples were loaded in duplicate as crude, 1:2, 1:10 and 1:100 dilutions in HPLC water. Once loaded, 200 µL of working reagent was added to each well and mixed thoroughly. Plate was covered with parafilm and incubated at 37 °C, 30 min and absorbance was measured at 550 nm.

3.4.2.3 Phenol-chloroform total carbohydrate quantification

As these preparations were designed to purify carbohydrate, it was important to determine the total carbohydrate concentration. This assay kit (Merck, MAK104-11CT) utilises the phenol-sulfuric acid method, during which the concentrated sulphuric acid breaks down polysaccharides, oligosaccharides and disaccharides to monosaccharides. Monosaccharides then react with phenol to produce a yellow-gold gradient for quantification by absorbance. In 2 mL locking-cap Eppendorf tubes, 30 µL of sample diluted in HPLC water was added alongside glucose controls for a standard curve (0-20 µgtube^{-1}). To the samples, 150 µL of 96% sulphuric acid was added and mixed for 1 min, RT, 100 rpm. Samples were incubated for 15 min, 90 °C then allowed to cool to RT. Once cooled, 30 µL of developer solution (containing phenol) was added and mixed for 5 min, RT, 100 rpm. Samples were transferred to a clear, flat-bottomed, 96-well plate in duplicate, covered with optically clear film and absorbance measured at 490 nm.

3.4.3 Generation of primary immune cells

Human monocytes were isolated from peripheral blood mononuclear cells (PBMCs) obtained from buffy coats (Blood Transfusion Service, Barnsley) by Histopaque 1077 (Sigma, 10771-100ML) density gradient centrifugation followed by positive selection using CD14+ beads (Miltenyi, 130-050-201). Monocytes were re-suspended in complete RPMI medium (RPMI-1640, Sigma, R0883), 10% (v/v) human AB serum (Sigma, H4522-

100ML), 2 mM Glutamax (Sigma, 35050-038), 10 mM HEPES (Gibco, 15630056) with relevant cytokines depending on cell type required and $1x10^6$ cells seeded to each well of a 24-well plate in 500 µL. For macrophages, monocytes required 50 $ngmL^{-1}$ M-CSF (R&D Systems, 130-093-963) in Ultra Low Attachment plates (Costar Corning, 3473), for monocyte-derived dendritic cells (moDCs), 50 $ngmL^{-1}$ each IL-4 (Miltenyi, 130-093-922) and GM-CSF (Miltenyi, 130-093-866) in TC-treated plates (Corning Costar, 3524) and for inflammatory monocytes, +/- 10 $ngmL^{-1}$ GM-CSF in UpCell plates (Thermo Scientific, 174899). For monocytes, plates were incubated for 48 h, while moDCs and macrophages required 6-7 days with feeding with complete RPMI medium with relevant cytokines on day 3. All were incubated at 37 °C, 5% CO_2. Differentiated cells were harvested by incubating on ice for 30 min and collected by gentle pipetting. Cells were counted and diluted to required cell densities for each experiment and stored on ice until needed.

For cell counting, cells were mixed with 0.4% Trypan blue (1:1 dilution, Sigma, T8154-100ML) and counted using a TC20™ automated cell counter (Bio-Rad).

3.4.4 Cytotoxicity analysis of carbohydrate preparations incubated with primary immune cells

Samples were applied in 50 µL to 96-well, TC-treated plates at a range of concentrations (10-0.01 μgmL^{-1} in X-Vivo15) followed by 50 µL immune cell suspension ($5x10^4$ $cellswell^{-1}$ in X-Vivo15 supplemented with 10 $ngmL^{-1}$ each IL-4 and GM-CSF) and incubated for 4 or 24 h, 37 °C, 5% CO_2. For controls, immune cells were incubated in media alone (100% survival) or in 2% Triton X. Following incubation, plates were centrifuged (400 x g, 4 °C, acc/dec 3/3, 5 min) and supernatants collected, pooled and stored at -20 °C before LDH analysis.

3.4.5 Assessment of cell cytotoxicity using lactate dehydrogenase (LDH) assay

The cytotoxicity kit by Roche (11644793001) utilises LDH production as an indicator of pyroptosed cells, and was used to assess percentage cytotoxicity in comparison to low (DC only) and high cell death (Triton X-100-treated DC cells (Sigma, T8787-100ML)) control groups by measuring lactate dehydrogenase activity. For this assay, 50 µL of cell supernatant was added to wells of a 96-well, medium binding flat-bottom plate (Corning Costar, 9017) and treated with an equal volume of assay reagent as provided in the kit and incubated at 37 °C in the dark. Absorbance was read at 650 nm and 492 nm between 15 and 30 min at 5-min intervals.

3.4.6 Development and optimisation of a competitive binding ELISA for purified carbohydrates against known lectin ligands

Due to concerns that the ELISA-type binding assay was insufficient to show true binding of *P. aeruginosa* and *S. aureus* EPS to CLRs, a competitive ELISA was developed to determine how well the EPS competed for lectin binding sites against their known ligands (**Figure 3.1**). Wells were coated with 2 µgmL^{-1} of control sugar as polymers (L-fucose-PAA, Lewis^{X}-PAA) or Zymosan in saline and incubated overnight at 37 °C. The following day, EPS at a range of concentrations was incubated with 2 µgmL^{-1} of relevant Fc-conjugated lectin in 1.5 mL Eppendorf tubes for 1 h in µL TSB buffer (10 mM Tris-HCl pH 7.5, 10 mM $CaCl_2$, 154 mM NaCl and 0.05% (v/v) Tween20), RT to allow for binding. Wells were washed 3x with 200 µL TSB buffer and incubated with 50 µL of protein-carbohydrate mixture before incubation for 1 h, RT. Wells were washed 3x with TSB then incubated with 50 µL anti-human IgG conjugated to alkaline phosphatase (1:1000 in TSB) for 1 h, RT. Wells were washed 2x with TSB and 1x with AP buffer (100 mM Tris HCl pH

9, 100 mM NaCl, 1 mM $MgCl_2$). For all experiments, 50 µL of p-Nitrophenyl phosphate substrate solution (1 $mgmL^{-1}$ PNPP tablet and 0.2 M Tris buffer tablet in HPLC water) was added to each well and incubated at RT in the dark. Absorbance was read at 405 nm between 5 and 30 minutes at 5 min intervals.

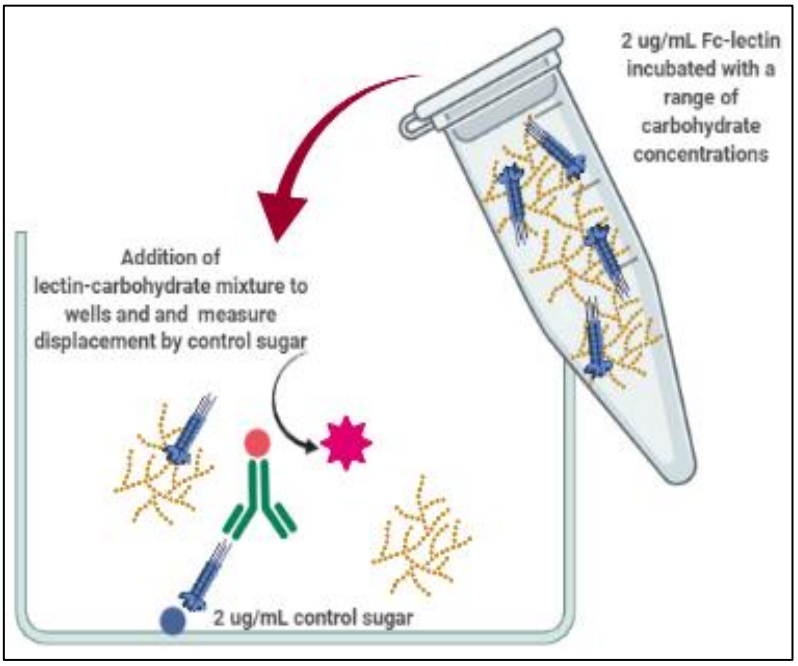

Figure 3. 1: Schematic representation of competitive binding ELISA for purified carbohydrates against known lectin ligands.

3.4.7 Optimisation of *P. aeruginosa* growth in minimal media for carbohydrate extraction and purification

Due to suspected contribution of TSB carbohydrates to binding activity of lectins, we optimised the carbohydrate extraction process for DMEM-BSA as explored in Section **3.5.4**. For the final protocol, PAO1*ΔwspFΔpel* was streaked from glycerol stocks to LB agar and incubated overnight at 37 °C. Single colonies were inoculated to 3x 20 mL sterile DMEM-4921 supplemented with 5 or 2% (w/v) BSA, 10 mM HEPES and 2 mM L-glutamine (DMEM-BSA) and incubated overnight at 37 °C, 200 rpm then each culture inoculated to 400 mL pre-warmed DMEM-BSA and incubated statically for 5 days, 37 °C.

Cultures were fixed in 0.219% (v/v) formaldehyde and incubated at RT, 100 rpm for 1 h, then carbohydrate solubilised in 285 mM NaOH for 3 h, RT, 100 rpm. The resulting solution was centrifuged at 16,000 x *g*, 4 °C for 1 h and supernatant diluted 1:1 in HPLC water. Supernatants underwent vacuum filtration through a CytoOne® 0.2 µM filtration unit (Starlab, CC6032-9233) to remove remaining bacteria before storage overnight at 4 °C.

Supernatants were dialysed against HPLC water at RT using VIVAFLOW 200, 12-14 kDa MWCO to a volume <100 mL. To precipitate proteins and nucleic acid, 20% (v/v) TCA (70% v/v stock in HPLC water) was added slowly while stirring at 4 °C, incubated on ice for 30 min before centrifugation at 16,000 x *g*, 4 °C for 1 h. Supernatant was collected to a glass bottle and lyophilised. Lyophilate was resuspended in the minimum volume of HPLC water possible and neutralised using saturated Tris-Base (Fisher Scientific, BBP152). Final extract was dialysed against 4 L HPLC water (1 L for every 6 h) using 8-10 kDa MWCO Spectra/Poe Float-A-Lyzer G2 Dialysis Device at 4 °C, 48 h and final product stored at -80 °C. At each stage, aliquots were taken for protein and carbohydrate quantification.

3.5 Results

3.5.1 Development of carbohydrate preparation and purification protocol for SH1000 biofilm.

Work conducted previously in the lab involved carbohydrate extraction and purification from PAO1*ΔwspFΔpel*, adapted from (351), that involves fixing and removal of bacterial cells as well as nucleic acids, proteins and lipids. This strain was chosen as the assumption was made that mannose-containing Psl, would be the dominant carbohydrate present within the preparation and hence, characterisation would be easier. Further, due to high levels of mannose described within Psl, it was more likely to engage with the receptors of interest to produce a downstream immunomodulatory effect. Growth conditions were optimised for this strain, by setting up multiple shallow, static cultures that allowed for maximum pellicle formation. Taking this into consideration, we aimed to optimise this method for *S. aureus* SH1000, initially attempting the same technique as used for *P. aeruginosa* (**Figure 3.3**). Unfortunately, using this method, SH1000 growth was not supported during long-term culture, as the biofilm did not appear to form a pellicle and that overall bacterial growth was poor, denoted by a culture that was almost completely clear.

Therefore, the protocol was modified after considering the literature. It has been widely observed that *S. aureus* biofilms are incredibly plastic and will adapt depending on specific environmental conditions. Most relevant here, protein and carbohydrate incorporation into the EPS matrix is heavily associated with salt and glucose levels in the media. Interestingly, the ratio between salt and glucose level is indicative of protein and carbohydrate, where increased glucose, such as in diabetic conditions, produces a more proteinaceous biofilm and vice versa (217). Therefore, it was in our interests to optimise

for high-salt in order to extract maximum carbohydrate. However, growth was still not supported in static conditions, hence gentle agitation and higher culture volume (1 L) were tested and good biofilm formation was observed (**Figure 3.2**). Biofilm was harvested at 40 h for the first culture, when a clear pellicle was visible. For the following 2 replicates, cultures were incubated for 5 days.

Figure 3. 2: S. aureus SH1000 requires alternative growth conditions to P. aeruginosa PAO1ΔwspFΔpel when extracting carbohydrate. *SH1000 grown statically in TSB alone in 400 mL volume produced poor pellicle formation (**A**). For good biofilm formation, SH1000 requires high-salt (3% NaCl w/v), high volume (1 L) and static conditions to produce extensive biofilm (**B**).*

Carbohydrate was extracted as depicted in **Figure 3.3**, in the same way as *P. aeruginosa* preparations. Cultures required fixation due to the presence of such large class II bacterial populations, and cells were removed to ensure only secreted, assumed biofilm-specific, carbohydrate was purified. Formaldehyde does not lyse the bacteria, and hence internal or cell wall-associated carbohydrate such as capsular polysaccharides should have been minimised. For most effective precipitation of nucleic acid, protein and lipids by TCA and ethanol precipitation, dialysis was performed to remove excess salt and water, concentrating the solution. Ethanol precipitation was performed twice for maximum efficacy. Final dialysis was performed to remove any remaining salt before

lyophilisation and reconstitution in water for a final crude concentration of 5 mgmL^{-1}. For each of the 3 replicates, aliquots were taken for biochemical characterisation and binding analysis to lectins. Following, samples were pooled for FPLC analysis.

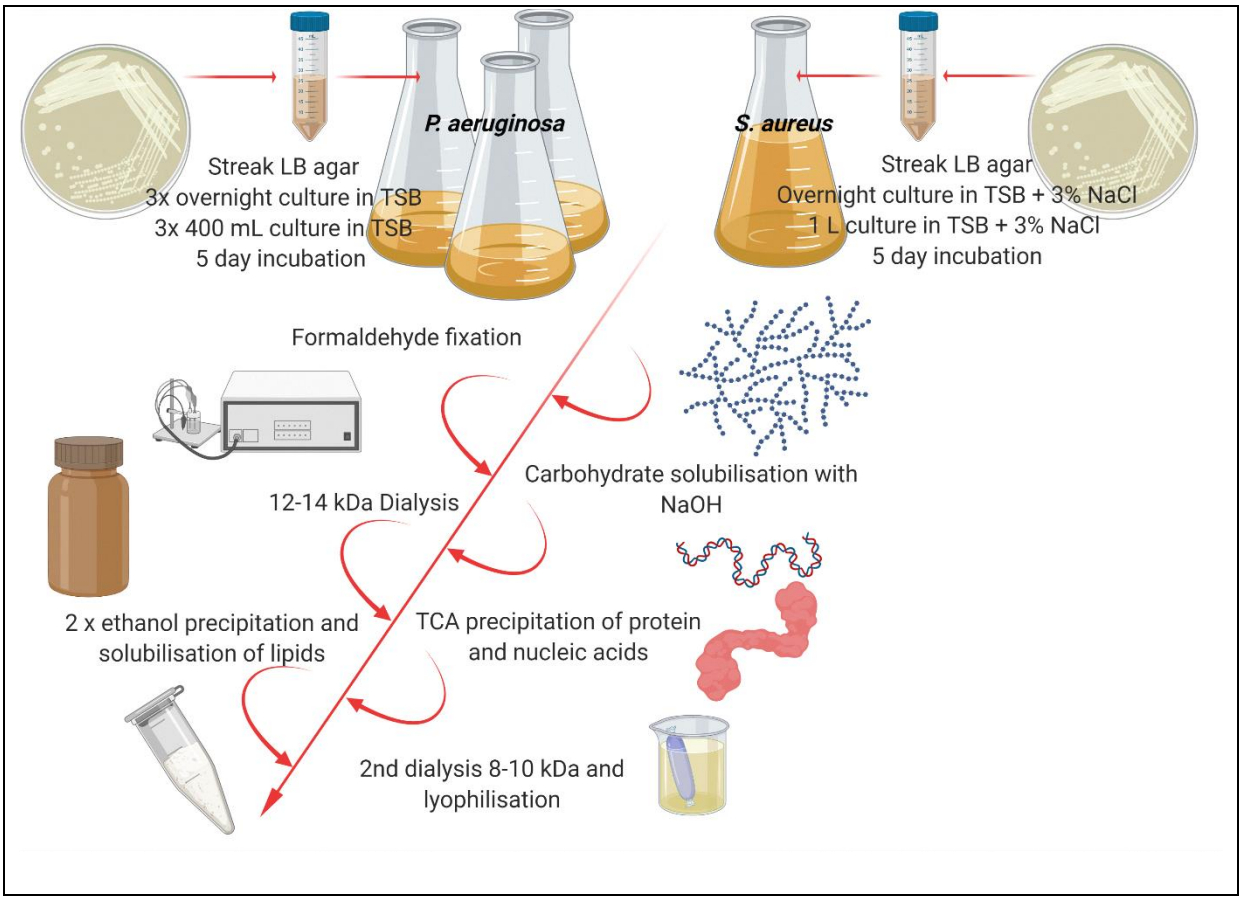

Figure 3. 3: Schematic for biofilm growth and carbohydrate extraction from P. aeruginosa and S. aureus in TSB medium.

3.5.2 Biochemical analysis of SH1000 carbohydrate preparation shows low to undetectable levels of contaminants, with high carbohydrate yield.

The most important analysis here was total carbohydrate content of our preparations, as the goal of this work. The phenol-sulfuric acid method was utilised for a range of dilutions for each preparation, with 12.8, 36.3 and 23.6 $mgmL^{-1}$ concentrations of carbohydrate obtained for preparations 1-3 respectively (**Table 3.1**). For preparation 1, the low raw and relative concentration (66.5%) was potentially due to the much shorter incubation time. The BCA assay was used to determine total protein composition. The overall protein percentage for preparations 1-3 were 0.985, 3.56 and 0.413 $mgmL^{-1}$ respectively. Before FPLC, preparations 1 and 2 were assessed by SDS-PAGE and silver staining to determine the presence of LPS. Although *S. aureus* does not produce LPS itself, equipment in the laboratory is shared and hence LPS from previous *P. aeruginosa* preparations may have contaminated here. For both samples, the classic banding pattern for *P. aeruginosa* LPS was not observed, but there was a smeared pattern with some product unable to enter the gel or pass the stacking gel, with some product unresolved at the dye front (**Figure 3.4**). This was reassessed post-FPLC.

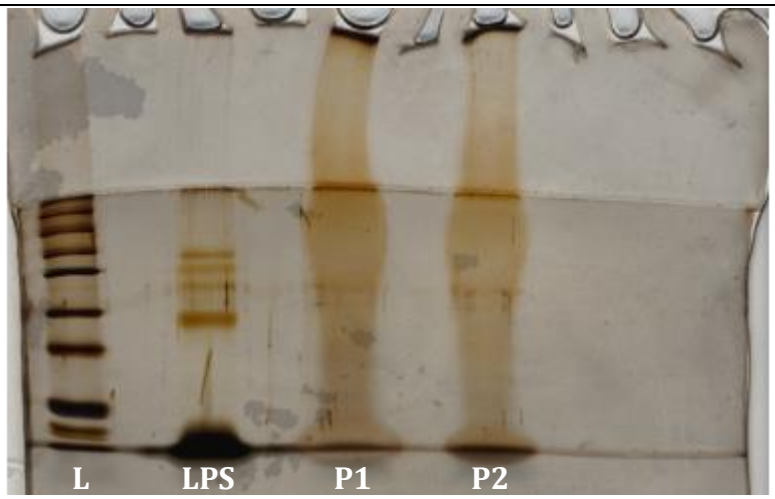

Figure 3. 4: SDS-PAGE gel with silver staining to assess potential LPS contamination of SH1000 EPS preparations*. Stacking and resolving gels were prepared and allowed to polymerise. Samples were mixed with 4x loading buffer and incubated for 5 min at 80 °C before incubation on ice for 5 min. Tubes were centrifuged for 1 min, 13000 rpm before 30 µg was loaded to relevant wells. 10 µL ladder (L) was loaded to each gel for reference, and for the silver stain, 5 µg P. aeruginosa LPS was loaded for comparison. Silver staining was performed according to materials and methods. For both preparations 1 and 2 (P1 and P2), a smeared pattern was observed, but there was no LPS detected.*

Table 3.1: S. aureus carbohydrate purification profile with total protein and carbohydrate contributions*.*

	Total material / mg	**Concentration (in 5 mL) / mgmL^{-1}**	**Total protein / mgmL^{-1}**	**Total carbohydrate / mgmL^{-1}**
Preparation 1	96.0	19.2	0.985 (5.13%)	12.8 (66.5%)
Preparation 2	207.5	41.5	0.356 (0.858%)	36.3 (87.4%)
Preparation 3	166.0	33.3	0.413 (1.24%)	23.6 (70.9%)

Also, before proceeding to FPLC, we wanted to compare binding of plant lectins to preparations 1 and 2 to get an initial idea of binding characteristics. Interestingly, Con A was the only lectin that showed noteworthy binding, while it was low to undetectable for all others tested, suggesting the presence of mannose/fucose ligands within this carbohydrate preparation (**Figure 3.5**). In contrast to the whole biofilms, no lectin bound the diluent used for these assays (saline), so we may consider this result real. As stated

previously, the major polysaccharide component of *S. aureus* biofilms is PIA, made up of GlcNAc polymers (275). However, it has been shown that up to 52.8% of the *S. epidermidis* EPS corresponds to mannose, so it is possible that *S. aureus* shows similar proportions (351). In ratification, Con A has been described as able to bind *S. aureus*, although in this case, ligands were predicted to come from the high-sugar cell glycocalyx and biofilm slime (369). Although whole bacterial cells were removed during the purification, it is possible that glycocalyx was dissociated during this process, so it is difficult to rule out this possibility.

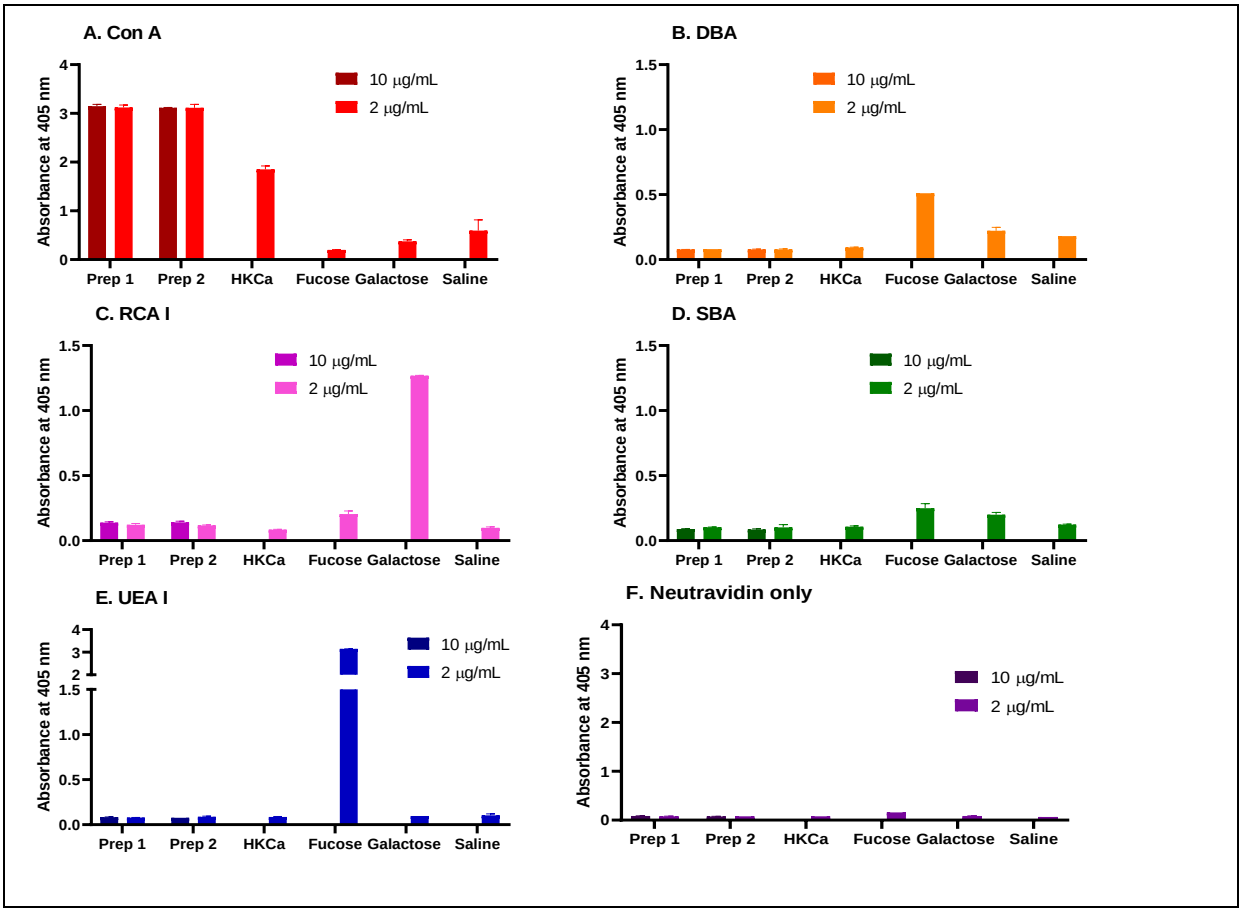

Figure 3. 5: Binding activity of plant lectins against S. aureus SH1000 EPS preparations 1 and 2, pre-FPLC. *Relevant wells of 96-well plate were coated with between 10 and 2 µgmL^{-1} in 50 µL of carbohydrate preparation or 10 µgmL^{-1} of control sugars, followed by incubation with 10 µgmL^{-1} of relevant lectin. After washing, wells were incubated with Neutravadin conjugated with alkaline phosphatase. On addition of substrate, absorbance was read at 405 nm after 10 min. Lectins tested were (**A**) Con A, (**B**) DBA, (**C**), RCA I, (**D**) SBA, (**E**) UEA I and (**F**) Neutravidin. Only Con A showed binding to preparations. Results were analysed using Graphpad Prism 9.*

Preparations 1-3 were pooled and FPLC gel filtration using the GE HiPrep 26/60 Sephacryl S-200 HR column was performed. Using protein standard myoglobin as a reference for 17 kDa, the distance was measured and compared with the spectrum produced by the sample (**Figure 3.6**). During the sample run, points were marked on the graph-paper to indicate respective fractions, therefore a value could be calculated for volume in each centimetre of spectrum. Here, 1 cm corresponded to 11 mL and the myoglobin peak fell at 19.1 cm, therefore, the first 210 mL of the sample run includes products 17 kDa or larger (**Figure 3.6**). As fractions were collected in 5 mL increments,

this corresponds to fractions 1-42. These were pooled (another bottle was also collected containing the void volume of fractions 43-69) and lyophilised. Lyophilised samples were re-suspended in sterile, endotoxin free water and dialysed overnight against HPLC water to remove products less than 8-10 kDa in size before final lyophilisation and reconstitution to a concentration of 5 $mgmL^{-1}$. This final sample was used for binding assay and cytotoxicity analysis. Ideally, as with carbohydrate purified from PAO1*ΔwspFΔpel*, we would have performed more thorough biochemical analysis of this product via NMR and gel permeation chromatography to determine specific residues and linkages (191).

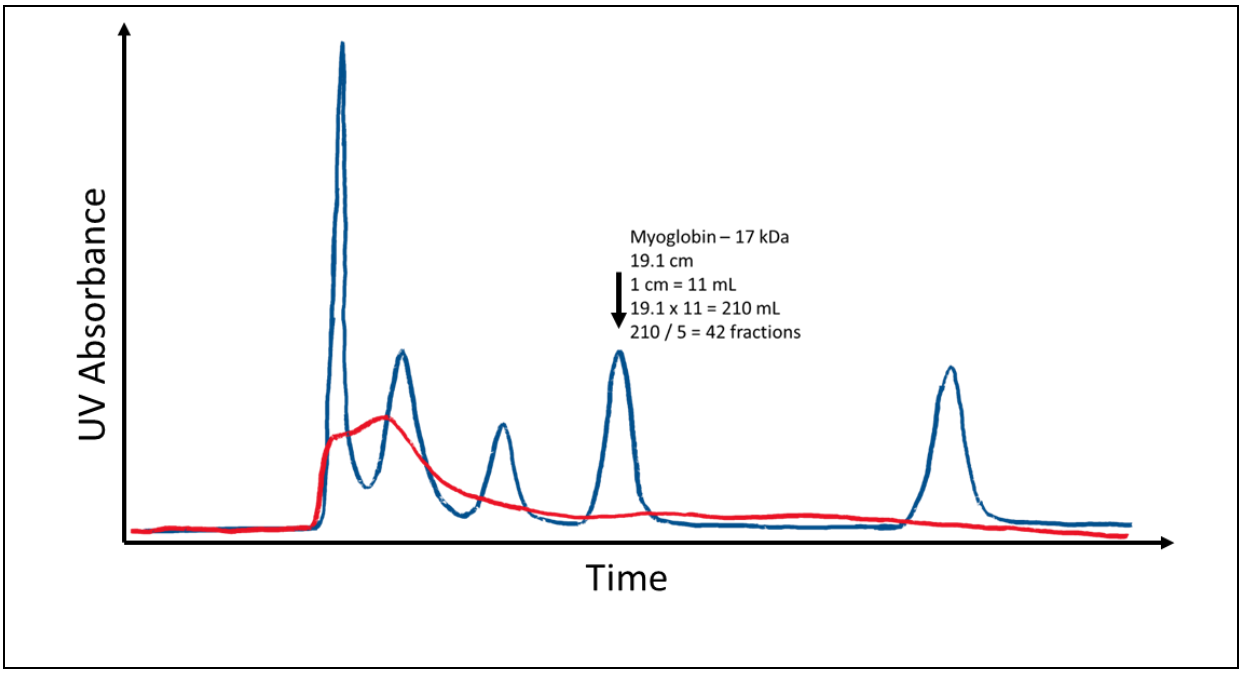

Figure 3. 6: Purification of high molecular weight fractions by FPLC. *Protein standards were used to calibrate a HiPrep 26/60, Sephacryl S-200 HR gel filtration column to generate a standard curve of known molecular weight markers (blue) in relation to retention time. Following, pooled carbohydrate extracts (red) were fed through the column and fractions ≥ 17 kDa were collected for analysis, relative to the myoglobin peak (black arrow). To calculate, time-points were marked on original trace and $mLmin^{-1}$ determined, corresponding to 1 cm = 11 mL. To reach the myoglobin peak, 19.1 cm was required, corresponding to 210 mL. Each fraction constitutes 5 mL, so fractions 1-42 were pooled for the high molecular weight portion. Image shown is a representative trace with arbitrary axes, produced in Microsoft PowerPoint (to correct scale).*

After FPLC and dialysis, Coomassie blue was performed, showing no bands and hence undetectable protein levels (**Figure 3.7A**). Similarly, Silver staining, where the LPS control showed the banded pattern characteristic of *P. aeruginosa* (395), *Staphylococcus* preparation showed no product (**Figure 3.7B**). Interestingly, the smeared pattern observed previously (**Figure 3.4**) was lost after FPLC, suggesting that this observation was caused by residual small proteins.

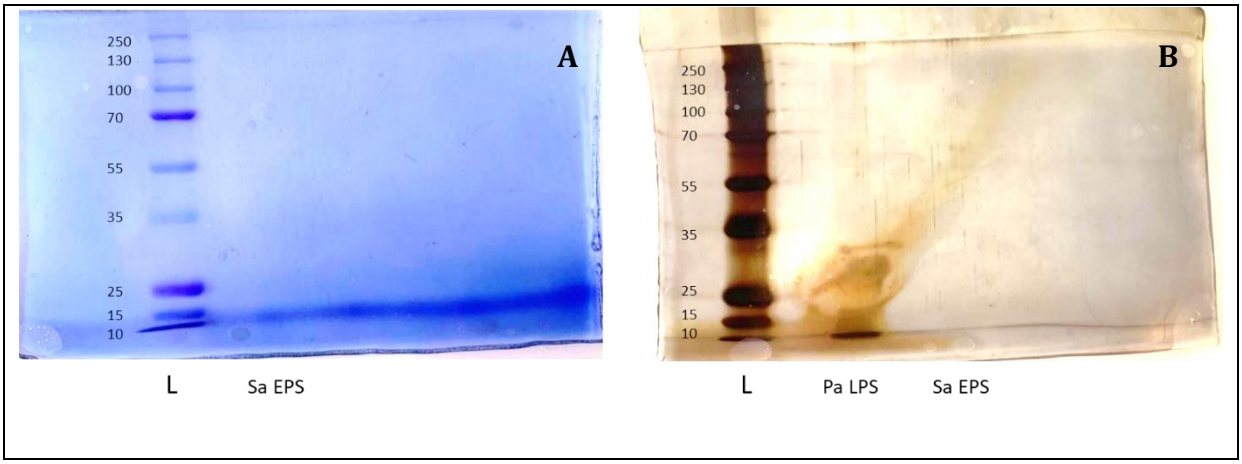

Figure 3. 7: SDS-PAGE gels with Coomassie Blue (A) and silver (B) staining to assess protein and LPS content of SH1000 EPS preparation. *Stacking and resolving gels were prepared (10 % polyacrylamide) and allowed to polymerise. Samples were mixed with 4x loading buffer and incubated for 5 min at 80 °C before incubation on ice for 5 min. Tubes were centrifuged for 1 min, 13000 rpm before 30 µg was loaded to relevant wells. 10 µL ladder was loaded to each gel for reference, and for the silver stain, 5 µg P. aeruginosa LPS was loaded for comparison. Coomassie and silver staining was performed according to materials and methods.*

3.5.3 LDH analysis of primary immune cells incubated with purified carbohydrate preparation shows low levels of cytotoxicity.

Once carbohydrate was purified, we began its characterisation using biotinylated and Fc-conjugated lectins. As the carbohydrate product was confirmed to contain little contamination, we incubated it with human immune cells in order to assess cytotoxicity. Here, primary monocyte derived dendritic cells (moDCs) were incubated for 4 h with 0, 0.1 or 1.0 μgmL^{-1} of the preparation before supernatants were collected for LDH analysis (**Figure 3.8**). Here, cytotoxicity remained low for all conditions tested, only exceeding 5% in one sample and for all 3 donors, cytotoxicity was lowest at 1.0 μgmL^{-1}, potentially suggesting a protective effect. In addition, some samples incubated with carbohydrate remained more viable than the untreated, indicated in **Figure 3.8** by the negative calculated values. However, due to the exceedingly small values, this variation may be insignificant. Therefore, the simple conclusion here is that in these conditions, carbohydrates extracted from *S. aureus* biofilm do not cause cytotoxicity in moDCs.

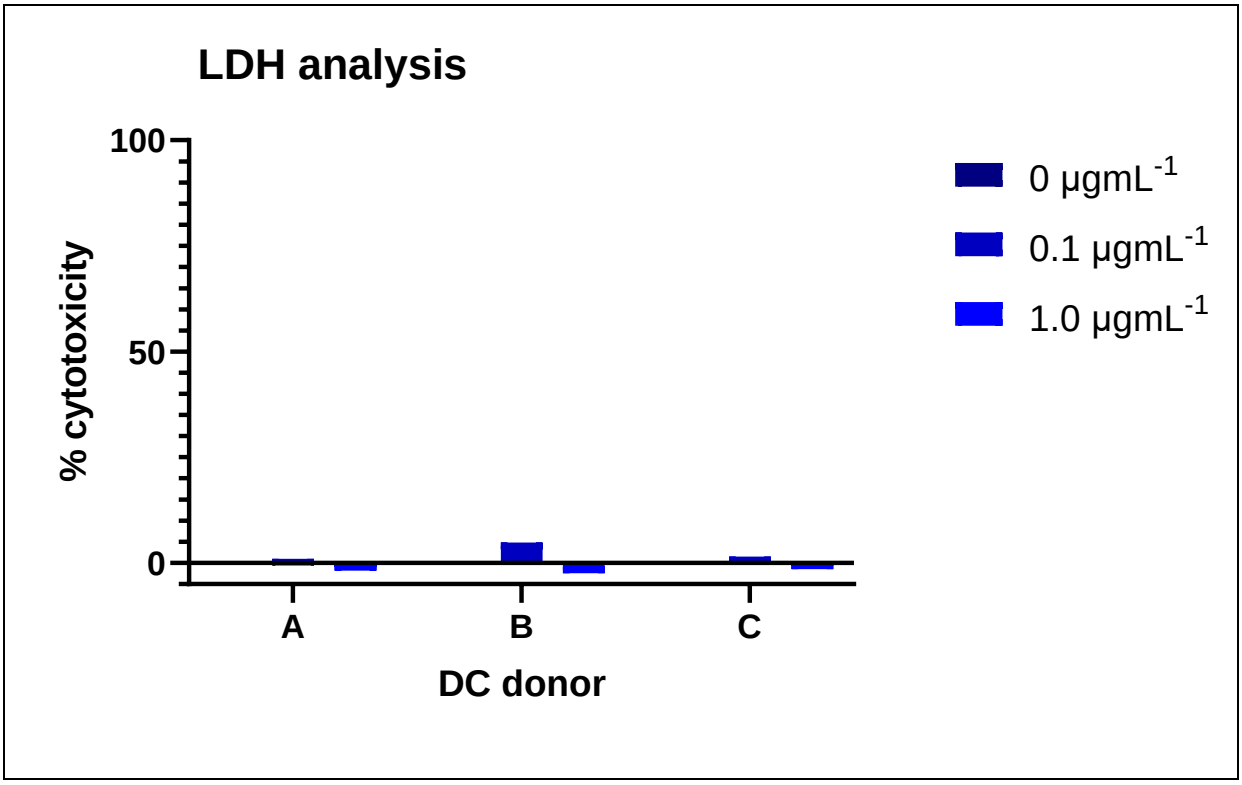

Figure 3. 8: LDH analysis of moDCs incubated with S. aureus biofilm carbohydrate. *Wells were loaded with 0-1.0 µgmL^{-1} EPS preparation before seeding with 5x10^4 moDCs. Plates were incubated for 24 h, 37 °C, 5% CO_2 before centrifugation at 400 x g, 4 °C, acc/dec 3/3, 5 min. Samples were incubated with LDH reagent and absorbance measured at 650 and 492 nm and values normalised against untreated (0 µgmL^{-1} EPS) DCs, presented as a %-cell death of 0. Results were analysed using Graphpad Prism 9.*

3.5.4 High levels of binding is observed by Dectin-2-Fc, MR CTLD4-7-Fc and Fc-DC-SIGN to carbohydrate purified from SH1000, PAO1 and its *ΔwspF* mutants and TSB alone in both standard and competitive binding ELISAs.

Due to the binding of Con A to the crude EPS, we were interested to next investigate whether the same EPS could interact with the CLRs, Fc-DC-SIGN, MR CTLD4-7-Fc and m/hDectin-2-Fc after gel filtration (**Figure 3.9**). Here, a range of 10 to 0.01 μgmL^{-1} of EPS preparation was used to test CLR binding, as 10 and 2 as initially used showed no clear differences (data not shown). Here, greatest level of binding was observed by MR CTLD4-7-Fc and Fc-DC-SIGN, with very little difference between the two receptors (**Figure 3.9A-B**), although the dose-effect between 2 and 10 μgmL^{-1} MR CTLD4-7-Fc is more apparent, perhaps due to slightly less abundant ligands (**Figure 3.9B**). For Dectin-2-Fc, the overall level of binding was diminished for both human and mouse clones compared to MR CTLD4-7-Fc and Fc-DC-SIGN, but the dose-effect was much more apparent (**Figure 3.9C-D**). All lectins were observed to bind to their respective controls. These results mirror previous observation with Con A, suggesting mannose structures within the matrix carbohydrate, at comparable levels to that of *P. aeruginosa* EPS (191). However, this is still surprising as consistently within the literature, the major component of *S. aureus* biofilms polysaccharide GlcNAc. As with Con A, the lectins tested here are all primarily specific to mannosylated ligands, which explains binding to *P. aeruginosa* but less so *S. aureus*, unless it does indeed share this similarity with *S. epidermidis* and contain mannose (351).

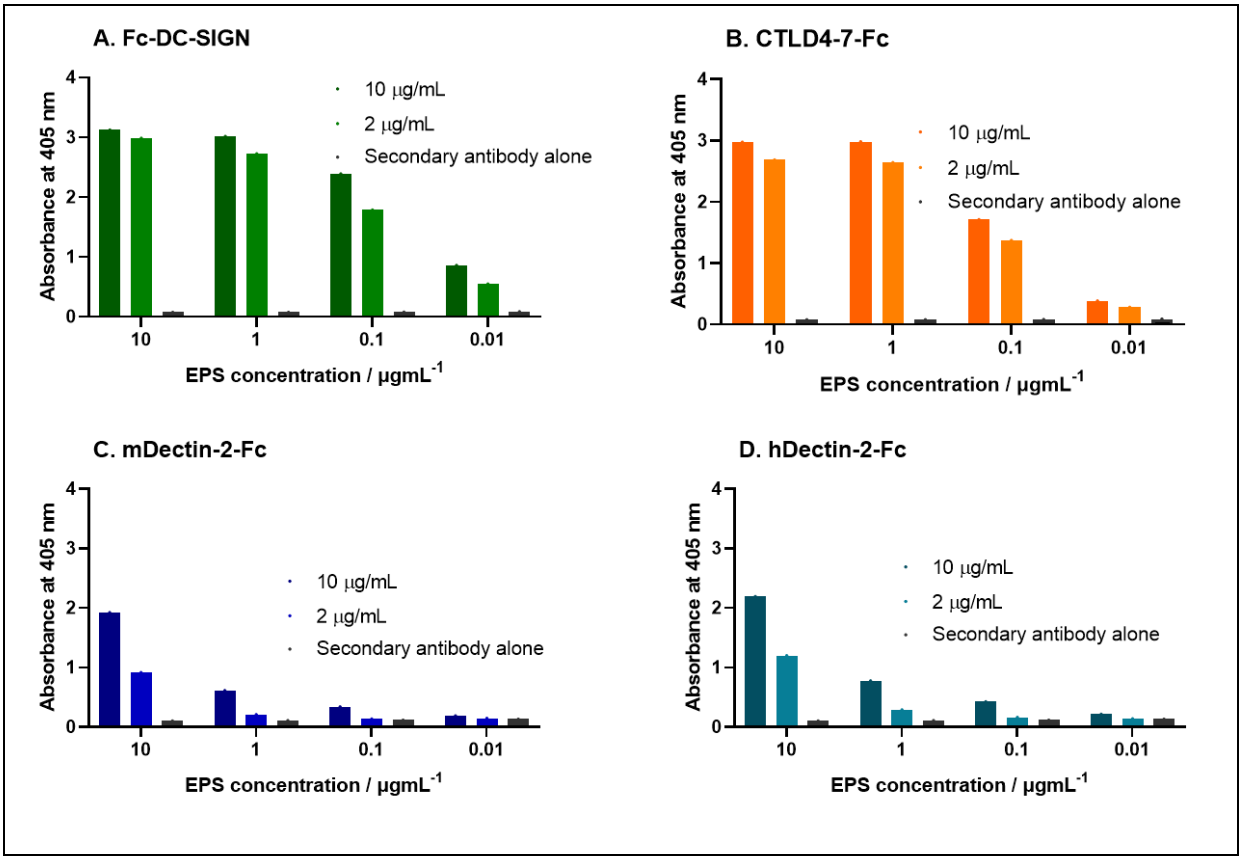

Figure 3. 9: Binding of Fc-conjugated CLRs to S. aureus SH1000 biofilm carbohydrate post-FPLC shows similar levels of binding to PAO1ΔwspFΔpel carbohydrate*. Relevant wells of 96-well plate was coated with between 10 and 0.01 µgmL^{-1} in 50 µL of carbohydrate preparation, followed by incubation with 10 and 2 µgmL^{-1} of relevant lectin. After washing, wells were incubated with IgG2 conjugated with alkaline phosphatase. On addition of substrate, absorbance was read at 405 nm after 10 min. (**A**) Fc-DC-SIGN and (**B**) MR CTLF4-7-Fc showed highest levels of binding. (**C**) mouse- and (**D**) human-Dectin-2-Fc bound at lower levels, but were comparable with each other, and showed greater dose-effect. Results were analysed using Graphpad Prism 9, n=1.*

A competitive ELISA assay was developed as it was unclear whether binding observed in the previous assays was true or an artefact. For binding assays, Maxisorb plates are used to allow for maximum adherence of samples to the well surface. For the assay, plates were coated with 2 µgmL^{-1} of fucose, the positive binding control for MR CTLD4-7-Fc and Fc-DC-SIGN and incubated overnight. MR CTLD4-7-Fc and Fc-DC-SIGN at 2 µgmL^{-1} each were incubated with 10, 1, 0.1, 0.01 or 0 µgmL^{-1} of carbohydrate preparation from PAO1 Δ*wspF*Δ*pel* to saturate the receptor, then added to fucose-containing wells to determine

if fucose could compete for the binding pocket. As we suspected, *P. aeruginosa* EPS was able to compete for binding, indicated by lower absorbance values at higher concentrations, where lectins previously anchored in the plate by control sugar were washed away (**Figure 3.9**). *P. aeruginosa* EPS showed the greatest binding avidity to Fc-DC-SIGN when compared with fucose, able to significantly displace at concentrations as low as 0.1 μgmL^{-1} (**Figure 3.10A**). EPS was also able to compete with $Lewis^X$, but to a lower extent, requiring 50 μgmL^{-1} to significantly displace $Lewis^X$ (**Figure 3.10B**). For MR CTLD4-7-Fc, EPS was able to significantly compete with fucose, although to a lower extent than with Fc-DC-SIGN, only reaching significance at 1 μgmL^{-1} or higher (**Figure 3.10C**). Finally, EPS was able to significantly displace Dectin-2-Fc's known ligand, Zymosan, from 10 μgmL^{-1} and higher (**Figure 3.10D**).

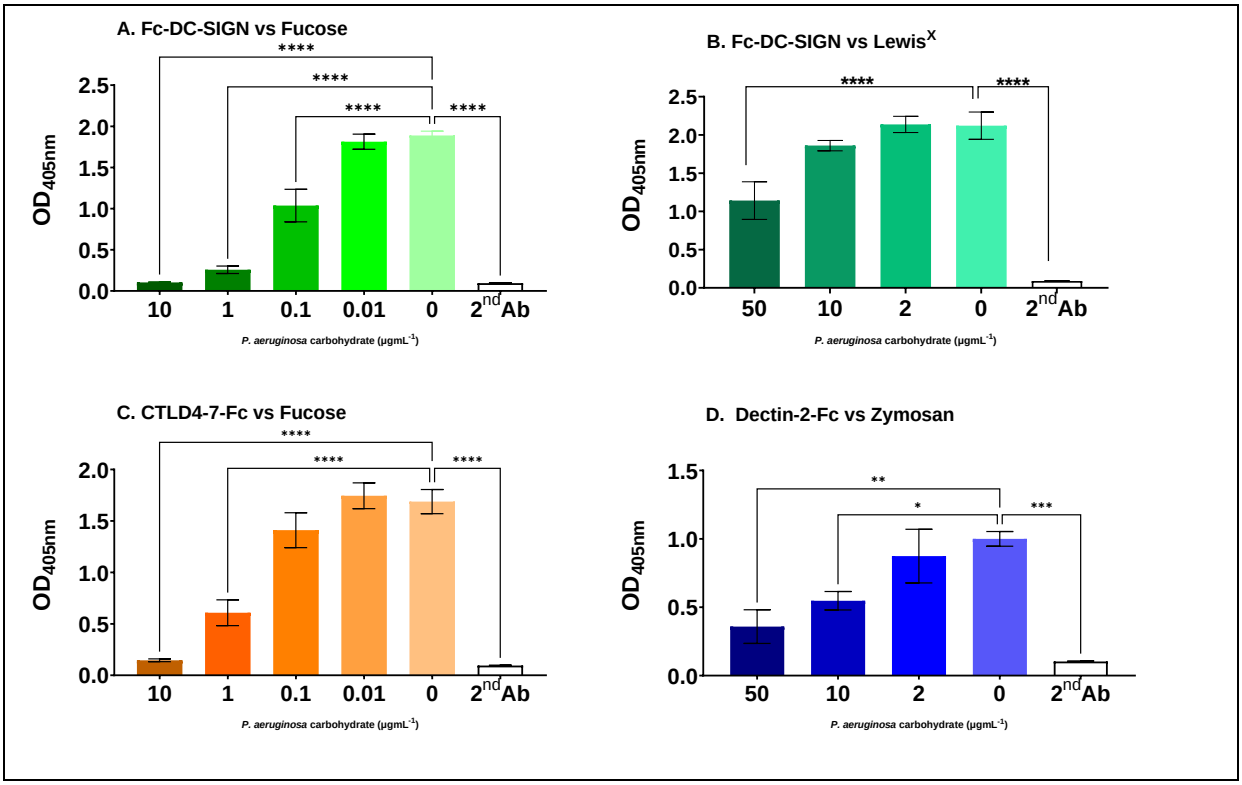

Figure 3. 10: Competitive binding of lectins with P. aeruginosa PAO1ΔwspFΔpel carbohydrate with known ligands*. Wells were coated with 2 μgmL^{-1} of control sugar and incubated overnight. In separate 1.5 mL Eppendorf tubes, 2 μgmL^{-1} of relevant Fc-conjugated lectin incubated with a range of carbohydrate concentrations for 1 h. Wells containing sugars were incubated with protein-carbohydrate mixture before washing and incubation with anti-human IgG conjugated to alkaline phosphatase before addition of substrate and reading absorbance at 405 nm. Results were analysed using Graphpad Prism 9, and one-way ANOVA corrected for Dunnett's multiple comparisons showed that carbohydrate significantly outcompeted fucose with Fc-DC-SIGN from 0.1 μgmL^{-1}(**A**, ($F_{5,18}$) = 80.89, p = <0.0001), and Lewis^X with Fc-DC-SIGN at 50 μgmL^{-1} (**B,** ($F_{4,10}$) = 105.2, p = <0.0001). With MR CTLD4-7-Fc, carbohydrate competed significantly with fucose from 1 μgmL^{-1} (**C,** ($F_{5,17}$) = 46.06, p = <0.0001), while for Dectin-2-Fc, carbohydrate was able to significantly compete with Zymosan from 10 μgmL^{-1} (**D,** ($F_{4,10}$) = 11.9, p = 0.0493). Secondary antibody alone showed very low levels of binding (**A, C**) n=4, (**B, D**) n=3.*

Once assay was optimised, we compared the ability of various carbohydrate preparations (kindly provided by Darryl Jackson) to displace fucose in Fc-DC-SIGN binding assays. Differences in binding between each *P. aeruginosa* preparations and the *S. aureus* preparation were not detected (**Figure 3.11**). Two different preparations of *P. aeruginosa* carbohydrates were tested here, as the purification process was slightly different between the two (**Figure 3.11 – green**). For the first preparation, FPLC was performed

at 4 °C while subsequent preparations were performed at RT. Due to this, we were concerned the final product may have been affected, altering binding capacity to the lectins. However, this was not the case.

Due to the indistinguishable binding between *S. aureus* and *P. aeruginosa* EPS, and previous reactivity between Fc-DC-SIGN and another media type, X-Vivo15 (**Section 3.5.2, Figure 3.3C**), we were wary that the media itself was providing ligands, so endeavoured to extract and purify carbohydrate from media alone (i.e. without bacteria) to test binding in the high and low molecular weight fractions. As expected, the low molecular weight fraction was unable to compete with fucose (**Figure 3.11 – light blue**), showing that ligands remain in the fraction >17kDa. However, as with *S. aureus* EPS, high molecular weight carbohydrates from TSB alone were able to compete with fucose to bind Fc-DC-SIGN, indistinguishable from that of *P. aeruginosa* (**Figure 3.11 – dark blue**). Therefore, we were able to conclude that a substantial portion of our product derived from the media and could contribute strongly to our EPS interactions with CLRs.

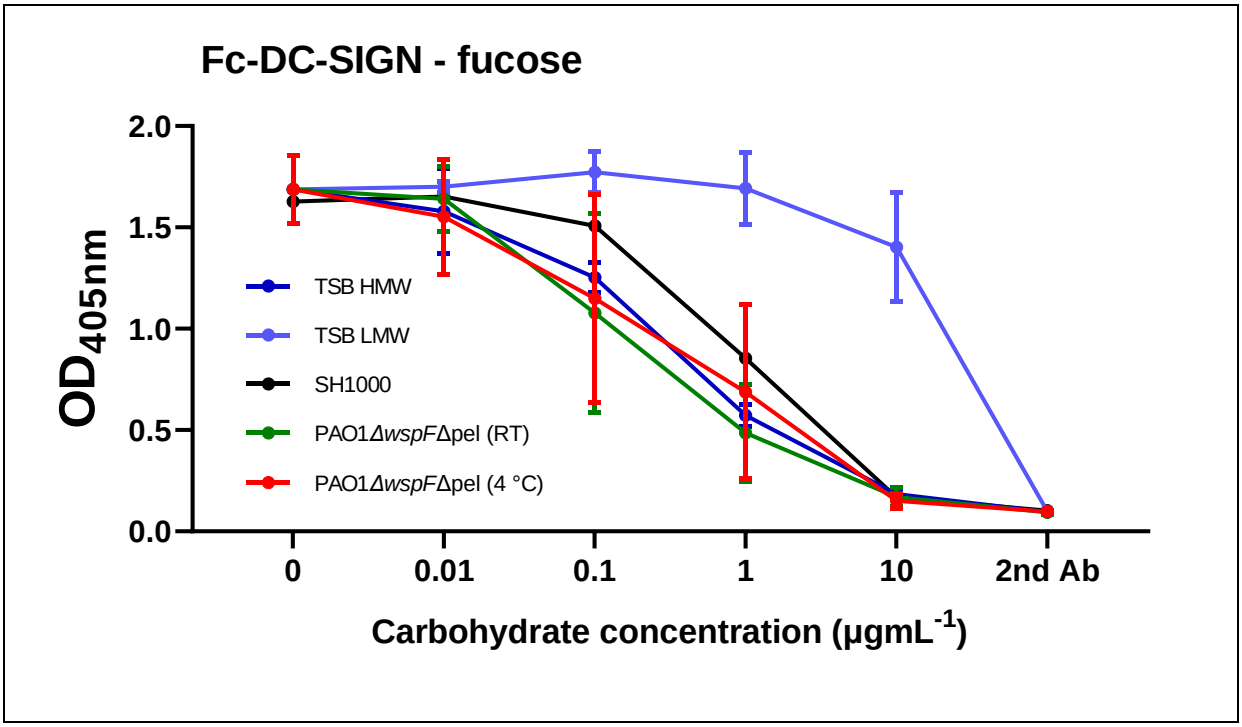

Figure 3. 11: Competitive binding of P. aeruginosa PAO1ΔwspFΔpel, S. aureus SH1000 biofilm and TSB-only carbohydrates with fucose for Fc-DC-SIGN binding shows a binding artefact in culture medium*. Wells were coated with 2 µgmL^{-1} of control sugar and incubated overnight. In separate 1.5 mL Eppendorf tubes, 2 µgmL^{-1} of relevant Fc-conjugated lectin incubated with a range of carbohydrate concentrations for 1 h. Wells containing sugars were incubated with protein-carbohydrate mixture before washing and incubation with anti-human IgG conjugated to alkaline phosphatase before addition of substrate and reading absorbance at 405 nm. P. aeruginosa PAO1ΔwspFΔpel carbohydrates (green and red), S. aureus SH1000 carbohydrate (black) and high molecular weight portion of TSB-only carbohydrate (dark blue) showed comparable levels of competition, while the low molecular weight portion of TSB-only carbohydrate (light blue) was unable to compete. Results were analysed using Graphpad Prism 9 with one-way ANOVA with corrections for multiple comparisons, n=3 (except SH1000, n=1).*

3.5.5 Optimisation of *P. aeruginosa* growth in minimal media for carbohydrate extraction produces a new carbohydrate without carbohydrate contaminants from culture medium.

Now it was clear that there are indeed ligands for our receptors directly in the TSB medium, it was important to optimise biofilm growth in a new, defined medium that did not contribute ligands in the same way. In the previous chapter, we optimised bacterial growth in plate-format to determine lectin binding characteristics using DMEM-BSA (DMEM-5921 supplemented with 5% BSA, 10 mM HEPES, 2 mM L-glutamine) and showed that there were indeed ligands for Fc-DC-SIGN and Dectin-2-Fc, but not to media alone (**Section 3.5.4, Figure 2.12**). Therefore, we intended to optimise the large-scale method for carbohydrate extraction and purification to incorporate this medium, providing us with a product where potential CLR ligands are solely provided by *P. aeruginosa* biofilms.

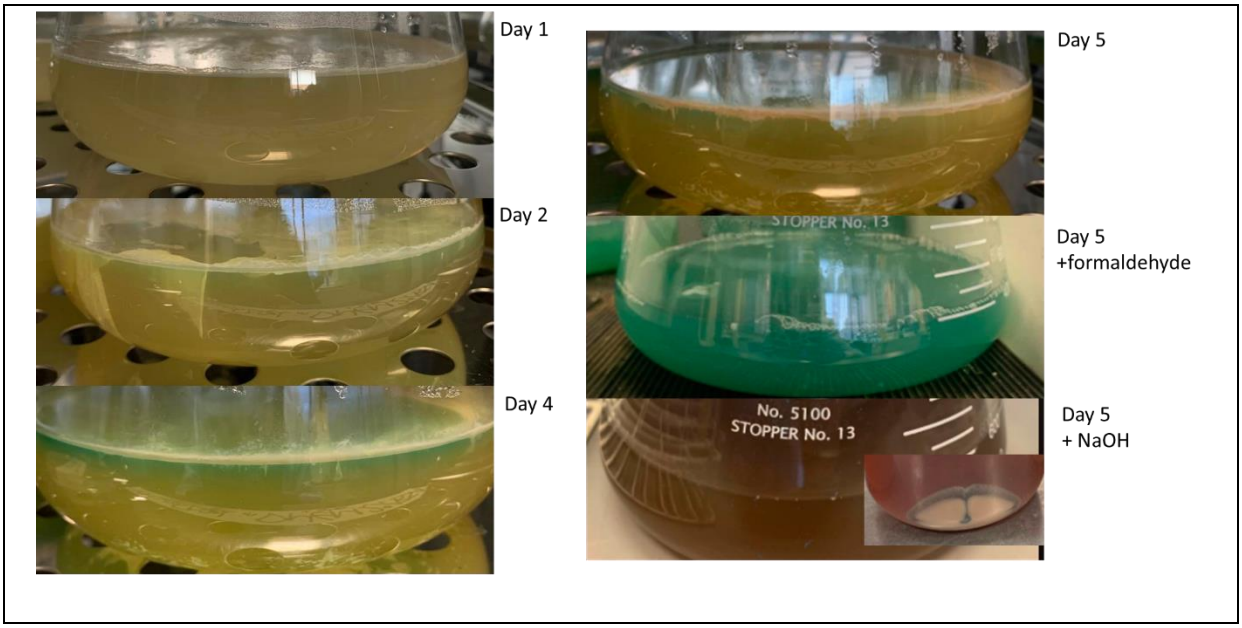

Figure 3. 12: Formation of PAO1ΔwspFΔpel biofilm pellicle over 5 days in DMEM-BSA, with formaldehyde and NaOH treatment. *Overnight cultures of PAO1ΔwspFΔpel in DMEM-BSA was added to 400 mL DMEM-BSA (5%) and incubated statically at 37 °C for 5 days. Pellicle formation was observed from day 2, and green colouration from day 4. This blue colouration was distributed throughout the culture during formaldehyde fixation. On addition of NaOH, blue colouration was replaced with brown. After centrifugation, bacterial pellet was small.*

We attempted initial biofilm growth using the method for *P. aeruginosa* described previously (**Figure 3.3**), where we were able to produce a robust, thick pellicle over the 5 day incubation (**Figure 3.12**). Interestingly, from around day 2, green colouration was clearly visible directly below the pellicle, indicating the presence of pyocyanin and/or pyoverdin. Both of these products are secreted by *P. aeruginosa* under high-stress conditions, acting as oxidising agents for competing species, suggesting that directly below the pellicle, oxygen is reduced and bacteria are changing phenotype, similarly to the chronic wound environment. Further, on addition of formaldehyde on day 5, this distinct layer became distributed throughout the culture. On addition of NaOH for carbohydrate solubilisation, the solution turned brown. This was surprising, as it is pH of 4.8 and below that is associated with the pyocyanin colour change to red/brown (396), whereas this culture was strongly basic on addition on NaOH. Also, compared to *P.*

aeruginosa in TSB, on centrifugation, the bacterial pellet was much more compact and had no jelly-like component, indicating a very different type of growth and supporting the hypothesis that the growth environment heavily influences biofilm characteristics and architecture.

Unfortunately, at this stage, we were unable to pass our carbohydrate-containing supernatant through the 0.22 μM filter to remove any remaining bacteria. Therefore, we took a step back and considered the proportion of BSA required to a) produce good biofilms while b) allowing us to effectively filter away all bacteria. Using a scaled-down version of the protocol, 50 mL in 250 mL conical flasks (compared to 400 mL in 2 L flasks), we tested various concentrations of BSA, showing that biofilm thickness increased with percentage of BSA (**Figure 3.13**). Bacterial growth was not supported in the absence of BSA. Further, pyocyanin production was only observed at 5% BSA (**Figure 3.13** – top row), as well as the brown colouration on NaOH addition (**Figure 3.13** – bottom picture row). Biofilm thickness related to the number of filter units required for complete filtration (**Figure 3.13** – bottom row). As with the full-scale culture, 5% BSA required extensive filtering, so was unsuitable. Therefore, a compromise was formed going forward, opting for utilisation of 2% BSA, where biofilm wasn't as substantial as with 5%, but was still present and allowed for filtering.

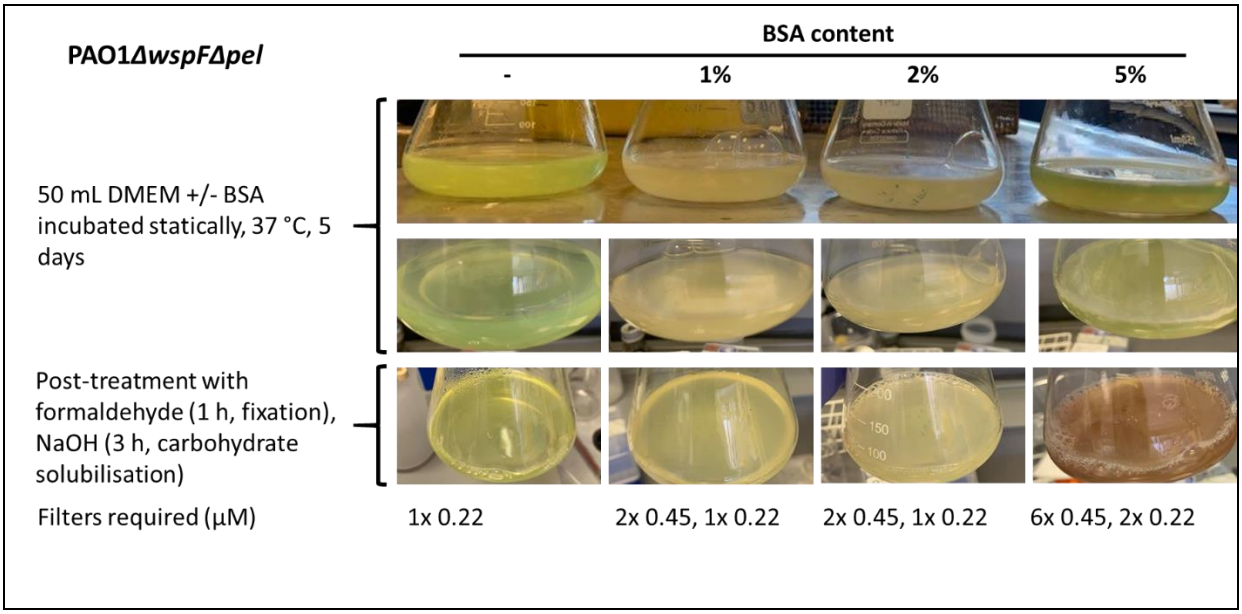

Figure 3. 13: Scale-down biofilm pellicle formation of PAO1ΔwspFΔpel in varying proportions of BSA before and after formaldehyde and NaOH treatment. *Overnight cultures were incubated in 0-5% DMEM-BSA and incubated statically at 37 °C for 5 days before formaldehyde fixation and carbohydrate solubilisation with NaOH. Biofilms were not supported at 0% BSA, and biofilms were poor at 1% BSA, increasing in thickness as BSA% increased. Bottom row denotes number of filters required for complete removal of bacterial cells.*

In addition, we were interested to determine whether glucose concentration affected biofilm growth in the culture, for the current strain as well as PAO1*ΔwspF*, where bacteria produced maximum biofilm biomass (**Section 2.5.4, Figure 2.11**). Here, biofilm growth was supported in all conditions (DMEM-2%BSA), with better pellicle formation at higher glucose concentration (**Figure 3.14**). Interestingly, even at 2% BSA, pyocyanin production was restored at high-glucose concentration after 5 days. This initially seemed counterintuitive, as bacteria here had access to more carbon sources and should therefore be less stressed, but it is also possible that due to rapid bacterial growth in the presence of glucose, that oxygen was depleted rapidly as in the high-BSA conditions, causing bacteria to secrete these stress-responders. In addition, regardless of the presence of more glucose, *Pseudomonas* tends to prefer succinate as a carbon source during its metabolism, allowing for maximum virulence (397, 398). Therefore, it would

be interesting to use succinate as a limiting factor in future experiments. Although this high-glucose condition was not pursued going forward here, it will be explored in later work.

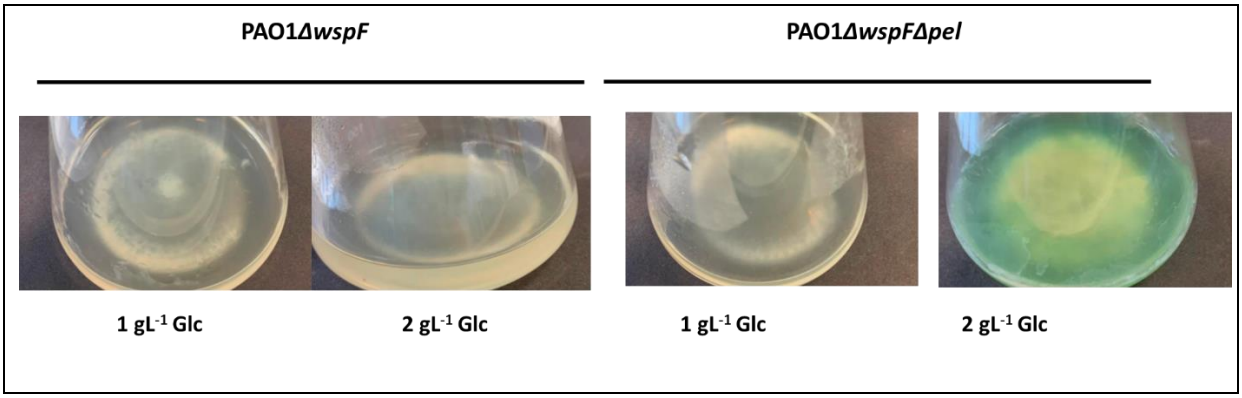

Figure 3. 14: Scale-down biofilm pellicle formation of PAO1ΔwspFΔpel and PAO1ΔwspF in DMEM-BSA with normal physiological and high, diabetes-associated levels of glucose.

Using normal, physiological concentration of glucose alongside 2% BSA, cultures were produced for carbohydrate extraction. The protocol was originally attempted as before, but as carbohydrate levels were likely lower than in TSB, during addition of ethanol to the extract, concentration was not high enough to precipitate out of solution, hence it was lost. To combat this, after TCA precipitation of proteins and nucleic acids, supernatant was lyophilised, concentrated and underwent second dialysis before ethanol precipitation. However, product was lost here again due to damage of the dialysis membrane caused by the low pH (pH 1-2), causing it to rupture. After this realisation, product was neutralised using Tris-base after reconstitution after lyophilisation to a pH of 7. In addition, this run utilised TCA in 70% solution rather than solid, and was added gradually during stirring at 4 °C. This allowed for improved distribution of the TCA within the extract, for more effective precipitation. The final protocol is summarised in **Figure 3.15**. When the product was characterised for total protein and carbohydrate

concentration, we showed that the product had considerable protein, 1,015.5 μgmL^{-1}, but maintained carbohydrate content.

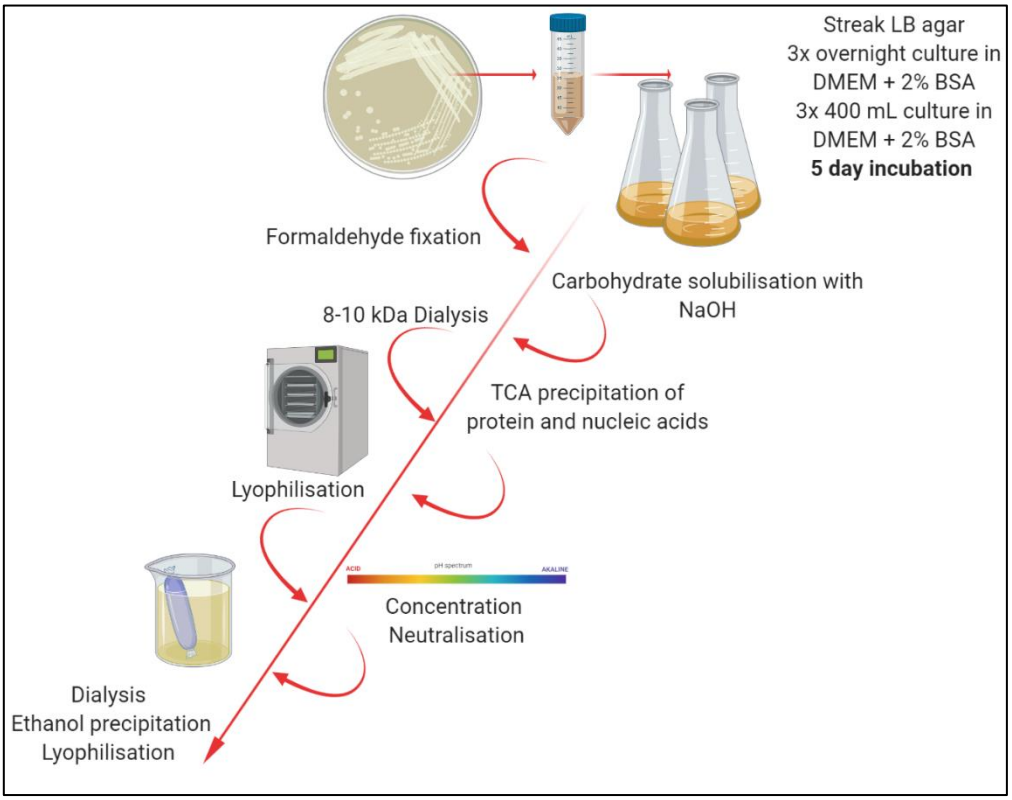

Figure 3. 15: Schematic for carbohydrate extraction and purification final protocol for PAO1ΔwspFΔpel.

Due to time constraints, ethanol precipitation of this new product was not conducted during this project, but has been continued by another lab member (Dr. Sonali Singh). Here, a pellet was found after ethanol precipitation which is ready for lyophilisation. A binding ELISAs was been performed against crude extracts to determine if carbohydrate produced using this method produces any ligands for our CLRs. So far only Fc-DC-SIGN (**Figure 3.16A**) and MR CTLD4-7-Fc (**Figure 3.16B**) have been tested. Fortunately, ligands were maintained for DC-SIGN, albeit at low binding levels compared to that of whole biofilms. For MR, like in whole biofilms, binding was not achieved for this preparation.

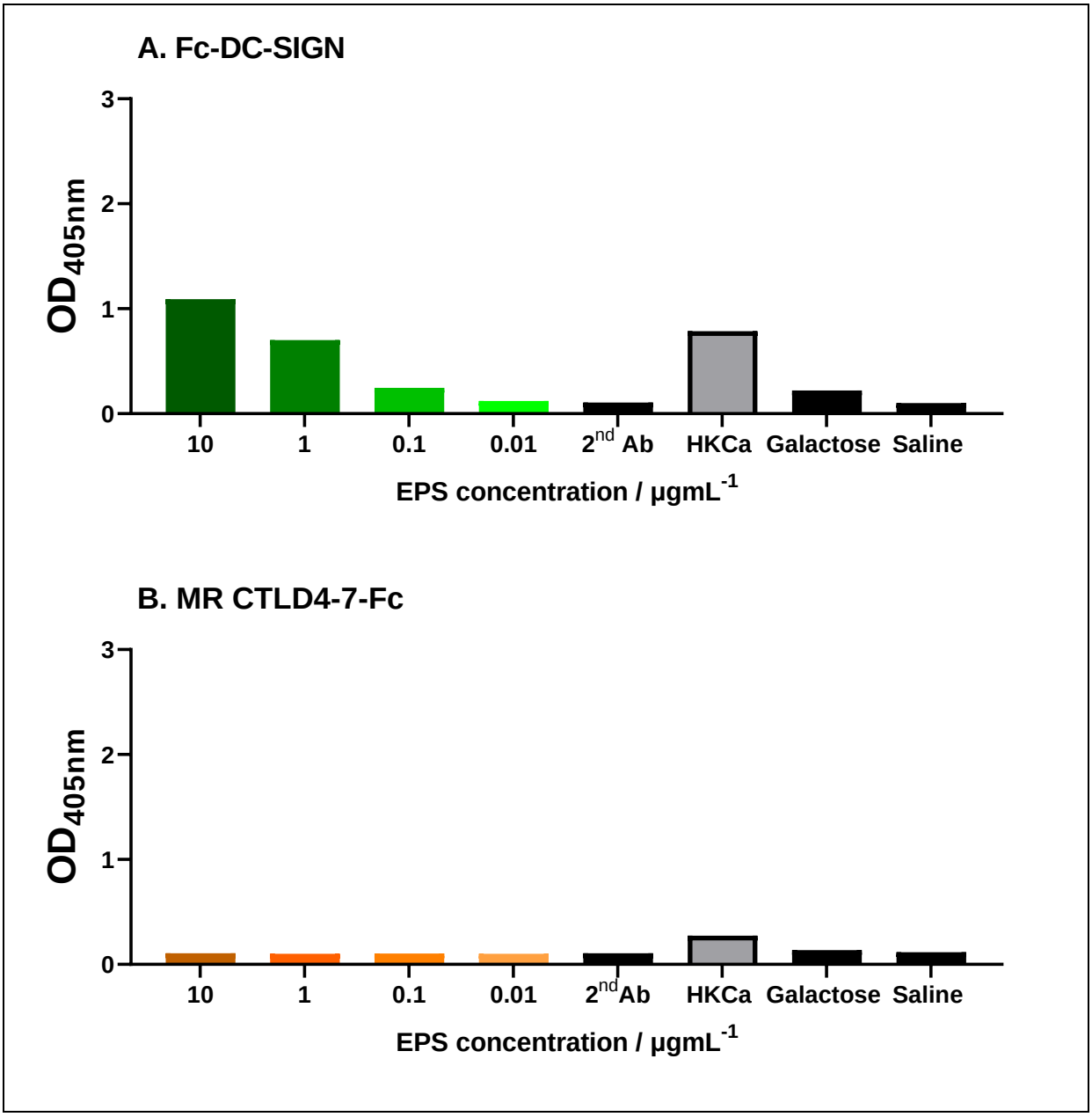

Figure 3. 16: Binding assays of Fc-conjugated CLRs to PAO1ΔwspFΔpel biofilm carbohydrate from DMEM-BSA show maintained binding to Fc-DC-SIGN, but not CTLD4-7-Fc*. Relevant wells of 96-well plate was coated with between 10 and 0.01 µgmL-1 in 50 µL of carbohydrate preparation, followed by incubation with 5 or 01 µgmL-1 of relevant lectin. After washing, wells were incubated with IgG2 conjugated to alkaline phosphatase. On addition of substrate, absorbance was read at 405 nm after 10 min. (**A**) Fc-DC-SIGN was able to maintain binding at low levels, while (**B**) MR CTLF4-7-Fc showed no binding. Results were analysed using Graphpad Prism 9.*

3.6 Discussion and future work

Several conclusions may be drawn from this chapter. Firstly, that using the methodology adopted previously in the laboratory, we can success produce, extract and purify biofilm carbohydrate from *S. aureus*, when its specific culture requirements are taken into consideration, with high carbohydrate yield and little protein contamination (**Table 3.1, Figure 3.4**). From here, we were able to show that plant lectins and CLRs bind this purified carbohydrate, in a similar fashion to *P. aeruginosa* carbohydrate, indicating high-mannose content (**Figure 3.5-7**). However, on comparison with carbohydrate extracted directly from TSB, we could confirm that some proportion of CLR ligands were provided directly from the media, not the bacteria (**Figure 3.8**). Finally, that the protocol can be altered to accommodate defined media that lacks CLR ligands, while still maintaining biofilm production at a large scale for effective carbohydrate extraction and purification (**Figure 3.12**). The key message here, similarly with the previous chapter, is that biofilm characteristics are highly dependent on their environmental niche, and carbohydrate production specifically is differs depending on this, allowing for a multitude of possibilities for immune interaction and infection outcome.

It has been established during this project that bacteria are able to adapt to their surroundings depending on their environment, including media compositions, agitation level and culture volumes. In blood, NaCl concentration is 154 mM (0.9%) to remain isotonic with red blood cells, dictating the minimum concentration for our assay to remain clinically relevant (399). Increased salt intake in humans is associated with vascular hypertension, mostly because of the effects of kidney retention of NaCl and salt-dependant manifestations of high blood pressure such as arterial remodelling and augmented Ca^{2+} signalling in cardiomyocytes amongst others (400). However, even in

these patients, blood NaCl levels only tend to increase by up to 3mM due to rebalancing of sodium levels via natriuresis, alongside muscle and skin accumulation (400, 401). This increase in cutaneous salt is associated with macrophage activation via M1-polarisation, resulting in increased T cell activation, in particular an enhanced Th17 response, and reactive nitric oxide synthesis for pathogen control (402). Similarly, in chronic wounds, immune cells are associated with dysregulation and promotion of an inappropriate development of pro-inflammatory macrophage and T cells, linking the phenotype with this high-salt culture condition. Further, it was not surprising that TSB medium itself heavily influenced the properties of carbohydrate extracted, regardless of bacterial presence. Although a 'simple' culture medium, consisting of only 5 components (**Table 3.2**), both casein and soybean digests contain various products, including polysaccharides. Caseins, the major phosphoproteins in mammalian milk, provide the majority of peptides for TSB (403). Soytone, the enzymatic digest of soybeans, contains high concentrations of vitamins and carbohydrates, potentially providing ligands for our lectins. However, the carbohydrate composition is not currently defined, so without internal biochemical analysis, we cannot be certain.

Table 3.2: TSB formula per 1 L sterile water (from supplier).

Tryptone (pancreatic digest of casein)	17.0 g
Soytone (peptic digest of soybean)	3.0 g
Glucose	2.5 g
Sodium Chloride	5.0 g
Dipotassium phosphate	2.5 g

Although all 3 CLRs tested binding to *S. aureus* EPS was potentially a result of the media alone, there is evidence that these interactions do occur *in vivo*. Dectin-2 is most heavily

associated with fungal infection, including that of *C. albicans*, due to abundant mannosylated ligands in the fungal cell wall, essential for phagocytosis and killing using the FcRγ pathway (404). Although less common, bacterial recognition by Dectin-2 has been described, including *Klebsiella* and *Mycobacterium spp*. (151). Further, although the carbohydrate recognition domains of Dectin-2 show highest affinity for mannose, GlcNAc residues are indeed recognised, although to a smaller extent and affinity, allowing for *S. aureus* recognition (151). This is also the case for MR, where high-throughput binding characterisation determined that the receptor is able to bind GlcNAc, but with a much lower affinity than mannose (405).

The interaction between DC-SIGN with *S. aureus* biofilms appears to be more nuanced. In the study described above, DC-SIGN did not bind GlcNAc (405). Similarly, DC-SIGN binding affinity has been investigated in a range of whole organisms and carbohydrate motifs, showing extremely low to undetectable interaction with GlcNAc or whole *S. aureus* cells (163). However, this idea has been contradicted in multiple studies. DC-SIGN interacts with *Schistosoma mansoni* surface antigen, containing both GalNAc and GlcNAc residues, resulting in a downstream, humoral immune response (406). Further, DC-SIGN binds strongly with various Lewis blood antigens, importantly Lewis^X which is used during this project as a positive binding control sugar, also containing GlcNAc residues (191, 407, 408). Finally, DC-SIGN binds GlcNAc-containing, *N*-linked oligomannose structures, although affinity is proportional to the number of mannose moieties, implying that mannose is the major contributing component here (407).

On optimisation of DMEM-BSA to the purification process, we knew from work in the previous chapter that this media alone did not provide ligands for our CLRs but was able to support bacterial growth at a BSA proportion of 5% (**Section 2.5.4, Figure 2.12**).

Therefore, this was a good starting, although due to issues in filtration, BSA was reduced to 2%. It has previously been described that bacteria may change their cell size based on stress levels, which may affect the ability of bacteria to pass through the 0.22 μM filter. However, high-stress such as that implied here by pyocyanin production in DMEM-BSA, is associated with 'starvation forms' and cell shrinking (409), which would in turn make them easier to filter, the opposite of what happened here. Therefore, the difficulty is more likely a result of a more heavily proteinacious and 'sticky' biofilm pellicle, as evidenced by extensive precipitant during TCA treatment compared to TSB culture (data not shown). Although protein precipitation efficiency was improved using liquid (70%) rather than solid TCA, it was clear that it was not 100% effective. This could have been remedied by multiple precipitation steps, as is the case in other protocols where lower concentrations using multiple, long incubations are used, alongside incorporation of Proteinase K (410). Proteinase K digests proteins indiscriminately in their native form, unlike TCA which denatures proteins allowing them to precipitate, allowing for removal via centrifugation (411). However, protein activity relies on 37 °C conditions, and as this protocol is not performed under sterile conditions, it may allow for contamination. Further, at 29 kDa, Proteinase K would be too large for removal by dialysis, requiring re-introduction of TCA precipitation, reducing efficiency. Other methods of protein and lipid precipitation are also described, including the use of ammonium sulphate (412) and the chloroform/methanol method (413), but under inspection, these methods are either ineffective or unnecessarily hazardous respectively. It is difficult to deduce whether protein content post-second dialysis is comparable to that during TSB culture here, as quantification was not performed at intermediate stages during those processes. Therefore, although purification and characterisation is halted at this stage at present, it

is important to continue into carbohydrate precipitation using ethanol, as this may truly compare composition.

Although extremely effective with TSB culture, ethanol precipitation was not possible using the original protocol with the DMEM-BSA culture, likely due to lower concentrations of carbohydrate. Ethanol precipitation is the most commonly used method for extraction of polysaccharides from mixed samples, the yield depending heavily on the ethanol concentration. Indeed, on investigation of a range of ethanol concentrations to extract polysaccharides of different size and structure type, the most important factor was consistently the ethanol concentration, with maximum yields obtained >80%, although the average reported in the literature is between 70-80% (414). This implied to us therefore, that our concentration of 95% was not incorrect, and rather the failure due to the low carbohydrate concentration, prompting the incorporation of a concentration step. Now that the neutralisation has been incorporated, preventing the degradation of the cellulose dialysis membrane during second dialysis, and presence of carbohydrate confirmed, we are hopeful that ethanol precipitation will be successful.

It has been unfortunate during this project that complex biochemical characterisation of our products by our collaborators has been impossible. Biochemical analysis is invaluable due to specific identification of polysaccharide residues, sizes and linkages that may give us more accurate clues as to composition and hence, their binding activities with our lectins. For example, gel permeation chromatography (GPC) would confirm more accurately the specific molecular weight of our products, as opposed to a range determined by FPLC. Further, our FPLC standards rely on protein masses rather than polysaccharide to stay consistent with previous preparations, calling into question the accuracy of the product masses stated. In addition, proton-NMR analysis would provide

the monomer composition of our products in relation to proportionate weight. This was indeed incredibly useful in our previous study, where mannose was confirmed to constitute between 74.9-80.9% of the HMW fractions (191). Further, proton-NMR provides clues as to the overall polymer structure from which identifiable monomers arise, as was the case with TSB-cultured P. aeruginosa EPS, where linkage organisation heavily implied a 1-3/1-6-linked β-D-mannan precursor, a fungal-associated polysaccharide, in contrast with previous reports of Psl structure (245, 415).

Alongside this, in work going forward is essential that we analyse interaction with primary immune cells and immortalised cell lines expressing receptors of interest in order to determine cytotoxicity, ligand uptake, overall cytokine response and intracellular signalling using reporter cell lines to name a few. We have confirmed that carbohydrate extracted from *S. aureus* grown in TSB is not cytotoxic, and hence unlikely to induce a significant pro-inflammatory response, as was the case with *P. aeruginosa* (191), but it would be interesting to identify any small changes in basal cytokines or chemokines which may dictate immune response later, perhaps on addition of whole bacteria. As implicated in our previous study, although there was no direct cytokine response caused by our carbohydrate, it did inhibit signalling for Dectin-2, acting as an antagonist, as well as inhibiting uptake of known receptor ligands in the case of DC-SIGN and MR (191). In blocking these receptor, we may imply that EPS plays a role in T cell interaction with APCs, influencing proliferation and differentiation characteristics. It would be interesting to undertake this route for investigation. Ultimately, the goal in the lab is to purify carbohydrates from poly-microbial biofilm cultures, incorporating species associated with infected wounds, as it has been suggested that in these conditions,

carbohydrate structures physically change in comparison to monoculture, producing something novel that interacts divergently with immune cells (416).

All these things considered, the clinical implications for purified carbohydrates are broad. *S. aureus* produces glycopolymers throughout the biofilm cycle, including PIA, poly-β(1-6)-*N*-acetylglucosamine (PNAG), capsular polysaccharide (CP) and teichoic acids (354). PNAG is not specific for *S. aureus*, but synthesised by various other bacteria, fungi and parasites, leaving it a prime candidate in vaccine development (417). For example, both native and deacetylated PNAG conjugated to diphtheria toxin raised antibodies that showed opsonophagocytic killing in various animal models, the latter being the most effective (418). Further, it is possible to control ratios of acetylated vs deacetylated PNAG to optimise immune reactivity, incorporating additional groups for improved functionalisation (419). Capsular polysaccharide, situated outside the cell wall, acts as a defence against phagocytosis and killing as well as contributing to invasive biofilm formation (420, 421). Of *S. aureus* CPs, CP5 and CP8 are most abundant amongst clinical isolates, both constituting combinations of *N*-acetyl mannuronic acid and *N*-acetyl-$_{L/D}$-fucose moieties (354). Although there have been no studies to date, (422) has shown a relevance for longer chain CPs in immunogenic activity. Wall teichoic acids and lipotechoic acids, associated with peptidoglycan and the periplasmic space respectively, are associated with various virulence pathways and are recognised by various host lectins, and are therefore prime vaccine candidates (423-425). As discussed previously, WTAs may be accessorised with GalNAc and GlcNAc substituents that contribute to the escape host defence (426). Indeed, the WTA RboP backbone including its accessories has been successfully produced synthetically with a BSA conjugate as a prototype vaccine, although no subsequent efficacy data is available (427).

The production of biomimetics for lectin ligands with downstream immune function has also been explored previously. Neoglycopolymer-protein hybrids of varying mannose densities conjugated to BSA, produced by transition-metal-mediated living radical polymerisation and Huisgen cycloaddition, are able to bind proportionally MBL when measured by surface plasmon resonance (428). Further, glycopolymer-BSA conjugates show significantly enhanced complement activation and deposition of complement protein C9 in comparison to BSA alone, indicating their value in vaccines and enhanced drug efficacy. MBL is an interesting lectin, as it exists as a serum circulating CLR within the collectin family as part of a protein complex, and induces complement activation on binding to its ligands, which is enhanced in the presence of *S. aureus* (429, 430). Interestingly, in the absence of MBL in mice, *S. aureus* infection increased systemic inflammation after injury compared to controls, including increase in IL-6, implying its important role in homeostasis (431). As well as pathogen recognition, MBL is associated with cryptic self-antigen recognition after injury, cell death or modified disease states for immune fine-tuning (431, 432).

Targeting immune cells via carbohydrate receptors such as MR and MBL are attractive for both vaccine development and drug discovery due to their broad expression and known links to downstream immune effects (433). Indeed, development of high-affinity ligands has been attempted via reversible addition-fragmentation chain transfer (RAFT) polymerisation of functional mannose and GlcNAc monomers with fluorescent probes, able to specifically target murine bone marrow-derived macrophages *in vitro* and *in vivo*, with enhanced uptake in M2-polarised macrophages compared to galactose polymers, providing a promising route for specific drug delivery via these conjugates (434). Further, DC-SIGN has been implemented in direct blocking of HIV virus entry via gp120, where

incubation of soluble receptor with mannose showed decreased interaction (435). As well as these promising applications in drug delivery, synthetic polymers are attractive due to their low toxicity to immune cells. Also, their interaction with other blood components does not appear detrimental. Importantly, polymers of glucose and lactose derivatives produced using RAFT polymerisation do not trigger blood coagulation *in vivo*, as well as platelet and complement activation, and therefore highly haemocompatible (436).

In conclusion, this chapter has explored the optimisation of different bacterial species within the context of our carbohydrate purification methods, implementing new conditions and media types to investigate biofilm polysaccharides and their interactions with the human immune system. As with the previous chapter, this work has highlighted stark differences between *S. aureus* and *P. aeruginosa* and growth conditions. It has become apparent during this work that ligands for our receptors provided by the media itself are not insignificant, and hence we have taken this into consideration going forward, controlling conditions more carefully and adapting purification accordingly. In conducting this work, we have demonstrated that bacteria are adaptable, and polysaccharide ligands for our receptors come from a broad range of sources, increasing the nuance of immune interaction and modulation.

Chapter 4. Responses of human immune cells to biofilms

4.1 Introduction

Biofilms of bacteria and/or fungal communities exhibiting classical group behaviour and are inherently complex, producing a 3D environment with combinations of polysaccharides, extracellular nucleic acids, proteins and other components as discussed in previous chapters (216, 219). Biofilms form on both biological and abiotic surfaces and are particularly troublesome due to their insensitivity to antibiotics, phagocyte tolerance and quorum sensing, leading to diminished treatment effectiveness. Immune responses to biofilm and planktonic infections are also extremely complex, with generally poor understanding of the nuance within these types of infection. It is generally accepted that initial recognition of bacteria-derived material elicits a pro-inflammatory immune response via engagement of innate PRRs expressed by phagocytic cells such as macrophages and dendritic cells. These receptors are specific for groups of ligands (molecular patterns), including nucleic acids, lipids or polysaccharides. Throughout the previous chapters, we have shown that both whole biofilms and purified biofilm carbohydrates are able to interact with specific CLRs, namely DC-SIGN, Dectin-2 and MR which engage with high mannose structures, and hence biofilms containing Psl (191). It seemed logical progression therefore, to begin investigation of the whole immune response to biofilm infection, beyond simple interaction.

Severe compromise of the skin barrier through burns or trauma leaves an exposed surface for bacterial colonisation and biofilm formation, particularly in those subjects slow to heal. Local immune cells produce pro-inflammatory cytokines that enter the bloodstream and signal to other cells promoting inflammation; most notably, interleukin

(IL)-1β, IL-6 and tumour necrosis factor-α (TNF-α) (22). Chronic wounds comprise granulation tissue with new capillaries, extracellular matrix (ECM), including collagen, and immune cells, with micro-colonies of biofilm observed within the damaged tissue. Local infection of chronic wounds can lead to systemic infection and organ dysfunction and failure, and it is often worsened if bacteria exhibit the biofilm mode of growth (437).

In 2019 the International Wound Infection Institute consensus provided key definitions and terminology for diagnosing and treating chronic wounds (438). Diagnosis of infected chronic wounds is multifaceted, with requirements for a positive diagnosis including microbiological evidence of infection, presence of bacterial glycocalyx, recurrent infection within wound and fibrinous or necrotic tissue in the wound bed. The polymicrobial diversity goes hand-in-hand with the range of characteristics within the chronic wound, in that the heterologous population is instrumental in stimulating and maintaining the inappropriate and excessive inflammatory response that inhibits wound healing. Of the various treatments available, the most strongly recommended for ulcers and other wounds with suspected biofilm are debridement with antiseptic soaks and dressings (439).

S. aureus is a common skin commensal and, together with the environmental organism *P. aeruginosa* is frequently found in chronic wounds. In a longitudinal study of chronic wounds in patients, 93.5% of wounds were colonised by *S. aureus* while 52.2% were colonised with *P. aeruginosa* (329), with *S. aureus* located at the surface and *P. aeruginosa* deep in the wound bed, highlighting that multiple species within a wound might play unique roles in pathology. *S. aureus* biofilms circumvent TLR-2- and TLR-9-dependant recognition and clearance *in vivo*, with decreases in pro-inflammatory macrophage secretions, including TNF-α, IL-1β, CCL2 (MCP-1), CXCL2, iNOS, and increases in anti-

inflammatory arginase-1 with diminished phagocytosis (267). Flagellin and LPS of *P. aeruginosa* engage TLR-5 and -4 respectively to initiate an inflammatory response during acute infection (103). However, it has been observed that during chronic infections associated with cystic fibrosis, *P. aeruginosa* undergoes mutations in LPS or peptidoglycan that are no longer recognised by their receptors, TLR-4/-2, alongside flagellum being completely lost when the bacteria enters the biofilm mode of growth (440). Therefore, the immune response to biofilm is characterised by excessive respiratory burst by neutrophils, stratified hypoxia and dysregulation of innate immune cells, particularly macrophages (252).

Amongst this, the chemokine CCL2 is particularly relevant, as it is associated with the promotion of wound healing, likely by inducing innate immune infiltration soon after injury (441). Interestingly, CCL2 along with TNFα have also been associated with M1-type, classically activated macrophage response, which is more aligned with pathogen clearance and pro-inflammation rather than wound healing (442). Taken together, this further emphasises the almost paradoxical nature by which each individual immune component influences inflammation. Unravelling the nuance of this balance is particularly relevant in patients with diabetes, where dysregulation of the healing process leaves long term wounds highly susceptible to infection, often with poor prognosis and with a high risk of amputation due to limited success in treatment regimens (443).

My project initially focused on the comparison of the immune responses to *S. aureus* and *P. aeruginosa* biofilms, ultimately leading to the analysis of mixed species communities, which are more characteristic of clinical infections. However, it was decided that a new approach should be followed which includes comparison of planktonic vs biofilm

cultures, use of live instead of fixed cultures and inclusion of a 3D collagen matrix to create a wound-like environment.

4.2 Hypothesis

Previous work in the lab and results from the previous chapter show that the CLRs Dectin-2, DC-SIGN and the CTLD4-7 portion of MR bind to whole biofilms of *P. aeruginosa* PAO1 and its mutants in different media types as well as SH1000 *S. aureus* grown X-Vivo15. Hence, it was important to establish the biological relevance of these findings. In this chapter, we wanted to investigate immune cell interactions with whole biofilms, using 2D and 3D wound models. We hypothesised that **interaction of immune cells with biofilms will promote inflammation.**

4.3 Aims

Immune cell assays performed in the lab previously used fixed *P. aeruginosa* biofilms with different carbohydrate compositions and monocyte-derived dendritic cells and failed to identify any clear differences in downstream responses i.e. cytokines output. There was also high cell death in some of the cultures. Part of this could be due to poor bacteria fixation in the biofilm structures generating non-culturable, live bacteria. The overall aim of this chapter is to set the basis for the establishment of a physiologically relevant model to study the interaction of innate immune cells with bacterial biofilms. The next step would be to investigate how CLRs affect this interaction. Towards this aim we performed different studies to guide the selection of experimental settings.

- Normalise live biofilm cell numbers using known OD_{600nm} values of planktonic cultures.

- Optimise 2D infection assays using live bacterial cultures and 96-well plate format.

- Design a novel 3D model to mimic the chronic wound environment. This included:

    - Optimise production of biofilms embedded in a collagen matrix

    - Optimise culture of primary immune cells within collagen matrix

    - Optimise co-culture of bacteria and immune cells within the 3D wound model

    - Analyse bacterial and immune cell behaviour within the 3D wound model

4.4 Materials and Methods

4.4.1 Bacterial quantification using colony forming units.

To quantify bacterial numbers, live biofilms were washed carefully 3x with 200 µL PBS without calcium or magnesium (Sigma, D8537-500ML). PBS was then completely aspirated and 100 µL per well of X-Vivo15 medium added. Plates were stored at 4 °C while planktonic cultures were prepared. For planktonic cultures, overnights prepared as described in Section **2.4.1** were corrected to a range of OD_{600nm} values as appropriate and serially diluted tenfold in X-Vivo15 to a final dilution of $1x10^{-7}$. For biofilms, wells were scraped, and supernatants pooled to a sterile 1.5 ml Eppendorf tube before serial tenfold dilutions were performed as above. For each dilution, three 20 µL aliquots were inoculated onto sections of LB agar plates and incubated overnight. Colony forming units (CFU) were counted for each dilution and $CFUmL^{-1}$ calculated.

4.4.2 Fixation optimisation

Due to high levels of cell death in previous biological assays, it was hypothesised that live bacteria may remain after fixation of the biofilms. In previous experiments, biofilms grown for 22-24 hours were fixed in 4% paraformaldehyde (PFA) (16% EM grade, Electron Microscopy Sciences, 10710-S) in PBS for 10 min. In order to optimise the fixation technique, Δ*wspF* biofilms were grown as described above and treated with PFA as described in **Table 4.1**. Wells were then washed 3x with PBS and 50 µL PBS added to wells before UV sterilisation as indicated. PBS was then aspirated and 100 µL of X-Vivo15 medium added to wells. Plates were incubated for 4 or 24 h at 37 °C, 5% CO_2. After incubation, wells were scraped, and supernatants pooled to a sterile Eppendorf tube before CFU were calculated as described in Section **4.4.1**.

Table 4.1: Fixation conditions tested against ΔwspF biofilms.

Condition number	Fixation method
1	No treatment
2	10 minutes 4% PFA
3	20 minutes 4% PFA, 15 minutes UV

4.4.3 Interaction of human monocyte-derived macrophages with biofilm cultures and planktonic bacteria

Biofilms and planktonic cell cultures (100 µl per well) were prepared as described in Section **2.4.1** and human macrophages as described in **3.4.3**. To each well, $5x10^4$ macrophages were seeded in 50 µL in X-Vivo15 and plates incubated for 4 or 24 h at 37 °C, 5% CO_2. Plates were centrifuged (300 x g, acc/decc 3/3, 4 °C, 5 min), and supernatants collected for further analysis. In separate plates, wells were scraped and CFUs quantified as described in Section **4.4.1**.

4.4.4 Incubation of primary immune cells with 3D collagen matrix

Type I rat-tail collagen (Corning, 354249) was used to produce the 3D matrix as follows. In one 15 mL Falcon tube, 2 $mgmL^{-1}$ collagen (final) and 10 mM acetic acid (final, Honeywell Fluka, 34256-1L) was mixed by gentle rolling, followed by addition of X-Vivo15 medium and 10% human AB serum, rolled again and kept on ice. To begin polymerisation, 10 mM NaOH (Sigma, 52770-100ML) was added and the tube rolled carefully to not introduce bubbles (**Table 4.2**). Required volumes of resulting solution were added to 48- or 96-well TC-treated plates and to allow polymerisation at 37 °C, 5% CO_2.

Table 4.2: Example collagen tube volumes used during infection assays.

		Volume (µl)				Total volume (µl)
	Collagen stock (10 mg/ml)	Acetic acid stock (1 M)	AB Human Serum	NaOH stocks (1 M)	X-Vivo 15 medium	
Collagen tube	2000	100	1000	100	6800	10000

For immune cell incubation assays, 100 µL of X-Vivo15 medium or collagen prepared as described above was added to relevant wells of a 96-well TC-treated plate and incubated for 1 h, 5% CO_2, 37 °C allowed to polymerise. Untreated monocytes, GM-CSF-treated monocytes or moDCs were seeded at $5x10^4$ cells per well in 50 µl and incubated for 24 or 48 h 37 °C, 5% CO_2. Final volume 150 µl. Collagen matrix was then digested using an equivalent volume of collagenase (Sigma, C6885) at 500 μgmL^{-1} in PBS at 37 °C, 5% CO_2 for 1 h. Well contents were collected to assess cell numbers and viability using Trypan blue.

4.4.5 Embedding biofilm into collagen matrix for quantification by colony forming units

Biofilms were produced in 96-well plates as described in Section **2.4.1**, but allowed to grow for 4, 16 or 24 h before washing 3x with 200 µL PBS without calcium and magnesium. To these wells, collagen solution was added (100 $\mu Lwell^{-1}$) and allowed to polymerise as described above. After incubation, an equivalent volume of collagenase (500 µgmL-1 in PBS) to that of collagen was added directly to wells and incubated at 37 °C for 1 h. Well contents were pooled and vortexed and 1:10 serial dilutions performed as in Section **4.4.3**.

4.4.6 Development of the 3D collagen model to incorporate bacteria and immune cells.

moDCs were generated as described in **3.4.3**. In parallel, PAO1 biofilms in X-Vivo15 were produced as described in **2.4.1** and allowed to mature for 16 h, before washing and coating with collagen as described in **4.4.5**.

While matrix polymerised, moDCs were harvested and washed 2x in 20 mL X-Vivo15 before incubation with 20 μgmL^{-1} anti-DC-SIGN (clone AZN-D1) or ultra-LEAF mouse IgG1κ isotype control (Biolegend, 400166) antibodies for 1 h at 37 °C, 5% CO_2. Cells were seeded to relevant wells (5 x10^4 cellswell^{-1}) in X-Vivo15 medium and incubated for 4 or 24 h at 37°C, 5% CO_2. Assays were set up with 6 wells for each condition (**Figure 4.1**). For collection of initial supernatants, plates were centrifuged (350 x *g*, acc/dec 3/3, 4 °C, 5 min) and surface liquid was carefully aspirated and pooled in 2 separate tubes (for 2 technical replicates) before storage on ice. Afterwards, collagen was digested by adding collagenase as described above. Once digested, samples were pooled to corresponding tubes already on ice. Tubes were mixed by inversion and cells tested for cell viability using Trypan blue. Remaining samples were vortexed thoroughly and an aliquot taken for CFU quantification as described in Section **4.4.1**. For the first 1:10 dilution, samples were diluted into sterile water and vortexed to lyse any remaining immune cells. Following dilutions were performed in PBS.

(*Note: during first experiment, supernatants were collected and stored separately to collagenase-digested samples for separate testing by Trypan blue and ELISA*).

A

	1	2	3	4	5	6	7	...
A								
B								
C								
D								
E								
F								
G								
H								

B

	1	2	3	4	5	6	7	...
A								
B		DCs only						
C		DC + antiDC-SIGN (20 µg/mL)						
D		DC + antiIgG (20 µg/mL)						
E		DCs only						
F		DC + antiDC-SIGN (20 µg/mL)						
G		DC + antiIgG (20 µg/mL)						
H								

Figure 4. 1: Plate layouts for collagen assay. *(**A**) plates were incubated for 16 h at 37 ^{0}C, 5% CO_2 with PAO1 to produce biofilms (green) or X-Vivo 15 alone (yellow) before washing and addition of collagen. (**B**) moDCs were incubated for 1 h with blocking antibodies or X-Vivo15 alone before mixing and seeding of 50,000 cells to each well and incubation for 4 or 24 h.*

4.4.7 Enzyme-linked immunosorbent assay

Cytokines were quantified following manufacturers' instruction (R&D systems). In brief, wells of a 96-well clear, flat-bottomed plate were coated with 100 µL capture antibody (concentration depending on kit, in PBS) for each cytokine tested and plate incubated overnight at RT. Wells were washed 3x in wash buffer (PBS without calcium or magnesium with 0.05% Tween20, Sigma-Aldrich, P1379-25ML) between each step. After the first wash, 300 µL 1X reagent diluent (R&D Systems, DY995) diluted from 10X stock in deionised water was added for blocking for 1 h, RT. After washing, 100 µL samples or standards were added to wells and plates incubated at RT for 2 h. Next, 100 µL detection antibody (concentration depending on kit, in reagent diluent) was added to wells before incubating for 2 h at RT. Following washing, wells were incubated for 20 min in the dark with 100 µL Streptavidin-HRP (1:40 dilution in reagent diluent). After a final wash, 100 µL substrate solution (1:1 colour reagent A (H_2O_2): colour reagent B (tetramethylbenzidine)) was added. Plates were incubated in the dark for 20 min for colour development. To end the reaction, 50 µL of stop solution (2 N H_2SO_4 in HPLC water) was added directly to wells and mixed by gently tapping and absorbance measured at 450 and 595 nm.

4.4.8 Flow cytometry analysis of moDCs

Following biological assay, cells were harvested by gentle pipetting, pooled and stored on ice. Cells were washed with 5 mL PBA (0.5% FBS (Sigma-Aldrich, F7524) and 0.1% sodium azide (Sigma-Aldrich, S2002) in PBS without calcium or magnesium) and centrifuged at 300 x *g*, acc/dec 3/3, 4 ^{0}C for 5 min. Supernatants were carefully aspirated and 0.5-1.0 mL PBA with 5% human AB serum was added to tubes for blocking, mixed by inversion and incubated at 4 ˚C for 1 h. After incubation, 100 µL of cell suspension (2-4x10^{5} cellstube^{-1}) was added to relevant FACS tubes (Fisher Scientific, 10100151) and single colour control antibodies or antibody cocktails added (**Table 4.3**). Tubes were shaken gently and incubated at 4 °C in the dark for 45 min. For the final 20 min of incubation, 1X Zombie UV was added to relevant tubes. Cells were washed with 2 mL PBA (300 x *g*, acc/dec 3/3, 4 ^{0}C for 5 min), supernatants discarded and pellets re-suspended in 0.5 mL 0.5% PFA in PBS without calcium and magnesium. These fixed samples were stored in the dark at 4 ^{0}C until analysis using an ID7000 Spectral Flow Cytometer where 2x10^{4} events were collected. Analyses were performed using Kaluza software.

Table 4.3: Antibodies and isotype control antibodies used during experiments.

Antibody	Supplier	Catalogue number	Clone	Isotype	Antibody per test (µg)
MR-Brilliant Violet 421	BioLegend	321126	15-2	IgG1	0.25
IgG1-Brilliant Violet 421	BioLegend	400158	MOPC-21	IgG1	0.25
CD11b-Brilliant Violet 711	BioLegend	301344	ICRF44	IgG1	0.25
IgG1-Brilliant Violet 711	BioLegend	400168	MOPC-21	IgG1	0.25
HLA-DR-Brilliant Violet 605	BioLegend	307640	L243	IgG2a	0.25
IgG2a-Brilliant Violet 605	BioLegend	400270	MOPC-173	IgG2a	0.25
DC-SIGN-Alexa Fluor 647	BioLegend	330112	9E9A8	IgG2a	0.125
IgG2a-Alexa Fluor 647	BioLegend	400234	MOPC-173	IgG2a	0.125
Zombie UV	Biolegend	423107	-	-	1:1000

4.4.9 Comparison of cytokine response by moDCs in the presence of collagen and LPS

Collagen solution was produced as described in **4.4.4** with or without inclusion of 50 ngmL^{-1} *E. coli* LPS (strain K12, InvivoGen, tlrl-eklps). For media-only conditions, X-Vivo15 was supplemented with 10% human AB serum and 10 mM each acetic acid and NaOH with or without inclusion of 50 ngmL^{-1} *E. coli* LPS so that the only difference in composition was that of collagen. Once polymerised, 5x10^4 moDCs were seeded to each well in 50 µL and incubated for 4 or 24 h, 37 ^{0}C, 5% CO_2 before collagenase digestion. Plates were centrifuged (350 x *g*, ac/dec 3/3, 4 °C, 5 min) and supernatants collected and pooled for ELISA (Section **4.4.7**).

4.4.10 Analysis of cytokine stability in the presence of bacterial biofilms

Biofilms of strains PAO1-L and PAO1-L*ΔlasR* were produced as described in Section **2.4.1** for 16 h in X-Vivo15 and washed 3x with 200 µL PBS without calcium or magnesium. After washing, 100 µL X-Vivo15 was added back to wells with known concentrations of cytokines (**Table 4.4**, cytokine standards from ELISA kits as described in **4.4.7**) with or without 1X cOmplete protease inhibitor (Merck, 11836170001) and incubated for 4 h at 37 ^{0}C, 5% CO_2. After incubation, plates were centrifuged (400 x *g*, ac/dec 3/3, 4 °C, 5 min), supernatant pooled and ELISA performed as described in Section **4.4.7**.

Table 4.4: cytokine concentrations used for protease degradation assay.

Cytokine	**Stock concentration / pgmL^{-1}**	**Working concentration / pgmL^{-1}**
MCP-1	3000	250
TNF-α	3250	250

4.4.11 Production of supernatants from biofilms grown in collagen for immunological assays

Biofilms of strains PAO1-L and PAO1-L*ΔlasR* were produced in X-Vivo15 as described in Section **2.4.1** for 16 h in TC-treated 96-well plates. Biofilms were washed 3x with 200 µL PBS without calcium or magnesium and collagen solution added and polymerised as described in Section **4.4.5**. Plates were incubated for 6 h at 37 ^{0}C, 5% CO_2. At the 2 h point, 50 µL media with or without 1X cOmplete protease inhibitor was added. After incubation, 100 µL collagenase (500 µgmL^{-1}) was added to wells and incubated for 1 h, at 37 ^{0}C, 5% CO_2. Once digested, samples were pooled and filtered through 0.22 µM filters to remove bacteria. An aliquot was taken from the each sample (except those treated with protease

inhibitor) and incubated for 10 min at 95 ^{0}C to denature all protein. Samples were aliquoted and stored at -80 ^{0}C for later experiments.

4.4.12 Immune response to bacterial supernatants

moDCs were produced and harvested as described in Section **3.4.3**. After washing, wells were counted and corrected to relevant cell density in X-Vivo15 with 10 ngmL^{-1} each IL-4 and GM-CSF. To each well of a 24-well TC-treated plate, 50 µL or 5 µL of supernatants from Section **4.4.11** was added, followed by 1x10^{6} cells in 450 µL, for a final supernatant dilution of 1:10 or 1:100. Plates were incubated for 4 h, 37 ^{0}C, 5% CO_2. Following incubation, samples were prepared for flow cytometry as in Section **4.4.8**.

4.5 Results

4.5.1 Normalisation of biofilm and planktonic cultures allows for comparison of both growth forms on ability to stimulate immune cells.

In previous studies performed in the laboratory, biofilms grown for 22-24 hours were fixed using 4% PFA in PBS without calcium or magnesium before incubation with primary immune cells. Biofilm biomass was quantified using a crystal violet assay before fixation, but live bacterial populations could not be analysed after incubation with immune cells ((191), supplementary information). Because of this, it was impossible to quantify MOI for these experiments or normalise different conditions for bacterial numbers during experiments. Further, after assays were performed to investigate the fixation efficiency, it was shown that the standard method was not always enough to eliminate all bacteria and hence, results from immune cell assays may have been compromised (**Figure 4.2A-B**). Interestingly, at 4 h after fixation, none of the replicates showed culturable bacteria. Although bacteria are not able to proliferate here to form colonies, perhaps due to shock from PFA treatment, live cells are residing within the biofilm as shown by their detection at 24 h. These cells may be contributing to the excessive inflammatory environment for the moDCs, leading to cell death. Therefore, for subsequent experiments, an alternative protocol was developed. It was also considered that comparing responses to biofilms and planktonic cultures normalised for CFU would yield relevant results for understanding of how biofilms modulate immunity. These experiments were performed with *P. aeruginosa* PA01 and *S. aureus* SH1000.

During initial experiments, we used exponential-phase bacterial cultures to produce biofilms; cultures were seeded at a set volume (100 µl) and optical density (OD_{600nm} 0.04) before incubation for 24 h. We also prepared sequential dilutions of planktonic cultures

to determine which dilution produced CFU numbers comparable to those obtained with biofilms. Here, PAO1 biofilms showed a mean CFU of $4.9x10^7$ cellsmL^{-1}, which was not significantly different to that of planktonic cultures with OD_{600nm} values between 0.02 and 0.3 (**Figure 4.2C**). Conversely, SH1000 biofilms showed much greater biofilm cell densities, with a mean of $3.0x10^8$ cellsmL^{-1}, which was not significantly different to planktonic cultures with an OD_{600nm} of 1.0 and 1.5 (**Figure 4.2D**). This difference in cell numbers values correlates with the differences in biomass observed in crystal violet readings between both pathogens (**Figure 4.2E**).

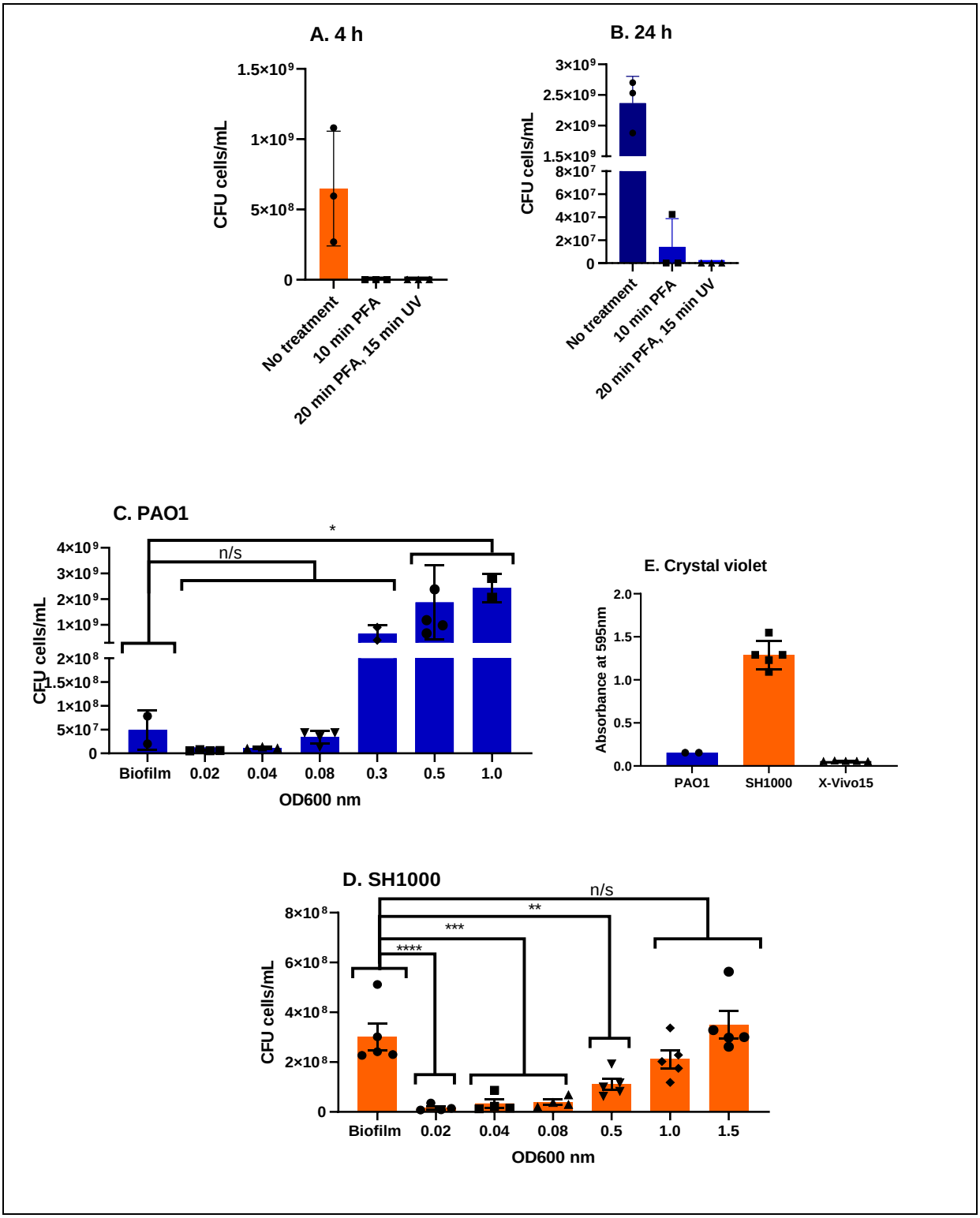

Figure 4. 2: Normalisation of planktonic cells against biofilm cultures using CFU. A-B. *Assessment of cell viability after fixation and UV exposure using ΔwspF biofilms. Biofilms were produced by plating 100 µL exponential-phase bacterial cultures at an* OD_{600nm} *of 0.04 and incubated at 37 °C, 5%* CO_2 *for 24 h. Biofilms were treated using the conditions shown and incubated with X-Vivo15 medium for* ***(A)*** *4 or* ***(B)*** *24 hours before harvesting, pooling, 1:10 serial dilution and inoculation to LB agar plates. CFUs were calculated for each condition and time-point.* ***C-E.*** *Normalisation of planktonic*

*and biofilms cultures using CFU. For live cultures, biofilms were produced as above. Remaining overnight culture was incubated overnight at 37 °C to produce new overnight planktonic cultures. For planktonic cultures, overnights were diluted to a range of OD_{600nm} values and serially diluted. For biofilm plates, wells were scraped, and supernatants pooled to a sterile Eppendorf tube before serial dilution. CFUs were calculated using the Miles Misra method and statistical analysis was performed using Graphpad Prism 9 with one-way ANOVA corrected for Dunnett's multiple comparisons test (n=4 (PAO1) or 5 (SH1000). PAO1 biofilm showed an average cell density of $4.91x10^7$, corresponding to OD_{600nms} from 0.02 to 0.3, defined by a non-significant difference to planktonic CFU values (**C,** ($F_{6,15}$) = 5.461, p = 0.0275). SH1000 biofilm produced an average cell density of $3.02x10^8$ $cellsmL^{-1}$, which was not significantly different to OD_{600nm} values of 1.0 and 1.5 (**D,** ($F_{6,25}$) = 13.41, p = 0.0045). Crystal violet analysis showed biofilm biomass consistent with CFU values (**E**).*

4.5.2 Viability of *S. aureus* biofilms and planktonic cells cultures is not affected by human macrophages, but both induce high macrophage cytotoxicity.

From the initial experiments where biofilm and planktonic cell densities were normalised, we were able to compare bacterial behaviour in the presence and absence of human macrophages. For this, *S. aureus* 24 h biofilms and planktonic cultures were incubated with human macrophages ($5x10^4$ $cellswell^{-1}$) generated as described Section **3.4.3** for 4 and 24h. There were no clear differences in bacterial cell numbers in the presence of macrophages compared to bacteria alone for planktonic or biofilm cultures at any time point (**Figure 4.3A-C**). This suggests that although these immune cells are generally highly phagocytic, they are not effective in killing bacteria alone in this assay. Rather, macrophages are generally described to clear other phagocytic cells that have internalised bacteria, such as neutrophils (444). At the time of seeding, the bacterial cell densities were between $1.3x10^8$ and $4.1x10^8$ $cellsmL^{-1}$ across all conditions, providing a multiplicity of infection (MOI) of around 225 for each well. Usually during infection assays, MOI should not exceed 10, and more likely fall between 0.1-1, which would prevent immune cells being overwhelmed by pathogens. Hence, unless the method for growing biofilms is altered to reduce bacteria numbers, it will be difficult to reduce the MOI during these assays. This formed part of the justification for moving on to the collagen model in Section **4.5.3**, where some of these issues may be alleviated.

In these experiments, macrophages were seeded into wells containing biofilms and planktonic bacterial cultures, wells without bacteria and wells containing Triton X (100% cell death) and incubated for 4 or 24 h before collection of supernatants to quantify cytotoxicity using the LDH assay. The first thing of note is that cell death appeared

extremely inconsistent between experiments. The LDH assay was repeated multiple times for the two experiments, yet there were no useable samples for cytotoxicity analysis using this method. It has been noted in the literature that many *S. aureus* strains are able to produce lactate dehydrogenase within certain metabolic pathways, particularly in response to innate immune attack which would likely interfere with the LDH assay output (445). Therefore, during the second run through of this experiment, supernatants were collected for SH1000 only for all conditions as well as SH1000 with macrophages to test this. Indeed, SH1000 alone did induce a colour change during the assay (**Figure 4.3D**). Therefore, an alternative method to measure immune cell cytotoxicity will be required for these experiments. However, the decision was made at this point that this line of investigation should be abandoned, with the new goal of prioritising the 3D collagen model as described in the next section.

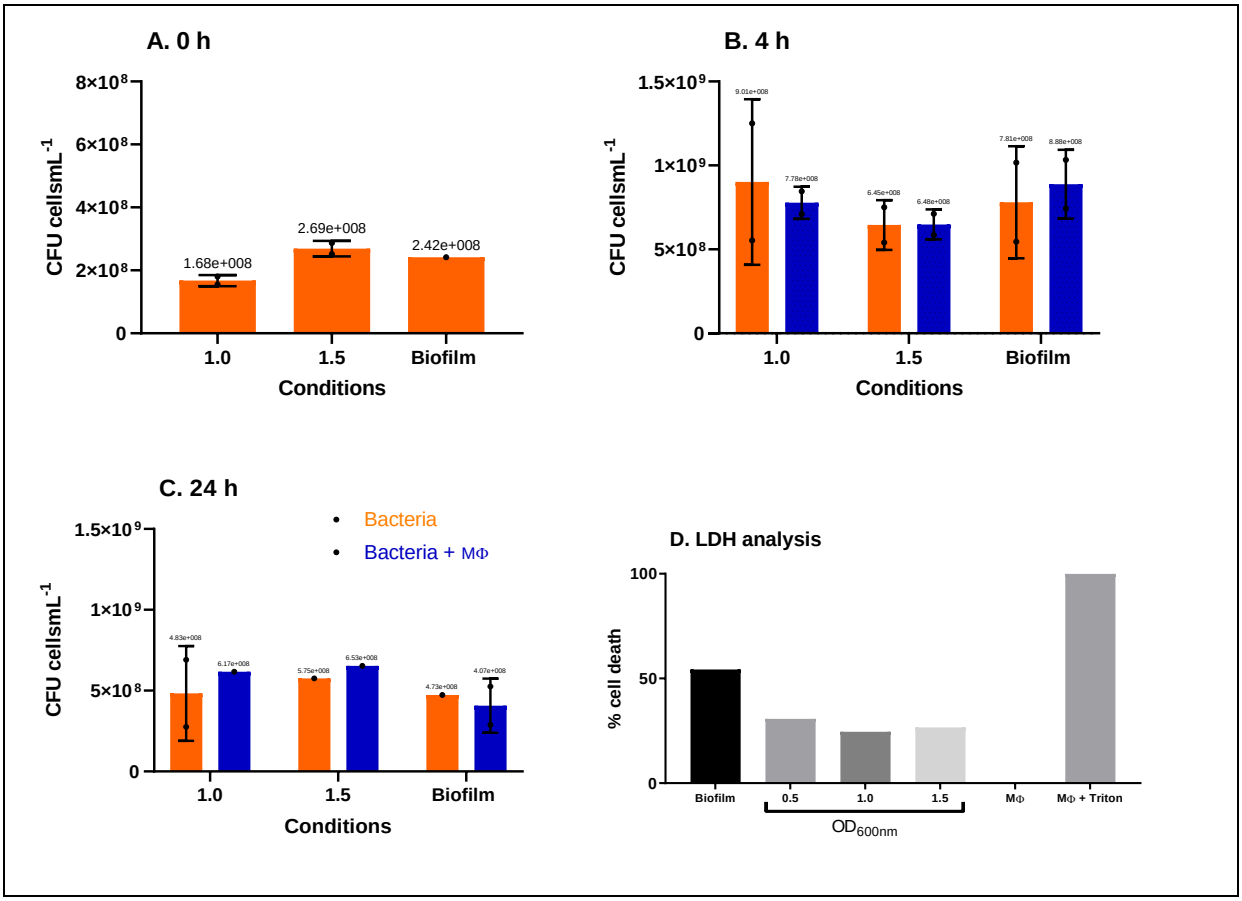

Figure 4. 3: Bacteria cell densities are not affected by presence of macrophage cells for both planktonic and biofilm SH1000 cultures. *Biofilms and planktonic cells were produced as described previously. After 24 h, biofilms were washed and 50 (planktonic) or 100 µL (biofilm) X-Vivo15 medium added. Macrophages were harvested on day 6 after differentiation of monocytes with 50 ng/mL M-CSF. When biofilms were ready, 5x10⁴ macrophages in 50 µL were seeded and incubated for (**B**) 4 or (**C**) 24 h. For 0 h, a plate was prepared separately for CFUs (**A**). Wells were scraped, pooled and serially diluted and CFUs counted. For the second set of cultures, plates were centrifuged, and supernatants collected for storage at -20 °C. Supernatants collected were analysed using the LDH assay to measure cytotoxicity. Here, cytotoxicity results were mostly unusable, likely due to interference by SH1000 in the assay (data not shown). Biofilm and planktonic culture supernatants were tested using the LDH assay and values normalised against untreated macrophages (0% cell death), showing that a colour change does indeed occur in the absence of immune cells (**D**).*

4.5.3 Development of 3D, collagen-embedded biofilm model using SH1000 and PAO1.

Within the chronic wound there are many complex interactions and components that make up the 3D space, such as the presence of infectious agents, host cells including immune cells and other tissue cells, extracellular matrix (ECM) and wound fluid as well as mechanical forces that are constantly exerted on the wound bed. The initial protocol used here was adapted from a study during which a sub-group of tumour-associated macrophages acquired a wound healing-like phenotype characterised by expression of certain factors (300). For the first attempt at this assay, 24-, 48- and 96-well TC-treated plates, two media types and a high and low volume of collagen were used to assess whether polymerisation would occur as expected, and that collagen plugs would be of adequate quality for culture (**Figure 4.4**). After some alterations to the original protocol, we successfully produced 3D matrices, using both RPMI-1640 and X-Vivo15. In the original protocol, a ratio of 1:1.5 of acetic acid to NaOH was used to trigger the polymerisation reaction, which did not successfully produce a plug here, perhaps due to the more complex nature of the mixture. Therefore, the protocol was adapted to alter the reaction to a 1:1 ratio for neutralisation. Further, we noted that using a high (10 $mgmL^{-1}$) stock concentration of collagen was essential for plugs to form, as we believe that when a low stock concentration (3.71 $mgmL^{-1}$), skewed the pH balance and hence, polymerisation was hampered.

For the next set of experiments, live biofilms of *P. aeruginosa* PAO1 and *S. aureus* SH1000 were produced over 24 h before washing and addition of collagen (**Figure 4.4**). Collagen readily polymerised on top of the PAO1 biofilm but was unable to do so in the presence of SH1000. The initial explanation for this was the physical size of the SH1000 biofilm. As

the polymerisation is triggered by a neutralisation reaction, the large, complex biofilm structure may have skewed the delicate pH balance, preventing the reaction from occurring. Therefore, for the next attempt with SH1000 biofilms, 24, 16 and 4 h biofilms were compared at both high and low seeding volumes. For the 4 and 16 h (immature) biofilms, polymerisation occurred regardless of seeding volume. For these assays, CFUs for biofilms grown in collagen were comparable to those grown in media alone (**Figure 4.4**). This was not the case with 24 h (mature) biofilms grown with either seeding volumes. For experiments going forwards, 16 h biofilms were selected as this time-point was more sustainable for the entire wound assay going forward.

For PAO1, bacterial cell numbers were compared between collagen and media to ensure growth was supported over time. Reassuringly, bacterial numbers increased over time for both conditions, and at 4 h were not significantly different from each other. However at 24 h, biofilms embedded within the collagen matrix significantly outgrew those incubated in media alone, with cell counts of $3.5x10^8$ and $8.1x10^8$ $cellswell^{-1}$ respectively (**Figure 4.5B**). This increase in proliferative capacity of the bacteria may be in response to serum or collagen. Here, it would be beneficial to expand the model to include fluorescently labelled bacteria and confocal microscopy, where we would be able to clearly visualise the bacteria within the matrix structure, confirming the preservation of the whole biofilm architecture, as well as any escaping planktonic cells. Finally, although optimisation of both *P. aeruginosa* and *S. aureus* biofilm embedding within the collagen occurred at this stage in the project, it was decided early in the investigation that we would only proceeding with *P. aeruginosa*. At this time, reagents and laboratory facilities were scarce and hence working had to be streamlined, with the hope of picking up more

avenues of investigation at a later date. Unfortunately, due to timing limitations of the project, this did not occur.

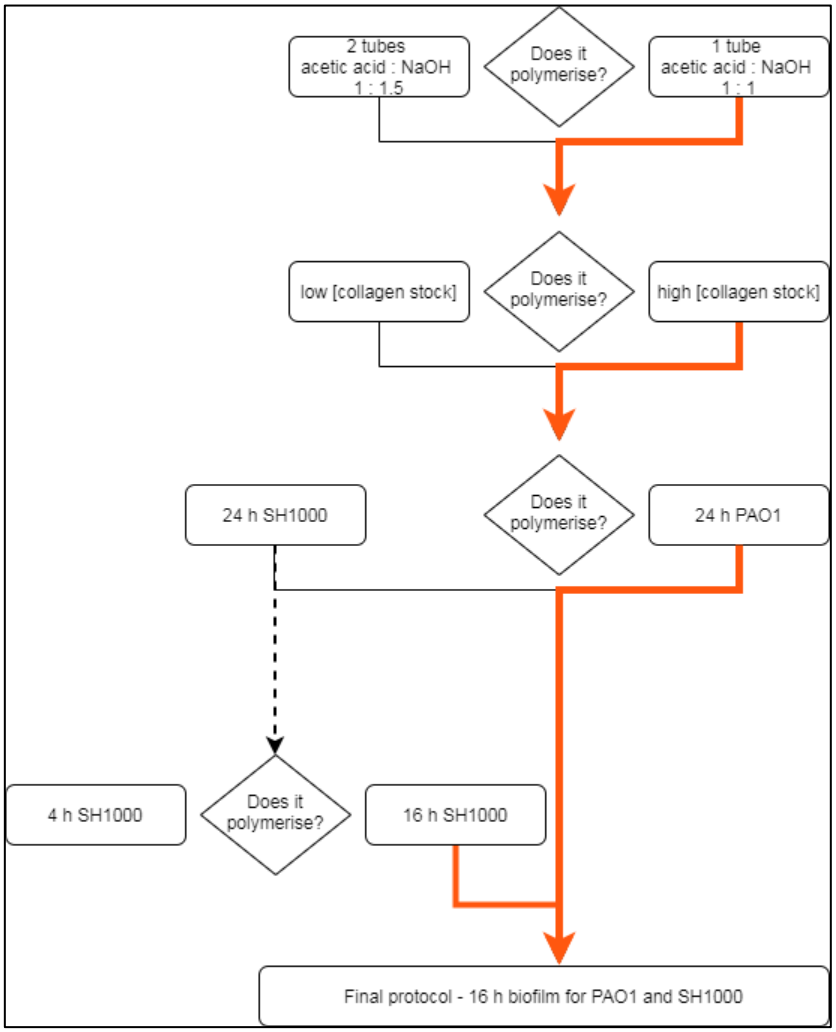

Figure 4. 4: Development of 3D collagen model of the infected chronic wound environment*. On ice, a final concentration of 2 mgmL^{-1} collagen and 10 mM acetic acid was mixed by gentle rolling, followed by addition of X-Vivo15 medium and 10% human AB serum. 10 mM NaOH was added and mixed carefully. Required volume of resulting solution was added to 96-well TC-treated plates and allowed to polymerise at 37 °C, 5% CO_2. Matrices were digested in 500 µgmL^{-1} collagenase for 1 h. Both PAO1 and SH1000 produced biofilms in the presence of collagen when grown for 16 h.*

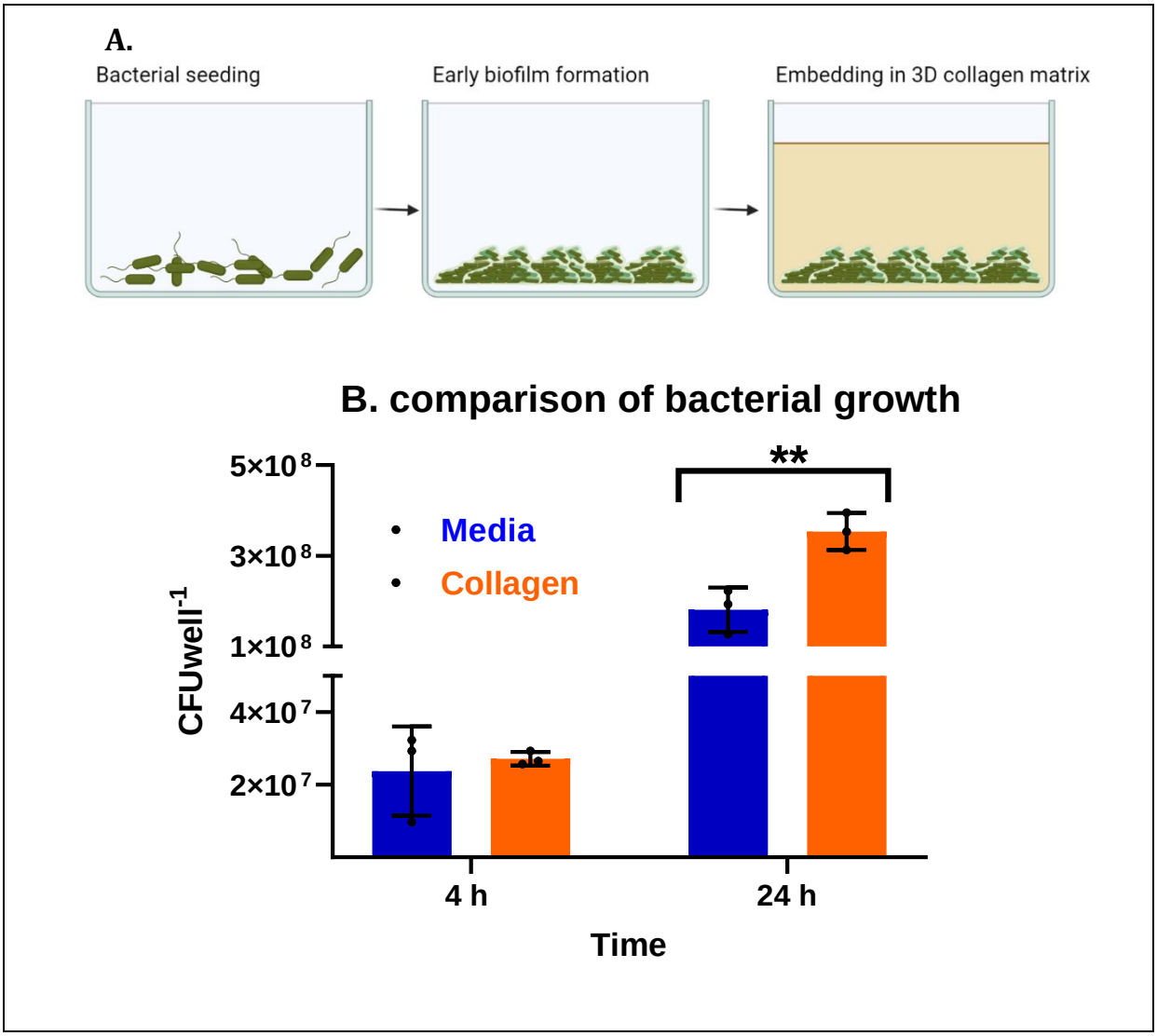

Figure 4. 5: Comparison of biofilm growth in media vs collagen. *Biofilms were produced for 16 h as described in previous sections and washed 3x in PBS before addition of collagen or X-vivo-15 alone (**A**) and incubation for 4 or 24 h. After incubation, collagen was digested for 1 h in 500 µgmL^{-1} collagenase before scraping and pooling wells and plating for CFU using the Miles Misra method (**B**). Growth was supported in both growth conditions. Analysis was performed using Graphpad Prism 9, where a paired t-test for values at 24 h showed that collagen contained significantly higher bacterial numbers than liquid medium (t = 5.624, df = 2, p = 0.03).*

4.5.4 Analysis of myeloid cell viability within collagen matrix shows high levels of survival and active migration into the matrix

Experiments in parallel to those in Section **4.5.3** focused on the interaction of primary immune cells with collagen (**Figure 4.6**). Here, 100 µL of collagen was seeded into wells of a 96-well TC-treated plate and allowed to polymerise before addition of $5x10^4$ immune cells to relevant wells and incubation for 24 or 48 h. As serum is used within the collagen matrix, LDH assay was not suitable for these experiments. Therefore, Trypan blue was utilised to assess cell viability. This assay was suitable here as the blue dye is unable to penetrate the bacterial cell walls, so do not interfere with detection. Bacterial cells are also too small to be detected on the counter.

For inflammatory monocytes (± GM-CSF) and monocyte-derived dendritic cells, viability remained very high throughout the essay (**Table 4.5**). These were very promising result as it shows that the matrix itself and the harvest method are not cytotoxic to immune cells. We therefore proceeded with optimisation. Interestingly, the initial protocol for this experiment called for separate viability testing on the top liquid portion of the wells followed by the digested semi-solid portion. However, when assessed, no myeloid cells, alive or dead, were detected within the top liquid portion, indicating that these cells actively migrated into the matrix following seeding.

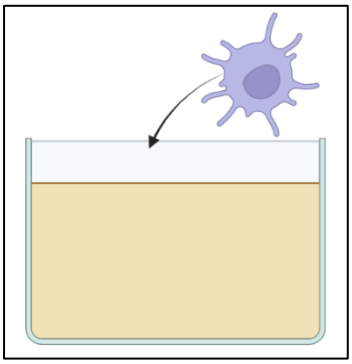

Figure 4. 6: Survival of immune cells in the collagen matrix. *To determine whether immune cells can survive within the collagen matrix, Type I rat-tail collagen was used to produce the 3D matrix as described in Figure 3 and 100 µL added to wells of a 96-well TC-treated plate and allowed to polymerise. Immune cells were harvested and 5x10⁴ cells seeded to each well at the collagen surface. Plates were incubated at 37 ^{0}C, 5% CO_2 for 24 or 48 h, then 500 µgmL^{-1} collagenase was added and plates incubated for a further 1 h.*

Table 4.5: Viability was measured using Trypan blue*. At both 24 and 48 h, cell viabilities remained above the 70% generally accepted for use in assays. Media used was X-Vivo15 + 10% human AB serum ± collagen, n=1.*

Cell type	Incubation time (h)	Cell viability
Inflammatory monocytes (collagen)	24	71%
Inflammatory monocytes + GM-CSF (collagen)		87%
Monocyte-derived dendritic cells (media)	24	99%
	48	92%
Monocyte-derived dendritic cells (collagen)	24	80%
	48	85%

4.5.5 Analysis of monocyte-derived dendritic cell response to *P. aeruginosa* PAO1 biofilms using the 3D collagen model

For the complete co-culture assay, moDCs were seeded onto 16 h-old PAO1 biofilm encased in collagen matrix (**Figure 4.7**). DCs were selected here due to their high levels of expression of DC-SIGN, the CLR that best binds *P. aeruginosa* biofilms as indicated from the previous chapter (446). Before seeding, cells were incubated with blocking antibodies for DC-SIGN or left untreated to determine whether this receptor plays a role in the interaction of moDCs with biofilms. DC-SIGN was selected here due to its ability to recognise *P. aeruginosa* biofilms (191), and its association with immune regulation during infection, and protection from excess inflammation within wounds (447). Therefore, engagement of this receptor during colonisation and establishment of biofilm may directly contribute to chronicity by promoting dysregulation of immune interaction and increased non-resolving pro-inflammation (448).

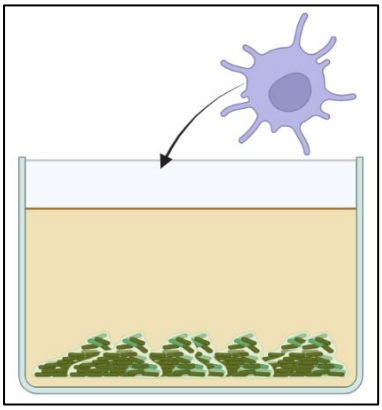

Figure 4. 7: Construction of the complete model. *PAO1 biofilms grown for 16 h in X-Vivo15 and were encased in collagen for 1h at 37 °C. moDCs were harvested and incubated with anti-DC-SIGN antibody, anti-IgG1 as an isotype control or left untreated and added to the biofilm matrix before 4 or 24 h incubation. Matrix was digested and collected for CFU and viability analysis as described in Section* ***5.4.1****.*

Here, high viability was observed in the absence of bacteria at 4 h, and although it appears to fall slightly at 24 h, the decrease was not statistically significant. Understandably, in the presence of bacteria, moDC viability was significantly decreased but still relatively high, very rarely falling below 60% (**Figure 4.8A-B**). Further, the blocking of DC-SIGN did not have any significant effect on cell viability, with or without the presence of bacteria.

Initially, cellular viability was tested from the pre-digested, liquid layer and the digested collagen layer (Section **4.4.6**, note). However, cells were only retrieved from the samples collected after collagenase digestion, suggesting that cells actively migrated toward the bacteria at the base of the well. These results were promising as they showed that although bacterial cell numbers were likely equivalent to those in the 2D plate assay, immune cells were still able to survive for long periods in co-culture. This supports the hypothesis that having more space in which to interact with biofilms, alongside a semi-solid matrix, would allow for enhanced survival of immune cells, like the environmental niche of a chronic wound. One reason for this may be that in this semi-solid model, individual niches may form in different areas of the wells, rather than a homogenous mixture as in liquid. It has been shown that bacteria form individual, separate aggregates in collagen *in vitro*, even when seeded as a mixed culture (449), and that in the skin, several microenvironments coexist containing different cell types, human and bacterial (450, 451). It is likely therefore that although we only use mono-species biofilms here, they have still formed a niche separate to the immune cells, which are able to aggregate in close proximity while maintaining a 'safe distance' from direct contact leading to cytotoxicity.

Following the testing of cell viability, bacterial counts were obtained using serial dilution and the Miles Misra method, with the first dilution performed in sterile water to lyse any remaining human cells, followed by PBS. As expected, bacteria numbers increased from 4 to 24 h in all conditions, with around a 10-fold increase in bacterial counts between time-points (**Figure 4.8C**). Here, although MOIs were still high, averaged at 125 and 785 for 4 and 24 h respectively, they were reduced in comparison to the 2D assay using PAO1, at least at 4 h. Bacterial populations did not significantly decrease in the presence of

immune cells, with or without blocking antibody. The reason for this is unclear, but could be due to the fact that the main role of DCs is antigen presentation rather than pathogen clearance. Generally, moDCs *in vivo* develop from monocytes under inflammatory conditions and have a variety of roles during infection including tissue repair, cytokine production and cell-cell signalling (452). In addition, DC-SIGN specifically is not inherently associated with pathogen clearance, but rather cell signalling and early immune decision making (447). Alternatively, even if this receptor does have a role in pathogen clearance, blocking antibody effectiveness may have diminished by bacterial-derived factors such as proteases, which may have directly degraded the proteins, preventing them from influencing the immune cells. *P. aeruginosa* is known to produce a plethora of proteases, including LasB that is able to digest various host proteins, including immunoglobulins and cytokines, and has been recently implicated in stimulating an allergic-type response by promoting host-cell mucus production (195, 453). There is evidence also, that antibodies against certain *Pseudomonas* proteases act as an agonist in pathogenicity during infection, such as those against alkaline protease that when produced, promote degradation of neutrophil extracellular traps (NETs) that are essential for pathogen clearance, worsening overall disease outcome in patients (196). Later in this chapter, we investigate the potential role of secreted proteases on the degradation of cytokines but not immunoglobulins (Section **4.5.8**). It would be useful therefore, to investigate this in future.

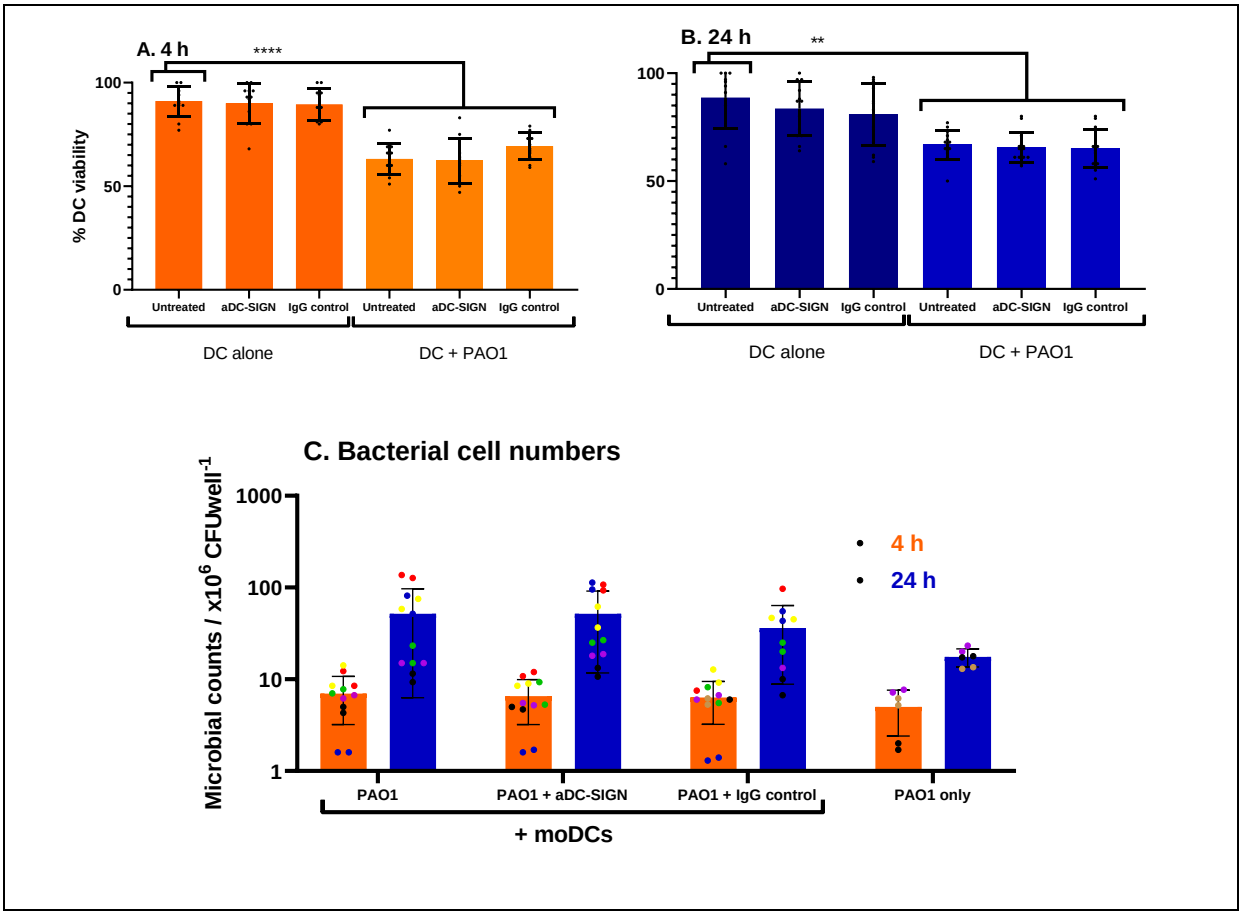

Figure 4. 8: Analysis of moDC and bacteria viability in biofilm-mDC 3D co-cultures*. Viability of moDCs was assessed using Trypan blue, and CFUs were calculated in pooled duplicates for each condition using the Miles Misra method as described in previous sections. For these assays, technical replicates are shown as individual points on the graph. For statistical analysis, means were calculated for each biological replicate. moDCs remained highly viable at both 4 and 24 h when bacteria were absent as expected but dropped slightly in the presence of PAO1. Cell viabilities were unaffected by the presence of blocking antibodies (**A, B**; n=7 biological repeats, in duplicate). Here, one-way ANOVA was utilised using Graphpad Prism 9 with Dunnett's multiple comparison test, where presence of anti-DC-SIGN or isotype control antibodies did not significantly affect viability but was significant in the presence of bacteria at 4 ($(F_{5,30}) = 24.75$, $p = <0.0001$) and 24 h ($(F_{5,35}) = 7.148$, $p = 0.0018$). Bacterial numbers were not significantly different across all 3 conditions at 4 h ($(F_{3,18}) = 0.2553$, $p = 0.8566$), and all increased similarly by 24 h by a factor of approximately 10, but again were not significantly different between conditions within this time-point ($(F_{3,17}) = 0.6683$, $p = 0.5830$). As in **A** and **B**, technical replicates are plotted individually, with colours corresponding to each biological replicate (**C**; n=7).*

4.5.6 Analysis of cytokine production by monocyte-derived dendritic cells incubated with *P. aeruginosa* PAO1 biofilms in collagen matrix

For these assays, it was important to test supernatant at a range of dilution factors to ensure absorbance fell within the range of the standard curve of the ELISAs. Therefore, several dilutions were tested, and it was determined that 1:10 provided good readouts. As indicated in the previous section, supernatants were initially collected separately, both pre- and post-digest with collagenase, hence we tested TNF-α concentration measured in each compartment (**Figure 4.9A-B**). Here, values were similar, but the pre-digested supernatants (above collagen matrix) appeared to give higher overall values than the post-digest. Therefore, it was decided to combine the supernatants, and continue doing so for subsequent experiments. Dendritic cells produced very low to undetectable levels of TNF-α at both 4 and 24 h incubation within the uninfected collagen matrix (**Figure 4.9C**). Conversely, when incubated with PAO1 biofilms, levels of TNF-α were high at 4 h, but dropped considerably at 24 h (**Figure 4.9C**).

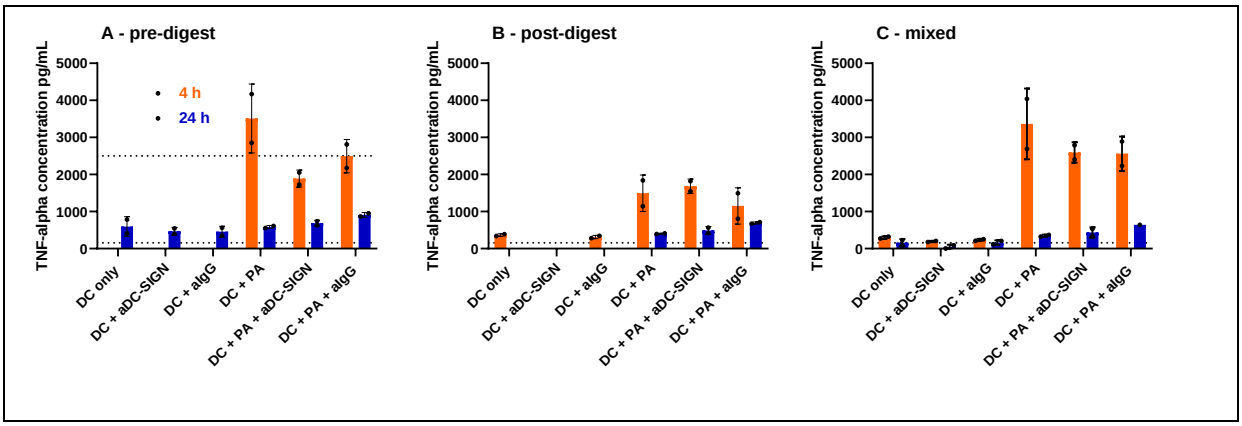

Figure 4. 9: Localisation of TNF-α in 3D collagen infection assays*. After the running of the 3D collagen infection model, ELISAs were performed to compare cytokine production by moDCs in all conditions and time-points. ELISAs to measure TNFα were performed on (**A**) pre- and (**B**) post-digest supernatants, and later (**C**) mixed supernatants to negate variation, first using a range of sample dilutions to find one best suited for the standard curve. Here, TNF-α production was low for moDCs alone, but high at 4 h for cells incubated with PAO1 which was depleted by 24 h. Graphs show data from two technical repeats from a single experiment, missing bars indicate samples that were lost due to experimental error.*

Once the final protocol was established, subsequent pre- and post-digestion supernatants were combined on collection and used to quantify cytokine production. So far, focus has been on classical pro-inflammatory cytokines IL-1β and TNF-α, and the chemoattractant MCP-1 (CCL2). As with the initial experiment (**Figure 4.9**), TNF-α was produced by moDCs at low to undetectable levels when incubated in the matrix without bacteria but is increased in the presence of PAO1. This high level of cytokine is diminished at 24h (**Figure 4.10A**). Although this trend is observed graphically, these changes do not reach statistical significance. Conversely, moDCs showed accumulation of IL-1β production over time when incubated without bacteria. However, when PAO1 was present, IL-1β was produced at 4 h but was diminished after 24 h to levels seen in cultures lacking bacteria (**Figure 4.10B**), again no statistically significant. Similarly, MCP-1 that is produced at a basal level by moDCs, showed an accumulation from 4 to 24 h in the matrix alone as expected, but levels were completely abrogated at both time-points in the presence of bacteria (**Figure 4.10C**). For all these experiments, it is unclear whether blocking DC-SIGN influences cytokine production.

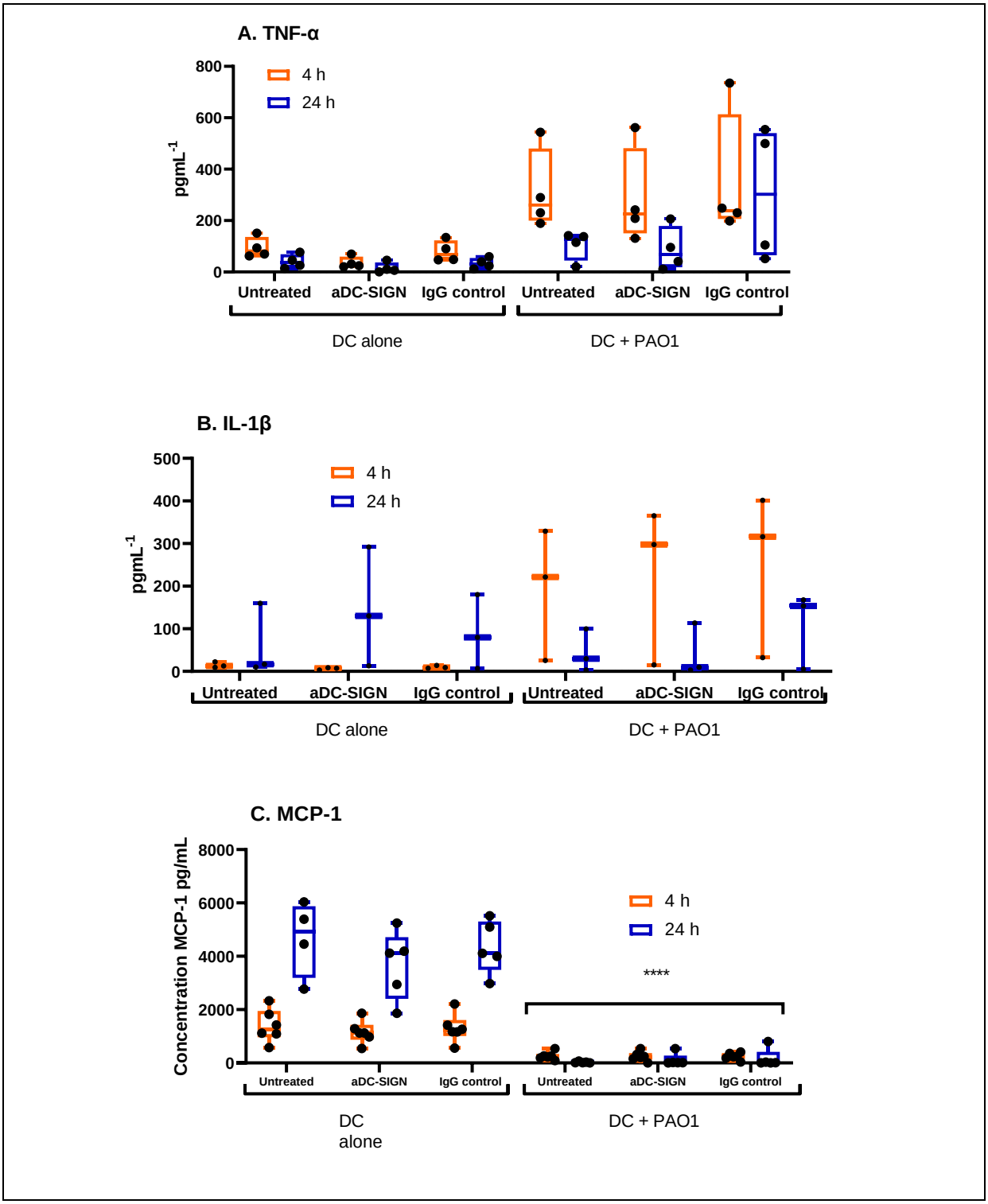

Figure 4. 10: Cytokine analysis of 3D collagen infection model shows variations in inflammatory cytokine production at 4 h and 24 h in response to biofilms not affected by blocking antibodies for DC-SIGN. *Biofilms embedded in collagen matrix were produced as in the previous sections and 5x10⁴ moDCs seeded in 100 µL X-Vivo 15 on top of the matrix, blocked with anti-DC-SIGN antibody, anti-IgG1 isotype control or left untreated. Plates were incubated at 37 °C, 5% CO_2 for 4 or 24 h. Initially, supernatants on top of the matrix were collected and stored separately to digested matrix, and ELISAs also performed separately. However, due to variation in the cytokine levels in samples of the same*

*condition, it was decided that pre- and post-digestion supernatants would be pooled. Therefore, all ELISA data comes from the total content of pooled wells. ELISA assays were performed to test for levels of (**A**) TNF-α (n=5), (**B**) IL-1β (n=3) and (**C**) MCP-1 (n=6). Statistical analysis was performed using two-way ANOVA, correcting for multiple comparisons in Graphpad Prism 9. For TNF- α and IL-1β, there was no significant interacting factors (($F_{5,36}$) = 0.7996, p = 0.5573 and ($F_{5,24}$) = 2.400, p = 0.067 respectively). For MCP-1, concentration was significantly increased between 4 and 24 h in uninfected samples (($F_{1,53}$) = 75.13, p = <0.0001, as well between infected vs uninfected samples (($F_{5,53}$) = 51.58, p = <0.0001), with an overall interaction of ($F_{5,53}$) = 18.57, p = <0.0001).*

4.5.7 Expression of cell surface markers in moDCs is diminished upon incubation with PAO1 biofilms grown in collagen.

Alongside supernatants, the infection assay allowed for the harvest of moDCs to stain for flow cytometry with the aim of investigating levels of cell surface markers. We investigated 4 different markers, HLA-DR (MHC class II), CD11b, DC-SIGN and MR (**Figure 4.11-12**). The two former molecules are general markers of DCs, as MHCII is only expressed on antigen presenting cells, and CD11b is a marker for myeloid cells (64). Quantifying these markers also allowed us to ensure moDCs exhibited expected phenotypes in the collagen than is described elsewhere using *in vitro* or *in vivo* samples (63). As shown in previous chapters, the CLRs DC-SIGN and MR are able to bind biofilms due to their affinity with high-mannose structures that are present in *P. aeruginosa* biofilms (191). Because of this, we were interested to determine if receptor surface levels were altered during infection with PAO1 compared to those incubated in the collagen alone for 4 or 24 h. MR is a broadly distributed lectin, present on primarily Kuppfer cells and alveolar macrophages, but also DCs, non-vascular endothelial cells and kidney mesangial cells amongst others (454-456). Indeed, despite its broad distribution, studies primarily focus on myeloid cells, including DCs as utilised in this study. Generally, circulating DCs express low levels of MR, but upregulate it under stimulation by IL-4 and GM-CSF, as was performed here (457). Generally, MR expression dampened in the presence of LPS in both macrophages and DCs. DC-SIGN expression appears to correlate with immune suppression, where engagement of the receptor appears to induce IL-10 production and a Th2-dominant T cell response during infection (164).

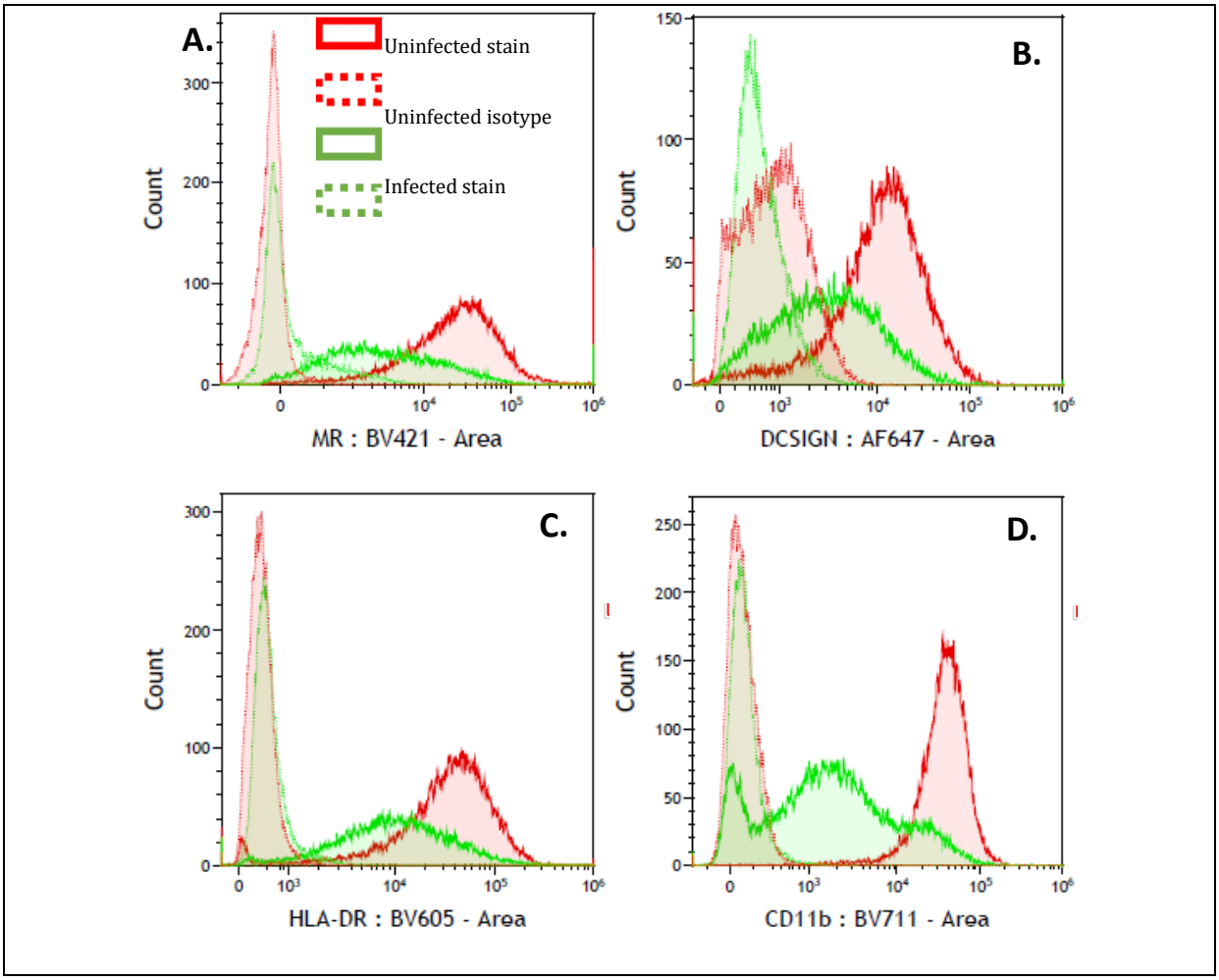

Figure 4. 11: Flow cytometry analysis shows a general decrease in surface marker expression levels when incubated with live biofilms for 4 h. *The 3D collagen infection assay was performed as in Section* ***4.4.6****, and cells collected after digestion for staining. Cells were blocked using AB human serum before staining with single or combined antibodies for the markers (**A**) MR, (**B**) DC-SIGN, (**C**) HLA-DR and (**D**) CD11b with viability dye Zombie UV used for additional gating of live cells. Overlays are representative images for samples collected at 4 h and show uninfected (red-solid line) and infected (green-solid line) counts. Isotype control counts are indicated using dotted lines. Flow cytometry was performed on an ID7000 Spectral Flow Cytometer analysed using Kaluza.*

For all markers tested, we observed a general decrease in surface marker expression when DCs were exposed to PAO1 (**Figure 4.11-12**), this depletion reaching significance in all but HLA-DR at 4 h (**Figure 4.13A**). Even here, a general decrease was observed in HLA-DR, but high levels of variability between donors in the uninfected samples as well as small numbers might have affected statistical analysis. Further, over time, the mean fluorescence intensities (MFIs) of HLA-DR and CD11b do not appear to change in their

raw values, and significance is regained in HLA-DR (**Figure 4.13B**). Importantly, when cell viability was determined prior to processing these samples via Trypan blue, cell death remained low (**Figure 4.13C**), comparable to those recorded in **Figures 4.8A-B**. These findings suggest that there is not a continual degradation of the markers in the presence of PAO1 biofilms, such as by protease digestion for example, but rather the downregulation is immediate and maintained from the onset of infection.

Concerning the CLRs tested, expression of MR decreased initially, but appeared to be rescued by 24 h, visibly showing increased expression in the infected samples, the levels comparable with that of the uninfected (**Figure 4.13B**). However, there appeared to be background binding by the isotype control for the MR antibody, so this must be taken into consideration (**Figure 4.12A**). Like with the APC markers, there is no cumulative degradation of MR here, and even if directly downregulated by degradation occurs upstream, this effect is antagonised later, perhaps due to recycling the protein in the cytoplasm (131). In contrast, although significance was lost in the comparison between infected vs uninfected samples (due to high variability in the uninfected), expression of DC-SIGN continues to be depleted beyond the 4 to 24 h time-point to an almost undetectable level (**Figure 4.13B**). Here, DC-SIGN expression appears to be permanently affected by the presence of live PAO1, perhaps lending itself to maintained activation of moDCs. It should be noted however, that background fluorescence in our isotypes for DC-SIGN may have affected the results here, so potential alternative staining methods should be considered (**Figure 4.11B**).

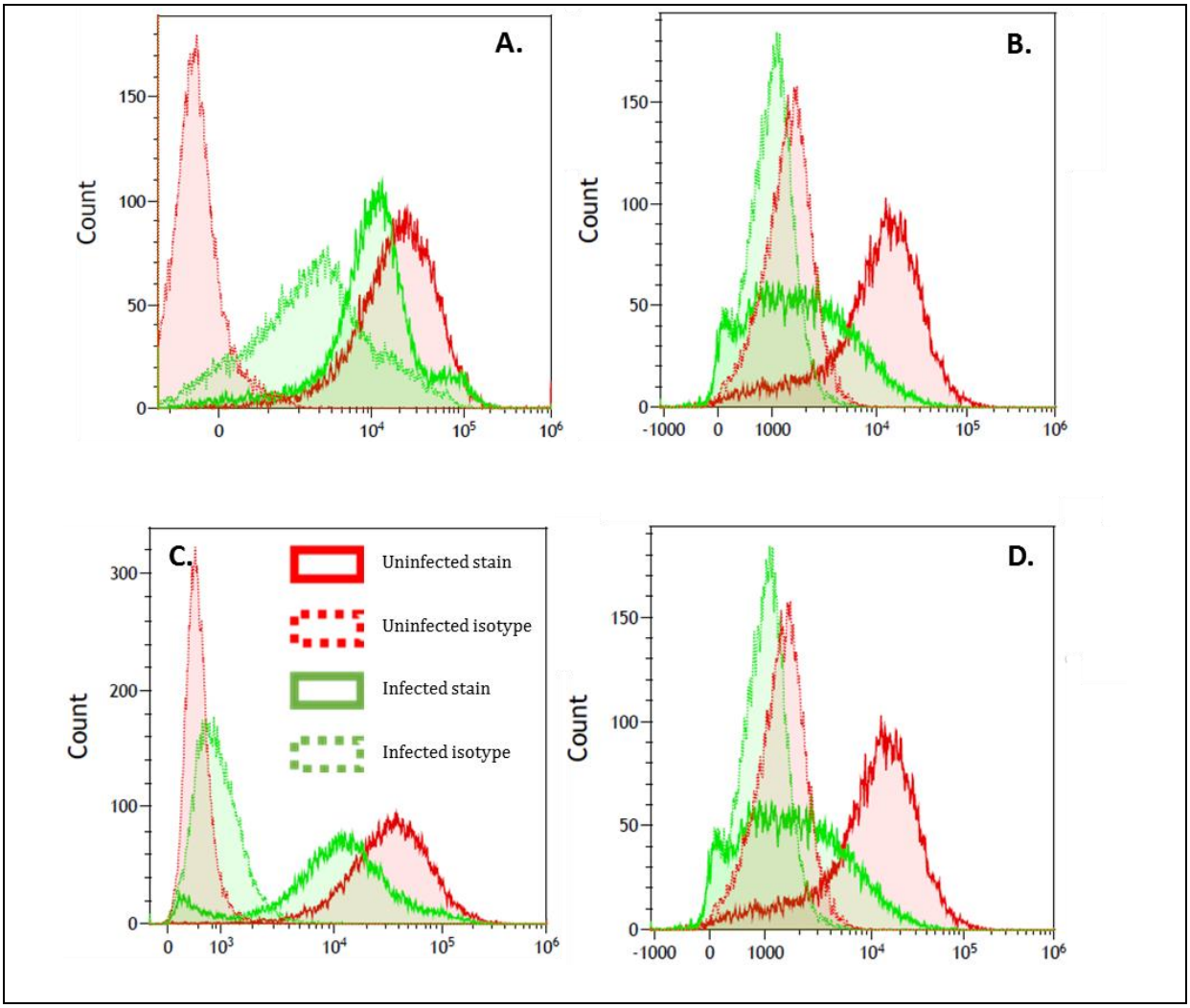

Figure 4. 12: Flow cytometry analysis shows a general decrease in surface marker expression levels when incubated with live biofilms for 24 h. *The 3D collagen infection assay was performed as in Section* ***4.4.6****, and cells collected after digestion for staining. Cells were blocked using AB human serum before staining with single or combined antibodies for the markers (****A****) MR, (****B****) DC-SIGN, (****C****) HLA-DR and (****D****) CD11b with viability dye Zombie UV used for additional gating of live cells. Overlays are representative images for samples collected at 24 h and show uninfected (red-solid line) and infected (green-solid line) counts. Isotype control counts are indicated using dotted lines. Flow cytometry was performed on an ID7000 Spectral Flow Cytometer analysed using Kaluza.*

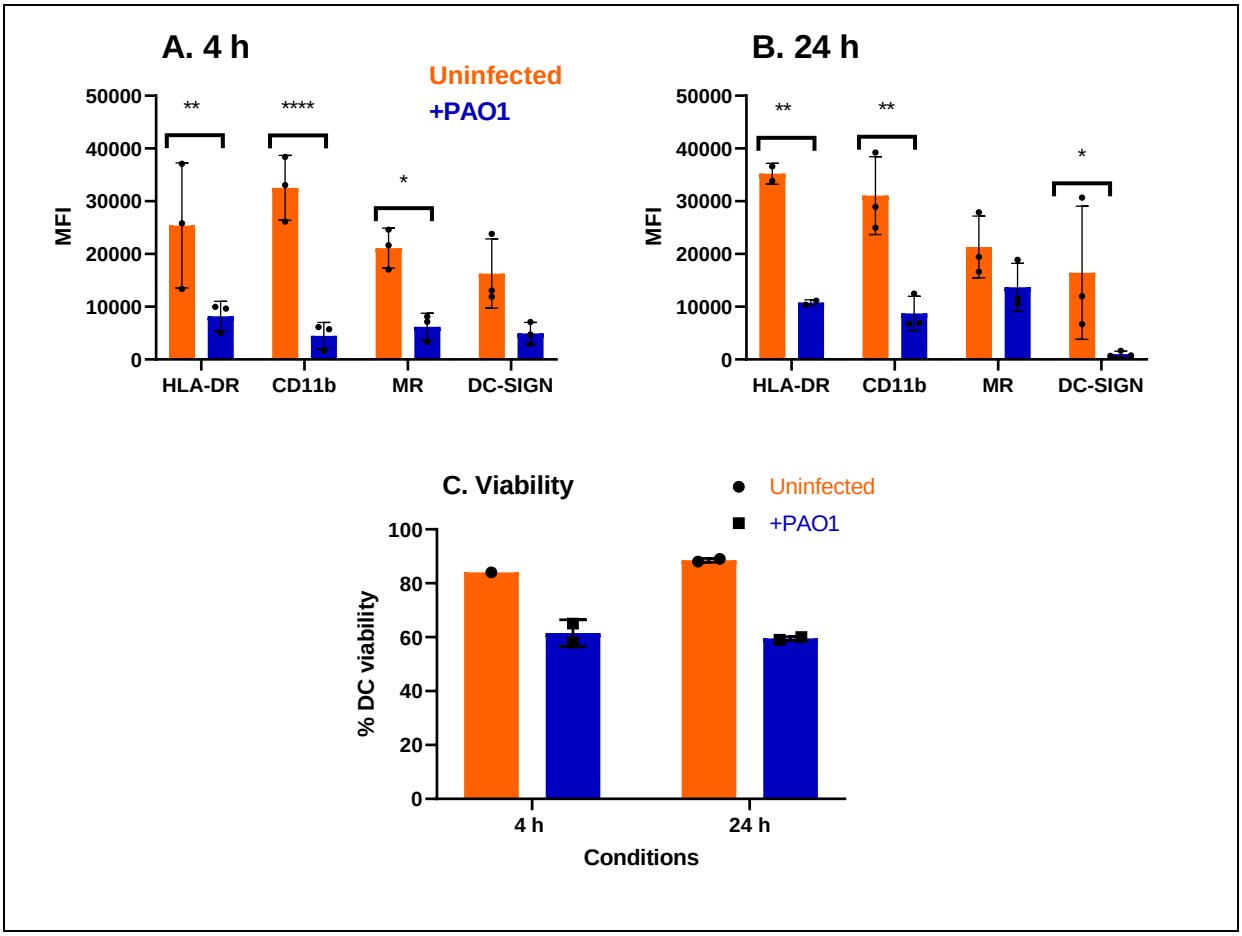

Figure 4. 13: Flow cytometry analysis shows a general decrease in levels of surface markers when incubated with live PAO1 biofilms. *The 3D collagen infection assay was performed as in Section* ***4.4.6****, and cells collected after collagen digestion for flow cytometry staining. Cells were blocked using AB human serum before staining with single or combined antibody cocktails for MR, DC-SIGN, HLA-DR and CD11b. Results were analysed using two-way ANOVA in Graphpad Prism 9 Šídák's multiple comparisons test to compare means of each row factor (infected vs uninfected). Here, expression was significantly different between infected and uninfected samples at 4 h ($(F_{1,16}) = 58.77$, p = <0.0001), but not between expression levels of each marker ($(F_{3,16}) = 2.251$, p = 0.1218). When corrected for multiple comparisons, decreases in infected samples reached significance in CD11b (p = <0.0001), MR (p = 0.0224) and HLA-DR (p = 0.0079) but not DC-SIGN (p = 0.1041) (**A**). At 24 h under the same analysis (**B**), the same overall result was observed, with significant differences between infected and uninfected samples ($(F_{1,14}) = 40.37$, p = <0.0001), but not between markers ($(F_{3,14}) = 5.000$, p = 0.0146). When corrected for multiple comparisons, decreases in infected samples reached significance in CD11b (p = 0.0029) and HLA-DR (p = 0.0070) as before, but was gained in DC-SIGN (p = 0.0394) and lost in MR (p = 0.0224). Viabilities remained comparable with previous experiments when measured by Trypan blue (**C**). Mean fluorescence intensities (MFI) were calculated using Kaluza.*

4.5.8 MCP-1 production by moDCs is not inherently affected by collagen even after LPS stimulation, and is not directly degraded by PAO1 supernatants

For functional assays going forwards, we focused on the stark reduction of MCP-1 as it appeared to be specific for this cytokine over the others tested. The important difference in this model compared to those conducted previously was the implementation of collagen over liquid medium, so initial investigations focused on this. Further, we tested the effects of LPS alone (50 $ngmL^{-1}$) on moDC in the presence of media and collagen (**Figure 4.14A**). We know that live biofilms are inherently very complex, so wanted to isolate specific virulence factors that might be involved here. LPS seemed a logical route of investigation here, as it has been indicated throughout the literature as an activator of immune cells, promoting inflammation (458). Here, MCP-1 increased from 4 to 24 h in all conditions as expected, complementing results collected in Section **4.5.6**. Interestingly, the increase was not significantly affected by the presence of collagen or LPS, suggesting that the live bacteria are responsible for the depletion (**Figure 4.14B**).

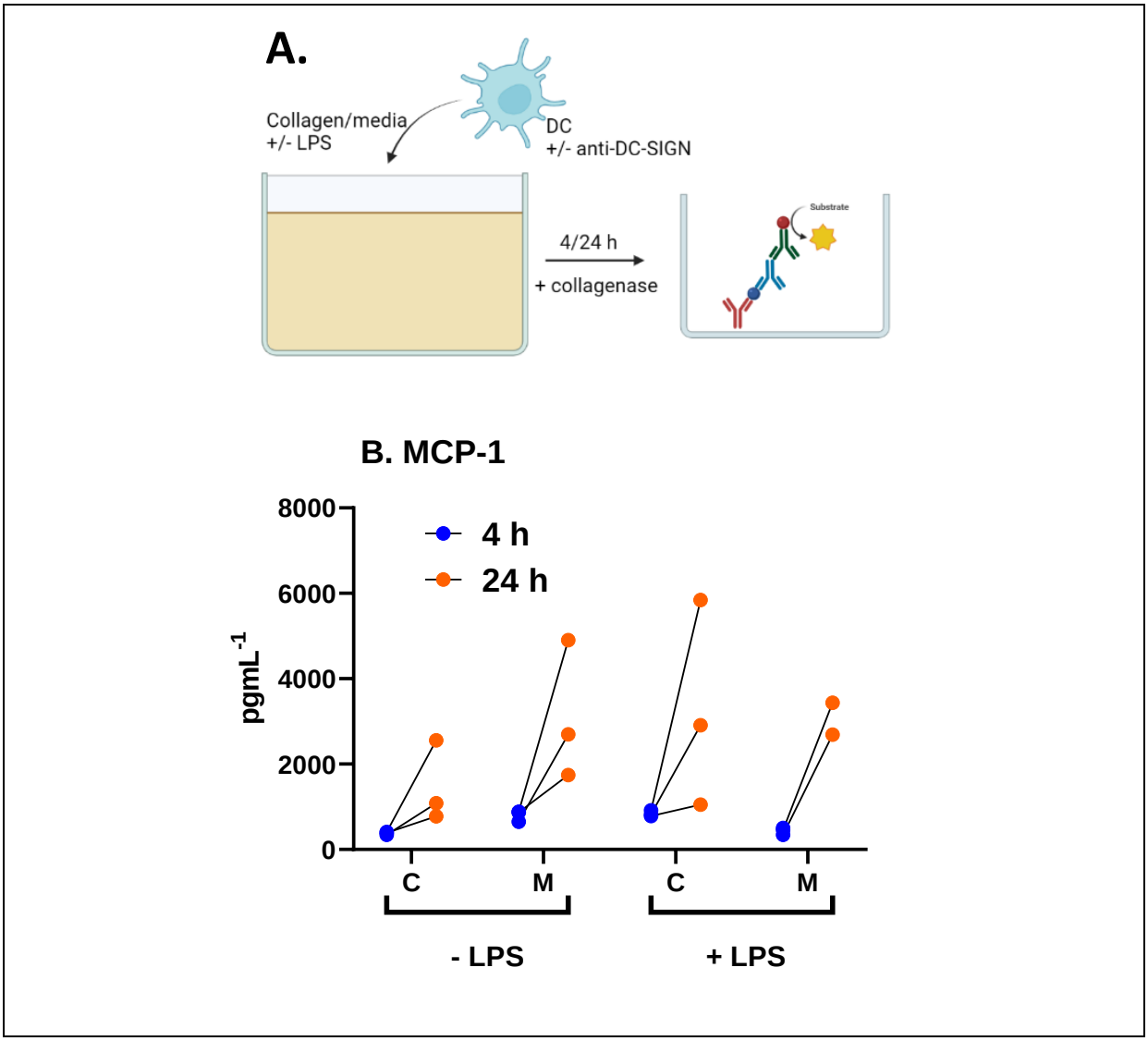

Figure 4. 14: MCP-1 production by moDCs is not inherently affected by collagen even after LPS stimulation. *Collagen or media was added to sterile wells with or without the presence of protease inhibitor, followed by seeding of moDCs and incubation for 4 or 24 h. Supernatants were harvested and cytokine concentrations determined using ELISA (**A**). As expected, MCP-1 levels increased from 4 (blue) to 24 h (orange), but there were no significant differences between media (M) and collagen (C), and was neither affected by the presence of LPS (**B**). Results were analysed using Graphpad Prism 9 (n=3).*

It is well established that *Pseudomonas spp.* produce a multitude of proteases and other virulence factors that play a role in its pathogenesis (459). It is possible therefore, that these proteases are responsible for the depletions we observed. A small assay was designed where biofilms were produced in the same way as during the collagen model, but after washing were incubated in media containing known concentrations of purified

cytokine (from R&D Systems kits used for ELISA) with and without cOmplete protease inhibitor in order to determine if there are any depletions from the values shown (**Figure 4.15A**). We used both the wild-type PAO1 from previous infection assays, and a Δ*lasR* knock-out mutant (**Table 2.1**). LasR is a regulator of a range of virulence factors, including major proteases such as LasB and elastase. Ideally, strains with specific knock-outs for proteases of interested would have been used here, but these were unavailable at the time of testing (460, 461). Work is ongoing to produce these mutants in collaboration with another laboratory. Here, reduction in cytokine concentration not observed for either MCP-1 or TNFα in wild-type PAO1 (**Figure 4.15B-C**), regardless of the presence of protease inhibitor. However, there was a significant reduction in the lasR-mutant for both cytokines in the absence of protease inhibitor. In the case of MCP-1, this is to a vastly smaller extent than in the complete infection model (**Figure 4.15B**). These results suggest that that lasR may directly some factor that depletes MCP-1 and TNF-α, and this is likely a protease due to the loss of this effect in the presence of protease inhibitor. Importantly, this experiment was only performed three times due to time constraints, increasing replicates may clarify the results observed. Further, experiments were conducted solely in medium rather than collagen due to supply issues, we may therefore speculate that the collagen is in fact very important in the whole infection assay.

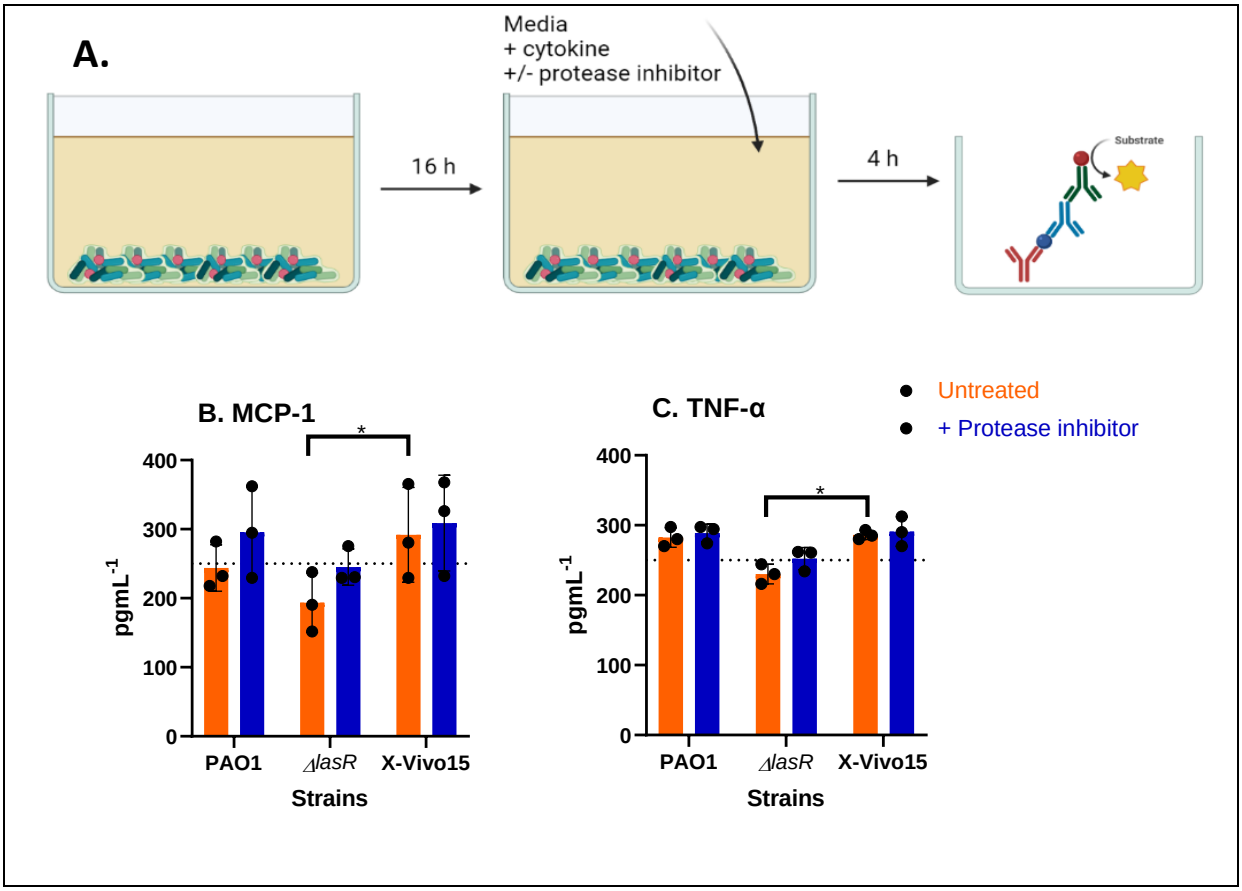

Figure 4. 15: Biofilms supernatants from wild-type PAO1 do not degrade TNF-α or MCP-1 regardless of treatment with protease inhibitor, but in a PAO1ΔlasR mutant strain, both cytokines are degraded in the absence of protease inhibitor*. Biofilms were produced as described in Section* ***2.4.1*** *before addition of fresh X-Vivo15 with known concentrations of cytokines, with (blue) or without (orange) protease inhibitor (****A****). After 4 h incubation, cytokine concentrations were determined using ELISA. For analysis, paired t-tests were performed between supernatants exposed to bacteria and the corresponding media-only control to account for variations in cytokine measurement. Here, significance was not reached for any value except in PAO1ΔlasR vs media (without protease inhibitor) for both MCP-1 (p = 0.0227,* ***B****) and TNF-α (p = 0.0132,* ***C****). Dotted lines indicate concentrations of cytokines chosen for analysis. Results were analysed by paired t-test using Graphpad Prism 9 (n=3).*

Following the potential reduction in MCP-1 in relation to lasR-regulated proteases, we aimed to investigate the 4 markers tested previously using flow cytometry, using supernatants collected from uninfected, PAO1-infected and PAO1*ΔlasR*-infected that had been exposed to a range of conditions. From work conducted previously in this chapter, it seemed likely that during the whole infection model, the presence of whole bacterial cells had a significant effect on immune cells, so we collected supernatants in order to

identify any specific interactions with secreted products. Also, the lack of collagen in Figure **4.15B** may have contributed to the minor downregulation of MCP-1, therefore biofilms were implanted in collagen for this experiment. Here, biofilms were produced with and without protease inhibitor to determine differences in surface expression in relation to secreted proteases. Also, in biofilms produced without inhibitor, a fraction of supernatants were boiled in order to denature any proteins present, inactivating any component that may be involved in immune interaction, protease or otherwise. Supernatants were incubated with moDCs and underwent flow cytometric analysis using the same parameters as in Section **4.5.7**. During this preliminary experiment, HLA-DR and CD11b surface levels were not affected by bacterial supernatants under any condition (**Figure 4.16**).

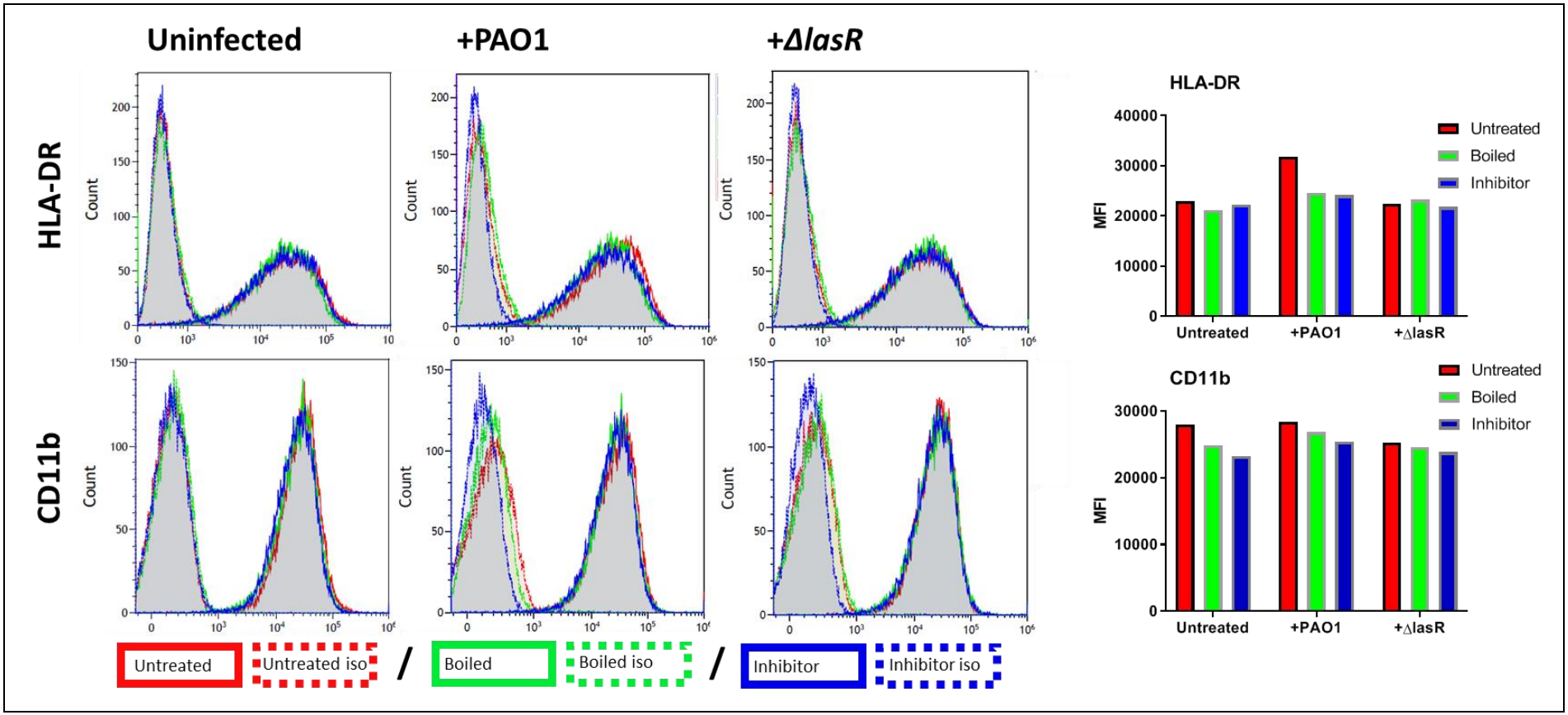

Figure 4. 16: Surface expression of CD11b and HLA-DR are not affected by bacterial supernatants. *Biofilms were produced as described in Section* ***2.4.1*** *for 16 h, followed by addition and polymerisation of collagen. After 2 h, media +/- protease inhibitor was added and incubated for 4 h, 37 °C, 5% CO_2. Collagen was digested with collagenase and samples filtered at 0.22 µM with an aliquot taken for boiling. Supernatants were incubated with moDCs for 4 h 37 °C, 5% CO_2 before flow cytometry analysis. Under all conditions, HLA-DR (top row) and CD11b (bottom row) surface expression was consistent. Results were analysed using Kaluza and MFIs displayed using Graphpad Prism 9.*

Similarly, MR and DC-SIGN surface expression was not specifically affected by presence of bacteria in this model (**Figure 4.17**). However, for both receptors, the boiled samples provided unexpected results for both conditions. Boiled samples resulted in reduced expression of MR, regardless of bacterial presence (**Figure 4.17** – top row). In contrast, DC-SIGN surface expression was increased drastically when moDCs were exposed to boiled supernatants (**Figure 4.17** – bottom row). These results suggest that some protein in the collagen matrix, or the collagenase for digestion of the matrix, is involved in the regulation of these receptors.

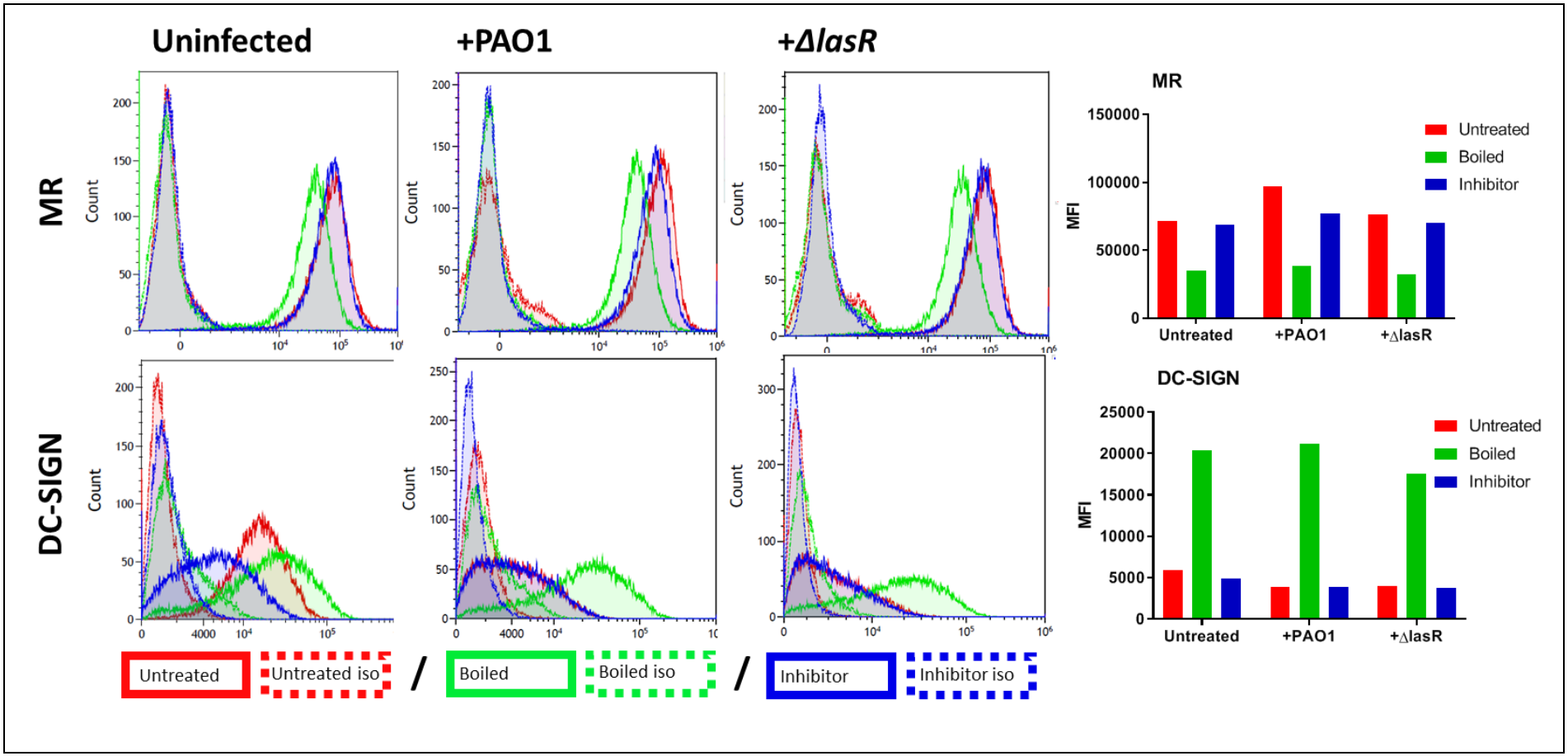

Figure 4. 17: Surface expression of MR and DC-SIGN are not affected by bacterial supernatants. *Biofilms were produced as described in Section* ***2.4.1*** *for 16 h, followed by addition and polymerisation of collagen. After 2 h, media +/- protease inhibitor was added and incubated for 4 h, 37 °C, 5% CO_2. Collagen was digested with collagenase and samples filtered at 0.22 µM with an aliquot taken for boiling. Supernatants were incubated with moDCs for 4 h 37 °C, 5% CO_2 before flow cytometry analysis. Expression of MR (top row) and DC-SIGN (bottom row) was not affected by supernatants from bacteria. In boiled supernatants (green), for all conditions, MR was decreased while DC-SIGN increased. Results were analysed using Kaluza and MFIs displayed using Graphpad Prism 9.*

4.6 Discussion and future work

From the work carried out during this section, several conclusions can be made. Firstly, that biofilms can be normalised against planktonic cells in order to expose immune cells to comparable bacterial cell numbers (**Figure 4.2**). Secondly, that during 2D cell assays, bacterial counts are not affected by the presence of primary monocyte derived macrophages, but that previous methods for cytotoxicity analysis are unsuitable for *S. aureus* cultures (**Figure 4.3**). Thirdly, that a 3D wound model can be optimised to maintain high levels of immune cell survival regardless of high MOI (**Figure 4.8**). Finally, that classical pro-inflammatory cytokines TNF-α and IL-1β are upregulated at 4 h in the presence of PAO1 biofilms, while MCP-1 is completely abrogated alongside surface markers (**Figures 4.10-12**). When this was investigated further, we concluded that MCP-1 depletion was not solely attributed to secreted proteases, or stimulation by LPS alone within the collagen (**Figures 4.14-15**). The key message we can take from this work, is that when immune cells are incubated in a wound-like environment, the presence of bacteria directly modulates their production of immune mediators to some extent, which may promote dysregulation of the healing process and infection chronicity, but is not reliant on DC-SIGN.

Although cells were fixed in previous assays using PFA, it proved insufficient to consistently remove all bacteria. This, alongside an indication that low levels of PFA might directly affect cytokine output of immune cells (data not shown) prompted the decision to optimise use of live bacteria during immune cell assays. After normalisation with planktonic cultures to determine MOIs and introduction of macrophages, no real differences were noted in bacterial clearance. This data aligns with the previous observation that *S. aureus* biofilms are able to circumvent recognition by receptors TLR-

2 and TLR-9 leading to reduced clearance *in vivo*, as well as depletion of M1-type macrophage secretions of pro-inflammatory cytokines (267). Interestingly, has been reported that macrophages show high levels of phagocytic uptake of *S. aureus* compared to other species, although these bacteria are not always killed (462). Likely the most important factor here, however, was that the calculated MOI during these assays was around 225, so it was likely that during infection, high cell death occurred because of over stimulation. However, due to the production of LDH by some *S. aureus* strains, we could not accurately analyse cytotoxicity (445, 463). Therefore, an alternative method to measure immune cell cytotoxicity will be required for these experiments. Taking this conundrum in mind, alongside various external factors within the laboratory, it was decided that the next approach would be to focus on the 3D collagen wound model, as well as the use of *P. aeruginosa* strain PAO1 to align with previous work conducted.

A wound is defined as a cut or other damage to the tissue, in this case skin, that compromises barrier integrity. Over the decades, the chronology of wound healing has been well described; in summary, the initial stage is characterised by a pro-inflammatory phase, which subsides on entering the second, anti-inflammatory and proliferative stage, then concluding in extracellular matrix remodelling and scar formation (464). Key in the initial inflammatory stages of wound healing is the activation of tissue resident macrophages and other immune cells by inflammatory mediators including complement components, coagulation cascade products and damage associated molecular patterns (DAMPs) released by the damaged tissues. On activation, macrophages upregulate chemoattractant production, leading to leukocyte recruitment and infiltration into the wound. These cells have an antimicrobial function, utilising various, well described inflammatory processes including reactive oxygen and nitrogen species, extracellular

traps in the case of neutrophils, inflammatory cytokines and chemokines, defensins and proteases (12). To a lesser extent, mast cells also infiltrate and further support the pro-inflammatory environment (11). Wounds that have dysregulated healing and become chronic due to persistence of pro-inflammation are often associated with various opportunistic pathogens, particularly *S. aureus* and *P. aeruginosa* (327, 330).

From this understanding of the complex nature of a wound bed, we wanted to design a model to incorporate and control key components to allow for analysis. Here, we considered the use of collagen to act as the ECM to encase mature biofilms grown on plastic. We also aimed to incorporate immune cells including macrophages, dendritic cells and monocytes. These assays can also be carried out in a 24- or 48-well format to provide a larger area if required. In utilising a larger space and having physical separation between the cell types, passive and active communication may occur over time while also diminishing the overwhelming MOI that we observed in the 2D plate assay. From here, bacterial cell numbers were calculated over time using CFUs, as well as immune cell cytotoxicity, cytokine output and surface marker expression. Using this information, we were able to analyse the interactions between biofilms and immune cells in a model that is more representative of the *in vivo* environment. Therefore, optimisation began with incorporation of serum, collagen, DCs and PAO1 biofilms.

This model was successful, with the niche able to support both bacteria and immune cells. Going forward, we aim to test similar parameters using macrophages and neutrophils and different bacterial species including *S. aureus*. Further, we aim to combine cell types, combining immune cells with keratinocytes and mixed species biofilms, using bacteria and fungi, to better represent real wounds observed in the clinic (327, 465). In the model, immune cells appeared to behave as expected, as the observation of immune cell

migration towards biofilms is supported in the literature, where neutrophils were able to migrate towards *Staphylococcus* biofilms when seeded to chambered cover slides and visualised with time-lapse microscopy (462). It is important for future assays to compare immune cell behaviour within the 3D model and media alone, perhaps via visualisation immune cell migration, and determine behaviours under different conditions. As suggested in (300), the presence of collagen promotes a wound healing phenotype in mouse bone marrow-derived macrophages, causing upregulation of fibroblast activation protein alpha and heme-oxygenase-1. So far, assays have been performed to compare this, with and without the presence of LPS to determine differences in cytokine output. Interestingly, MCP-1 levels do not seem affected by LPS in this model, or the collagen. It would be beneficial therefore, to expand these experiments to measure a broader range of cytokines, as well as incorporating other virulence factors, such as purified proteases etc.

Once the ELISAs were optimised and the decision made to combine sample fractions, cytokine analysis could proceed. Experiments did indeed show that presence of bacteria promoted production of classical pro-inflammatory cytokines at the 4 h time-point IL-1β and TNF-α, which is in line with the literature (466). Interestingly, in the absence of bacteria, IL-1β appeared to accumulate over time, posing the possibility that collagen itself is able to activate DCs, requiring further investigation

It would be beneficial in later experiments to assess complement and inflammasome activation during this infection assay, as IL-1β secretion is associated heavily with this process, often associated with pyroptosis, although not intrinsically responsible. Indeed, *P. aeruginosa* infection has been associated with IL-1β processing in relation to the NLRC4 inflammasome and caspase-1 (467, 468), but both have been shown to be non-

essential, as IL-1β processing has been reported in their absence, rather modulated by neutrophil serine proteases (469). However, in work conducted previously in our laboratory where IL-1β was production was assessed in macrophage-neutrophil co-cultures in the presence of caspase and neutrophil elastase (a neutrophil protease) inhibitors during planktonic *P. aeruginosa* infection, caspase was the mediating factor (470). Further, it has been reported that in certain clinical isolates of chronic *P. aeruginosa* from cystic fibrosis patients, that complement signalling is impaired during planktonic cell infection of THP-1 monocyte-like cells, exacerbating the inflammatory response by enhancement of TNF-α, IL-6 and IL-8 production (471). During our biofilm infection assays, extremely high viability in both infected and uninfected conditions implies that pyroptosis was not occurring, although this does not necessarily affect IL-1β production. Variability between repeats was extremely high, so difficult to accurately interpret, perhaps due to the use of biofilm over planktonic *P. aeruginosa*.

Conversely, MCP-1 was produced in the absence of bacteria, which was expected due to its basal production by DCs (472). Interestingly though, this cytokine is completely abrogated in the presence of bacteria. There are several explanations for this. Firstly, that secreted products such as proteases by PAO1 directly degrade cytokines (252), although if this was the case, it would be more likely observed across all cytokines. However, it has been described previously that certain *P. aeruginosa* metalloproteinases do specifically degrade MCP-1 (473). Perhaps in future experiments, a specific knockout of some of these metalloproteinases would shed some light on this possibility. Secondly, DCs may be experiencing the phenomenon of 'exhaustion', generally described as an inability of immune cells to produce cytokines after maintained stimulation over a long period. It has been suggested however, that rather than total exhaustion, these over-stimulated cells

are programmed to alter their expression profile with the aid of various signals from other cells (474). Additionally, it has been suggested that long-term stimulation of DCs, in this case with LPS and IFNγ, results in variation of cytokine response and apoptosis in certain cell subsets (475). In this study, IL-10 and IL-12p70 appear to be key during this long-term stimulation, a potential avenue for investigation within our laboratory. For all of these assays, it is assumed that the effect is caused specifically by biofilm-type bacteria, rather than expelled planktonic cells, however we cannot be certain. It is therefore important that bright field and confocal microscopy is performed using fluorescent bacteria to visualise and confirm this.

For all conditions, the presence of blocking antibodies to DC-SIGN did not appear to affect cytokine production or CFUs. This is not necessarily surprising when combined with flow cytometry data, where in the presence of PAO1, surface expression of this receptor was almost completely abrogated by 24 h (**Figure 4.12**). Here, there was concern that the depletion of DC-SIGN signal was due to protease production by the biofilms degrading blocking or fluorescent antibodies during the infection assay and flow cytometry respectively rather than DC-SIGN itself. Indeed, during binding assays in Chapter 2, DC-SIGN binding is extensive when incubated with biofilms, at comparative levels to sugar controls, indicating some downstream effect as a result of recognition. However, this observation may be a result of biofilm fixation, preventing production of any degrading factors of DC-SIGN that might be produced by live bacteria. It has been described that *P. aeruginosa* produces proteases that cleave complement proteins and alginate and Psl directly interfere with antibody opsonisation during infection, so an alternative method of blocking DC-SIGN activity may need to be implemented (329). We were reassured however, during incubations of known concentrations of cytokines with bacterial

supernatants that this was potentially not the case, but needs to be determined in DC-SIGN specifically. Regardless, work is currently to develop an RNA-interference or CRISPR-Cas9 platform to tackle this potential issue. Although there have been no other studies to investigate this, it has been shown that MR is instrumental in the pro-inflammatory response to *P. aeruginosa* infection (466). It is interesting therefore, that even after an initial depletion of MR, its levels increase again over time in the assay, suggesting that in some way, immune cells may recover and re-model their phenotype during long term infection.

In whole cells harvested and flow cytometry used to investigate a range of surface markers. Although CD11b and HLA-DR are both drastically downregulated in the presence of bacteria, a consistent level is maintained for the whole infection assay, even at 24 h. Work performed previously in the lab showed that moDCs are able to change their physical shape in the presence of purified biofilm carbohydrates, where cells significantly reduced their surface area and increased circularity without altering their cytokine output. It is possible therefore, that rather than secretory products, DCs stimulated by biofilm-products alter their cell-cell communication methods. Here, reduced HLA-DR in infected moDCs may hamper T cell communication downstream, which raises the question as to whether the moDCs *in vivo* communicate differentially with T cells in the presence of PAO1, diminishing effective clearance. Indeed, it has been reported in the literature that DCs appear to reduce dendrite formation on engagement of DC-SIGN, so this mechanism may be at play here (476).

Interestingly, supernatants collected from bacterial biofilms in collagen did not appear to have any specific effect on either HLA-DR, CD11b, MR or DC-SIGN when incubated with moDCs. However, the process of boiling supernatants appeared to affect expression of

the two CLRs. MR itself is able to bind collagen via its fibronectin type II domain (477), suggesting an involvement in clearance of collagen fragments during wound healing, or in cell-matrix adhesion in tissues. In the context of this model, denaturing of the collagen itself may have resulted in reduced recognition by MR, and hence its upregulation in that environment. Additionally, DC-SIGN, although not directly able to bind collagen, has been described to undergo protein-protein interaction with surfactant protein D which contains a collagen-like domain (478). It is not impossible therefore, that collagen or collagen-like moieties play some role in DC-SIGN regulation and that here, on collagen denaturation during boiling, DC-SIGN expression became dysregulated. Some forms of collagenase itself are also able to degrade some immune receptors, including CD1c, CD91 and CCR5 by type IV collagenase, which may explain some of the decreases in surface expression during the whole infection assay (479). However, collagenase used in this assay, a type II, does not degrade MR or DC-SIGN (479). However, this experiment was only performed once, and therefore it would be useful to investigate this observation further.

The power of current flow cytometry facilities allows for co-staining of single cells with a multitude of fluorescent markers within individual samples to more effectively unravel the true cell surface landscape. For example, costimulatory molecules CD80 and CD86 are heavily implicated in the propagation of the pro-inflammatory response during *S. aureus* infection *in vitro*, and hence should be investigated in this model (480). Conversely, it will be valuable to differentiate DCs based on their flavour, as conventional DC types 1 and 2 (cDC1/2) or plasmacytoid DCs. Importantly, cDC1s are noted for their antigen cross presentation to T cells and coordinate polarisation of CD4+ T cells to Th1s while cDC2s are more heavily associated in triggering polarisation to Th2s (481-483). To distinguish

between cDC1s and cDC2s, antibodies for CD103, XCR1 and SERPα can be utilised which we could incorporate to the model, as a general trend towards one of the groups may give us some insight as to the T cell involvement during these types of infection (481). In a previous study, it has been shown that planktonic *P. aeruginosa* is able to interfere with DC signatures by reducing cDC1 (CD103+XCR1+) populations, favouring cDC2 (484). Therefore, it would be interesting to see if a similar trend is observed with *P. aeruginosa* biofilms. Finally, OX40L has been investigated by collaborators and shown to be down-regulated by moDCs when incubated with purified biofilm carbohydrate, which may lead to immune modulation, but it is not known whether this effect is shown on exposure to whole biofilms. Ultimately, it would be interesting to perform experiments using *ex vivo* skin explants or an *in vivo* model, ideally incorporating purified carbohydrates as described in the next results chapter.

In summary, during this chapter, we have demonstrated an interaction of immune cells with *P. aeruginosa* biofilms in a novel wound model format and have shown direct effects of this interaction on cytokine production and cell surface markers. In doing so, we have highlighted the possibility that this growth mode contributes to and modulates the immune response during *P. aeruginosa* infection of chronic wounds.

Chapter 5. General discussion and future perspectives

The human immune system is complex, with a plethora of interconnecting pathways that dictate homeostasis, wound healing and protection from infection. Non-self-antigens are recognised by a range of PRRs, able to identify PAMPs specific to bacteria, likely in their planktonic form, as they breach immune barriers, namely TLRs, CLRs and inflammasomes, resulting in the promotion of pro-inflammation, immune clearance and healing.

Numerous bacteria have the ability to switch from planktonic to the biofilm mode of growth, granting the ability to persist during infection, impeding clearance by both antibiotics and the host immune system (216). Biofilms have various unique characteristics compared to planktonic cells. Namely, the production of EPS that encases and protects the bacterial community. EPS contains eDNA, carbohydrates and proteins that make up the 3D matrix (258). Two important species, *P. aeruginosa* and *S. aureus*, pose a major clinical burden worldwide, significantly owing to their ability for form biofilms (168). *P. aeruginosa* produces three carbohydrates, alginate, Pel and Psl, presence of at least one being essential for biofilm production. Importantly, the Psl structure contains D-mannose, D-glucose and L-rhamnose, while Pel contains *N*-acetylgalactosamine and *N*-acetylglucosamine (254). In contrast *S. aureus* produces only one type of biofilm carbohydrate, PIA, constituting partially acetylated *N*-acetylglucosamine (274).

During biofilm formation, various virulence factors are lost from planktonic cells, including flagellin, LPS O-antigen (*P. aeruginosa*) and staphyloxanthin (*S. aureus*), seemingly diminishing the repertoire of PAMPs for PRR recognition (485, 486). However,

upregulation of biofilm products divulges a new avenue for recognition by carbohydrate-specific CLRs, where little is currently known about their role in immune recognition, modulation and effector function in response to biofilms. Therefore, the overall aim of this thesis was to investigate the interaction of biofilms with human immune cells, in the context of carbohydrate recognition by CLRs. The three avenues for investigation were explored in depth in Chapters 2, 3 and 4, and will be summarised and discussed here.

The basis for this project drew from the work of previous lab members (191, 416, 487), where it was revealed that both whole *P. aeruginosa* biofilms and carbohydrate purified from these biofilms engaged with CLRs MR, DC-SIGN and Dectin-2. Therefore, during Chapter 2, the main aim was to reproduce and expand these data, and investigate potential CLR interaction with a new species, *S. aureus*, under various growth conditions to identify any changes. Chapter 3 focused solely on carbohydrates purified from biofilms and their interactions with CLRs. Previously, PAO1*ΔwspFΔpel* biofilms were shown to produce a carbohydrate containing 74.9% mannose, which engaged the 3 CLRs discussed (191). From here, the aim of this chapter was to investigate CLR interactions with carbohydrates purified from different *P. aeruginosa* strains, as well as *S. aureus* to investigate its role in immune recognition. Finally, using previously optimised *in vitro* methods, immune cell responses to fixed *P. aeruginosa* biofilms did not seem influenced by carbohydrate composition within the tested parameters, could not be normalised for bacteria load and viability because of differences in fixation and hence, difficult to interpret (191). Therefore, Chapter 4 aimed to design and optimise a 3D chronic wound model that could be used to investigate immune cell interactions with live biofilms using a range of parameters. For the project, DC-SIGN in particular was of interest as it has been implicated in various types of infection, including bacterial (*H. pylori*), viral (HIV-1) and

parasitic (*S. mansoni*) (66, 163) With this broad range of ligands in species that are associated with chronic infection, it seemed logical that DC-SIGN would be involved in immune modulation during infection, dampening the inflammatory response and allowing *P. aeruginosa* to establish itself in the tissue. However, the mechanism of this is unlikely to be straightforward, as receptor engagement has been described to both directly hinder and promote infection. Namely, DC-SIGN engagement with HIV-1 protein gp120 directly facilitates viral particle entry to T cells, while in contrast, DC-SIGN engagement by *M. tuberculosis* specifically promotes IL-10 upregulation and a Th-2 response which promotes colonisation (66, 164). With this in mind, it was uncertain what role DC-SIGN would provide during this model.

For this study, we utilised a range of *P. aeruginosa* strains to specifically investigate the role of biofilm carbohydrate in immune recognition and response, which each overproduced one, both or none of the carbohydrates associated with PAO1 biofilms, Pel and Psl. This overproduction was achieved through increased cellular cdiGMP as a result of *wspF* mutation and hence overexpression of various downstream genes associated with biofilm production, most notably those involved in EPS production (238, 258). Mutations were confirmed at the start of the project. We also selected the strain SH1000 for investigation of *S. aureus*, as it originates from the parent strain *S. aureus* 8325-4, with an inserted functional copy of the *rsbU* gene, which is defective in the parent strain, encoding a regulator for the general stress response protein, accessory sigma factor-β (488). This strain is used extensively in laboratory studies, and the lineage originates from a sepsis isolate, deeming it clinically relevant for this study (489). The proceeding sections provide a brief summary of each results chapter including aims and main findings, followed by an overview of future work and implications going forward.

5.1 Analysis of carbohydrate composition of *P. aeruginosa* and *S. aureus* biofilms using lectins (Chapter 2)

During chapter 2, we explored the optimisation of *P. aeruginosa* and *S. aureus* biofilm growth in a range of conditions to investigate innate immune interactions with these structures. For this chapter, the main aim was optimising biofilm growth in a range of conditions to determine alterations in growth characteristics via the interactions of lectins (**Ch. 2**), which would then be utilised for carbohydrate purification (**Ch. 3**) and whole immune cell interactions (**Ch. 4**). Following previous work where biofilms of *P. aeruginosa* PAO1 with its *ΔwspF* mutants were produced and characterised in the eukaryotic media X-Vivo15 (191), we were able to produce biofilms of consistent biomass based on crystal violet quantification (**Figure 2.3A**). We aimed to use these biofilms for composition analysis using lectins and confocal microscopy in this chapter, as well as in a novel chronic wound model designed and used in Chapter 4.

Using an ELISA-type binding assay, we investigated CLR interactions with both whole biofilms and culture medium alone which was overlooked previously, confirming that at up to 5 μgmL^{-1}, Fc-DC-SIGN did not bind to X-Vivo15, while MR CTLD4-7-Fc and Dectin-2-Fc did not bind at any concentration tested (**Figures 2.3-5**), proving that ligands observed were of bacterial-origin and not an artefact from the culture medium. All these CLRs tested reportedly bind high-mannose structures (127, 151, 161), and this has been demonstrated in these strains by previous lab members. These high-mannose ligands within biofilms produced in X-Vivo15 were also observed in this chapter for all three CLRs tested (**Figure 2.3-5**). Generally, highest levels of binding were observed by Fc-DC-SIGN, which did not directly correlate with overall biofilm biomass, as Fc-DC-SIGN was the only CLR able to bind planktonic bacteria (PAO1*ΔwspFΔpelΔpsl*). Of note, using

commercially available biotinylated lectins with a range of specificities, no ligands were observed in either strain, namely GlcNAc, GalNAc, galactose, mannose, glucose or fucose (**Table 2.2, Figure 2.8**). However, some lectins tested, namely Con A, RCA I, SBA and WGA, bound X-Vivo15 alone at high levels, deeming these results inconclusive, as ligands originating from biofilm vs media alone could not be differentiated (**Figure 2.6A**).

Also in this chapter, biofilms of *S. aureus* SH1000 were successfully produced using the model developed for *P. aeruginosa*, although requiring higher seeding densities to produce exponential-phase cultures in the time-frame required for experiments due to its longer lag-phase (**Figure 2.2**). These biofilms produced consistent, high-quantities of biomass and were analysed using biotin-, but not Fc-conjugated lectins due to interference by secreted virulence factor protein A, described to bind the Fc-portion of immunoglobulins *in vivo* (287). Here, the presence of GalNAc was indicated within *S. aureus* biofilms, but not *P. aeruginosa*, based on unique binding of DBA to *S. aureus* (**Figure 2.8**).

Finally, we optimised production of *P. aeruginosa* biofilms in a defined minimal tissue-culture medium, DMEM-BSA, to determine if this had an effect on biofilm growth or ligand distribution. *S. aureus* growth was not supported in DMEM-BSA, perhaps due to the general antimicrobial effect of BSA on this species (490). Overall, biofilms were of lower biomass in this medium, with PAO1*ΔwspFΔpsl* showing highly diminished biofilm growth (**Figure 2.11**). Further, binding by MR CTLD4-7-Fc was completely lost (**Figure 2.12B**). For Fc-DC-SIGN and Dectin-2-Fc, binding was generally diminished compared to biofilms grown in X-Vivo15, but remained significant for PAO1*ΔwspfΔpsl* for both CLRs (**Figure 2.12A, C**). As well as lack of biomass, this strain also lacks Psl, the carbohydrate produced by *P. aeruginosa* confirmed to contain high proportions of mannose in its structure. The

remaining carbohydrate, Pel, constitutes partially acetylated GalNAc, which has been described as a ligand for DC-SIGN, but not Dectin-2 (349). In DMEM-BSA, distribution of Fc-DC-SIGN is consistent with that in X-Vivo15 when analysed using confocal microscopy (**Figure 2.13**).

Overall, the most important finding from this chapter was that even within the same model parameters, biofilm architecture and ligand combinations are altered when changing environmental resources. Plasticity in biofilm characteristics then results in altered CLR binding and hence, changes in overall immune response during different types of *P. aeruginosa* infection, perhaps promoting or inhibiting inflammation to facilitate persistent infections.

5.2 Preparation and analysis of purified EPS from biofilms (Chapter 3)

In Chapter 3, we expanded on work performed in Chapter 2 by extracting biofilm carbohydrate from *P. aeruginosa* and *S. aureus* biofilms, with the aim to analyse it both biochemically and in the context of immune receptor recognition (**Ch. 2**) and whole-cell interactions (**Ch. 4**). We established during the last chapter that whole biofilms provide ligands for various lectin receptors, including DBA (*S. aureus*), DC-SIGN, Dectin-2 and MR CTLD4-7 (*P. aeruginosa*), but using this model, it is difficult to establish the specific contribution from EPS carbohydrates compared to other factors that interact with immune receptors. Therefore, in extracting total carbohydrate from mature biofilms, we may be able to characterise its specific contributions to immune recognition and response during these types of biofilm-associated infection.

All 3 CLRs Dectin-2, MR and DC-SIGN bind a range of pathogens via high-mannose structures, with a general association with chronic infection types. As discussed in the previous section, past work in the laboratory identified CLR ligands in whole *P. aeruginosa* biofilms, and these ligands were maintained when biofilm carbohydrate was purified from the strain PAO1*ΔwspFΔpel*, predicted to overexpress Psl only, which is reported to contain a high proportion of mannose (245). Unlike *with P. aeruginosa* strains, we were unable to definitively identify mannose within the biofilm, but binding of DBA suggested the presence of GalNAc, not generally associated with *S. aureus* biofilms (280). To more clearly determine the true carbohydrate content in this *S. aureus* biofilms, we aimed to optimise extraction and purification for biochemical and immunological analysis.

Using a medium utilised extensively in the literature for biofilm culture, tryptic soy broth (TSB), we adopted and optimised *S. aureus* growth for the 5-day incubation period, increasing salt-levels, volume and introducing medium agitation to maximise carbohydrate output for extraction. Using this culture method, we were able to extract and purify a carbohydrate product that showed little protein contamination when assessed by BCA and Coomassie staining that was used for analysis (**Figure 3.5**). Before pooling, we coated wells with *S. aureus* carbohydrate preparations 1 and 2 and incubated them with biotin-conjugated plant lectins used in Chapter 2 to obtain preliminary data for binding characteristics. Interestingly, high levels of Con A (mannose-specific) binding was observed here, at similar levels to that of X-Vivo15-cultured biofilms and X-Vivo15 alone. Here, carbohydrates were diluted in saline solution, so we can confirm that the binding observed came directly from the carbohydrate preparation. In contrast, DBA (GalNAc-specific) binding was lost when compared to whole-biofilm interactions, suggesting a loss of GalNAc (**Figure 3.7**). This gain of mannose-containing structures was taken into consideration going forward, post-FPLC.

FPLC was performed in relation to protein-standards to isolate high molecular weight (HMW) products within the extract, >17 kDa, excluding small sugar contaminants that do not originate from PIA. The extract underwent Coomassie and silver staining and unlike with Gram-negative *P. aeruginosa*, *S. aureus* EPS showed no LPS contamination, although some smearing was observed in the individual preparations before pooling, suggesting a low molecular weight contaminant that was lost after FPLC. The relevance of this will be discussed in Section **5.5.4**. The product was incubated with moDCs, the cell type most utilised during Chapter 4, to assess cytotoxicity, with cells showing high viability up to 1 μgmL^{-1}.

After this initial characterisation, we coated wells with HMW carbohydrate at a range of concentrations (10-0.01 μgmL^{-1}) and incubated them with CLRs Dectin-2-Fc, MR CTLD4-7-Fc and Fc-DC-SIGN. All three CLRs bound the *S. aureus* product at very high levels, comparable with *P. aeruginosa* extract, validating the Con A binding discussed previously (**Figure 3.8**). To further validate this observation, we designed a competitive ELISA where we tested the purified product's ability to compete with known lectin ligands, by preventing its displacement by the relevant ligand in the binding pocket during incubation. We started here with carbohydrate from *P. aeruginosa* PAO1*ΔwspFΔpel* which was the previous focus in the lab, which was able to actively compete for all three CLRs as expected (**Figure 3.9**).

Alongside the two preparations discussed previously, carbohydrate was extracted from TSB alone that had not housed any bacterial biofilms. During binding assays to *S. aureus* carbohydrate, we were concerned at the appearance of high-mannose structures that were unexpected when considered with the literature (280). From here, we could compare all three preparations and determine if TSB provided any considerable proportion of binding by the CLRs. The low molecular weight TSB extract did not bind, but unfortunately, the HMW competed with fucose for Fc-DC-SIGN binding at comparable levels to *S. aureus* and *P. aeruginosa* preparations, confirming our doubts that binding may be an artefact of the specific culture conditions (**Figure 3.10**).

As shown in Chapter 2, DMEM-5921 supplemented with 5% BSA, 10 mM HEPES and 2 mM L-glutamine (DMEM-BSA) was able to support *P. aeruginosa* biofilm growth that produced CLR ligands, and this binding was dependant on the presence of bacteria, as no binding was observed to media alone (**Figure 2.12**). PAO1*ΔwspFΔpel* was able to form a good pellicle in DMEM-BSA over the 5-day incubation, but filtration at 5% BSA was

extremely difficult, and hence a 2% BSA content was utilised going forward. For extraction, the protocol was altered to accommodate a lower overall carbohydrate content, incorporating a concentration step post-TCA precipitation of protein/lipids, with neutralisation before dialysis to prevent damage of the cassette membrane (**Figure 3.14**). This work is currently ongoing in the laboratory, and further preparation, purification and characterisation of this carbohydrate will be carried out by postdoctoral researcher Dr Sonali Singh.

Overall, the main message during this chapter was similar to that of Section **5.1**, that biofilms develop differently depending on their environment, and that carbohydrate characteristics in the overall biofilm environment are dictated by those provided in that environment, all of which contributing to combined recognition and response by immune receptors of the host.

5.3 Responses of human immune cells to biofilms (Chapter 4)

For Chapter 4, the initial aim was to optimise the previously utilised laboratory infection model to effectively fix all bacteria present, as well as normalise planktonic and biofilm cell numbers for adoption of a live infection model. This investigation was successful (**Figure 4.2**), but on incubation with monocyte-derived human macrophages with live biofilm and planktonic cells, cytotoxicity remained exceptionally high and results were difficult to interpret (**Figure 4.3**). Therefore, the ultimate endeavour was to produce a 3D collagen model which allowed us to incubate immune cells alongside live biofilms to investigate the interactions that occur, providing some insight into chronic infections caused by the clinically relevant species, *P. aeruginosa.* Here, *P. aeruginosa* PAO1 wild-type strain was used to ensure there were no outlying effects of the Δ*wspF* mutation in addition to carbohydrate production, such as virulence factor production, that may influence immune cells. Although still a laboratory strain, PAO1 is extensively used in various *in vitro* and *in vivo* studies, so is relevant during this investigation. In future, this model may be adapted to include clinical isolates of *P. aeruginosa*, as well as other bacterial species, pathogenic or commensal, which will be discussed in Section **5.5.2**.

The collagen model was optimised individually to ensure consistent bacterial growth at 4 and 24 h (**Figure 4.5**) and high immune cell viability (**Table 4.5**), followed by combination of bacteria and moDCs to produce the final, complete model. Here, in the presence of immune cells, bacterial cell numbers were not affected compared to control wells containing no human cells, indicating that moDCs are not directly involved in pathogen killing in this context. However, cytokines levels were altered in the presence of bacteria, discussed in more depth in the proceeding paragraph. Briefly, we may infer from these changes that rather than killing bacteria directly, immune cells in this model

are involved in cellular signalling during inflammation, perhaps via recruitment of peripheral cells such as neutrophils and monocytes, and in doing so would dysregulate wound homeostasis, healing, and infection progression. During infection assays, DC-SIGN was inhibited using blocking antibodies to determine if this receptor played a role in bacterial clearance, cell cytotoxicity or cytokine production, as this receptor bound whole biofilms at high levels in ELISA assays, indicating a role in infection (**Ch. 2, Ch. 3**). However, blocking of DC-SIGN did not significantly affect either parameter tested (**Figures 4.8-9**), suggesting that in fact, this receptor does not play a role during *P. aeruginosa* infection in the context of moDCs.

When comparing infected and uninfected cells outwith DC-SIGN blocking, cytokines TNF-α and IL-1β are upregulated by PAO1 biofilms, but only in the short term (4 h), as levels appear to diminish by 24 h, suggesting some kind of exhaustion effect (**Figures 4.10A-B**, (474)). Interestingly, at 24 h, IL-1β is produced even in the absence of bacteria, suggesting that collagen itself may have some pro-inflammatory properties in this model (**Figure 4.10B**). Interestingly, chronic wounds in diabetes are associated with dysregulation in ECM deposition, so perhaps in this context, the concentration of collagen used may have mimicked this environment, triggering IL-1β production (443). In stark contrast, MCP-1 chemokine, alongside surface proteins HLA-DR, CD11b, MR and DC-SIGN, were abrogated in the presence of PAO1, prompting further investigation (**Figure 4.10C, Figure 4.12A-B**). When moDCs were incubated with *E. coli* LPS alone within the collagen matrix, MCP-1 production was not significantly affected compared to untreated moDCs, concluding that this was not the determining factor of the abrogation (**Figure 4.14B**). Further, PAO1 biofilms alone were unable to directly degrade purified MCP-1 or TNF-α (**Figure 4.15B, C**), and in the presence of bacterial supernatants, surface expression of all 4 markers

tested (HLA-DR, CD11b, MR, DC-SIGN, **Figures 4.16-17**) were not affected, leaving the final assumption that live bacteria within the collagen matrix were required for downregulation of the production of certain immune factors, rather than secreting products that degrade directly them.

For this final chapter, the key message we could decipher, is that in a simple wound-like environment, live bacteria are able to directly modulate immune outcome, via both their secretion of specific immune mediators such as immune cell chemoattractant and production of surface markers that may contribute to immune response. In doing so, bacteria may directly promote immune dysregulation and infection chronicity, although we are still unsure of the specific mechanisms that cause this.

5.4 Ongoing Work

Following the work presented during this thesis, the project will be continued by PhD student Nusrat Abedin, who has adopted the 3D collagen model and successfully reproduced data presented in Chapter 4. For her PhD, she has accrued the following aims that will expand on the knowledge developed during this project, answering some of the questions raised here:

- Validate findings previously reported to establish the mechanisms and biological consequences involved in MCP-1 abrogation and moDC surface marker changes in response to PAO1 biofilms (eg. proteomics and RNAseq).

- Expand the range of moDCs markers and cytokines investigated to broaden understanding.

- Assess moDC role in T cell activation, proliferation and differentiation in response to bacteria cultured in collagen.

- Determine the role of *P. aeruginosa* proteases by investigating their expression under different conditions and use of specific mutants.

- Utilise the 3D collagen model to study monocyte and neutrophil contributions to biofilm recognition, focusing on the role of Dectin-2.

In addition, carbohydrate purification from biofilms grown in DMEM-BSA is continuing with Sonali Singh undertaking biochemical characterisation and biological assays.

5.5 Clinical implications and future prospective

5.5.1 Refinement of the wound model

In its current state, the 3D collagen model provides very general depiction of the chronic wound environment, housing a single bacterial species and immune cell type (discussed in depth during in Sections **5.5.2** and **5.5.3**). Alongside the resident species, specific environmental parameters may be altered to more specifically mimic different types of niche in the context of infection and immune infiltration. The wound environment in diabetic patients differs from that of healthy individuals. Perhaps most prominently, diabetic patients harbour dysregulated glucose metabolism, which can be replicated within this model by supplementing glucose at normal physiological or hyperglycaemic levels, perhaps by incorporating DMEM-BSA over X-Vivo15 as in Chapter 2 and 3. Additionally, in diabetes *in vivo* models, macrophages exhibit impaired phagocytic ability as well as reduced VEGF secretion, leading to failed tissue repair (491). It would be interesting to utilise macrophages treated in a diabetes-like environment for this model compared to M-CSF macrophages as used generally in our lab to determine changes in phenotype and secretory output. Finally, the matrix itself may be impregnated with additional components such as antibiotics or other drugs to determine their effects on human or bacterial cells.

5.5.2 Expanding species and poly-microbial biofilms

During this study, we utilised single-species biofilms using two lab strains of clinically relevant species *S. aureus* and *P. aeruginosa*. However, there are various other important pathogens that are relevant in the clinical setting, including bacteria and fungi, which may be incorporated into this *in vitro* infection model as well as for carbohydrate purification. Alongside these two species, the ESKAPE organisms compose *Enterococcus faecium*, *Klebsiella pneumoniae*, *Acinetobacter baumannii* and *Enterobacter spp*. that all pose significant burden to the healthcare system by causing nosocomial infections and would be interesting to investigate using this model (177). Importantly, it is also rare in the clinic that infection sites are colonised with a single species, but rather polymicrobial communities that rely on interspecies interactions to promote successful colonisation, resistance and virulence (492-494).

Enterococcal species commonly colonise the human gastrointestinal tract, but opportunistic infections are often reported in the urinary tract during catheterisation and are associated with poly-microbial biofilm formation (495). Indeed, Enterococci are frequently co-isolated with the other ESKAPE species, with co-culture having important effects on each species (496). For example, when co-cultured with uropathogenic *E. coli in vitro, E. faecalis* attachment and biofilm formation is partially inhibited, but *K. pneumoniae* and *E. coli* biofilm formation is promoted by *E. faecalis* (492). *E. coli* is a member of the Enterobacteriaceae family, which includes a range of Gram-negative bacilli that commonly populate the mammalian gut flora, and also includes *Shigella* and *Salmonella spp.* It would be interesting to assess these interactions in the context of our model. In addition, Enterococcal species are mainly limited to *in vivo* studies for investigation, as *in vitro* methods are currently lacking (495). This collagen model may

pose an opportunity here, as Enterococci produce a range of virulence factors specifically associated with collagen interaction. Namely, Ace and Enterococcal fibronectin-binding protein (EfbA) both facilitate collagen adhesion in the host extracellular matrix, and their gene deletions have been shown to significantly attenuate *E. faecalis* virulence in a rat *in vivo* model, while immunisation with these proteins provided protection against infective endocarditis (497, 498). In our model, we may be able to further explore the specific roles of these proteins in the context of collagen binding during immune interaction.

Additionally, hypervirulent-hypermucoid *K. pneumoniae* is an important invasive pathogen and the leading cause of pyogenic liver abscesses in the USA and Europe, while non-hypervirulent strains also commonly cause highly antibiotic-resistant infections of the urinary and respiratory tracts and bacteraemia in immunocompromised patients (499, 500). The most common species co-isolated with this species is *E. coli*, although as yet, there is no reported influence on virulence in either species during co-culture (501). Although it is understood that on entry to the bloodstream, *K. pneumoniae* are subject to phagocytosis by macrophage populations, the specific clearance mechanisms are still poorly understood. Generally considered obligate extracellular, *K. pneumoniae* has been reported to survive within macrophages *in vitro,* via avoiding lysosome uptake (502), and that on occasion, can actively form a niche replicate intracellularly as demonstrated using an *in vivo* pig organ perfusion model (503). Using our model, we may be able to more closely study this bacteria-macrophage interaction in the 3D setting, providing some insight as to the specific interactions taking place.

Alongside bacteria, fungal species are also associated with HAI and may be explored in the context of our *in vitro* model. Importantly, *C. albicans* is a member of the skin microbiome, but under certain conditions is able to cause a range of diseases, from

superficial skin infections to life threatening, systemic fungaemia. *C. albicans* harbours the ability to switch between yeast and fungal growth forms, the latter associated with multiple adhesins, invasins and biofilm formation that contribute to virulence within the host. However, the triggers for switching between these two forms is poorly understood, which could be explored in this 3D setting.

Further, *C. albicans* is frequently co-isolated with *S. aureus* and *P. aeruginosa* in the clinic, and has been investigated in various *in vivo* and *in vitro* scenarios. In an *in vivo* murine model, *C. albicans* has been shown to augment *S. aureus* virulence and lethality (504), and also promotes *S. aureus* growth in poly-microbial *in vitro* models (505). Generally, *P. aeruginosa* growth is also enhanced by *C. albicans*, as it is able to attach fungal hyphae via type IV pili and lectin-interactions for parasitic nutrient filtering (506). Further, LPS from *P. aeruginosa* interferes with *C. albicans* filamentation, metabolism and growth (507). All of this combined makes *C. albicans* an attractive addition to this model, where these interactions can be investigated in the 3D environment.

As discussed above, *E. coli* and *C. albicans* alongside various other bacterial and fungal species naturally populate the mammalian microbiome of the skin, gut and all other niches. Importantly for this thesis, the skin flora is a robust population that survives in this harsh environment of desiccation, high-salt and nutrient deficiency, and acts as a secondary barrier for the body against invading pathogens as well as immune education (508, 509). Skin as an organ can be subdivided into sebaceous, moist or oily, which determine the specific combinations of colonising bacteria. Historically, the microbiome was investigated using strictly culture-based methods, however developments in 16S ribosomal, Illumina and amplicon sequencing have allowed for in depth analysis of microbial communities (510). It may be useful going forward therefore, to utilise

important commensal species to determine their interactions and outputs during both health and in contact with pathogens.

5.5.3 Expanding human cell subsets and receptors

As discussed throughout this thesis, wound healing and infection control involved a broad range of immune cells, including macrophages, monocytes and neutrophils that populate the wound bed (**Section 1.2**). Currently, work is being carried out in the lab to incorporate inflammatory monocytes (GM-CSF-treated) to the collagen model in order to investigate the role of Dectin-2 in response to *P. aeruginosa* as well as *C. albicans* (Khawalah Munshi, Nusrat Abedin, PhD students). This investigation could be extended to macrophages which also express this receptor (155, 511). As discussed here, little effect on bacterial numbers has been observed using moDCs (**Figure 4.8C**). This is unsurprising due to their primary role in antigen presentation over killing, so investigation of monocytes and neutrophils in this context may give us some new information.

Alongside innate immune cells, work has been designed for the investigation of T cell roles during biofilm infection, although due to time restraints we could not proceed with experiments. From work conducted previously, we showed that moDCs reduce surface area and ligand uptake in the presence of purified biofilm carbohydrate (191), and hence implies that this plays some role in antigen presentation to T cells. This would support the idea that these biofilms do promote chronicity of infection, as T cell effector function would be inhibited and inflammation maintained. Using the discarded fraction of leukocytes from donor blood, CD4+ T cells may be isolated by positive selection and maintained using IL-2 during differentiation of monocytes to macrophages or DCs (512). From here, APCs incubated with carbohydrate may be stimulated using LPS while CD4+ cells are activated by CPI, a cocktail of Cytomegalo-, Parainfluenza- and Influenza virions,

and added to APCs (513). From here, T cell differentiation, proliferation capability and cytokine output may be measured to identify changes in these interactions (514).

Alongside classical immune cells, keratinocytes and epithelial cells are heavily involved in wound healing. Keratinocytes are the most prolific skin cell type and play vital structural roles in healing, modulated by chemokines, cytokines and matrix metalloproteinases (515, 516). They also contribute to immunity, including production of cytokines, chemokines and extracellular vesicles for communication with leukocytes (517). In addition, these cells directly contribute to pathogen clearance by producing antimicrobial peptides (518). These cells undergo epithelial restitution in the early stages of wound healing to initiate closure and remodelling and actively communicate with immune cells to initiate inflammation (12). Recently, air liquid interface culturing methods have been developed to replicate the 3D respiratory tract environment, allowing for investigation of infection and pollutants on multiple cell types, including goblet and epithelial cells amongst others (519). Development and incorporation of this type of culture method would be invaluable here, particularly in relation to cystic fibrosis.

It was suggested during Chapter 4 that in the context of the collagen model, DC-SIGN did not appear to play a role in the immune response (**Figures 4.8, 4.10**). However, there are many other receptors that could be investigated using this system that may be relevant. As shown in Chapter 2, both MR and Dectin-2 are able to bind *P. aeruginosa* biofilms (**Figure 2.4-5**), which may also be investigated. In addition, dendritic cell immunoreceptor (DCIR, CLEC4A/CLECSF6) is highly expressed on moDCs as well as other immune subsets, and has broad carbohydrate specificity, including mannose and fucose (520). When co-stimulated alongside DC-SIGN, DCIR inhibits antigen presentation

to T cells, which may explain the apparent redundancy of DC-SIGN alone during this study (521).

Finally, it would be interesting to investigate the synergistic effect of CLRs with other receptors during infection, as it was clear during previous work that carbohydrates were able to antagonise certain receptors from inflammatory function (191). For example, TLRs -4, -9 and -2 recognise LPS, nucleic acid and peptidoglycans respectively, all of which are produced by biofilms (100). It would be interesting therefore, to determine if signalling by these receptors is affected by carbohydrate, perhaps during blocking of other receptors like DC-SIGN and MR whose cooperation with TLRs has been described previously (142, 522).

5.5.4 The role of carbohydrate vs LPS

During our previous study, EPS extracted from *P. aeruginosa* biofilm underwent extensive LPS-removal during the purification process to ensure that any immune effect was a result of the carbohydrate alone and not a by-product of LPS stimulation (191). Indeed biofilm carbohydrate did not appear to have a large effect on moDCs, although it did inhibit uptake of Lewis^X ligands by DC-SIGN and acted as a Dectin-2 antagonist in response to zymosan stimulation (191). Although the protocols for biofilm production and carbohydrate purification have been optimised during this thesis and have yet to be investigated in biological assays, the question still remains as to the true relevance of Psl during infection. LPS is a highly inflammatory virulence factor and is used extensively during *in vitro* studies to activate immune cells (523). It is also produced extensively by Gram-negative bacteria, confirmed during purification of our product, where a minimum of six rounds of LPS-removal was required to remove all traces (191). Therefore, we must question whether any specific effect of carbohydrate engagement of immune cells is completely overshadowed by LPS stimulation. To determine this, it would be useful to compare LPS+ and LPS- carbohydrate alongside LPS-alone in ongoing experiments to determine any differences. Interestingly, in previous work, preparations that had/had not undergone LPS removal were compared in previous preliminary experiments in the lab, the LPS-contaminated preparation appeared to have less of an effect on immune cells (as described in (191)). Further, investigation of carbohydrates purified biofilms of Gram-positive bacteria or fungi would alleviate the issue of LPS but may introduce other virulence factors. Finally, alongside repeating experiments conducted previously, it would be interesting to incorporate carbohydrate into the collagen model, as presence of EPS within the matrix may affect immune cell function. In particular, incorporation of

carbohydrate from one species with live cells of another may provide some insight into communication between bacteria in the wound environment via these specific products.

5.5.5 Diagnostics and treatment of biofilm infections

Often, signs and symptoms of wound infection are subtle and covert, so efforts were made by the International Wound Infection Institute in 2019 to propose a consensus on diagnosis by considering the latest clinical evidence, alongside an extensive literature review and an online consensus survey with 14 international experts to define biofilms, and chronic infections and implement correct terminologies (438). With this taken into consideration, in the clinic diagnostics are multifaceted, with various requirements in place for positive bacterial biofilm diagnosis. Namely, microbiological evidence of infection via culture-based methods, confocal or SEM evidence of bacteria glycocalyx or evidence of fibrous or necrotic tissue within a wound bed. Further, observation of recurrent infection within a chronic wound with clonally identical organisms when compliance with recommended antimicrobial treatment was maintained alongside signs of local or systemic infection that subside then return after treatment indicate resistant infection most associated with biofilms (438).

In 2016, a similar consensus was discussed, and voting performed to determine the most strongly recommended therapeutic interventions for wounds, venous leg, pressure and diabetic foot ulcers with suspected biofilm infection (439). Importantly, debridement alongside antiseptic soaks and dressings remove necrotic tissue and limit bacterial overgrowth during treatment. Work is already being conducted within our laboratory to determine effectiveness of various antimicrobial compounds on poly-microbial biofilms using collagen and synthetic wound fluid (Iona Willingham, PhD project), but as yet, immune cells have not been incorporated into this model. The model developed during this project may provide insight here, as the parameters may be adjusted to incorporate

these compounds with the species already tested, alongside immune cells and other antimicrobials.

Summary

To conclude this work, we have shown that DC-SIGN, MR and Dectin-2 are able to bind biofilms and purified biofilm-derived carbohydrates in a range of culture conditions and strains using *P. aeruginosa*, and that experimental methods may be expanded to new species, namely *S. aureus*. We were also able to optimise carbohydrate extraction and purification from biofilms using a new methodology that excludes medium-derived ligands for biological investigation. Finally, we designed and optimised a 3D, collagen wound model where we successfully co-cultured *P. aeruginosa* with moDCs with high viability, causing various immune effects including MCP-1 and surface marker depletion in response to biofilm. Although there were limitations within this study, we have gained some exciting insight into immune interaction with the human immune system, opening many interesting avenues for investigation in the near future (**Figure 5.1**).

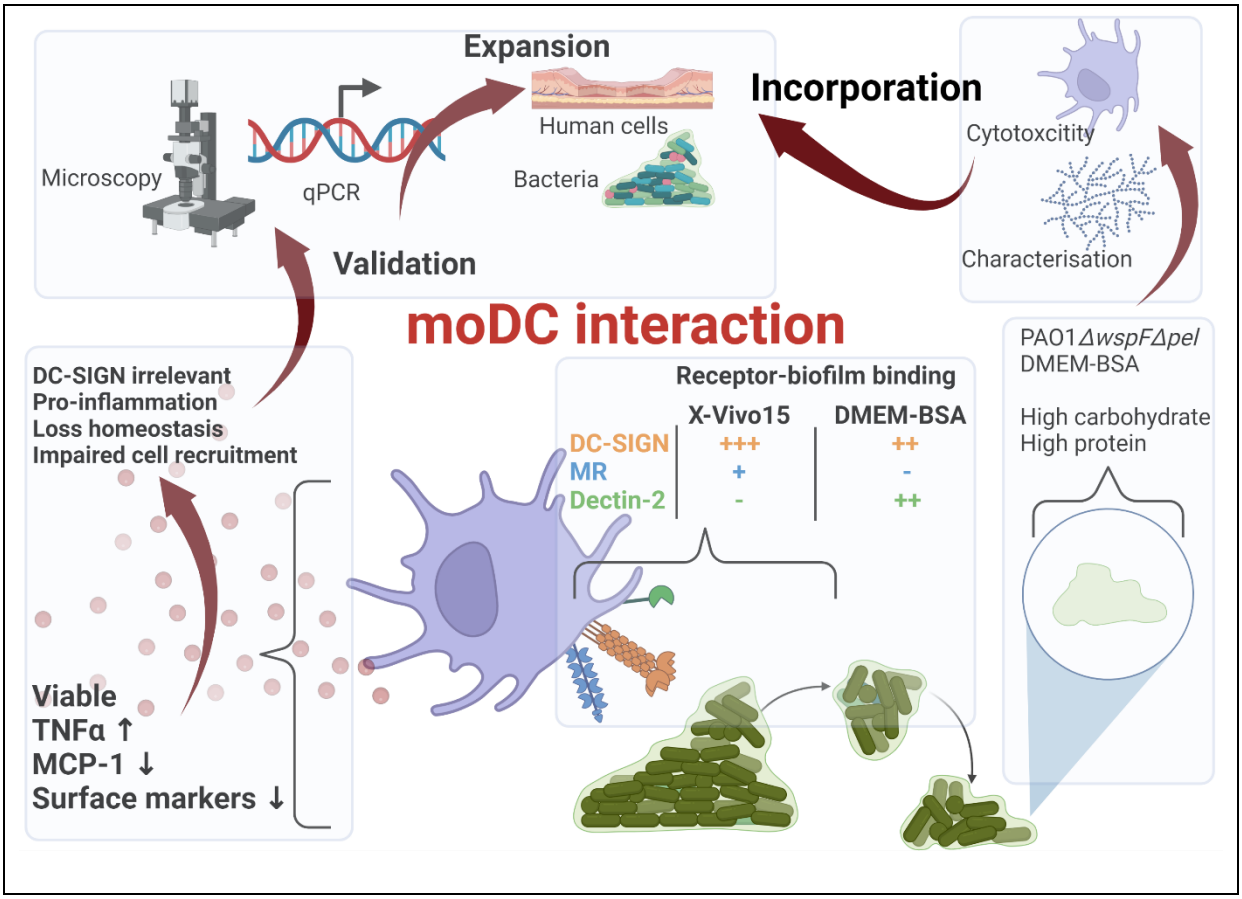

Figure 5. 1: Interaction of human immune cells via C-type lectin receptors with P. aeruginosa biofilms. *P. aeruginosa biofilms and purified biofilm carbohydrates were able to interact with clinically relevant CLRs: DC-SIGN, MR and Dectin-2, with most prominent binding by DC-SIGN to both X-Vivo15 and DMEM-BSA biofilms. Purified biofilm carbohydrate did bind these CLRs, but artefacts in TSB medium prompted optimisation of extraction using DMEM-BSA grown biofilms. This work is ongoing. Using biofilms embedded in collagen matrix, moDCs were exposed to PAO1 with and without DC-SIGN blocking, but there was no significant effect in any parameters tested. In response to PAO1, moDCs increased TNF-α production but reduced MCP-1 and surface markers, suggesting a preference for inflammation, loss of homeostasis and impaired cell recruitment, leading to chronic infection. In future, biofilm carbohydrate from DMEM-BSA will be incorporated into this model, alongside validation of functional observations by microscopy and qPCR. Ultimately, we will include a range of prokaryotic and human cell types to our 3D co-culture model.*

Covid Statement

It can't be denied that for the last year, the pandemic has taken a huge toll. When the outbreak started early in 2020, I had only recently started to recover from some very difficult times, as for the first 6 months of my PhD I was situated in a different lab which I had to leave when I could not continue with my supervisor. Towards the end of 2019, I had settled into my current lab and had many experiments optimised ready for data collection in 2020, but Covid hit then and lockdown shortly followed.

When the pandemic started in 2020, I was beginning large-scale data collection which was cut short while we were forced to leave the lab during the first lockdown. Due to the lab-based nature of my project, I had no bioinformatics data that I could work through or incorporate into my work, and had too little data at this point to begin constructing thesis chapters. Further, there were several aspects of this project that relied on collaborations with other labs that were discontinued. Of note, our collaborator Prof. David Williams was heavily involved in carbohydrate analysis and will no longer be able to assist with various biochemistry aspects of the project, and therefore work did not go ahead, hindering a large part of the second results chapter. In addition, before lockdown I had begun to development of a DC-T cell co-culture assay which was outsourced to Prof. Yvette van Kooyk's lab in Holland in order to accelerate the data collection process. However, due to the various lockdowns and ongoing pandemic work did not proceed as expected.

In a more specific sense, the lab has faced many logistical issues throughout the pandemic. There have been various important reagents and equipment that have been difficult to procure which made progress slow. Also, certain orders coming from overseas,

including new cell lines, were delayed or completely eliminated. It was also impossible to procure blood products until relatively recently. My work centres on human donors, so this caused a lot of problems. The use of immortalised cell lines was attempted, but due to various issues those experiments could not continue. Another major issue was the lack of access to FPLC and freeze-drying equipment. Various machines were dismantled on returning to the lab to better utilise space, and until recently there were no alternatives.

My project initially focused on the comparison of the immune interaction to *S. aureus* and *P. aeruginosa* biofilms, ultimately leading to the analysis of mixed species communities, with addition of fungal species at a later date, which are more characteristic of clinical infections. However, due to the pandemic and subsequent lockdown, we were forced to reconsider some of the project aims based on what was possible in the new lab environment. Therefore, we decided to focus now on the comparison of planktonic vs biofilm *S. aureus* monocultures as growth of these has already been optimised for our lab, which is unfortunate as it makes my work less clinically relevant. The 3D collagen model was not previously considered, but over lockdown the system was optimised for use in the lab by other members going forward.

References

1. Luu M, Riester Z, Baldrich A, Reichardt N, Yuille S, Busetti A, et al. Microbial short-chain fatty acids modulate CD8(+) T cell responses and improve adoptive immunotherapy for cancer. Nat Commun. 2021;12(1):4077.
2. Mayer EA, Knight R, Mazmanian SK, Cryan JF, Tillisch K. Gut microbes and the brain: paradigm shift in neuroscience. J Neurosci. 2014;34(46):15490-6.
3. Ly NP, Litonjua A, Gold DR, Celedon JC. Gut microbiota, probiotics, and vitamin D: interrelated exposures influencing allergy, asthma, and obesity? J Allergy Clin Immunol. 2011;127(5):1087-94; quiz 95-6.
4. Wong R, Geyer S, Weninger W, Guimberteau JC, Wong JK. The dynamic anatomy and patterning of skin. Exp Dermatol. 2016;25(2):92-8.
5. Baroni A, Buommino E, De Gregorio V, Ruocco E, Ruocco V, Wolf R. Structure and function of the epidermis related to barrier properties. Clin Dermatol. 2012;30(3):257-62.
6. Dabrowska AK, Spano F, Derler S, Adlhart C, Spencer ND, Rossi RM. The relationship between skin function, barrier properties, and body-dependent factors. Skin Res Technol. 2018;24(2):165-74.
7. Byrd MS, Sadovskaya I, Vinogradov E, Lu H, Sprinkle AB, Richardson SH, et al. Genetic and biochemical analyses of the Pseudomonas aeruginosa Psl exopolysaccharide reveal overlapping roles for polysaccharide synthesis enzymes in Psl and LPS production. Mol Microbiol. 2009;73(4):622-38.
8. Tecle T, Tripathi S, Hartshorn KL. Review: Defensins and cathelicidins in lung immunity. Innate Immun. 2010;16(3):151-9.
9. Jogi A, Rono B, Lund IK, Nielsen BS, Ploug M, Hoyer-Hansen G, et al. Neutralisation of uPA with a monoclonal antibody reduces plasmin formation and delays skin wound healing in tPA-deficient mice. PLoS One. 2010;5(9):e12746.
10. Herter JM, Rossaint J, Zarbock A. Platelets in inflammation and immunity. J Thromb Haemost. 2014;12(11):1764-75.
11. Karhausen J, Choi HW, Maddipati KR, Mathew JP, Ma Q, Boulaftali Y, et al. Platelets trigger perivascular mast cell degranulation to cause inflammatory responses and tissue injury. Sci Adv. 2020;6(12):eaay6314.
12. Leoni G, Neumann PA, Sumagin R, Denning TL, Nusrat A. Wound repair: role of immune-epithelial interactions. Mucosal Immunol. 2015;8(5):959-68.
13. Smigiel KS, Parks WC. Matrix Metalloproteinases and Leukocyte Activation. Prog Mol Biol Transl Sci. 2017;147:167-95.
14. Penn JW, Grobbelaar AO, Rolfe KJ. The role of the TGF-beta family in wound healing, burns and scarring: a review. Int J Burns Trauma. 2012;2(1):18-28.
15. Hong WX, Hu MS, Esquivel M, Liang GY, Rennert RC, McArdle A, et al. The Role of Hypoxia-Inducible Factor in Wound Healing. Adv Wound Care (New Rochelle). 2014;3(5):390-9.
16. Schultz GS, Chin GA, Moldawer L, Diegelmann RF. Principles of Wound Healing. In: Fitridge R, Thompson M, editors. Mechanisms of Vascular Disease: A Reference Book for Vascular Specialists. Adelaide (AU)2011.
17. Schumacher C, Clark-Lewis I, Baggiolini M, Moser B. High- and low-affinity binding of GRO alpha and neutrophil-activating peptide 2 to interleukin 8 receptors on human neutrophils. Proc Natl Acad Sci U S A. 1992;89(21):10542-6.
18. Deshmane SL, Kremlev S, Amini S, Sawaya BE. Monocyte chemoattractant protein-1 (MCP-1): an overview. J Interferon Cytokine Res. 2009;29(6):313-26.
19. Zhang JM, An J. Cytokines, inflammation, and pain. Int Anesthesiol Clin. 2007;45(2):27-37.
20. Yu P, Zhang X, Liu N, Tang L, Peng C, Chen X. Pyroptosis: mechanisms and diseases. Signal Transduct Target Ther. 2021;6(1):128.
21. Tie R, Li H, Cai S, Liang Z, Shan W, Wang B, et al. Interleukin-6 signaling regulates hematopoietic stem cell emergence. Exp Mol Med. 2019;51(10):1-12.

22. Parameswaran N, Patial S. Tumor necrosis factor-alpha signaling in macrophages. Crit Rev Eukaryot Gene Expr. 2010;20(2):87-103.
23. Lubbers R, van Essen MF, van Kooten C, Trouw LA. Production of complement components by cells of the immune system. Clin Exp Immunol. 2017;188(2):183-94.
24. Murphy KM, Weaver C, Mowat A, Berg L, Chaplin D, Janeway CA, et al. Janeway's immunobiology2017.
25. Reid KBM. Complement Component C1q: Historical Perspective of a Functionally Versatile, and Structurally Unusual, Serum Protein. Front Immunol. 2018;9:764.
26. Nauta AJ, Trouw LA, Daha MR, Tijsma O, Nieuwland R, Schwaeble WJ, et al. Direct binding of C1q to apoptotic cells and cell blebs induces complement activation. Eur J Immunol. 2002;32(6):1726-36.
27. Paidassi H, Tacnet-Delorme P, Lunardi T, Arlaud GJ, Thielens NM, Frachet P. The lectin-like activity of human C1q and its implication in DNA and apoptotic cell recognition. FEBS Lett. 2008;582(20):3111-6.
28. Paidassi H, Tacnet-Delorme P, Verneret M, Gaboriaud C, Houen G, Duus K, et al. Investigations on the C1q-calreticulin-phosphatidylserine interactions yield new insights into apoptotic cell recognition. J Mol Biol. 2011;408(2):277-90.
29. Roumenina LT, Popov KT, Bureeva SV, Kojouharova M, Gadjeva M, Rabheru S, et al. Interaction of the globular domain of human C1q with Salmonella typhimurium lipopolysaccharide. Biochim Biophys Acta. 2008;1784(9):1271-6.
30. Sjoberg AP, Trouw LA, Blom AM. Complement activation and inhibition: a delicate balance. Trends Immunol. 2009;30(2):83-90.
31. Noris M, Remuzzi G. Overview of complement activation and regulation. Semin Nephrol. 2013;33(6):479-92.
32. Rooijakkers SH, Wu J, Ruyken M, van Domselaar R, Planken KL, Tzekou A, et al. Structural and functional implications of the alternative complement pathway C3 convertase stabilized by a staphylococcal inhibitor. Nat Immunol. 2009;10(7):721-7.
33. Pangburn MK, Ferreira VP, Cortes C. Discrimination between host and pathogens by the complement system. Vaccine. 2008;26 Suppl 8:I15-21.
34. Beltrame MH, Catarino SJ, Goeldner I, Boldt AB, de Messias-Reason IJ. The lectin pathway of complement and rheumatic heart disease. Front Pediatr. 2014;2:148.
35. Ammitzboll CG, Kjaer TR, Steffensen R, Stengaard-Pedersen K, Nielsen HJ, Thiel S, et al. Non-synonymous polymorphisms in the FCN1 gene determine ligand-binding ability and serum levels of M-ficolin. PLoS One. 2012;7(11):e50585.
36. Chaplin DD. Overview of the immune response. J Allergy Clin Immunol. 2010;125(2 Suppl 2):S3-23.
37. Leoni G, Alam A, Neumann PA, Lambeth JD, Cheng G, McCoy J, et al. Annexin A1, formyl peptide receptor, and NOX1 orchestrate epithelial repair. J Clin Invest. 2013;123(1):443-54.
38. Tauzin S, Starnes TW, Becker FB, Lam PY, Huttenlocher A. Redox and Src family kinase signaling control leukocyte wound attraction and neutrophil reverse migration. J Cell Biol. 2014;207(5):589-98.
39. Krzyszczyk P, Schloss R, Palmer A, Berthiaume F. The Role of Macrophages in Acute and Chronic Wound Healing and Interventions to Promote Pro-wound Healing Phenotypes. Front Physiol. 2018;9:419.
40. Castellana D, Paus R, Perez-Moreno M. Macrophages contribute to the cyclic activation of adult hair follicle stem cells. PLoS Biol. 2014;12(12):e1002002.
41. Larson-Casey JL, Deshane JS, Ryan AJ, Thannickal VJ, Carter AB. Macrophage Akt1 Kinase-Mediated Mitophagy Modulates Apoptosis Resistance and Pulmonary Fibrosis. Immunity. 2016;44(3):582-96.
42. Desmouliere A, Redard M, Darby I, Gabbiani G. Apoptosis mediates the decrease in cellularity during the transition between granulation tissue and scar. Am J Pathol. 1995;146(1):56-66.
43. Boothby IC, Cohen JN, Rosenblum MD. Regulatory T cells in skin injury: At the crossroads of tolerance and tissue repair. Sci Immunol. 2020;5(47).
44. Strbo N, Yin N, Stojadinovic O. Innate and Adaptive Immune Responses in Wound Epithelialization. Adv Wound Care (New Rochelle). 2014;3(7):492-501.

45. Vivier E, Tomasello E, Baratin M, Walzer T, Ugolini S. Functions of natural killer cells. Nat Immunol. 2008;9(5):503-10.
46. Bonilla FA, Oettgen HC. Adaptive immunity. J Allergy Clin Immunol. 2010;125(2 Suppl 2):S33-40.
47. Mauri C, Bosma A. Immune regulatory function of B cells. Annu Rev Immunol. 2012;30:221-41.
48. Leibovich SJ, Ross R. The role of the macrophage in wound repair. A study with hydrocortisone and antimacrophage serum. Am J Pathol. 1975;78(1):71-100.
49. Yang J, Zhang L, Yu C, Yang XF, Wang H. Monocyte and macrophage differentiation: circulation inflammatory monocyte as biomarker for inflammatory diseases. Biomark Res. 2014;2(1):1.
50. Davies LC, Jenkins SJ, Allen JE, Taylor PR. Tissue-resident macrophages. Nat Immunol. 2013;14(10):986-95.
51. Lucas T, Waisman A, Ranjan R, Roes J, Krieg T, Muller W, et al. Differential roles of macrophages in diverse phases of skin repair. J Immunol. 2010;184(7):3964-77.
52. Sindrilaru A, Peters T, Wieschalka S, Baican C, Baican A, Peter H, et al. An unrestrained proinflammatory M1 macrophage population induced by iron impairs wound healing in humans and mice. J Clin Invest. 2011;121(3):985-97.
53. Orecchioni M, Ghosheh Y, Pramod AB, Ley K. Macrophage Polarization: Different Gene Signatures in M1(LPS+) vs. Classically and M2(LPS-) vs. Alternatively Activated Macrophages. Front Immunol. 2019;10:1084.
54. Shibuya M. Vascular Endothelial Growth Factor (VEGF) and Its Receptor (VEGFR) Signaling in Angiogenesis: A Crucial Target for Anti- and Pro-Angiogenic Therapies. Genes Cancer. 2011;2(12):1097-105.
55. Stanislavova R, Nalbanski B. [Comparison of results obtained from two tests to determine spermatozoid penetration of cervical mucus]. Akush Ginekol (Sofiia). 1976;15(5):359-65.
56. Das UN. Essential Fatty Acids and Their Metabolites in the Pathobiology of Inflammation and Its Resolution. Biomolecules. 2021;11(12).
57. Vijayan V, Wagener F, Immenschuh S. The macrophage heme-heme oxygenase-1 system and its role in inflammation. Biochem Pharmacol. 2018;153:159-67.
58. Weis N, Weigert A, von Knethen A, Brune B. Heme oxygenase-1 contributes to an alternative macrophage activation profile induced by apoptotic cell supernatants. Mol Biol Cell. 2009;20(5):1280-8.
59. Maceyka M, Harikumar KB, Milstien S, Spiegel S. Sphingosine-1-phosphate signaling and its role in disease. Trends Cell Biol. 2012;22(1):50-60.
60. Figueroa G, Parira T, Laverde A, Casteleiro G, El-Mabhouh A, Nair M, et al. Characterization of Human Monocyte-derived Dendritic Cells by Imaging Flow Cytometry: A Comparison between Two Monocyte Isolation Protocols. J Vis Exp. 2016(116).
61. Haniffa M, Ginhoux F, Wang XN, Bigley V, Abel M, Dimmick I, et al. Differential rates of replacement of human dermal dendritic cells and macrophages during hematopoietic stem cell transplantation. J Exp Med. 2009;206(2):371-85.
62. Platt CD, Ma JK, Chalouni C, Ebersold M, Bou-Reslan H, Carano RA, et al. Mature dendritic cells use endocytic receptors to capture and present antigens. Proc Natl Acad Sci U S A. 2010;107(9):4287-92.
63. Collin M, McGovern N, Haniffa M. Human dendritic cell subsets. Immunology. 2013;140(1):22-30.
64. Merad M, Sathe P, Helft J, Miller J, Mortha A. The dendritic cell lineage: ontogeny and function of dendritic cells and their subsets in the steady state and the inflamed setting. Annu Rev Immunol. 2013;31:563-604.
65. Harding CV, Song R. Phagocytic processing of exogenous particulate antigens by macrophages for presentation by class I MHC molecules. J Immunol. 1994;153(11):4925-33.
66. Geijtenbeek TB, Torensma R, van Vliet SJ, van Duijnhoven GC, Adema GJ, van Kooyk Y, et al. Identification of DC-SIGN, a novel dendritic cell-specific ICAM-3 receptor that supports primary immune responses. Cell. 2000;100(5):575-85.

67. Dalod M, Chelbi R, Malissen B, Lawrence T. Dendritic cell maturation: functional specialization through signaling specificity and transcriptional programming. EMBO J. 2014;33(10):1104-16.
68. Dauer M, Obermaier B, Herten J, Haerle C, Pohl K, Rothenfusser S, et al. Mature dendritic cells derived from human monocytes within 48 hours: a novel strategy for dendritic cell differentiation from blood precursors. J Immunol. 2003;170(8):4069-76.
69. Lutz MB, Strobl H, Schuler G, Romani N. GM-CSF Monocyte-Derived Cells and Langerhans Cells As Part of the Dendritic Cell Family. Front Immunol. 2017;8:1388.
70. Sichien D, Lambrecht BN, Guilliams M, Scott CL. Development of conventional dendritic cells: from common bone marrow progenitors to multiple subsets in peripheral tissues. Mucosal Immunol. 2017;10(4):831-44.
71. Cavanagh LL, Saal RJ, Grimmett KL, Thomas R. Proliferation in monocyte-derived dendritic cell cultures is caused by progenitor cells capable of myeloid differentiation. Blood. 1998;92(5):1598-607.
72. Wimmers F, Schreibelt G, Skold AE, Figdor CG, De Vries IJ. Paradigm Shift in Dendritic Cell-Based Immunotherapy: From in vitro Generated Monocyte-Derived DCs to Naturally Circulating DC Subsets. Front Immunol. 2014;5:165.
73. Whiteson K, Agrawal S, Agrawal A. Differential responses of human dendritic cells to metabolites from the oral/airway microbiome. Clin Exp Immunol. 2017;188(3):371-9.
74. Dodge IL, Carr MW, Cernadas M, Brenner MB. IL-6 production by pulmonary dendritic cells impedes Th1 immune responses. J Immunol. 2003;170(9):4457-64.
75. Nathan C. Neutrophils and immunity: challenges and opportunities. Nat Rev Immunol. 2006;6(3):173-82.
76. Guentsch A, Puklo M, Preshaw PM, Glockmann E, Pfister W, Potempa J, et al. Neutrophils in chronic and aggressive periodontitis in interaction with Porphyromonas gingivalis and Aggregatibacter actinomycetemcomitans. J Periodontal Res. 2009;44(3):368-77.
77. Dahlgren C, Karlsson A. Respiratory burst in human neutrophils. J Immunol Methods. 1999;232(1-2):3-14.
78. Delgado-Rizo V, Martinez-Guzman MA, Iniguez-Gutierrez L, Garcia-Orozco A, Alvarado-Navarro A, Fafutis-Morris M. Neutrophil Extracellular Traps and Its Implications in Inflammation: An Overview. Front Immunol. 2017;8:81.
79. Desai J, Mulay SR, Nakazawa D, Anders HJ. Matters of life and death. How neutrophils die or survive along NET release and is "NETosis" = necroptosis? Cell Mol Life Sci. 2016;73(11-12):2211-9.
80. Theilgaard-Monch K, Knudsen S, Follin P, Borregaard N. The transcriptional activation program of human neutrophils in skin lesions supports their important role in wound healing. J Immunol. 2004;172(12):7684-93.
81. Wilgus TA, Roy S, McDaniel JC. Neutrophils and Wound Repair: Positive Actions and Negative Reactions. Adv Wound Care (New Rochelle). 2013;2(7):379-88.
82. Widgerow AD. Cellular resolution of inflammation--catabasis. Wound Repair Regen. 2012;20(1):2-7.
83. Serhan CN, Chiang N, Van Dyke TE. Resolving inflammation: dual anti-inflammatory and pro-resolution lipid mediators. Nat Rev Immunol. 2008;8(5):349-61.
84. . !!! INVALID CITATION !!! {}.
85. Joffre OP, Segura E, Savina A, Amigorena S. Cross-presentation by dendritic cells. Nat Rev Immunol. 2012;12(8):557-69.
86. Pennock ND, White JT, Cross EW, Cheney EE, Tamburini BA, Kedl RM. T cell responses: naive to memory and everything in between. Adv Physiol Educ. 2013;37(4):273-83.
87. Gao Y, Williams AP. Role of Innate T Cells in Anti-Bacterial Immunity. Front Immunol. 2015;6:302.
88. Walker JA, McKenzie ANJ. TH2 cell development and function. Nat Rev Immunol. 2018;18(2):121-33.
89. Tesmer LA, Lundy SK, Sarkar S, Fox DA. Th17 cells in human disease. Immunol Rev. 2008;223:87-113.

90. Veldhoen M, Hocking RJ, Atkins CJ, Locksley RM, Stockinger B. TGFbeta in the context of an inflammatory cytokine milieu supports de novo differentiation of IL-17-producing T cells. Immunity. 2006;24(2):179-89.
91. Singh S, Barr H, Liu YC, Robins A, Heeb S, Williams P, et al. Granulocyte-macrophage colony stimulatory factor enhances the pro-inflammatory response of interferon-gamma-treated macrophages to Pseudomonas aeruginosa infection. PLoS One. 2015;10(2):e0117447.
92. Omilusik KD, Goldrath AW. The origins of memory T cells. Nature. 2017;552(7685):337-9.
93. Zhang N, Bevan MJ. CD8(+) T cells: foot soldiers of the immune system. Immunity. 2011;35(2):161-8.
94. Mogensen TH. Pathogen recognition and inflammatory signaling in innate immune defenses. Clin Microbiol Rev. 2009;22(2):240-73, Table of Contents.
95. Takeuchi O, Akira S. Pattern recognition receptors and inflammation. Cell. 2010;140(6):805-20.
96. Vilaplana L, Marco MP. Phenazines as potential biomarkers of Pseudomonas aeruginosa infections: synthesis regulation, pathogenesis and analytical methods for their detection. Anal Bioanal Chem. 2020;412(24):5897-912.
97. Wojcik-Bojek U, Rozalska B, Sadowska B. Staphylococcus aureus-A Known Opponent against Host Defense Mechanisms and Vaccine Development-Do We Still Have a Chance to Win? Int J Mol Sci. 2022;23(2).
98. Botos I, Segal DM, Davies DR. The structural biology of Toll-like receptors. Structure. 2011;19(4):447-59.
99. Kawai T, Akira S. The role of pattern-recognition receptors in innate immunity: update on Toll-like receptors. Nat Immunol. 2010;11(5):373-84.
100. Kawasaki T, Kawai T. Toll-like receptor signaling pathways. Front Immunol. 2014;5:461.
101. Mourits VP, Arts RJW, Novakovic B, Matzaraki V, de Bree LCJ, Koeken V, et al. The role of Toll-like receptor 10 in modulation of trained immunity. Immunology. 2020;159(3):289-97.
102. Male DK. Immunology : an illustrated outline. New York: Garland Science; 2014.
103. McIsaac SM, Stadnyk AW, Lin TJ. Toll-like receptors in the host defense against Pseudomonas aeruginosa respiratory infection and cystic fibrosis. J Leukoc Biol. 2012;92(5):977-85.
104. Takeuchi O, Kawai T, Muhlradt PF, Morr M, Radolf JD, Zychlinsky A, et al. Discrimination of bacterial lipoproteins by Toll-like receptor 6. Int Immunol. 2001;13(7):933-40.
105. Takeuchi O, Hoshino K, Akira S. Cutting edge: TLR2-deficient and MyD88-deficient mice are highly susceptible to Staphylococcus aureus infection. J Immunol. 2000;165(10):5392-6.
106. Travassos LH, Girardin SE, Philpott DJ, Blanot D, Nahori MA, Werts C, et al. Toll-like receptor 2-dependent bacterial sensing does not occur via peptidoglycan recognition. EMBO Rep. 2004;5(10):1000-6.
107. Hidmark A, von Saint Paul A, Dalpke AH. Cutting edge: TLR13 is a receptor for bacterial RNA. J Immunol. 2012;189(6):2717-21.
108. Li XD, Chen ZJ. Sequence specific detection of bacterial 23S ribosomal RNA by TLR13. Elife. 2012;1:e00102.
109. de Jong SD, Basha G, Wilson KD, Kazem M, Cullis P, Jefferies W, et al. The immunostimulatory activity of unmethylated and methylated CpG oligodeoxynucleotide is dependent on their ability to colocalize with TLR9 in late endosomes. J Immunol. 2010;184(11):6092-102.
110. Mathur R, Oh H, Zhang D, Park SG, Seo J, Koblansky A, et al. A mouse model of Salmonella typhi infection. Cell. 2012;151(3):590-602.
111. El-Zayat SR, Sibaii H, Mannaa FA. Toll-like receptors activation, signaling, and targeting: an overview. Bulletin of the National Research Centre. 2019;43(1):187.
112. Guo H, Callaway JB, Ting JP. Inflammasomes: mechanism of action, role in disease, and therapeutics. Nat Med. 2015;21(7):677-87.

113. Lamkanfi M, Dixit VM. Inflammasomes and their roles in health and disease. Annu Rev Cell Dev Biol. 2012;28:137-61.
114. Strowig T, Henao-Mejia J, Elinav E, Flavell R. Inflammasomes in health and disease. Nature. 2012;481(7381):278-86.
115. Bergsbaken T, Fink SL, Cookson BT. Pyroptosis: host cell death and inflammation. Nat Rev Microbiol. 2009;7(2):99-109.
116. Yang X, Chang HY, Baltimore D. Autoproteolytic activation of pro-caspases by oligomerization. Mol Cell. 1998;1(2):319-25.
117. Gu Y, Kuida K, Tsutsui H, Ku G, Hsiao K, Fleming MA, et al. Activation of interferon-gamma inducing factor mediated by interleukin-1beta converting enzyme. Science. 1997;275(5297):206-9.
118. Sutterwala FS, Haasken S, Cassel SL. Mechanism of NLRP3 inflammasome activation. Ann N Y Acad Sci. 2014;1319:82-95.
119. Vanaja SK, Rathinam VA, Fitzgerald KA. Mechanisms of inflammasome activation: recent advances and novel insights. Trends Cell Biol. 2015;25(5):308-15.
120. Vance RE. The NAIP/NLRC4 inflammasomes. Curr Opin Immunol. 2015;32:84-9.
121. Tenthorey JL, Kofoed EM, Daugherty MD, Malik HS, Vance RE. Molecular basis for specific recognition of bacterial ligands by NAIP/NLRC4 inflammasomes. Mol Cell. 2014;54(1):17-29.
122. Kroken AR, Chen CK, Evans DJ, Yahr TL, Fleiszig SMJ. The Impact of ExoS on Pseudomonas aeruginosa Internalization by Epithelial Cells Is Independent of fleQ and Correlates with Bistability of Type Three Secretion System Gene Expression. mBio. 2018;9(3).
123. Bouillot S, Pont S, Gallet B, Moriscot C, Deruelle V, Attree I, et al. Inflammasome activation by Pseudomonas aeruginosa's ExlA pore-forming toxin is detrimental for the host. Cell Microbiol. 2020;22(11):e13251.
124. Jin T, Perry A, Jiang J, Smith P, Curry JA, Unterholzner L, et al. Structures of the HIN domain:DNA complexes reveal ligand binding and activation mechanisms of the AIM2 inflammasome and IFI16 receptor. Immunity. 2012;36(4):561-71.
125. Brown GD, Willment JA, Whitehead L. C-type lectins in immunity and homeostasis. Nat Rev Immunol. 2018;18(6):374-89.
126. van Kooyk Y, Rabinovich GA. Protein-glycan interactions in the control of innate and adaptive immune responses. Nat Immunol. 2008;9(6):593-601.
127. Martinez-Pomares L. The mannose receptor. J Leukoc Biol. 2012;92(6):1177-86.
128. Leteux C, Chai W, Loveless RW, Yuen CT, Uhlin-Hansen L, Combarnous Y, et al. The cysteine-rich domain of the macrophage mannose receptor is a multispecific lectin that recognizes chondroitin sulfates A and B and sulfated oligosaccharides of blood group Lewis(a) and Lewis(x) types in addition to the sulfated N-glycans of lutropin. J Exp Med. 2000;191(7):1117-26.
129. Taylor ME, Bezouska K, Drickamer K. Contribution to ligand binding by multiple carbohydrate-recognition domains in the macrophage mannose receptor. J Biol Chem. 1992;267(3):1719-26.
130. Schweizer A, Stahl PD, Rohrer J. A di-aromatic motif in the cytosolic tail of the mannose receptor mediates endosomal sorting. J Biol Chem. 2000;275(38):29694-700.
131. Gazi U, Martinez-Pomares L. Influence of the mannose receptor in host immune responses. Immunobiology. 2009;214(7):554-61.
132. Rajaram MVS, Arnett E, Azad AK, Guirado E, Ni B, Gerberick AD, et al. M. tuberculosis-Initiated Human Mannose Receptor Signaling Regulates Macrophage Recognition and Vesicle Trafficking by FcRgamma-Chain, Grb2, and SHP-1. Cell Rep. 2017;21(1):126-40.
133. Yamasaki S, Ishikawa E, Sakuma M, Hara H, Ogata K, Saito T. Mincle is an ITAM-coupled activating receptor that senses damaged cells. Nat Immunol. 2008;9(10):1179-88.
134. Miyake Y, Toyonaga K, Mori D, Kakuta S, Hoshino Y, Oyamada A, et al. C-type lectin MCL is an FcRgamma-coupled receptor that mediates the adjuvanticity of mycobacterial cord factor. Immunity. 2013;38(5):1050-62.

135. Squadrito ML, Pucci F, Magri L, Moi D, Gilfillan GD, Ranghetti A, et al. miR-511-3p modulates genetic programs of tumor-associated macrophages. Cell Rep. 2012;1(2):141-54.
136. Taylor PR, Gordon S, Martinez-Pomares L. The mannose receptor: linking homeostasis and immunity through sugar recognition. Trends Immunol. 2005;26(2):104-10.
137. Allavena P, Chieppa M, Bianchi G, Solinas G, Fabbri M, Laskarin G, et al. Engagement of the mannose receptor by tumoral mucins activates an immune suppressive phenotype in human tumor-associated macrophages. Clin Dev Immunol. 2010;2010:547179.
138. McKenzie EJ, Taylor PR, Stillion RJ, Lucas AD, Harris J, Gordon S, et al. Mannose receptor expression and function define a new population of murine dendritic cells. J Immunol. 2007;178(8):4975-83.
139. Akilov OE, Khachemoune A, Hasan T. Clinical manifestations and classification of Old World cutaneous leishmaniasis. Int J Dermatol. 2007;46(2):132-42.
140. Lee SJ, Zheng NY, Clavijo M, Nussenzweig MC. Normal host defense during systemic candidiasis in mannose receptor-deficient mice. Infect Immun. 2003;71(1):437-45.
141. Polando RE, Jones BC, Ricardo C, Whitcomb J, Ballhorn W, McDowell MA. Mannose receptor (MR) and Toll-like receptor 2 (TLR2) influence phagosome maturation during Leishmania infection. Parasite Immunol. 2018;40(4):e12521.
142. Loures FV, Araujo EF, Feriotti C, Bazan SB, Calich VL. TLR-4 cooperates with Dectin-1 and mannose receptor to expand Th17 and Tc17 cells induced by Paracoccidioides brasiliensis stimulated dendritic cells. Front Microbiol. 2015;6:261.
143. Brown GD. Dectin-1: a signalling non-TLR pattern-recognition receptor. Nat Rev Immunol. 2006;6(1):33-43.
144. Tone K, Stappers MHT, Willment JA, Brown GD. C-type lectin receptors of the Dectin-1 cluster: Physiological roles and involvement in disease. Eur J Immunol. 2019;49(12):2127-33.
145. Geijtenbeek TB, Gringhuis SI. Signalling through C-type lectin receptors: shaping immune responses. Nat Rev Immunol. 2009;9(7):465-79.
146. Dostert C, Tschopp J. DEteCTINg fungal pathogens. Nat Immunol. 2007;8(1):17-8.
147. Taylor PR, Tsoni SV, Willment JA, Dennehy KM, Rosas M, Findon H, et al. Dectin-1 is required for beta-glucan recognition and control of fungal infection. Nat Immunol. 2007;8(1):31-8.
148. Carvalho A, Giovannini G, De Luca A, D'Angelo C, Casagrande A, Iannitti RG, et al. Dectin-1 isoforms contribute to distinct Th1/Th17 cell activation in mucosal candidiasis. Cell Mol Immunol. 2012;9(3):276-86.
149. Ferwerda B, Ferwerda G, Plantinga TS, Willment JA, van Spriel AB, Venselaar H, et al. Human dectin-1 deficiency and mucocutaneous fungal infections. N Engl J Med. 2009;361(18):1760-7.
150. Goodridge HS, Underhill DM. Fungal Recognition by TLR2 and Dectin-1. Handb Exp Pharmacol. 2008(183):87-109.
151. Feinberg H, Jegouzo SAF, Rex MJ, Drickamer K, Weis WI, Taylor ME. Mechanism of pathogen recognition by human dectin-2. J Biol Chem. 2017;292(32):13402-14.
152. Robinson MJ, Osorio F, Rosas M, Freitas RP, Schweighoffer E, Gross O, et al. Dectin-2 is a Syk-coupled pattern recognition receptor crucial for Th17 responses to fungal infection. J Exp Med. 2009;206(9):2037-51.
153. McDonald JU, Rosas M, Brown GD, Jones SA, Taylor PR. Differential dependencies of monocytes and neutrophils on dectin-1, dectin-2 and complement for the recognition of fungal particles in inflammation. PLoS One. 2012;7(9):e45781.
154. Seeds RE, Gordon S, Miller JL. Characterisation of myeloid receptor expression and interferon alpha/beta production in murine plasmacytoid dendritic cells by flow cytomtery. J Immunol Methods. 2009;350(1-2):106-17.

155. Taylor PR, Reid DM, Heinsbroek SE, Brown GD, Gordon S, Wong SY. Dectin-2 is predominantly myeloid restricted and exhibits unique activation-dependent expression on maturing inflammatory monocytes elicited in vivo. Eur J Immunol. 2005;35(7):2163-74.
156. Miura T, Kawakami K, Kanno E, Tanno H, Tada H, Sato N, et al. Dectin-2-Mediated Signaling Leads to Delayed Skin Wound Healing through Enhanced Neutrophilic Inflammatory Response and Neutrophil Extracellular Trap Formation. J Invest Dermatol. 2019;139(3):702-11.
157. Sato K, Yang XL, Yudate T, Chung JS, Wu J, Luby-Phelps K, et al. Dectin-2 is a pattern recognition receptor for fungi that couples with the Fc receptor gamma chain to induce innate immune responses. J Biol Chem. 2006;281(50):38854-66.
158. Ritter M, Gross O, Kays S, Ruland J, Nimmerjahn F, Saijo S, et al. Schistosoma mansoni triggers Dectin-2, which activates the Nlrp3 inflammasome and alters adaptive immune responses. Proc Natl Acad Sci U S A. 2010;107(47):20459-64.
159. Saijo S, Ikeda S, Yamabe K, Kakuta S, Ishigame H, Akitsu A, et al. Dectin-2 recognition of alpha-mannans and induction of Th17 cell differentiation is essential for host defense against Candida albicans. Immunity. 2010;32(5):681-91.
160. Svajger U, Anderluh M, Jeras M, Obermajer N. C-type lectin DC-SIGN: an adhesion, signalling and antigen-uptake molecule that guides dendritic cells in immunity. Cell Signal. 2010;22(10):1397-405.
161. Drickamer K, Taylor ME. Recent insights into structures and functions of C-type lectins in the immune system. Curr Opin Struct Biol. 2015;34:26-34.
162. Geijtenbeek TB, Kwon DS, Torensma R, van Vliet SJ, van Duijnhoven GC, Middel J, et al. DC-SIGN, a dendritic cell-specific HIV-1-binding protein that enhances trans-infection of T cells. Cell. 2000;100(5):587-97.
163. Appelmelk BJ, van Die I, van Vliet SJ, Vandenbroucke-Grauls CM, Geijtenbeek TB, van Kooyk Y. Cutting edge: carbohydrate profiling identifies new pathogens that interact with dendritic cell-specific ICAM-3-grabbing nonintegrin on dendritic cells. J Immunol. 2003;170(4):1635-9.
164. Nigou J, Zelle-Rieser C, Gilleron M, Thurnher M, Puzo G. Mannosylated lipoarabinomannans inhibit IL-12 production by human dendritic cells: evidence for a negative signal delivered through the mannose receptor. J Immunol. 2001;166(12):7477-85.
165. van Vliet SJ, Garcia-Vallejo JJ, van Kooyk Y. Dendritic cells and C-type lectin receptors: coupling innate to adaptive immune responses. Immunol Cell Biol. 2008;86(7):580-7.
166. Geijtenbeek TB, Krooshoop DJ, Bleijs DA, van Vliet SJ, van Duijnhoven GC, Grabovsky V, et al. DC-SIGN-ICAM-2 interaction mediates dendritic cell trafficking. Nat Immunol. 2000;1(4):353-7.
167. Chen JT, Chen CH, Ku KL, Hsiao M, Chiang CP, Hsu TL, et al. Glycoprotein B7-H3 overexpression and aberrant glycosylation in oral cancer and immune response. Proc Natl Acad Sci U S A. 2015;112(42):13057-62.
168. Haque M, Sartelli M, McKimm J, Abu Bakar M. Health care-associated infections - an overview. Infect Drug Resist. 2018;11:2321-33.
169. Sydnor ER, Perl TM. Hospital epidemiology and infection control in acute-care settings. Clin Microbiol Rev. 2011;24(1):141-73.
170. Habboush Y, Yarrarapu SNS, Guzman N. Infection Control. StatPearls. Treasure Island (FL)2022.
171. Boev C, Kiss E. Hospital-Acquired Infections: Current Trends and Prevention. Crit Care Nurs Clin North Am. 2017;29(1):51-65.
172. Kung HC, Hoyert DL, Xu J, Murphy SL. Deaths: final data for 2005. Natl Vital Stat Rep. 2008;56(10):1-120.
173. Vincent JL. Nosocomial infections in adult intensive-care units. Lancet. 2003;361(9374):2068-77.
174. Loveday HP, Wilson JA, Pratt RJ, Golsorkhi M, Tingle A, Bak A, et al. epic3: national evidence-based guidelines for preventing healthcare-associated infections in NHS hospitals in England. J Hosp Infect. 2014;86 Suppl 1:S1-70.

175. Weiner-Lastinger LM, Pattabiraman V, Konnor RY, Patel PR, Wong E, Xu SY, et al. The impact of coronavirus disease 2019 (COVID-19) on healthcare-associated infections in 2020: A summary of data reported to the National Healthcare Safety Network. Infect Control Hosp Epidemiol. 2022;43(1):12-25.
176. Magill SS, O'Leary E, Janelle SJ, Thompson DL, Dumyati G, Nadle J, et al. Changes in Prevalence of Health Care-Associated Infections in U.S. Hospitals. N Engl J Med. 2018;379(18):1732-44.
177. Boucher HW, Talbot GH, Bradley JS, Edwards JE, Gilbert D, Rice LB, et al. Bad bugs, no drugs: no ESKAPE! An update from the Infectious Diseases Society of America. Clin Infect Dis. 2009;48(1):1-12.
178. Ventola CL. The antibiotic resistance crisis: part 1: causes and threats. P T. 2015;40(4):277-83.
179. Martin MJ, Thottathil SE, Newman TB. Antibiotics Overuse in Animal Agriculture: A Call to Action for Health Care Providers. Am J Public Health. 2015;105(12):2409-10.
180. Prestinaci F, Pezzotti P, Pantosti A. Antimicrobial resistance: a global multifaceted phenomenon. Pathog Glob Health. 2015;109(7):309-18.
181. Pendleton JN, Gorman SP, Gilmore BF. Clinical relevance of the ESKAPE pathogens. Expert Rev Anti Infect Ther. 2013;11(3):297-308.
182. Mulani MS, Kamble EE, Kumkar SN, Tawre MS, Pardesi KR. Emerging Strategies to Combat ESKAPE Pathogens in the Era of Antimicrobial Resistance: A Review. Front Microbiol. 2019;10:539.
183. Lyczak JB, Cannon CL, Pier GB. Establishment of Pseudomonas aeruginosa infection: lessons from a versatile opportunist. Microbes Infect. 2000;2(9):1051-60.
184. Thuong M, Arvaniti K, Ruimy R, de la Salmoniere P, Scanvic-Hameg A, Lucet JC, et al. Epidemiology of Pseudomonas aeruginosa and risk factors for carriage acquisition in an intensive care unit. J Hosp Infect. 2003;53(4):274-82.
185. Hauser AR. Pseudomonas aeruginosa: so many virulence factors, so little time. Crit Care Med. 2011;39(9):2193-4.
186. Huszczynski SM, Lam JS, Khursigara CM. The Role of Pseudomonas aeruginosa Lipopolysaccharide in Bacterial Pathogenesis and Physiology. Pathogens. 2019;9(1).
187. Henderson JC, Zimmerman SM, Crofts AA, Boll JM, Kuhns LG, Herrera CM, et al. The Power of Asymmetry: Architecture and Assembly of the Gram-Negative Outer Membrane Lipid Bilayer. Annu Rev Microbiol. 2016;70:255-78.
188. Pier GB. Pseudomonas aeruginosa lipopolysaccharide: a major virulence factor, initiator of inflammation and target for effective immunity. Int J Med Microbiol. 2007;297(5):277-95.
189. Korneev KV, Arbatsky NP, Molinaro A, Palmigiano A, Shaikhutdinova RZ, Shneider MM, et al. Structural Relationship of the Lipid A Acyl Groups to Activation of Murine Toll-Like Receptor 4 by Lipopolysaccharides from Pathogenic Strains of Burkholderia mallei, Acinetobacter baumannii, and Pseudomonas aeruginosa. Front Immunol. 2015;6:595.
190. Lam JS, Taylor VL, Islam ST, Hao Y, Kocincova D. Genetic and Functional Diversity of Pseudomonas aeruginosa Lipopolysaccharide. Front Microbiol. 2011;2:118.
191. Singh S, Almuhanna Y, Alshahrani MY, Lowman DW, Rice PJ, Gell C, et al. Carbohydrates from Pseudomonas aeruginosa biofilms interact with immune C-type lectins and interfere with their receptor function. NPJ Biofilms Microbiomes. 2021;7(1):87.
192. Moskowitz SM, Ernst RK. The role of Pseudomonas lipopolysaccharide in cystic fibrosis airway infection. Subcell Biochem. 2010;53:241-53.
193. Prasad ASB, Shruptha P, Prabhu V, Srujan C, Nayak UY, Anuradha CKR, et al. Pseudomonas aeruginosa virulence proteins pseudolysin and protease IV impede cutaneous wound healing. Lab Invest. 2020;100(12):1532-50.
194. Casilag F, Lorenz A, Krueger J, Klawonn F, Weiss S, Haussler S. The LasB Elastase of Pseudomonas aeruginosa Acts in Concert with Alkaline Protease AprA To Prevent Flagellin-Mediated Immune Recognition. Infect Immun. 2016;84(1):162-71.
195. Santajit S, Kong-Ngoen T, Chongsa-Nguan M, Boonyuen U, Pumirat P, Sookrung N, et al. Human Single-Chain Antibodies That Neutralize Elastolytic Activity of Pseudomonas aeruginosa LasB. Pathogens. 2021;10(6).

196. Jing C, Liu C, Liu Y, Feng R, Cao R, Guan Z, et al. Antibodies Against Pseudomonas aeruginosa Alkaline Protease Directly Enhance Disruption of Neutrophil Extracellular Traps Mediated by This Enzyme. Front Immunol. 2021;12:654649.
197. Tang A, Caballero AR, Marquart ME, Bierdeman MA, O'Callaghan RJ. Mechanism of Pseudomonas aeruginosa Small Protease (PASP), a Corneal Virulence Factor. Invest Ophthalmol Vis Sci. 2018;59(15):5993-6002.
198. Hauser AR. The type III secretion system of Pseudomonas aeruginosa: infection by injection. Nat Rev Microbiol. 2009;7(9):654-65.
199. Lister PD, Wolter DJ, Hanson ND. Antibacterial-resistant Pseudomonas aeruginosa: clinical impact and complex regulation of chromosomally encoded resistance mechanisms. Clin Microbiol Rev. 2009;22(4):582-610.
200. Bassetti M, Vena A, Croxatto A, Righi E, Guery B. How to manage Pseudomonas aeruginosa infections. Drugs Context. 2018;7:212527.
201. Llano-Sotelo B, Azucena EF, Jr., Kotra LP, Mobashery S, Chow CS. Aminoglycosides modified by resistance enzymes display diminished binding to the bacterial ribosomal aminoacyl-tRNA site. Chem Biol. 2002;9(4):455-63.
202. Poole K. Efflux-mediated antimicrobial resistance. J Antimicrob Chemother. 2005;56(1):20-51.
203. Wertheim HF, Melles DC, Vos MC, van Leeuwen W, van Belkum A, Verbrugh HA, et al. The role of nasal carriage in Staphylococcus aureus infections. Lancet Infect Dis. 2005;5(12):751-62.
204. Tong SY, Davis JS, Eichenberger E, Holland TL, Fowler VG, Jr. Staphylococcus aureus infections: epidemiology, pathophysiology, clinical manifestations, and management. Clin Microbiol Rev. 2015;28(3):603-61.
205. Tang Y-W, Yi-Wei T. Molecular Medical Microbiology (Second Edition): Academic Press; 2015.
206. Otto M. Staphylococcus aureus toxins. Curr Opin Microbiol. 2014;17:32-7.
207. Kulhankova K, King J, Salgado-Pabon W. Staphylococcal toxic shock syndrome: superantigen-mediated enhancement of endotoxin shock and adaptive immune suppression. Immunol Res. 2014;59(1-3):182-7.
208. Stapels DA, Ramyar KX, Bischoff M, von Kockritz-Blickwede M, Milder FJ, Ruyken M, et al. Staphylococcus aureus secretes a unique class of neutrophil serine protease inhibitors. Proc Natl Acad Sci U S A. 2014;111(36):13187-92.
209. Sutton JAF, Carnell OT, Lafage L, Gray J, Biboy J, Gibson JF, et al. Staphylococcus aureus cell wall structure and dynamics during host-pathogen interaction. PLoS Pathog. 2021;17(3):e1009468.
210. Vollmer W, Blanot D, de Pedro MA. Peptidoglycan structure and architecture. FEMS Microbiol Rev. 2008;32(2):149-67.
211. Mnich ME, van Dalen R, Gerlach D, Hendriks A, Xia G, Peschel A, et al. The C-type lectin receptor MGL senses N-acetylgalactosamine on the unique Staphylococcus aureus ST395 wall teichoic acid. Cell Microbiol. 2019;21(10):e13072.
212. Enright MC, Robinson DA, Randle G, Feil EJ, Grundmann H, Spratt BG. The evolutionary history of methicillin-resistant Staphylococcus aureus (MRSA). Proc Natl Acad Sci U S A. 2002;99(11):7687-92.
213. Hiramatsu K, Cui L, Kuroda M, Ito T. The emergence and evolution of methicillin-resistant Staphylococcus aureus. Trends Microbiol. 2001;9(10):486-93.
214. Katayama Y, Ito T, Hiramatsu K. A new class of genetic element, staphylococcus cassette chromosome mec, encodes methicillin resistance in Staphylococcus aureus. Antimicrob Agents Chemother. 2000;44(6):1549-55.
215. Howden BP, Davies JK, Johnson PD, Stinear TP, Grayson ML. Reduced vancomycin susceptibility in Staphylococcus aureus, including vancomycin-intermediate and heterogeneous vancomycin-intermediate strains: resistance mechanisms, laboratory detection, and clinical implications. Clin Microbiol Rev. 2010;23(1):99-139.
216. O'Toole G, Kaplan HB, Kolter R. Biofilm formation as microbial development. Annu Rev Microbiol. 2000;54:49-79.

217. Zapotoczna M, O'Neill E, O'Gara JP. Untangling the Diverse and Redundant Mechanisms of Staphylococcus aureus Biofilm Formation. PLoS Pathog. 2016;12(7):e1005671.
218. Kostakioti M, Hadjifrangiskou M, Hultgren SJ. Bacterial biofilms: development, dispersal, and therapeutic strategies in the dawn of the postantibiotic era. Cold Spring Harb Perspect Med. 2013;3(4):a010306.
219. Flemming HC, Neu TR, Wozniak DJ. The EPS matrix: the "house of biofilm cells". J Bacteriol. 2007;189(22):7945-7.
220. Flemming HC, Wingender J. Relevance of microbial extracellular polymeric substances (EPSs)--Part I: Structural and ecological aspects. Water Sci Technol. 2001;43(6):1-8.
221. Ibanez de Aldecoa AL, Zafra O, Gonzalez-Pastor JE. Mechanisms and Regulation of Extracellular DNA Release and Its Biological Roles in Microbial Communities. Front Microbiol. 2017;8:1390.
222. Sugimoto S, Sato F, Miyakawa R, Chiba A, Onodera S, Hori S, et al. Broad impact of extracellular DNA on biofilm formation by clinically isolated Methicillin-resistant and -sensitive strains of Staphylococcus aureus. Sci Rep. 2018;8(1):2254.
223. Whitchurch CB, Tolker-Nielsen T, Ragas PC, Mattick JS. Extracellular DNA required for bacterial biofilm formation. Science. 2002;295(5559):1487.
224. Wilton M, Charron-Mazenod L, Moore R, Lewenza S. Extracellular DNA Acidifies Biofilms and Induces Aminoglycoside Resistance in Pseudomonas aeruginosa. Antimicrob Agents Chemother. 2016;60(1):544-53.
225. Lindau D, Mussard J, Rabsteyn A, Ribon M, Kotter I, Igney A, et al. TLR9 independent interferon alpha production by neutrophils on NETosis in response to circulating chromatin, a key lupus autoantigen. Ann Rheum Dis. 2014;73(12):2199-207.
226. Alim D, Sircaik S, Panwar SL. The Significance of Lipids to Biofilm Formation in Candida albicans: An Emerging Perspective. J Fungi (Basel). 2018;4(4).
227. Rella A, Farnoud AM, Del Poeta M. Plasma membrane lipids and their role in fungal virulence. Prog Lipid Res. 2016;61:63-72.
228. Lattif AA, Mukherjee PK, Chandra J, Roth MR, Welti R, Rouabhia M, et al. Lipidomics of Candida albicans biofilms reveals phase-dependent production of phospholipid molecular classes and role for lipid rafts in biofilm formation. Microbiology (Reading). 2011;157(Pt 11):3232-42.
229. Krause J, Geginat G, Tammer I. Prostaglandin E2 from Candida albicans Stimulates the Growth of Staphylococcus aureus in Mixed Biofilms. PLoS One. 2015;10(8):e0135404.
230. Harriott MM, Noverr MC. Candida albicans and Staphylococcus aureus form polymicrobial biofilms: effects on antimicrobial resistance. Antimicrob Agents Chemother. 2009;53(9):3914-22.
231. Kong KF, Vuong C, Otto M. Staphylococcus quorum sensing in biofilm formation and infection. Int J Med Microbiol. 2006;296(2-3):133-9.
232. Papenfort K, Bassler BL. Quorum sensing signal-response systems in Gram-negative bacteria. Nat Rev Microbiol. 2016;14(9):576-88.
233. LaSarre B, Federle MJ. Exploiting quorum sensing to confuse bacterial pathogens. Microbiol Mol Biol Rev. 2013;77(1):73-111.
234. Stewart PS. Mechanisms of antibiotic resistance in bacterial biofilms. Int J Med Microbiol. 2002;292(2):107-13.
235. Anderl JN, Franklin MJ, Stewart PS. Role of antibiotic penetration limitation in Klebsiella pneumoniae biofilm resistance to ampicillin and ciprofloxacin. Antimicrob Agents Chemother. 2000;44(7):1818-24.
236. Fleming D, Rumbaugh K. The Consequences of Biofilm Dispersal on the Host. Sci Rep. 2018;8(1):10738.
237. Prabhakara R, Harro JM, Leid JG, Harris M, Shirtliff ME. Murine immune response to a chronic Staphylococcus aureus biofilm infection. Infect Immun. 2011;79(4):1789-96.
238. Hickman JW, Tifrea DF, Harwood CS. A chemosensory system that regulates biofilm formation through modulation of cyclic diguanylate levels. Proc Natl Acad Sci U S A. 2005;102(40):14422-7.

239. Hentzer M, Teitzel GM, Balzer GJ, Heydorn A, Molin S, Givskov M, et al. Alginate overproduction affects Pseudomonas aeruginosa biofilm structure and function. J Bacteriol. 2001;183(18):5395-401.
240. Mathee K, Ciofu O, Sternberg C, Lindum PW, Campbell JI, Jensen P, et al. Mucoid conversion of Pseudomonas aeruginosa by hydrogen peroxide: a mechanism for virulence activation in the cystic fibrosis lung. Microbiology. 1999;145 (Pt 6):1349-57.
241. Malhotra S, Limoli DH, English AE, Parsek MR, Wozniak DJ. Mixed Communities of Mucoid and Nonmucoid Pseudomonas aeruginosa Exhibit Enhanced Resistance to Host Antimicrobials. mBio. 2018;9(2).
242. Mann EE, Wozniak DJ. Pseudomonas biofilm matrix composition and niche biology. FEMS Microbiol Rev. 2012;36(4):893-916.
243. Ma L, Jackson KD, Landry RM, Parsek MR, Wozniak DJ. Analysis of Pseudomonas aeruginosa conditional psl variants reveals roles for the psl polysaccharide in adhesion and maintaining biofilm structure postattachment. J Bacteriol. 2006;188(23):8213-21.
244. Colvin KM, Irie Y, Tart CS, Urbano R, Whitney JC, Ryder C, et al. The Pel and Psl polysaccharides provide Pseudomonas aeruginosa structural redundancy within the biofilm matrix. Environ Microbiol. 2012;14(8):1913-28.
245. Franklin MJ, Nivens DE, Weadge JT, Howell PL. Biosynthesis of the Pseudomonas aeruginosa Extracellular Polysaccharides, Alginate, Pel, and Psl. Front Microbiol. 2011;2:167.
246. Ma L, Conover M, Lu H, Parsek MR, Bayles K, Wozniak DJ. Assembly and development of the Pseudomonas aeruginosa biofilm matrix. PLoS Pathog. 2009;5(3):e1000354.
247. Chew SC, Kundukad B, Seviour T, van der Maarel JR, Yang L, Rice SA, et al. Dynamic remodeling of microbial biofilms by functionally distinct exopolysaccharides. mBio. 2014;5(4):e01536-14.
248. Fleming D, Niese B, Redman W, Vanderpool E, Gordon V, Rumbaugh KP. Contribution of Pseudomonas aeruginosa Exopolysaccharides Pel and Psl to Wound Infections. Front Cell Infect Microbiol. 2022;12:835754.
249. Mishra M, Byrd MS, Sergeant S, Azad AK, Parsek MR, McPhail L, et al. Pseudomonas aeruginosa Psl polysaccharide reduces neutrophil phagocytosis and the oxidative response by limiting complement-mediated opsonization. Cell Microbiol. 2012;14(1):95-106.
250. Tseng BS, Reichhardt C, Merrihew GE, Araujo-Hernandez SA, Harrison JJ, MacCoss MJ, et al. A Biofilm Matrix-Associated Protease Inhibitor Protects Pseudomonas aeruginosa from Proteolytic Attack. mBio. 2018;9(2).
251. Rybtke M, Jensen PO, Nielsen CH, Tolker-Nielsen T. The Extracellular Polysaccharide Matrix of Pseudomonas aeruginosa Biofilms Is a Determinant of Polymorphonuclear Leukocyte Responses. Infect Immun. 2020;89(1).
252. Moser C, Jensen PO, Thomsen K, Kolpen M, Rybtke M, Lauland AS, et al. Immune Responses to Pseudomonas aeruginosa Biofilm Infections. Front Immunol. 2021;12:625597.
253. Ray VA, Hill PJ, Stover CK, Roy S, Sen CK, Yu L, et al. Anti-Psl Targeting of Pseudomonas aeruginosa Biofilms for Neutrophil-Mediated Disruption. Sci Rep. 2017;7(1):16065.
254. Jennings LK, Storek KM, Ledvina HE, Coulon C, Marmont LS, Sadovskaya I, et al. Pel is a cationic exopolysaccharide that cross-links extracellular DNA in the Pseudomonas aeruginosa biofilm matrix. Proc Natl Acad Sci U S A. 2015;112(36):11353-8.
255. Armbruster CR, Lee CK, Parker-Gilham J, de Anda J, Xia A, Zhao K, et al. Heterogeneity in surface sensing suggests a division of labor in Pseudomonas aeruginosa populations. Elife. 2019;8.
256. Fong JNC, Yildiz FH. Biofilm Matrix Proteins. Microbiol Spectr. 2015;3(2).
257. van Schaik EJ, Giltner CL, Audette GF, Keizer DW, Bautista DL, Slupsky CM, et al. DNA binding: a novel function of Pseudomonas aeruginosa type IV pili. J Bacteriol. 2005;187(4):1455-64.
258. Borlee BR, Goldman AD, Murakami K, Samudrala R, Wozniak DJ, Parsek MR. Pseudomonas aeruginosa uses a cyclic-di-GMP-regulated adhesin to reinforce the biofilm extracellular matrix. Mol Microbiol. 2010;75(4):827-42.

259. Reichhardt C, Jacobs HM, Matwichuk M, Wong C, Wozniak DJ, Parsek MR. The Versatile Pseudomonas aeruginosa Biofilm Matrix Protein CdrA Promotes Aggregation through Different Extracellular Exopolysaccharide Interactions. J Bacteriol. 2020;202(19).
260. Reichhardt C, Wong C, Passos da Silva D, Wozniak DJ, Parsek MR. CdrA Interactions within the Pseudomonas aeruginosa Biofilm Matrix Safeguard It from Proteolysis and Promote Cellular Packing. mBio. 2018;9(5).
261. Passos da Silva D, Matwichuk ML, Townsend DO, Reichhardt C, Lamba D, Wozniak DJ, et al. The Pseudomonas aeruginosa lectin LecB binds to the exopolysaccharide Psl and stabilizes the biofilm matrix. Nat Commun. 2019;10(1):2183.
262. Passos da Silva D, Schofield MC, Parsek MR, Tseng BS. An Update on the Sociomicrobiology of Quorum Sensing in Gram-Negative Biofilm Development. Pathogens. 2017;6(4).
263. Sakuragi Y, Kolter R. Quorum-sensing regulation of the biofilm matrix genes (pel) of Pseudomonas aeruginosa. J Bacteriol. 2007;189(14):5383-6.
264. Rampioni G, Falcone M, Heeb S, Frangipani E, Fletcher MP, Dubern JF, et al. Unravelling the Genome-Wide Contributions of Specific 2-Alkyl-4-Quinolones and PqsE to Quorum Sensing in Pseudomonas aeruginosa. PLoS Pathog. 2016;12(11):e1006029.
265. Diggle SP, Winzer K, Chhabra SR, Worrall KE, Camara M, Williams P. The Pseudomonas aeruginosa quinolone signal molecule overcomes the cell density-dependency of the quorum sensing hierarchy, regulates rhl-dependent genes at the onset of stationary phase and can be produced in the absence of LasR. Mol Microbiol. 2003;50(1):29-43.
266. Skindersoe ME, Zeuthen LH, Brix S, Fink LN, Lazenby J, Whittall C, et al. Pseudomonas aeruginosa quorum-sensing signal molecules interfere with dendritic cell-induced T-cell proliferation. FEMS Immunol Med Microbiol. 2009;55(3):335-45.
267. Thurlow LR, Hanke ML, Fritz T, Angle A, Aldrich A, Williams SH, et al. Staphylococcus aureus biofilms prevent macrophage phagocytosis and attenuate inflammation in vivo. J Immunol. 2011;186(11):6585-96.
268. Ji G, Beavis RC, Novick RP. Cell density control of staphylococcal virulence mediated by an octapeptide pheromone. Proc Natl Acad Sci U S A. 1995;92(26):12055-9.
269. Boisset S, Geissmann T, Huntzinger E, Fechter P, Bendridi N, Possedko M, et al. Staphylococcus aureus RNAIII coordinately represses the synthesis of virulence factors and the transcription regulator Rot by an antisense mechanism. Genes Dev. 2007;21(11):1353-66.
270. Vuong C, Saenz HL, Gotz F, Otto M. Impact of the agr quorum-sensing system on adherence to polystyrene in Staphylococcus aureus. J Infect Dis. 2000;182(6):1688-93.
271. Yarwood JM, Bartels DJ, Volper EM, Greenberg EP. Quorum sensing in Staphylococcus aureus biofilms. J Bacteriol. 2004;186(6):1838-50.
272. Le KY, Otto M. Quorum-sensing regulation in staphylococci-an overview. Front Microbiol. 2015;6:1174.
273. O'Gara JP. ica and beyond: biofilm mechanisms and regulation in Staphylococcus epidermidis and Staphylococcus aureus. FEMS Microbiol Lett. 2007;270(2):179-88.
274. Cramton SE, Gerke C, Schnell NF, Nichols WW, Gotz F. The intercellular adhesion (ica) locus is present in Staphylococcus aureus and is required for biofilm formation. Infect Immun. 1999;67(10):5427-33.
275. Lister JL, Horswill AR. Staphylococcus aureus biofilms: recent developments in biofilm dispersal. Front Cell Infect Microbiol. 2014;4:178.
276. Fluckiger U, Ulrich M, Steinhuber A, Doring G, Mack D, Landmann R, et al. Biofilm formation, icaADBC transcription, and polysaccharide intercellular adhesin synthesis by staphylococci in a device-related infection model. Infect Immun. 2005;73(3):1811-9.
277. Begun J, Gaiani JM, Rohde H, Mack D, Calderwood SB, Ausubel FM, et al. Staphylococcal biofilm exopolysaccharide protects against Caenorhabditis elegans immune defenses. PLoS Pathog. 2007;3(4):e57.
278. Francois P, Tu Quoc PH, Bisognano C, Kelley WL, Lew DP, Schrenzel J, et al. Lack of biofilm contribution to bacterial colonisation in an experimental model of foreign body infection by Staphylococcus aureus and Staphylococcus epidermidis. FEMS Immunol Med Microbiol. 2003;35(2):135-40.

279. Chokr A, Leterme D, Watier D, Jabbouri S. Neither the presence of ica locus, nor in vitro-biofilm formation ability is a crucial parameter for some Staphylococcus epidermidis strains to maintain an infection in a guinea pig tissue cage model. Microb Pathog. 2007;42(2-3):94-7.
280. Nguyen HTT, Nguyen TH, Otto M. The staphylococcal exopolysaccharide PIA - Biosynthesis and role in biofilm formation, colonization, and infection. Comput Struct Biotechnol J. 2020;18:3324-34.
281. Lund LD, Ingmer H, Frokiaer H. D-Alanylation of Teichoic Acids and Loss of Poly-N-Acetyl Glucosamine in Staphylococcus aureus during Exponential Growth Phase Enhance IL-12 Production in Murine Dendritic Cells. PLoS One. 2016;11(2):e0149092.
282. Kropec A, Maira-Litran T, Jefferson KK, Grout M, Cramton SE, Gotz F, et al. Poly-N-acetylglucosamine production in Staphylococcus aureus is essential for virulence in murine models of systemic infection. Infect Immun. 2005;73(10):6868-76.
283. Al-Ishaq R, Armstrong J, Gregory M, O'Hara M, Phiri K, Harris LG, et al. Effects of polysaccharide intercellular adhesin (PIA) in an ex vivo model of whole blood killing and in prosthetic joint infection (PJI): A role for C5a. Int J Med Microbiol. 2015;305(8):948-56.
284. Fredheim EG, Granslo HN, Flaegstad T, Figenschau Y, Rohde H, Sadovskaya I, et al. Staphylococcus epidermidis polysaccharide intercellular adhesin activates complement. FEMS Immunol Med Microbiol. 2011;63(2):269-80.
285. Stevens NT, Sadovskaya I, Jabbouri S, Sattar T, O'Gara JP, Humphreys H, et al. Staphylococcus epidermidis polysaccharide intercellular adhesin induces IL-8 expression in human astrocytes via a mechanism involving TLR2. Cell Microbiol. 2009;11(3):421-32.
286. Arciola CR, Campoccia D, Ravaioli S, Montanaro L. Polysaccharide intercellular adhesin in biofilm: structural and regulatory aspects. Front Cell Infect Microbiol. 2015;5:7.
287. Peterson PK, Verhoef J, Sabath LD, Quie PG. Effect of protein A on staphylococcal opsonization. Infect Immun. 1977;15(3):760-4.
288. Falugi F, Kim HK, Missiakas DM, Schneewind O. Role of protein A in the evasion of host adaptive immune responses by Staphylococcus aureus. MBio. 2013;4(5):e00575-13.
289. Goodyear CS, Silverman GJ. Staphylococcal toxin induced preferential and prolonged in vivo deletion of innate-like B lymphocytes. Proc Natl Acad Sci U S A. 2004;101(31):11392-7.
290. Roche FM, Meehan M, Foster TJ. The Staphylococcus aureus surface protein SasG and its homologues promote bacterial adherence to human desquamated nasal epithelial cells. Microbiology (Reading). 2003;149(Pt 10):2759-67.
291. Burke FM, Di Poto A, Speziale P, Foster TJ. The A domain of fibronectin-binding protein B of Staphylococcus aureus contains a novel fibronectin binding site. FEBS J. 2011;278(13):2359-71.
292. Peters BM, Jabra-Rizk MA, O'May GA, Costerton JW, Shirtliff ME. Polymicrobial interactions: impact on pathogenesis and human disease. Clin Microbiol Rev. 2012;25(1):193-213.
293. Kragh KN, Hutchison JB, Melaugh G, Rodesney C, Roberts AE, Irie Y, et al. Role of Multicellular Aggregates in Biofilm Formation. mBio. 2016;7(2):e00237.
294. Cai YM. Non-surface Attached Bacterial Aggregates: A Ubiquitous Third Lifestyle. Front Microbiol. 2020;11:557035.
295. El Ghalbzouri A, Hensbergen P, Gibbs S, Kempenaar J, van der Schors R, Ponec M. Fibroblasts facilitate re-epithelialization in wounded human skin equivalents. Lab Invest. 2004;84(1):102-12.
296. Werthen M, Henriksson L, Jensen PO, Sternberg C, Givskov M, Bjarnsholt T. An in vitro model of bacterial infections in wounds and other soft tissues. APMIS. 2010;118(2):156-64.
297. Yang Q, Phillips PL, Sampson EM, Progulske-Fox A, Jin S, Antonelli P, et al. Development of a novel ex vivo porcine skin explant model for the assessment of mature bacterial biofilms. Wound Repair Regen. 2013;21(5):704-14.
298. Brackman G, Garcia-Fernandez MJ, Lenoir J, De Meyer L, Remon JP, De Beer T, et al. Dressings Loaded with Cyclodextrin-Hamamelitannin Complexes Increase Staphylococcus aureus Susceptibility Toward Antibiotics Both in Single as well as in Mixed Biofilm Communities. Macromol Biosci. 2016;16(6):859-69.

299. Oates A, Lindsay S, Mistry H, Ortega F, McBain AJ. Modelling antisepsis using defined populations of facultative and anaerobic wound pathogens grown in a basally perfused biofilm model. Biofouling. 2018;34(5):507-18.
300. Muliaditan T, Caron J, Okesola M, Opzoomer JW, Kosti P, Georgouli M, et al. Macrophages are exploited from an innate wound healing response to facilitate cancer metastasis. Nat Commun. 2018;9(1):2951.
301. Yoon DJ, Fregoso DR, Nguyen D, Chen V, Strbo N, Fuentes JJ, et al. A tractable, simplified ex vivo human skin model of wound infection. Wound Repair Regen. 2019;27(4):421-5.
302. Harrington NE, Sweeney E, Harrison F. Building a better biofilm - Formation of in vivo-like biofilm structures by Pseudomonas aeruginosa in a porcine model of cystic fibrosis lung infection. Biofilm. 2020;2:100024.
303. Rogers CS, Stoltz DA, Meyerholz DK, Ostedgaard LS, Rokhlina T, Taft PJ, et al. Disruption of the CFTR gene produces a model of cystic fibrosis in newborn pigs. Science. 2008;321(5897):1837-41.
304. Bobadilla JL, Macek M, Jr., Fine JP, Farrell PM. Cystic fibrosis: a worldwide analysis of CFTR mutations--correlation with incidence data and application to screening. Hum Mutat. 2002;19(6):575-606.
305. Bonfield TL, Hodges CA, Cotton CU, Drumm ML. Absence of the cystic fibrosis transmembrane regulator (Cftr) from myeloid-derived cells slows resolution of inflammation and infection. J Leukoc Biol. 2012;92(5):1111-22.
306. Baldan R, Cigana C, Testa F, Bianconi I, De Simone M, Pellin D, et al. Adaptation of Pseudomonas aeruginosa in Cystic Fibrosis airways influences virulence of Staphylococcus aureus in vitro and murine models of co-infection. PLoS One. 2014;9(3):e89614.
307. Bjarnsholt T, Jensen PO, Fiandaca MJ, Pedersen J, Hansen CR, Andersen CB, et al. Pseudomonas aeruginosa biofilms in the respiratory tract of cystic fibrosis patients. Pediatr Pulmonol. 2009;44(6):547-58.
308. Lau GW, Hassett DJ, Ran H, Kong F. The role of pyocyanin in Pseudomonas aeruginosa infection. Trends Mol Med. 2004;10(12):599-606.
309. Kharami A, Bibi Z, Nielsen H, Hoiby N, Doring G. Effect of Pseudomonas aeruginosa rhamnolipid on human neutrophil and monocyte function. APMIS. 1989;97(12):1068-72.
310. Jensen PO, Givskov M, Bjarnsholt T, Moser C. The immune system vs. Pseudomonas aeruginosa biofilms. FEMS Immunol Med Microbiol. 2010;59(3):292-305.
311. Kolpen M, Hansen CR, Bjarnsholt T, Moser C, Christensen LD, van Gennip M, et al. Polymorphonuclear leucocytes consume oxygen in sputum from chronic Pseudomonas aeruginosa pneumonia in cystic fibrosis. Thorax. 2010;65(1):57-62.
312. Moser C, Kjaergaard S, Pressler T, Kharazmi A, Koch C, Hoiby N. The immune response to chronic Pseudomonas aeruginosa lung infection in cystic fibrosis patients is predominantly of the Th2 type. APMIS. 2000;108(5):329-35.
313. Decraene A, Willems-Widyastuti A, Kasran A, De Boeck K, Bullens DM, Dupont LJ. Elevated expression of both mRNA and protein levels of IL-17A in sputum of stable Cystic Fibrosis patients. Respir Res. 2010;11:177.
314. Kushwah R, Gagnon S, Sweezey NB. Intrinsic predisposition of naive cystic fibrosis T cells to differentiate towards a Th17 phenotype. Respir Res. 2013;14:138.
315. Tiringer K, Treis A, Fucik P, Gona M, Gruber S, Renner S, et al. A Th17- and Th2-skewed cytokine profile in cystic fibrosis lungs represents a potential risk factor for Pseudomonas aeruginosa infection. Am J Respir Crit Care Med. 2013;187(6):621-9.
316. Percival SL, Hill KE, Williams DW, Hooper SJ, Thomas DW, Costerton JW. A review of the scientific evidence for biofilms in wounds. Wound Repair Regen. 2012;20(5):647-57.
317. Rumbaugh KP, Griswold JA, Iglewski BH, Hamood AN. Contribution of quorum sensing to the virulence of Pseudomonas aeruginosa in burn wound infections. Infect Immun. 1999;67(11):5854-62.
318. Gonzalez MR, Fleuchot B, Lauciello L, Jafari P, Applegate LA, Raffoul W, et al. Effect of Human Burn Wound Exudate on Pseudomonas aeruginosa Virulence. mSphere. 2016;1(2).

319. Radlinski L, Rowe SE, Kartchner LB, Maile R, Cairns BA, Vitko NP, et al. Pseudomonas aeruginosa exoproducts determine antibiotic efficacy against Staphylococcus aureus. PLoS Biol. 2017;15(11):e2003981.
320. Woods PW, Haynes ZM, Mina EG, Marques CNH. Maintenance of S. aureus in Co-culture With P. aeruginosa While Growing as Biofilms. Front Microbiol. 2018;9:3291.
321. Sun H, Saeedi P, Karuranga S, Pinkepank M, Ogurtsova K, Duncan BB, et al. IDF Diabetes Atlas: Global, regional and country-level diabetes prevalence estimates for 2021 and projections for 2045. Diabetes Res Clin Pract. 2022;183:109119.
322. Chiang JL, Kirkman MS, Laffel LM, Peters AL, Type 1 Diabetes Sourcebook A. Type 1 diabetes through the life span: a position statement of the American Diabetes Association. Diabetes Care. 2014;37(7):2034-54.
323. Alberti KG, Zimmet PZ. Definition, diagnosis and classification of diabetes mellitus and its complications. Part 1: diagnosis and classification of diabetes mellitus provisional report of a WHO consultation. Diabet Med. 1998;15(7):539-53.
324. Kitabchi AE, Umpierrez GE, Miles JM, Fisher JN. Hyperglycemic crises in adult patients with diabetes. Diabetes Care. 2009;32(7):1335-43.
325. Lotfy M, Adeghate J, Kalasz H, Singh J, Adeghate E. Chronic Complications of Diabetes Mellitus: A Mini Review. Curr Diabetes Rev. 2017;13(1):3-10.
326. Greenhalgh DG. Wound healing and diabetes mellitus. Clin Plast Surg. 2003;30(1):37-45.
327. Leaper D, Assadian O, Edmiston CE. Approach to chronic wound infections. Br J Dermatol. 2015;173(2):351-8.
328. Alhede M, Er O, Eickhardt S, Kragh K, Alhede M, Christensen LD, et al. Bacterial biofilm formation and treatment in soft tissue fillers. Pathog Dis. 2014;70(3):339-46.
329. Gjodsbol K, Christensen JJ, Karlsmark T, Jorgensen B, Klein BM, Krogfelt KA. Multiple bacterial species reside in chronic wounds: a longitudinal study. Int Wound J. 2006;3(3):225-31.
330. Fazli M, Bjarnsholt T, Kirketerp-Moller K, Jorgensen B, Andersen AS, Krogfelt KA, et al. Nonrandom distribution of Pseudomonas aeruginosa and Staphylococcus aureus in chronic wounds. J Clin Microbiol. 2009;47(12):4084-9.
331. Kirketerp-Moller K, Jensen PO, Fazli M, Madsen KG, Pedersen J, Moser C, et al. Distribution, organization, and ecology of bacteria in chronic wounds. J Clin Microbiol. 2008;46(8):2717-22.
332. Morgan SJ, Lippman SI, Bautista GE, Harrison JJ, Harding CL, Gallagher LA, et al. Bacterial fitness in chronic wounds appears to be mediated by the capacity for high-density growth, not virulence or biofilm functions. PLoS Pathog. 2019;15(3):e1007511.
333. Liu T, Zhang L, Joo D, Sun SC. NF-kappaB signaling in inflammation. Signal Transduct Target Ther. 2017;2.
334. S. Singh YA, M. Y. Alshahrani, D. Lowman, P. J. Rice, C. Gell, Z. Ma, B. Graves, D. Jackson, K. Lee, R. Kelkar, J. Koranteng, S. Muntaka, D. Mitchell, A. C. da Silva, F. Hussain, G. Yilmaz, F. Mastrotto, Y. Irie, P. Williams, D. Williams, M. Camara, and Luisa Martinez-Pomares. Pseudomonas aeruginosa biofilms display carbohydrate ligands for CD206 and CD209 that interfere with their receptor function. bioRxiv, 2020.04.20.051292 (Published). 2020.
335. Zhu LL, Zhao XQ, Jiang C, You Y, Chen XP, Jiang YY, et al. C-type lectin receptors Dectin-3 and Dectin-2 form a heterodimeric pattern-recognition receptor for host defense against fungal infection. Immunity. 2013;39(2):324-34.
336. Menon S, Rosenberg K, Graham SA, Ward EM, Taylor ME, Drickamer K, et al. Binding-site geometry and flexibility in DC-SIGN demonstrated with surface force measurements. Proc Natl Acad Sci U S A. 2009;106(28):11524-9.
337. Ezekowitz RA, Sastry K, Bailly P, Warner A. Molecular characterization of the human macrophage mannose receptor: demonstration of multiple carbohydrate recognition-like domains and phagocytosis of yeasts in Cos-1 cells. J Exp Med. 1990;172(6):1785-94.
338. Heinsbroek SE, Squadrito ML, Schilderink R, Hilbers FW, Verseijden C, Hofmann M, et al. miR-511-3p, embedded in the macrophage mannose receptor gene, contributes to intestinal inflammation. Mucosal Immunol. 2016;9(4):960-73.

339. Andrejko M, Zdybicka-Barabas A, Janczarek M, Cytrynska M. Three Pseudomonas aeruginosa strains with different protease profiles. Acta Biochim Pol. 2013;60(1):83-90.
340. Mun JJ, Tam C, Kowbel D, Hawgood S, Barnett MJ, Evans DJ, et al. Clearance of Pseudomonas aeruginosa from a healthy ocular surface involves surfactant protein D and is compromised by bacterial elastase in a murine null-infection model. Infect Immun. 2009;77(6):2392-8.
341. Kuang Z, Hao Y, Walling BE, Jeffries JL, Ohman DE, Lau GW. Pseudomonas aeruginosa elastase provides an escape from phagocytosis by degrading the pulmonary surfactant protein-A. PLoS One. 2011;6(11):e27091.
342. Wilder CN, Diggle SP, Schuster M. Cooperation and cheating in Pseudomonas aeruginosa: the roles of the las, rhl and pqs quorum-sensing systems. ISME J. 2011;5(8):1332-43.
343. Holloway BW, Krishnapillai V, Morgan AF. Chromosomal genetics of Pseudomonas. Microbiol Rev. 1979;43(1):73-102.
344. Irie Y, Starkey M, Edwards AN, Wozniak DJ, Romeo T, Parsek MR. Pseudomonas aeruginosa biofilm matrix polysaccharide Psl is regulated transcriptionally by RpoS and post-transcriptionally by RsmA. Mol Microbiol. 2010;78(1):158-72.
345. O'Neill AJ. Staphylococcus aureus SH1000 and 8325-4: comparative genome sequences of key laboratory strains in staphylococcal research. Lett Appl Microbiol. 2010;51(3):358-61.
346. Hall RA, Gow NA. Mannosylation in Candida albicans: role in cell wall function and immune recognition. Mol Microbiol. 2013;90(6):1147-61.
347. Valverde P, Delgado S, Martinez JD, Vendeville JB, Malassis J, Linclau B, et al. Molecular Insights into DC-SIGN Binding to Self-Antigens: The Interaction with the Blood Group A/B Antigens. ACS Chem Biol. 2019;14(7):1660-71.
348. Archer NK, Mazaitis MJ, Costerton JW, Leid JG, Powers ME, Shirtliff ME. Staphylococcus aureus biofilms: properties, regulation, and roles in human disease. Virulence. 2011;2(5):445-59.
349. Jarlov JO, Hansen JE, Rosdahl VT, Espersen F. The typing of Staphylococcus epidermidis by a lectin-binding assay. J Med Microbiol. 1992;37(3):195-200.
350. Jarlov JO, Rosdahl VT, Yeo M, Marples RR. Lectin typing of methicillin-resistant Staphylococcus aureus from Singapore, England and Wales, and Denmark. J Med Microbiol. 1993;39(4):305-9.
351. Bales PM, Renke EM, May SL, Shen Y, Nelson DC. Purification and Characterization of Biofilm-Associated EPS Exopolysaccharides from ESKAPE Organisms and Other Pathogens. PLoS One. 2013;8(6):e67950.
352. Chai Y, Beauregard PB, Vlamakis H, Losick R, Kolter R. Galactose metabolism plays a crucial role in biofilm formation by Bacillus subtilis. mBio. 2012;3(4):e00184-12.
353. Carvalho SM, de Jong A, Kloosterman TG, Kuipers OP, Saraiva LM. The Staphylococcus aureus alpha-Acetolactate Synthase ALS Confers Resistance to Nitrosative Stress. Front Microbiol. 2017;8:1273.
354. Berni F, Enotarpi J, Voskuilen T, Li S, van der Marel GA, Codee JDC. Synthetic carbohydrate-based cell wall components from Staphylococcus aureus. Drug Discov Today Technol. 2020;38:35-43.
355. Yan J, Nadell CD, Bassler BL. Environmental fluctuation governs selection for plasticity in biofilm production. ISME J. 2017;11(7):1569-77.
356. Liakat S, Bors KA, Huang TY, Michel AP, Zanghi E, Gmachl CF. In vitro measurements of physiological glucose concentrations in biological fluids using mid-infrared light. Biomed Opt Express. 2013;4(7):1083-90.
357. Smith AC, Rice A, Sutton B, Gabrilska R, Wessel AK, Whiteley M, et al. Albumin Inhibits Pseudomonas aeruginosa Quorum Sensing and Alters Polymicrobial Interactions. Infect Immun. 2017;85(9).
358. Cotter PA, Stibitz S. c-di-GMP-mediated regulation of virulence and biofilm formation. Curr Opin Microbiol. 2007;10(1):17-23.
359. Kulasakara H, Lee V, Brencic A, Liberati N, Urbach J, Miyata S, et al. Analysis of Pseudomonas aeruginosa diguanylate cyclases and phosphodiesterases reveals a role for bis-(3'-5')-cyclic-GMP in virulence. Proc Natl Acad Sci U S A. 2006;103(8):2839-44.

360. Starkey M, Hickman JH, Ma L, Zhang N, De Long S, Hinz A, et al. Pseudomonas aeruginosa rugose small-colony variants have adaptations that likely promote persistence in the cystic fibrosis lung. J Bacteriol. 2009;191(11):3492-503.
361. Hall CL, Lee VT. Cyclic-di-GMP regulation of virulence in bacterial pathogens. Wiley Interdiscip Rev RNA. 2018;9(1).
362. Geijtenbeek TB, van Kooyk Y. Pathogens target DC-SIGN to influence their fate DC-SIGN functions as a pathogen receptor with broad specificity. APMIS. 2003;111(7-8):698-714.
363. Sommer R, Wagner S, Varrot A, Nycholat CM, Khaledi A, Haussler S, et al. The virulence factor LecB varies in clinical isolates: consequences for ligand binding and drug discovery. Chem Sci. 2016;7(8):4990-5001.
364. Garcia-Vallejo JJ, van Kooyk Y. The physiological role of DC-SIGN: a tale of mice and men. Trends Immunol. 2013;34(10):482-6.
365. Feinberg H, Guo Y, Mitchell DA, Drickamer K, Weis WI. Extended neck regions stabilize tetramers of the receptors DC-SIGN and DC-SIGNR. J Biol Chem. 2005;280(2):1327-35.
366. Ruiz-Herrera J, Elorza MV, Valentin E, Sentandreu R. Molecular organization of the cell wall of Candida albicans and its relation to pathogenicity. FEMS Yeast Res. 2006;6(1):14-29.
367. Kim HJ, Bae IK, Jeong MH, Park HJ, Jung JS, Kim JE. A New HPLC-ELSD Method for Simultaneous Determination of N-Acetylglucosamine and N-Acetylgalactosamine in Dairy Foods. Int J Anal Chem. 2015;2015:892486.
368. Goldstein IJ, Hollerman CE, Merrick JM. Protein-Carbohydrate Interaction. I. The Interaction of Polysaccharides with Concanavalin A. Biochim Biophys Acta. 1965;97:68-76.
369. Akiyama H, Huh WK, Fujii K, Yamasaki O, Oono T, Iwatsuki K. Confocal laser microscopic observation of glycocalyx production by Staphylococcus aureus in vitro. J Dermatol Sci. 2002;29(1):54-61.
370. Meredith TC, Swoboda JG, Walker S. Late-stage polyribitol phosphate wall teichoic acid biosynthesis in Staphylococcus aureus. J Bacteriol. 2008;190(8):3046-56.
371. Peters BM, Noverr MC. Candida albicans-Staphylococcus aureus polymicrobial peritonitis modulates host innate immunity. Infect Immun. 2013;81(6):2178-89.
372. Carolus H, Van Dyck K, Van Dijck P. Candida albicans and Staphylococcus Species: A Threatening Twosome. Front Microbiol. 2019;10:2162.
373. van Dalen R, De La Cruz Diaz JS, Rumpret M, Fuchsberger FF, van Teijlingen NH, Hanske J, et al. Langerhans Cells Sense Staphylococcus aureus Wall Teichoic Acid through Langerin To Induce Inflammatory Responses. mBio. 2019;10(3).
374. McDermott R, Bausinger H, Fricker D, Spehner D, Proamer F, Lipsker D, et al. Reproduction of Langerin/CD207 traffic and Birbeck granule formation in a human cell line model. J Invest Dermatol. 2004;123(1):72-7.
375. Ng WC, Londrigan SL, Nasr N, Cunningham AL, Turville S, Brooks AG, et al. The C-type Lectin Langerin Functions as a Receptor for Attachment and Infectious Entry of Influenza A Virus. J Virol. 2016;90(1):206-21.
376. Zizzari IG, Napoletano C, Battisti F, Rahimi H, Caponnetto S, Pierelli L, et al. MGL Receptor and Immunity: When the Ligand Can Make the Difference. J Immunol Res. 2015;2015:450695.
377. Achouiti A, Van't Veer C, de Vos AF, van der Poll T. The receptor for advanced glycation end products promotes bacterial growth at distant body sites in Staphylococcus aureus skin infection. Microbes Infect. 2015;17(9):622-7.
378. Moffatt JD, Jeffrey KL, Cocks TM. Protease-activated receptor-2 activating peptide SLIGRL inhibits bacterial lipopolysaccharide-induced recruitment of polymorphonuclear leukocytes into the airways of mice. Am J Respir Cell Mol Biol. 2002;26(6):680-4.
379. Heuberger DM, Schuepbach RA. Protease-activated receptors (PARs): mechanisms of action and potential therapeutic modulators in PAR-driven inflammatory diseases. Thromb J. 2019;17:4.

380. Dulon S, Leduc D, Cottrell GS, D'Alayer J, Hansen KK, Bunnett NW, et al. Pseudomonas aeruginosa elastase disables proteinase-activated receptor 2 in respiratory epithelial cells. Am J Respir Cell Mol Biol. 2005;32(5):411-9.
381. Potempa J, Pike RN. Corruption of innate immunity by bacterial proteases. J Innate Immun. 2009;1(2):70-87.
382. Kida Y, Higashimoto Y, Inoue H, Shimizu T, Kuwano K. A novel secreted protease from Pseudomonas aeruginosa activates NF-kappaB through protease-activated receptors. Cell Microbiol. 2008;10(7):1491-504.
383. Li X, Syrovets T, Paskas S, Laumonnier Y, Simmet T. Mature dendritic cells express functional thrombin receptors triggering chemotaxis and CCL18/pulmonary and activation-regulated chemokine induction. J Immunol. 2008;181(2):1215-23.
384. Wittmann A, Lamprinaki D, Bowles KM, Katzenellenbogen E, Knirel YA, Whitfield C, et al. Dectin-2 Recognizes Mannosylated O-antigens of Human Opportunistic Pathogens and Augments Lipopolysaccharide Activation of Myeloid Cells. J Biol Chem. 2016;291(34):17629-38.
385. Zhang P, Snyder S, Feng P, Azadi P, Zhang S, Bulgheresi S, et al. Role of N-acetylglucosamine within core lipopolysaccharide of several species of gram-negative bacteria in targeting the DC-SIGN (CD209). J Immunol. 2006;177(6):4002-11.
386. Zhang P, Schwartz O, Pantelic M, Li G, Knazze Q, Nobile C, et al. DC-SIGN (CD209) recognition of Neisseria gonorrhoeae is circumvented by lipooligosaccharide variation. J Leukoc Biol. 2006;79(4):731-8.
387. Klausen M, Aaes-Jorgensen A, Molin S, Tolker-Nielsen T. Involvement of bacterial migration in the development of complex multicellular structures in Pseudomonas aeruginosa biofilms. Mol Microbiol. 2003;50(1):61-8.
388. Barken KB, Pamp SJ, Yang L, Gjermansen M, Bertrand JJ, Klausen M, et al. Roles of type IV pili, flagellum-mediated motility and extracellular DNA in the formation of mature multicellular structures in Pseudomonas aeruginosa biofilms. Environ Microbiol. 2008;10(9):2331-43.
389. Miller JK, Badawy HT, Clemons C, Kreider KL, Wilber P, Milsted A, et al. Development of the Pseudomonas aeruginosa mushroom morphology and cavity formation by iron-starvation: a mathematical modeling study. J Theor Biol. 2012;308:68-78.
390. Torres FG, Troncoso OP, Pisani A, Gatto F, Bardi G. Natural Polysaccharide Nanomaterials: An Overview of Their Immunological Properties. Int J Mol Sci. 2019;20(20).
391. Diener M, Adamcik J, Sánchez-Ferrer A, Jaedig F, Schefer L, Mezzenga R. Primary, Secondary, Tertiary and Quaternary Structure Levels in Linear Polysaccharides: From Random Coil, to Single Helix to Supramolecular Assembly. Biomacromolecules. 2019;20(4):1731-9.
392. Boyd A, Chakrabarty AM. Pseudomonas aeruginosa biofilms: role of the alginate exopolysaccharide. J Ind Microbiol. 1995;15(3):162-8.
393. Lin K, Kasko AM. Carbohydrate-Based Polymers for Immune Modulation. ACS Macro Lett. 2014;3(7):652-7.
394. Cordeiro AS, Alonso MJ, de la Fuente M. Nanoengineering of vaccines using natural polysaccharides. Biotechnol Adv. 2015;33(6 Pt 3):1279-93.
395. Fomsgaard A. Antibodies to lipopolysaccharides: some diagnostic and protective aspects. APMIS Suppl. 1990;18:1-38.
396. Mavrodi DV, Bonsall RF, Delaney SM, Soule MJ, Phillips G, Thomashow LS. Functional analysis of genes for biosynthesis of pyocyanin and phenazine-1-carboxamide from Pseudomonas aeruginosa PAO1. J Bacteriol. 2001;183(21):6454-65.
397. Valentini M, Lapouge K. Catabolite repression in Pseudomonas aeruginosa PAO1 regulates the uptake of C4 -dicarboxylates depending on succinate concentration. Environ Microbiol. 2013;15(6):1707-16.
398. Panayidou S, Georgiades K, Christofi T, Tamana S, Promponas VJ, Apidianakis Y. Pseudomonas aeruginosa core metabolism exerts a widespread growth-independent control on virulence. Sci Rep. 2020;10(1):9505.
399. van den Tillaart SA, Busard MP, Trimbos JB. The use of distilled water in the achievement of local hemostasis during surgery. Gynecol Surg. 2009;6(3):255-9.

400. Blaustein MP, Leenen FH, Chen L, Golovina VA, Hamlyn JM, Pallone TL, et al. How NaCl raises blood pressure: a new paradigm for the pathogenesis of salt-dependent hypertension. Am J Physiol Heart Circ Physiol. 2012;302(5):H1031-49.
401. Min B, Fairchild RL. Over-salting ruins the balance of the immune menu. J Clin Invest. 2015;125(11):4002-4.
402. Jantsch J, Schatz V, Friedrich D, Schroder A, Kopp C, Siegert I, et al. Cutaneous Na+ storage strengthens the antimicrobial barrier function of the skin and boosts macrophage-driven host defense. Cell Metab. 2015;21(3):493-501.
403. Holt C. Structure and stability of bovine casein micelles. Adv Protein Chem. 1992;43:63-151.
404. Haider M, Dambuza IM, Asamaphan P, Stappers M, Reid D, Yamasaki S, et al. The pattern recognition receptors dectin-2, mincle, and FcRgamma impact the dynamics of phagocytosis of Candida, Saccharomyces, Malassezia, and Mucor species. PLoS One. 2019;14(8):e0220867.
405. Haber L, Winthrop L, Weiner SS. Biomechanical findings in a random survey of fifth toe abnormalities. J Am Podiatry Assoc. 1975;65(3):206-11.
406. Nyame AK, Leppanen AM, Bogitsh BJ, Cummings RD. Antibody responses to the fucosylated LacdiNAc glycan antigen in Schistosoma mansoni-infected mice and expression of the glycan among schistosomes. Exp Parasitol. 2000;96(4):202-12.
407. van Liempt E, Bank CM, Mehta P, Garcia-Vallejo JJ, Kawar ZS, Geyer R, et al. Specificity of DC-SIGN for mannose- and fucose-containing glycans. FEBS Lett. 2006;580(26):6123-31.
408. van Die I, van Vliet SJ, Nyame AK, Cummings RD, Bank CM, Appelmelk B, et al. The dendritic cell-specific C-type lectin DC-SIGN is a receptor for Schistosoma mansoni egg antigens and recognizes the glycan antigen Lewis x. Glycobiology. 2003;13(6):471-8.
409. Velimirov B. Nanobacteria, Ultramicrobacteria and Starvation Forms: A Search for the Smallest Metabolizing Bacterium. Microbes and Environments. 2001;16(2):67-77.
410. Lee C, Verma R, Byun S, Jeun EJ, Kim GC, Lee S, et al. Structural specificities of cell surface beta-glucan polysaccharides determine commensal yeast mediated immuno-modulatory activities. Nat Commun. 2021;12(1):3611.
411. Hilz H, Wiegers U, Adamietz P. Stimulation of proteinase K action by denaturing agents: application to the isolation of nucleic acids and the degradation of 'masked' proteins. Eur J Biochem. 1975;56(1):103-8.
412. Wingfield P. Protein precipitation using ammonium sulfate. Curr Protoc Protein Sci. 2001;Appendix 3:Appendix 3F.
413. Jiang L, He L, Fountoulakis M. Comparison of protein precipitation methods for sample preparation prior to proteomic analysis. J Chromatogr A. 2004;1023(2):317-20.
414. Xu J, Yue RQ, Liu J, Ho HM, Yi T, Chen HB, et al. Structural diversity requires individual optimization of ethanol concentration in polysaccharide precipitation. Int J Biol Macromol. 2014;67:205-9.
415. Lowman DW, West LJ, Bearden DW, Wempe MF, Power TD, Ensley HE, et al. New insights into the structure of (1-->3,1-->6)-beta-D-glucan side chains in the Candida glabrata cell wall. PLoS One. 2011;6(11):e27614.
416. Almuhanna YSI. Role of lectin receptors in recognition of Pseudomonas aeruginosa biofilms [PhD]. Nottingham, UK: University of Nottingham; 2021.
417. Maira-Litran T, Kropec A, Abeygunawardana C, Joyce J, Mark G, 3rd, Goldmann DA, et al. Immunochemical properties of the staphylococcal poly-N-acetylglucosamine surface polysaccharide. Infect Immun. 2002;70(8):4433-40.
418. Maira-Litran T, Kropec A, Goldmann DA, Pier GB. Comparative opsonic and protective activities of Staphylococcus aureus conjugate vaccines containing native or deacetylated Staphylococcal Poly-N-acetyl-beta-(1-6)-glucosamine. Infect Immun. 2005;73(10):6752-62.
419. Gening ML, Tsvetkov YE, Pier GB, Nifantiev NE. Synthesis of beta-(1-->6)-linked glucosamine oligosaccharides corresponding to fragments of the bacterial surface polysaccharide poly-N-acetylglucosamine. Carbohydr Res. 2007;342(3-4):567-75.

420. O'Riordan K, Lee JC. Staphylococcus aureus capsular polysaccharides. Clin Microbiol Rev. 2004;17(1):218-34.
421. Karakawa WW, Sutton A, Schneerson R, Karpas A, Vann WF. Capsular antibodies induce type-specific phagocytosis of capsulated Staphylococcus aureus by human polymorphonuclear leukocytes. Infect Immun. 1988;56(5):1090-5.
422. Danieli E, Proietti D, Brogioni G, Romano MR, Cappelletti E, Tontini M, et al. Synthesis of Staphylococcus aureus type 5 capsular polysaccharide repeating unit using novel L-FucNAc and D-FucNAc synthons and immunochemical evaluation. Bioorg Med Chem. 2012;20(21):6403-15.
423. Theilacker C, Kaczynski Z, Kropec A, Fabretti F, Sange T, Holst O, et al. Opsonic antibodies to Enterococcus faecalis strain 12030 are directed against lipoteichoic acid. Infect Immun. 2006;74(10):5703-12.
424. Matias VR, Beveridge TJ. Native cell wall organization shown by cryo-electron microscopy confirms the existence of a periplasmic space in Staphylococcus aureus. J Bacteriol. 2006;188(3):1011-21.
425. Xia G, Kohler T, Peschel A. The wall teichoic acid and lipoteichoic acid polymers of Staphylococcus aureus. Int J Med Microbiol. 2010;300(2-3):148-54.
426. Gerlach D, Guo Y, De Castro C, Kim SH, Schlatterer K, Xu FF, et al. Methicillin-resistant Staphylococcus aureus alters cell wall glycosylation to evade immunity. Nature. 2018;563(7733):705-9.
427. Fekete A, Hoogerhout P, Zomer G, Kubler-Kielb J, Schneerson R, Robbins JB, et al. Synthesis of octa- and dodecamers of D-ribitol-1-phosphate and their protein conjugates. Carbohydr Res. 2006;341(12):2037-48.
428. Geng J, Mantovani G, Tao L, Nicolas J, Chen G, Wallis R, et al. Site-directed conjugation of "clicked" glycopolymers to form glycoprotein mimics: binding to mammalian lectin and induction of immunological function. J Am Chem Soc. 2007;129(49):15156-63.
429. Takahashi M, Ishida Y, Iwaki D, Kanno K, Suzuki T, Endo Y, et al. Essential role of mannose-binding lectin-associated serine protease-1 in activation of the complement factor D. J Exp Med. 2010;207(1):29-37.
430. Neth O, Jack DL, Johnson M, Klein NJ, Turner MW. Enhancement of complement activation and opsonophagocytosis by complexes of mannose-binding lectin with mannose-binding lectin-associated serine protease after binding to Staphylococcus aureus. J Immunol. 2002;169(8):4430-6.
431. Takahashi K. Mannose-binding lectin and the balance between immune protection and complication. Expert Rev Anti Infect Ther. 2011;9(12):1179-90.
432. Ip WK, Takahashi K, Ezekowitz RA, Stuart LM. Mannose-binding lectin and innate immunity. Immunol Rev. 2009;230(1):9-21.
433. Coffman RL, Sher A, Seder RA. Vaccine adjuvants: putting innate immunity to work. Immunity. 2010;33(4):492-503.
434. Song EH, Manganiello MJ, Chow YH, Ghosn B, Convertine AJ, Stayton PS, et al. In vivo targeting of alveolar macrophages via RAFT-based glycopolymers. Biomaterials. 2012;33(28):6889-97.
435. Pustylnikov S, Dave RS, Khan ZK, Porkolab V, Rashad AA, Hutchinson M, et al. Short Communication: Inhibition of DC-SIGN-Mediated HIV-1 Infection by Complementary Actions of Dendritic Cell Receptor Antagonists and Env-Targeting Virus Inactivators. AIDS Res Hum Retroviruses. 2016;32(1):93-100.
436. Ahmed M, Lai BF, Kizhakkedathu JN, Narain R. Hyperbranched glycopolymers for blood biocompatibility. Bioconjug Chem. 2012;23(5):1050-8.
437. Kirker KR, James GA. In vitro studies evaluating the effects of biofilms on wound-healing cells: a review. APMIS. 2017;125(4):344-52.
438. Haesler E, Swanson T, Ousey K, Carville K. Clinical indicators of wound infection and biofilm: reaching international consensus. J Wound Care. 2019;28(Sup3b):s4-s12.
439. Bianchi T, Wolcott RD, Peghetti A, Leaper D, Cutting K, Polignano R, et al. Recommendations for the management of biofilm: a consensus document. J Wound Care. 2016;25(6):305-17.

440. Rodriguez-Rojas A, Oliver A, Blazquez J. Intrinsic and environmental mutagenesis drive diversification and persistence of Pseudomonas aeruginosa in chronic lung infections. J Infect Dis. 2012;205(1):121-7.
441. Wood S, Jayaraman V, Huelsmann EJ, Bonish B, Burgad D, Sivaramakrishnan G, et al. Pro-inflammatory chemokine CCL2 (MCP-1) promotes healing in diabetic wounds by restoring the macrophage response. PLoS One. 2014;9(3):e91574.
442. Hutami IR, Izawa T, Khurel-Ochir T, Sakamaki T, Iwasa A, Tanaka E. Macrophage Motility in Wound Healing Is Regulated by HIF-1alpha via S1P Signaling. Int J Mol Sci. 2021;22(16).
443. Spampinato SF, Caruso GI, De Pasquale R, Sortino MA, Merlo S. The Treatment of Impaired Wound Healing in Diabetes: Looking among Old Drugs. Pharmaceuticals (Basel). 2020;13(4).
444. Silva MT. Macrophage phagocytosis of neutrophils at inflammatory/infectious foci: a cooperative mechanism in the control of infection and infectious inflammation. J Leukoc Biol. 2011;89(5):675-83.
445. Richardson AR, Libby SJ, Fang FC. A nitric oxide-inducible lactate dehydrogenase enables Staphylococcus aureus to resist innate immunity. Science. 2008;319(5870):1672-6.
446. Soilleux EJ, Morris LS, Leslie G, Chehimi J, Luo Q, Levroney E, et al. Constitutive and induced expression of DC-SIGN on dendritic cell and macrophage subpopulations in situ and in vitro. J Leukoc Biol. 2002;71(3):445-57.
447. den Dunnen J, Gringhuis SI, Geijtenbeek TB. Innate signaling by the C-type lectin DC-SIGN dictates immune responses. Cancer Immunol Immunother. 2009;58(7):1149-57.
448. van Kooyk Y, Geijtenbeek TB. DC-SIGN: escape mechanism for pathogens. Nat Rev Immunol. 2003;3(9):697-709.
449. da Silva AC. Understanding the diversity and evolution of complex wound infections. Nottingham, UK: University of Nottingham 2019.
450. Bjarnsholt T. The role of bacterial biofilms in chronic infections. APMIS Suppl. 2013(136):1-51.
451. Kvich L, Burmolle M, Bjarnsholt T, Lichtenberg M. Do Mixed-Species Biofilms Dominate in Chronic Infections?-Need for in situ Visualization of Bacterial Organization. Front Cell Infect Microbiol. 2020;10:396.
452. Bieber K, Autenrieth SE. Dendritic cell development in infection. Mol Immunol. 2020;121:111-7.
453. Agaronyan K, Sharma L, Vaidyanathan B, Glenn K, Yu S, Annicelli C, et al. Tissue remodeling by an opportunistic pathogen triggers allergic inflammation. Immunity. 2022;55(5):895-911 e10.
454. Boyle D, Tien LF, Cooper NG, Shepherd V, McLaughlin BJ. A mannose receptor is involved in retinal phagocytosis. Invest Ophthalmol Vis Sci. 1991;32(5):1464-70.
455. Linehan SA, Martinez-Pomares L, Stahl PD, Gordon S. Mannose receptor and its putative ligands in normal murine lymphoid and nonlymphoid organs: In situ expression of mannose receptor by selected macrophages, endothelial cells, perivascular microglia, and mesangial cells, but not dendritic cells. J Exp Med. 1999;189(12):1961-72.
456. Wilt SD, Greaton CJ, Lutz DA, McLaughlin BJ. Mannose receptor is expressed in normal and dystrophic retinal pigment epithelium. Exp Eye Res. 1999;69(4):405-11.
457. Sallusto F, Cella M, Danieli C, Lanzavecchia A. Dendritic cells use macropinocytosis and the mannose receptor to concentrate macromolecules in the major histocompatibility complex class II compartment: downregulation by cytokines and bacterial products. J Exp Med. 1995;182(2):389-400.
458. Liu X, Yin S, Chen Y, Wu Y, Zheng W, Dong H, et al. LPSinduced proinflammatory cytokine expression in human airway epithelial cells and macrophages via NFkappaB, STAT3 or AP1 activation. Mol Med Rep. 2018;17(4):5484-91.
459. Jurado-Martin I, Sainz-Mejias M, McClean S. Pseudomonas aeruginosa: An Audacious Pathogen with an Adaptable Arsenal of Virulence Factors. Int J Mol Sci. 2021;22(6).

460. Hennemann LC, LaFayette SL, Malet JK, Bortolotti P, Yang T, McKay GA, et al. LasR-deficient Pseudomonas aeruginosa variants increase airway epithelial mICAM-1 expression and enhance neutrophilic lung inflammation. PLoS Pathog. 2021;17(3):e1009375.
461. Hennemann LC, Nguyen D. LasR-regulated proteases in acute vs. chronic lung infection: a double-edged sword. Microb Cell. 2021;8(7):161-3.
462. Guenther F, Stroh P, Wagner C, Obst U, Hansch GM. Phagocytosis of staphylococci biofilms by polymorphonuclear neutrophils: S. aureus and S. epidermidis differ with regard to their susceptibility towards the host defense. Int J Artif Organs. 2009;32(9):565-73.
463. Van den Bossche S, Vandeplassche E, Ostyn L, Coenye T, Crabbe A. Bacterial Interference With Lactate Dehydrogenase Assay Leads to an Underestimation of Cytotoxicity. Front Cell Infect Microbiol. 2020;10:494.
464. Gonzalez AC, Costa TF, Andrade ZA, Medrado AR. Wound healing - A literature review. An Bras Dermatol. 2016;91(5):614-20.
465. Peleg AY, Hogan DA, Mylonakis E. Medically important bacterial-fungal interactions. Nat Rev Microbiol. 2010;8(5):340-9.
466. Xaplanteri P, Lagoumintzis G, Dimitracopoulos G, Paliogianni F. Synergistic regulation of Pseudomonas aeruginosa-induced cytokine production in human monocytes by mannose receptor and TLR2. Eur J Immunol. 2009;39(3):730-40.
467. Sutterwala FS, Mijares LA, Li L, Ogura Y, Kazmierczak BI, Flavell RA. Immune recognition of Pseudomonas aeruginosa mediated by the IPAF/NLRC4 inflammasome. J Exp Med. 2007;204(13):3235-45.
468. Patankar YR, Mabaera R, Berwin B. Differential ASC requirements reveal a key role for neutrophils and a noncanonical IL-1beta response to Pseudomonas aeruginosa. Am J Physiol Lung Cell Mol Physiol. 2015;309(8):L902-13.
469. Karmakar M, Sun Y, Hise AG, Rietsch A, Pearlman E. Cutting edge: IL-1beta processing during Pseudomonas aeruginosa infection is mediated by neutrophil serine proteases and is independent of NLRC4 and caspase-1. J Immunol. 2012;189(9):4231-5.
470. Muntaka S, Almuhanna Y, Jackson D, Singh S, Afryie-Asante A, Camara M, et al. Gamma Interferon and Interleukin-17A Differentially Influence the Response of Human Macrophages and Neutrophils to Pseudomonas aeruginosa Infection. Infect Immun. 2019;87(2).
471. Phuong MS, Hernandez RE, Wolter DJ, Hoffman LR, Sad S. Impairment in inflammasome signaling by the chronic Pseudomonas aeruginosa isolates from cystic fibrosis patients results in an increase in inflammatory response. Cell Death Dis. 2021;12(3):241.
472. Henkel JS, Beers DR, Siklos L, Appel SH. The chemokine MCP-1 and the dendritic and myeloid cells it attracts are increased in the mSOD1 mouse model of ALS. Mol Cell Neurosci. 2006;31(3):427-37.
473. Leidal KG, Munson KL, Johnson MC, Denning GM. Metalloproteases from Pseudomonas aeruginosa degrade human RANTES, MCP-1, and ENA-78. J Interferon Cytokine Res. 2003;23(6):307-18.
474. Abdi K, Singh NJ, Matzinger P. Lipopolysaccharide-activated dendritic cells: "exhausted" or alert and waiting? J Immunol. 2012;188(12):5981-9.
475. Carstensen LS, Lie-Andersen O, Obers A, Crowther MD, Svane IM, Hansen M. Long-Term Exposure to Inflammation Induces Differential Cytokine Patterns and Apoptosis in Dendritic Cells. Front Immunol. 2019;10:2702.
476. Hodges A, Sharrocks K, Edelmann M, Baban D, Moris A, Schwartz O, et al. Activation of the lectin DC-SIGN induces an immature dendritic cell phenotype triggering Rho-GTPase activity required for HIV-1 replication. Nat Immunol. 2007;8(6):569-77.
477. Napper CE, Drickamer K, Taylor ME. Collagen binding by the mannose receptor mediated through the fibronectin type II domain. Biochem J. 2006;395(3):579-86.
478. Dodagatta-Marri E, Mitchell DA, Pandit H, Sonawani A, Murugaiah V, Idicula-Thomas S, et al. Protein-Protein Interaction between Surfactant Protein D and DC-SIGN via C-Type Lectin Domain Can Suppress HIV-1 Transfer. Front Immunol. 2017;8:834.
479. Botting RA, Bertram KM, Baharlou H, Sandgren KJ, Fletcher J, Rhodes JW, et al. Phenotypic and functional consequences of different isolation protocols on skin mononuclear phagocytes. J Leukoc Biol. 2017;101(6):1393-403.

480. Parker D. CD80/CD86 signaling contributes to the proinflammatory response of Staphylococcus aureus in the airway. Cytokine. 2018;107:130-6.
481. Guilliams M, Dutertre CA, Scott CL, McGovern N, Sichien D, Chakarov S, et al. Unsupervised High-Dimensional Analysis Aligns Dendritic Cells across Tissues and Species. Immunity. 2016;45(3):669-84.
482. Gao Y, Nish SA, Jiang R, Hou L, Licona-Limon P, Weinstein JS, et al. Control of T helper 2 responses by transcription factor IRF4-dependent dendritic cells. Immunity. 2013;39(4):722-32.
483. Martinez-Lopez M, Iborra S, Conde-Garrosa R, Sancho D. Batf3-dependent CD103+ dendritic cells are major producers of IL-12 that drive local Th1 immunity against Leishmania major infection in mice. Eur J Immunol. 2015;45(1):119-29.
484. Brassard J, Roy J, Lemay AM, Beaulieu MJ, Bernatchez E, Veillette M, et al. Exposure to the Gram-Negative Bacteria Pseudomonas aeruginosa Influences the Lung Dendritic Cell Population Signature by Interfering With CD103 Expression. Front Cell Infect Microbiol. 2021;11:617481.
485. Bragonzi A, Paroni M, Nonis A, Cramer N, Montanari S, Rejman J, et al. Pseudomonas aeruginosa microevolution during cystic fibrosis lung infection establishes clones with adapted virulence. Am J Respir Crit Care Med. 2009;180(2):138-45.
486. Clauditz A, Resch A, Wieland KP, Peschel A, Gotz F. Staphyloxanthin plays a role in the fitness of Staphylococcus aureus and its ability to cope with oxidative stress. Infect Immun. 2006;74(8):4950-3.
487. Alshahrani M. The role of C-type lectin receptors in the recognition of Pseudiminas aeruginosa. Nottingham, UK: University of Nottingham; 2018.
488. Horsburgh MJ, Aish JL, White IJ, Shaw L, Lithgow JK, Foster SJ. sigmaB modulates virulence determinant expression and stress resistance: characterization of a functional rsbU strain derived from Staphylococcus aureus 8325-4. J Bacteriol. 2002;184(19):5457-67.
489. Baek KT, Frees D, Renzoni A, Barras C, Rodriguez N, Manzano C, et al. Genetic variation in the Staphylococcus aureus 8325 strain lineage revealed by whole-genome sequencing. PLoS One. 2013;8(9):e77122.
490. Lourenco C, Macdonald TJ, Gavriilidis A, Allan E, MacRobert AJ, Parkin IP. Effects of bovine serum albumin on light activated antimicrobial surfaces. RSC Adv. 2018;8(60):34252-8.
491. Khanna S, Biswas S, Shang Y, Collard E, Azad A, Kauh C, et al. Macrophage dysfunction impairs resolution of inflammation in the wounds of diabetic mice. PLoS One. 2010;5(3):e9539.
492. Galvan EM, Mateyca C, Ielpi L. Role of interspecies interactions in dual-species biofilms developed in vitro by uropathogens isolated from polymicrobial urinary catheter-associated bacteriuria. Biofouling. 2016;32(9):1067-77.
493. Hammer ND, Cassat JE, Noto MJ, Lojek LJ, Chadha AD, Schmitz JE, et al. Inter- and intraspecies metabolite exchange promotes virulence of antibiotic-resistant Staphylococcus aureus. Cell Host Microbe. 2014;16(4):531-7.
494. Ditu LM, Chifiriuc MC, Bezirtzoglou E, Voltsi C, Bleotu C, Pelinescu D, et al. Modulation of virulence and antibiotic susceptibility of enteropathogenic Escherichia coli strains by Enterococcus faecium probiotic strain culture fractions. Anaerobe. 2011;17(6):448-51.
495. Goh HMS, Yong MHA, Chong KKL, Kline KA. Model systems for the study of Enterococcal colonization and infection. Virulence. 2017;8(8):1525-62.
496. Pammi M, Zhong D, Johnson Y, Revell P, Versalovic J. Polymicrobial bloodstream infections in the neonatal intensive care unit are associated with increased mortality: a case-control study. BMC Infect Dis. 2014;14:390.
497. Singh KV, La Rosa SL, Somarajan SR, Roh JH, Murray BE. The fibronectin-binding protein EfbA contributes to pathogenesis and protects against infective endocarditis caused by Enterococcus faecalis. Infect Immun. 2015;83(12):4487-94.
498. Singh KV, Nallapareddy SR, Sillanpaa J, Murray BE. Importance of the collagen adhesin ace in pathogenesis and protection against Enterococcus faecalis experimental endocarditis. PLoS Pathog. 2010;6(1):e1000716.

499. Siu LK, Yeh KM, Lin JC, Fung CP, Chang FY. Klebsiella pneumoniae liver abscess: a new invasive syndrome. Lancet Infect Dis. 2012;12(11):881-7.
500. Bengoechea JA, Sa Pessoa J. Klebsiella pneumoniae infection biology: living to counteract host defences. FEMS Microbiol Rev. 2019;43(2):123-44.
501. Liu Q, Wu J, Wang Z, Wu X, Wang G, Ren J. Polymicrobial Bacteremia Involving Klebsiella pneumoniae in Patients with Complicated Intra-Abdominal Infections: Frequency, Co-Pathogens, Risk Factors, and Clinical Outcomes. Surg Infect (Larchmt). 2019;20(4):317-25.
502. Cano V, March C, Insua JL, Aguilo N, Llobet E, Moranta D, et al. Klebsiella pneumoniae survives within macrophages by avoiding delivery to lysosomes. Cell Microbiol. 2015;17(11):1537-60.
503. Wanford JJ, Hames RG, Carreno D, Jasiunaite Z, Chung WY, Arena F, et al. Interaction of Klebsiella pneumoniae with tissue macrophages in a mouse infection model and ex-vivo pig organ perfusions: an exploratory investigation. Lancet Microbe. 2021;2(12):e695-e703.
504. Todd OA, Fidel PL, Jr., Harro JM, Hilliard JJ, Tkaczyk C, Sellman BR, et al. Candida albicans Augments Staphylococcus aureus Virulence by Engaging the Staphylococcal agr Quorum Sensing System. mBio. 2019;10(3).
505. Todd OA, Peters BM. Candida albicans and Staphylococcus aureus Pathogenicity and Polymicrobial Interactions: Lessons beyond Koch's Postulates. J Fungi (Basel). 2019;5(3).
506. Brand A, Barnes JD, Mackenzie KS, Odds FC, Gow NA. Cell wall glycans and soluble factors determine the interactions between the hyphae of Candida albicans and Pseudomonas aeruginosa. FEMS Microbiol Lett. 2008;287(1):48-55.
507. Bandara HM, BP KC, Watt RM, Jin LJ, Samaranayake LP. Pseudomonas aeruginosa lipopolysaccharide inhibits Candida albicans hyphae formation and alters gene expression during biofilm development. Mol Oral Microbiol. 2013;28(1):54-69.
508. Scharschmidt TC, Fischbach MA. What Lives On Our Skin: Ecology, Genomics and Therapeutic Opportunities Of the Skin Microbiome. Drug Discov Today Dis Mech. 2013;10(3-4).
509. Belkaid Y, Segre JA. Dialogue between skin microbiota and immunity. Science. 2014;346(6212):954-9.
510. Byrd AL, Belkaid Y, Segre JA. The human skin microbiome. Nat Rev Microbiol. 2018;16(3):143-55.
511. Gavino AC, Chung JS, Sato K, Ariizumi K, Cruz PD, Jr. Identification and expression profiling of a human C-type lectin, structurally homologous to mouse dectin-2. Exp Dermatol. 2005;14(4):281-8.
512. Ross SH, Cantrell DA. Signaling and Function of Interleukin-2 in T Lymphocytes. Annu Rev Immunol. 2018;36:411-33.
513. Lehmann AA, Reche PA, Zhang T, Suwansaard M, Lehmann PV. CERI, CEFX, and CPI: Largely Improved Positive Controls for Testing Antigen-Specific T Cell Function in PBMC Compared to CEF. Cells. 2021;10(2).
514. Ten Brinke A, Marek-Trzonkowska N, Mansilla MJ, Turksma AW, Piekarska K, Iwaszkiewicz-Grzes D, et al. Monitoring T-Cell Responses in Translational Studies: Optimization of Dye-Based Proliferation Assay for Evaluation of Antigen-Specific Responses. Front Immunol. 2017;8:1870.
515. Pastar I, Stojadinovic O, Yin NC, Ramirez H, Nusbaum AG, Sawaya A, et al. Epithelialization in Wound Healing: A Comprehensive Review. Adv Wound Care (New Rochelle). 2014;3(7):445-64.
516. Souren JM, Ponec M, van Wijk R. Contraction of collagen by human fibroblasts and keratinocytes. In Vitro Cell Dev Biol. 1989;25(11):1039-45.
517. Piipponen M, Li D, Landen NX. The Immune Functions of Keratinocytes in Skin Wound Healing. Int J Mol Sci. 2020;21(22).
518. Roupe KM, Nybo M, Sjobring U, Alberius P, Schmidtchen A, Sorensen OE. Injury is a major inducer of epidermal innate immune responses during wound healing. J Invest Dermatol. 2010;130(4):1167-77.

519. Lacroix G, Koch W, Ritter D, Gutleb AC, Larsen ST, Loret T, et al. Air-Liquid Interface In Vitro Models for Respiratory Toxicology Research: Consensus Workshop and Recommendations. Appl In Vitro Toxicol. 2018;4(2):91-106.
520. Nagae M, Ikeda A, Hanashima S, Kojima T, Matsumoto N, Yamamoto K, et al. Crystal structure of human dendritic cell inhibitory receptor C-type lectin domain reveals the binding mode with N-glycan. FEBS Lett. 2016;590(8):1280-8.
521. Garcia-Vallejo JJ, Bloem K, Knippels LM, Garssen J, van Vliet SJ, van Kooyk Y. The Consequences of Multiple Simultaneous C-Type Lectin-Ligand Interactions: DCIR Alters the Endo-Lysosomal Routing of DC-SIGN. Front Immunol. 2015;6:87.
522. Hoving JC, Wilson GJ, Brown GD. Signalling C-type lectin receptors, microbial recognition and immunity. Cell Microbiol. 2014;16(2):185-94.
523. Meng F, Lowell CA. Lipopolysaccharide (LPS)-induced macrophage activation and signal transduction in the absence of Src-family kinases Hck, Fgr, and Lyn. J Exp Med. 1997;185(9):1661-70.